

# New polymer electrolytes for all-solid-state lithium batteries

Itziar Aldalur Ceberio  
Donostia, 2019



**Universidad del País Vasco  
Euskal Herriko Unibertsitatea**

Facultad de Química  
Kimika Fakultatea

Departamento de Ciencia y Tecnología de Polímeros  
Polimeroen Zientzia eta Teknologia Departamentua

**CIC Energigune**

**New polymer electrolytes for all-solid-state  
lithium batteries**

*A dissertation submitted to the University of the Basque Country  
in partial fulfillment of the requirements for the degree of Ph.D.*

By

**Itziar Aldalur Ceberio**

Thesis supervisors:

**Prof. Michel Armand**

**Dr. Michal Piszcz**

**Donostia, 18<sup>th</sup> October 2019**





*Mita, Ama eta Inigori*



*Every ending is a new beginning*





## *Acknowledgements / Eskerrak / Agradecimientos*

No me puedo creer que finalmente haya llegado este momento. Han sido muchas las personas que me han ayudado durante estos cuatro años sin las que esta tesis doctoral no podría haberse llevado a cabo. Por este motivo, y antes de entrar en más detalle, me gustaría agradecerlos a todos y cada uno de vosotros vuestro apoyo de todo corazón. Mila esker bihotz-bihotzez.

First of all, I would like to express my deepest gratitude to my thesis supervisors Prof. Michel Armand and Dr. Michal Piszcz for their support during my PhD period. Michel, thank you for allowing me to work on your wonderful scientific ideas, for always being available to answer to my queries and, above all, thank you for your kindness and patience to guide me back to the right path. Michal, thank you for introducing me into the world of polymer electrolytes. I will keep the good memories of all the time we spent in the lab trying to figure out how to solve all the problems related to the “Jeffys”. I would also like to thank you for your friendship, for taking my ideas into account and for always giving me the freedom to decide which direction I wanted to follow.

I would like to give a special acknowledgement to Dr. Heng Zhang, my good friend Hengi. Thank you for helping me since your arrival to CIC, for your unconditional support, for all the scientific discussion, for never making fun of my crazy ideas, for sharing your crazy ideas with me, for the university of life lessons, for encouraging me to assemble more coin cells even if the previous one hundred were short-circuited and, above everything, thank you for believing in me and in my work. I am sure our friendship will last forever, even if it is only for “postureo”.

My warmest appreciation to my research group and all the wonderful people that have been part of it: Roshan and Oihane thank you for your happiness and for always bringing a smile to the office; “big bro” Hicham for your kind support and good advice during these four years; a Esti por apoyarme siempre y por intentar encontrar una solución a nuestros problemas; a Edu por cantarnos flamenquito en el laboratorio y por esos comentarios que solo a ti se te pueden ocurrir; Kiddan for being so authentic and for making our days happier; a Leire por su optimismo y por los buenos recuerdos del congreso en Strasbourg; Lixin for being so sweet, for all the Chinese lessons and for honored me with a Chinese

name; a María M., mi boss, por ser la persona que más veces va a salir en mis agradecimientos; a Alex por todas las horas de terapia, los partidos del Baskonia y, sobre todo, por los bocadillos de pechuga, queso, bacon. Si llevamos tantos años de amistad será por algo. Finally, I would like to thank Marise for her kindness and for always looking after the whole group.

Me gustaría agradecer especialmente a una persona que no solo ha formado parte de mi grupo de investigación, sino que forma parte de mi vida y que ha sido uno de los pilares fundamentales durante estos cuatro años. Muchísimas gracias Uxue por tu amistad y por estar siempre a mi lado; para alegrarnos cuando todo iba bien, pero sobre todo para apoyarnos en los malos momentos. No puedo imaginar una compañera de mesa mejor que tú en ningún aspecto. Nunca olvidaré todas nuestras batallas, las risas, las lágrimas y, lo más importante de todo, los momentos vividos como las co-fundadoras del "Team Surikate".

También me gustaría dar las gracias al grupo de litio-azufre, especialmente a Lide por su optimismo, apoyo y energía positiva. Gracias por hacer de la unión Polymer-LiS una familia. Chunmei, thank you for your smile and happiness every day. Finalmente, me gustaría agradecer a Judez *et al.* su compañerismo, el buen ambiente y todos los buenos momentos.

A mis compañeros de doctorado: a Xabi, mi compañero de fatigas; a JS por financiar y amenizar los trayectos al trabajo; a Ane y a Jaione por todos los pintxopotes y momentos de devastación; a María A. por todas esas charlas y risas en el hall del segundo piso; a Oier A. por preocuparse de nuestra salud e informarnos sobre todas las actualidades de la OMS y a Begoña por recibirme siempre con una sonrisa. Estos cuatro años no hubiesen sido ni la mitad de buenos si no hubiese compartido esta experiencia con vosotros. Muchísimas gracias.

No me puedo olvidar de toda la gente del CIC que me ha mostrado su apoyo y cariño durante este camino. En especial, me gustaría dar las gracias a Giorgio por su amabilidad, por estar siempre dispuesto a echar una mano y por eso deliciosos postres italianos; a Cristina L. TES por las merecidas meriendas después de un duro día; a María E. por regalarme los momentos más divertidos e informarme de las últimas tendencias para ejercitarse; a Haizea por su simpatía, sus ocurrencias y por intentar poner algo de cordura en nuestro islote; a Ander, gracias por animarme cada día y por todas esas historias para no dormir, no

cambiaría las risas que nos echamos cada día por nada del mundo. Por último, me gustaría agradecer a Guillermo la difusión interna de información.

I thank Dr. Anna Krzton-Maziopa for the rheological measurements at Warsaw University which were really helpful for this PhD work.

I would also like to give a special thanks to Prof. Maria Forsyth and Prof. Patrick C. Howlett for hosting me at Deakin University for three months. I will always remember these months with a big smile on my face. Xiaoen for all his support and commitment; Nico for never letting me cry in front of the DMA and for crying with me when necessary, we still have some collaboration pending; Matze, for the warm welcome and the best Melbourne tour ever; Lane for all the crazy talks and spider hunting at home; Yafei, for her kindness and happiness; Sobhan for the salsa lessons and Tushan and Kalani for all the good memories during the lunch time. Thank you all!

My deepest gratitude goes to my Australian family, Danah and Laura. Thank you for all the weekend adventures, the movie nights, the popcorn and lollies, the never ending walks discovering new places, hours and hours of fun, the euro-trip, all the good memories...but above all, thank you for your friendship. I still wonder where have both of you been my whole life! I am sure we will meet soon. The world is not big enough to prevent our meetings.

Me gustaría agradecer a la gente de Polymat con la que empecé en el mundo de la investigación. Bea y María, me siento muy afortunada de haber podido formar parte del Bioteam con vosotras. Oihane, gracias por estar siempre pendiente y por esos desayunos que alegraban el día.

Muchísimas gracias a las “turbos” por acogerme en Vitoria con los brazos abiertos. Erika, eres sin duda la mejor compañera de piso que podría haber tenido jamás. Gracias por todas las noches de risas y por todas las anécdotas juntas, cada vez que me acuerdo de todas ellas me sale una sonrisa de oreja a oreja. A María, mi bossi, has estado presente en mi vida desde que nos conocimos, quizás por eso es la tercera vez que te menciono a lo largo de estas páginas. Podría escribir un montón de hojas agradeciéndote todo lo que has hecho por mí y todos los momentos que hemos vivido juntas. Pero seré breve, muchísimas gracias por tu amistad, por cuidarme siempre y por ser mi “amatxito” Vitoriana.

A “LaKuadri”, por entender mis ausencias, y por estar ahí para apoyarnos en los malos momentos y para celebrar por todo lo alto nuestras victorias. Laura, Leire García, María S., Teresa, Leyre A., Zuriñe, Sonia, María D., Maite, Amaia, Leire Goenaga y Clara muchísimas gracias a todas y cada una de vosotras por llenar mi vida de luz. Al fin y al cabo sois la familia que he elegido, y que elegiría una y otra vez.

A mi hermano Iñigo, por ser una de las personas a las que más admiro y mi mayor ejemplo a seguir. Gracias por tu apoyo a lo largo de toda mi vida. A mi kú Oihana, por tus ánimos y por sacarme siempre una sonrisa con la alegría que transmites.

Por último, quiero dar las gracias a mis padres ya que sin ellos no habría sido posible llegar hasta aquí. Aita, ama gracias por dármelo todo, por apoyarme siempre, por darme la libertad de elegir el camino que quiero seguir y por creer en mí incluso cuando yo no lo hago. Esta tesis os pertenece más a vosotros que a mí.

## Abstract

The field of lithium-ion batteries (LIBs) is rapidly expanding due to the growing demand of new technologies such as portable electronics, electric vehicles and stationary large-scale energy storage. LIBs are very promising storage systems because of their decent energy density, long lifetime and fast charge/discharge capacity. However, the use of flammable liquid electrolytes, which raises strong safety issues along with insufficient energy density, has incentivized the search for all-solid-state lithium metal ( $\text{Li}^\circ$ ) batteries (ASSLMBs).

Solid polymer electrolytes (SPEs) are considered as one of the viable solutions to replace their liquid counterparts due to their lower flammability, ease of processing and good contact with the electrodes. More importantly, SPEs have better compatibility with  $\text{Li}^\circ$  anode compared to liquid ones, thus allowing a stable operation of ASSLMBs which are supposed to remarkably boost the energy density of the state-of-art LIBs.

The development of SPEs have been the finding of a compromise between good mechanical properties and high ionic conductivity, since the SPEs with low glass transition temperature ( $T_g$ ) and suppressed crystallinity, which are crucial for facilitating fast ionic transport, can hardly form self-standing membranes. Among the different macromolecular hosts, poly(ethylene oxide) (PEO) is one of the most widely used polymer matrices as it contains suitably spaced ether coordination sites that facilitate lithium salt dissociation. PEO is a semi-crystalline polymer in which ionic transport occurs mainly in the amorphous phase, leading to a low ionic conductivity at temperatures below the melting point ( $T_m$ , *ca.* 65 °C) and resulting in PEO-based ASSLMBs operating at elevated temperatures (70–90 °C). Under this condition, PEO is extremely soft and too weak to prevent the growth of lithium metal soft dendrites upon cycling.

Trying to overcome above-mentioned drawbacks, tremendous efforts have been devoted to the design and synthesis of novel non-crystalline and low  $T_g$  polymer matrices, such as structural alteration by random, comb and/or block copolymerization. On the other hand, the incorporation of different type of salts is critical for improving transport properties of SPEs. Lithium bis(trifluoromethanesulfonyl)imide (LiTFSI) has been the most widely studied as

conducting salt owing to the sulfonimide  $-\text{[SO}_2\text{-N-SO}_2\text{]}-$  group. The outstanding thermal and electrochemical stability of this salt, as well as its highly delocalized charge distribution promoting the dissociation of  $\text{Li}^+$  cation and the plasticizing effect due to the flexible S–N bond make this salt suitable for developing reliable SPEs for Li-based batteries. In recent years, lithium bis(fluorosulfonyl)imide (LiFSI) has been widely studied due to the improved compatibility with various electrodes, such as lithium iron phosphate ( $\text{LiFePO}_4$ , LFP) and Li metal. This enhanced compatibility with  $\text{Li}^\circ$  anode is attributed to the formation of LiF-rich solid electrolyte interface (SEI) layer resulting in a stable cycling performance.

In the first stage of this thesis work, novel comb-like polymer matrices based on imide ring backbone and containing polyether hanging moieties (so-called Jeffamine<sup>®</sup>) are reported. These polymers have been doped with sulfonamide salts (*i.e.*, LiTFSI and LiFSI) with the aim of improving the conductivity and the interfacial compatibility with electrode of polymer-based ASSLMBs. The structures of these novel polymer matrices have been conceived on the basis of the following considerations: 1) the poly(ethylene-*alt*-maleimide) backbone is easy to modify in a clean reaction; 2) Jeffamine-side chain polymer is a polyether based on propylene oxide (PO) and ethylene oxide (EO) units ensuring low  $T_g$  and high amorphicity, thus favoring the ionic transport and 3) good adhesion properties and good compatibility against  $\text{Li}^\circ$  anode. These novel SPEs show appreciably higher ionic conductivity than conventional PEO at room temperature (RT) and good compatibility with  $\text{Li}^\circ$  electrode. These exceptional properties enable the operational temperature of  $\text{Li}^\circ \parallel \text{LFP}$  cells to be decreased from an elevated temperature (70 °C) to RT using LiFSI-based electrolytes. Despite these outstanding properties, further modifications were needed in order to improve the mechanical properties and processability of these materials, which we have addressed.

In the next chapter a new type of self-standing and highly conductive SPE based on tailor-made block copolymers (BCPs), containing highly flexible Jeffamine-based blocks and mechanically stable polystyrene (PS) moieties, is presented. The electrolytes exhibit improved mechanical properties without detriment to the ionic conductivity. The superior compatibility with  $\text{Li}^\circ$  electrode allows the electrolyte to be cycled in a  $\text{Li}^\circ \parallel \text{LFP}$  cell with good Coulombic efficiency and low capacity fading. However, the  $\text{Li}^\circ \parallel \text{LFP}$  cell using BCP-based electrolytes

showed inferior cell performance compared to the Jeffamine-based homopolymers.

As another alternative, physical modifications were carried out in the SPEs, obtaining a flowable polymer electrolyte (FPE). The high amorphicity and segmental mobility of the liquid-like polymer matrices facilitate fast ionic transport, thus leading to the highest ionic conductivity reported ( $6.6 \times 10^{-4} \text{ S cm}^{-1}$  at  $70 \text{ }^\circ\text{C}$  and  $1.4 \times 10^{-4} \text{ S cm}^{-1}$  at  $30 \text{ }^\circ\text{C}$ ). The introduction of FPE as a buffer layer between Li metal electrode and PEO-based SPE decreases the interfacial resistivity of  $\text{Li}^\circ/\text{Electrolyte}$  and improves remarkably the cyclability and Coulombic efficiency of  $\text{Li}^\circ \parallel \text{LFP}$  cells.

Finally, a nanofiber-reinforced polymer electrolyte (NRPE) comprising of poly(vinylidene fluoride) (PVDF) fibers along with the FPE is proposed as an innovative electrolyte for ASSLMs. These NRPEs are self-standing, highly conductive, and stable against Li metal electrode, endowing the  $\text{Li}^\circ \parallel \text{LFP}$  cells with good performances at operational temperature down to RT.





# INDEX

---



---

**Chapter 1:****INTRODUCTION**

<b>1.1. Global energy scenario</b> .....	<b>5</b>
<b>1.2. Electrochemical energy storage</b> .....	<b>6</b>
1.2.1. Battery classification.....	6
1.2.2. Rechargeable lithium batteries.....	7
1.2.3. The role of polymers in batteries.....	9
<b>1.3. Fundamentals of polymer electrolytes</b> .....	<b>11</b>
1.3.1. Why polymer electrolytes.....	11
1.3.2. Ionic conduction.....	13
1.3.3. Electrode/electrolyte interfacial chemistry and compatibility.....	16
<b>1.4. Type of polymer electrolytes</b> .....	<b>17</b>
1.4.1. Gel polymer electrolytes (GPEs).....	17
1.4.2. Solid polymer electrolytes (SPEs).....	18
<b>1.5. Towards room temperature solid-state batteries</b> .....	<b>26</b>
1.5.1. Basic requirements.....	26
1.5.2. State-of-the-art.....	26
<b>1.6. General objectives of the present work</b> .....	<b>28</b>
<b>References</b> .....	<b>30</b>

---

**Chapter 2:****EXPERIMENTAL FRAMEWORK**

<b>2.1. Introduction</b> .....	<b>49</b>
<b>2.2. Synthesis methods and sample preparation</b> .....	<b>49</b>
2.2.1. Materials.....	49
2.2.2. Synthesis of new polymer backbones.....	50
2.2.3. Electrolyte preparation.....	51
2.2.4. Poly(vinylidene fluoride) nanofiber preparation.....	52
<b>2.3. Cell preparation</b> .....	<b>53</b>
2.3.1. Electrode preparation.....	53
2.3.2. Cell assembly.....	54
<b>2.4. Characterization techniques</b> .....	<b>55</b>
2.4.1. Chemical characterization.....	55
2.4.2. Morphological and elemental characterization.....	56

---

2.4.3. Mechanical characterization.....	56
2.4.4. Thermal characterization .....	57
2.4.5. Electrochemical characterization .....	58
<b>References.....</b>	<b>61</b>

### **Chapter 3:**

---

## **JEFFAMINE®-BASED HIGHLY CONDUCTIVE SOLID POLYMER ELECTROLYTES**

<b>3.1. Introduction.....</b>	<b>67</b>
<b>3.2. Synthesis of Jeffamine-based polymer matrix.....</b>	<b>69</b>
<b>3.3. Chemical characterization.....</b>	<b>71</b>
5.3.1. Hydrogen-1 nuclear magnetic resonance ( <sup>1</sup> H NMR).....	71
5.3.2. Attenuated total reflectance-Fourier-transform infrared spectroscopy (ATR-FTIR) .....	72
<b>3.4. Thermal characterization.....</b>	<b>73</b>
3.4.1. Thermogravimetric analysis (TGA).....	73
3.4.2. Differential scanning calorimetry (DSC) .....	74
<b>3.5. Ionic conductivity.....</b>	<b>76</b>
<b>3.6. Conclusions.....</b>	<b>77</b>
<b>References.....</b>	<b>79</b>

### **Chapter 4:**

---

## **LOWERING THE OPERATIONAL TEMPERATURE OF ALL-SOLID-STATE LITHIUM METAL BATTERIES WITH HIGHLY CONDUCTIVE SOLID POLYMER ELECTROLYTES**

<b>4.1. Introduction.....</b>	<b>87</b>
<b>4.2. Solid polymer electrolyte preparation.....</b>	<b>89</b>
<b>4.3. Chemical characterization.....</b>	<b>90</b>
<b>4.4. Morphological characterization.....</b>	<b>91</b>
<b>4.5. Thermal characterization.....</b>	<b>92</b>
4.5.1. Thermogravimetric analysis (TGA).....	92
4.5.2. Differential scanning calorimetry (DSC) .....	93
<b>4.6. Electrochemical characterization.....</b>	<b>95</b>
4.6.1. Ionic conductivity.....	95
4.6.2. Li-ion transference number .....	97

4.6.3. Diffusion coefficient.....	98
4.6.4. Electrochemical stability toward oxidation.....	99
4.6.5. Compatibility with Li <sup>o</sup> electrode.....	100
4.6.6. Cycling of Li <sup>o</sup>     LiFePO <sub>4</sub> cell performance.....	104
4.6.6.1. LiTFSI-based cells.....	104
4.6.6.2. LiFSI-based cells.....	107
<b>4.7. Conclusions.....</b>	<b>111</b>
<b>References.....</b>	<b>112</b>

## Chapter 5:

### SELF-STANDING HIGHLY CONDUCTIVE BLOCK COPOLYMER ELECTROLYTES FOR LITHIUM METAL BATTERIES

<b>5.1. Introduction.....</b>	<b>119</b>
<b>5.2. Synthesis of polymer matrices.....</b>	<b>121</b>
<b>5.3. Selection of the best block copolymer matrix.....</b>	<b>123</b>
5.3.1. Chemical characterization of polymer matrices.....	124
5.3.1.1. Hydrogen-1 nuclear magnetic resonance ( <sup>1</sup> H NMR).....	124
5.3.1.2. Attenuated total reflectance-Fourier-transform infrared spectroscopy (ATR-FTIR).....	125
5.3.2. Mechanical properties.....	126
5.3.3. Thermal characterization.....	127
5.3.4. Ionic conductivity.....	128
<b>5.4. Characterization of BCP70 polymer matrix and electrolytes.....</b>	<b>129</b>
5.4.1. Chemical characterization.....	129
5.4.2. Thermal characterization.....	130
5.4.2.1. Thermogravimetric analysis (TGA).....	130
5.4.2.2. Differential scanning calorimetry (DSC).....	131
5.4.3. Electrochemical characterization.....	134
5.4.3.1. Ionic conductivity.....	134
5.4.3.2. Li-ion transference number.....	136
5.4.3.3. Electrochemical stability toward oxidation.....	138
5.4.3.4. Compatibility with Li <sup>o</sup> electrode.....	139
5.4.3.5. Cycling of Li <sup>o</sup>     LiFePO <sub>4</sub> cell performance.....	140
<b>5.5. Conclusions.....</b>	<b>141</b>
<b>References.....</b>	<b>143</b>

---

**Chapter 6:****FLOWABLE POLYMER ELECTROLYTES FOR LITHIUM METAL BATTERIES**

<b>6.1. Introduction</b>	<b>151</b>
<b>6.2. Synthesis of Jeffamine-based polymer matrix</b>	<b>152</b>
<b>6.3. Chemical characterization</b>	<b>154</b>
6.3.1. Hydrogen-1 nuclear magnetic resonance ( $^1\text{H}$ NMR)	154
6.3.2. Attenuated total reflectance-Fourier-transform infrared spectroscopy (ATR-FTIR)	155
<b>6.4. Morphological characterization: Scanning electron microscopy SEM</b>	<b>156</b>
<b>6.5. Mechanical properties</b>	<b>156</b>
<b>6.6. Thermal characterization</b>	<b>159</b>
6.6.1. Thermogravimetric analysis (TGA)	159
6.6.2. Differential scanning calorimetry (DSC)	160
<b>6.7. Electrochemical characterization of FPEs</b>	<b>162</b>
6.7.1. Ionic conductivity	162
6.7.2. Li-ion transference number	163
6.7.3. Electrochemical stability toward oxidation	164
6.7.4. Compatibility with $\text{Li}^\circ$ electrode	165
<b>6.8. Application of FPE as buffer layer</b>	<b>167</b>
6.8.1. Formation of buffer layer	168
6.8.2. Electrochemical stability of electrolyte/ $\text{Li}^\circ$ electrode	168
6.8.3. Cycling of $\text{Li}^\circ$    $\text{LiFePO}_4$ cell performance	170
<b>6.9. Conclusions</b>	<b>172</b>
<b>References</b>	<b>174</b>

---

**Chapter 7:****NANOFIBER-REINFORCED POLYMER ELECTROLYTES TOWARDS ROOM TEMPERATURE SOLID-STATE LITHIUM BATTERIES**

<b>7.1. Introduction</b>	<b>181</b>
<b>7.2. Preparation of NRPEs</b>	<b>183</b>
<b>7.3. Chemical characterization of NRPEs</b>	<b>185</b>
<b>7.4. Morphological characterization</b>	<b>186</b>
<b>7.5. Mechanical characterization</b>	<b>188</b>
<b>7.6. Thermal characterization</b>	<b>189</b>

7.6.1. Thermogravimetric analysis (TGA),.....	189
7.6.2. Differential scanning calorimetry (DSC),.....	190
<b>7.7. Electrochemical characterization</b> ,.....	<b>192</b>
7.7.1. Ionic conductivity,.....	192
7.7.2. Li-ion transference number,.....	195
7.7.3. Electrochemical stability toward oxidation,.....	196
7.7.4. Compatibility with Li <sup>o</sup> electrode,.....	196
7.7.5. Cycling of Li <sup>o</sup>    LiFePO <sub>4</sub> cell performance,.....	198
7.7.5.1. Solvent-casting method in LiFePO <sub>4</sub> -based cathodes ,.....	198
7.7.5.2. Cycling of Li <sup>o</sup>    LiFePO <sub>4</sub> cell performance at RT,.....	201
7.7.5.3. Cycling of Li <sup>o</sup>    LiFePO <sub>4</sub> cell performance at different temperatures,.....	201
<b>7.8. Conclusions</b> ,.....	<b>203</b>
<b>References</b> ,.....	<b>204</b>

## Chapter 8:

### CONCLUSIONS

<b>8.1. Conclusions</b> ,.....	<b>211</b>
--------------------------------	------------

### APPENDIX:

<b>A.1. List of abbreviations and symbols</b> ,.....	<b>219</b>
<b>A.2. SEM images of the cathodes</b> ,.....	<b>223</b>
<b>A.3. Supplementary information Chapter 3</b> ,.....	<b>224</b>
<b>A.4. Supplementary information Chapter 4</b> ,.....	<b>225</b>
<b>A.5. Supplementary information Chapter 5</b> ,.....	<b>228</b>
<b>A.6. Supplementary information Chapter 6</b> ,.....	<b>229</b>
<b>A.7. Supplementary information Chapter 7</b> ,.....	<b>235</b>
<b>References</b> ,.....	<b>241</b>

### LIST OF CONTRIBUTIONS

<b>Publications</b> ,.....	<b>243</b>
<b>Works submitted to national or international conferences</b> ,.....	<b>245</b>
<b>Internationally recognized awards</b> ,.....	<b>247</b>





# Chapter 1

---

## Introduction



The first part of the document discusses the importance of maintaining accurate records of all transactions. This includes not only sales and purchases but also expenses and income. Proper record-keeping is essential for determining the correct amount of tax owed and for identifying potential deductions.

Next, the document outlines the various methods for calculating taxable income. This involves starting with gross income and then subtracting allowable deductions and exemptions. The resulting amount is then subject to the appropriate tax rates based on the taxpayer's filing status and the amount of income.

The document also addresses the issue of tax credits, which can significantly reduce the amount of tax owed. These credits are available for a variety of expenses, including child care, education, and energy-efficient home improvements. It is important to understand the eligibility requirements for each credit and to ensure that all necessary documentation is provided to the tax authority.

Finally, the document provides information on how to file tax returns and the consequences of non-compliance. Taxpayers are required to file returns by a specific deadline, and failure to do so can result in penalties and interest. However, there are options for requesting extensions and for resolving any outstanding tax obligations.

## Chapter 1:

### INTRODUCTION

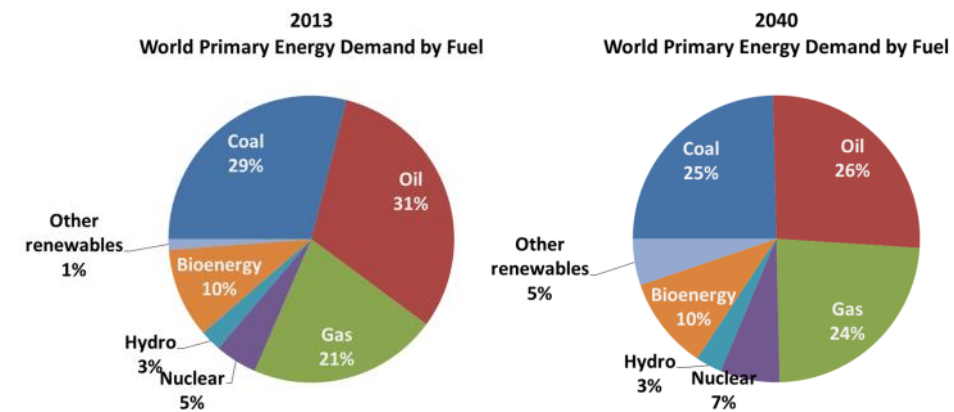
1.1.	Global energy scenario.....	5
1.2.	Electrochemical energy storage.....	6
1.2.1.	Battery classification.....	6
1.2.2.	Rechargeable lithium batteries.....	7
1.2.3.	The role of polymers in batteries.....	9
1.3.	Fundamentals of polymer electrolytes.....	11
1.3.1.	Why polymer electrolytes.....	11
1.3.2.	Ionic conduction.....	13
1.3.3.	Electrode/electrolyte interfacial chemistry and compatibility.....	16
1.4.	Type of polymer electrolytes.....	17
1.4.1.	Gel polymer electrolytes (GPEs).....	17
1.4.2.	Solid polymer electrolytes (SPEs).....	18
1.5.	Towards room temperature solid-state batteries.....	26
1.5.1.	Basic requirements.....	26
1.5.2.	State-of-the-art.....	26
1.6.	General objectives of the present work.....	28
	References.....	30



### 1.1. Global energy scenario

As a consequence of the increasing world population and raise in the average energy use per person due to the living standards derived from the continuous economic and social development, an increase of 35% in the world energy consumption is expected for the next 20 years, rising from  $1.7 \times 10^{13}$  KWh in 2018 to  $2.4 \times 10^{13}$  KWh in 2040 to cover the requirements [1, 2].

The actual energetic consumption and economic welfare is strongly dependent on the combustion of non-renewable fossil fuels including oil, natural gas and coal (**Figure 1.1**). However, the dependence on fossil fuels presents several environmental risks due to the large amount of pollutants produced during the combustion such as sulphur oxides ( $\text{SO}_x$ ), nitrogen oxides ( $\text{NO}_x$ ) and carbon dioxide ( $\text{CO}_2$ ). The raising level of these volatile compounds into the atmosphere has been identified as one of the major causes of global warming through greenhouse effect and pollution especially burdensome in urban spaces as resulting from car combustion engines [3].



**Figure 1.1.** World energy consumption by fuel type in 2013 according to the International Energy Agency (IEA) world energy outlook 2015 and the expected for 2040 [1].

Due to the awareness of the above-mentioned negative effects, a great investment in more sustainable energy sources has been carried out by worldwide governments resulting in a growth of the renewable energy production [4]. Renewable energy harvesting technologies have considerably evolved in the recent years; however, the intermittency of the main sources of alternative energy

is still a shortcoming. As an example, the solar and wind power generation strongly depends on the weather conditions and do not fulfil the electricity demand [5, 6]. Therefore, electrochemical energy storage (EES) systems will play a pivotal role in order to mitigate the above mentioned drawbacks.

## **1.2. Electrochemical energy storage**

Electrochemical energy storage systems are able to store the electric energy when required (off peaks) and release it at peak times when necessary. Several features such as safety, flexibility, rapid charging, high energy density and excellent cycle life are the basic requirements for energy storage devices. There is a full spectrum of energy-storage applications with varying storage time and charging/discharging rates, creating market opportunities for advanced batteries, fuel cells, supercapacitors, flywheels and other technologies.

One of the most widely used EES technologies in industry and daily life is the rechargeable batteries. Their simple design, relatively straightforward operational principle and portability are some of the essential properties that make them popular among energy storage systems. However, further modifications are needed in present technology in order to overcome drawbacks such as relatively low cycling times and high maintenance costs.

### **1.2.1. Battery classification**

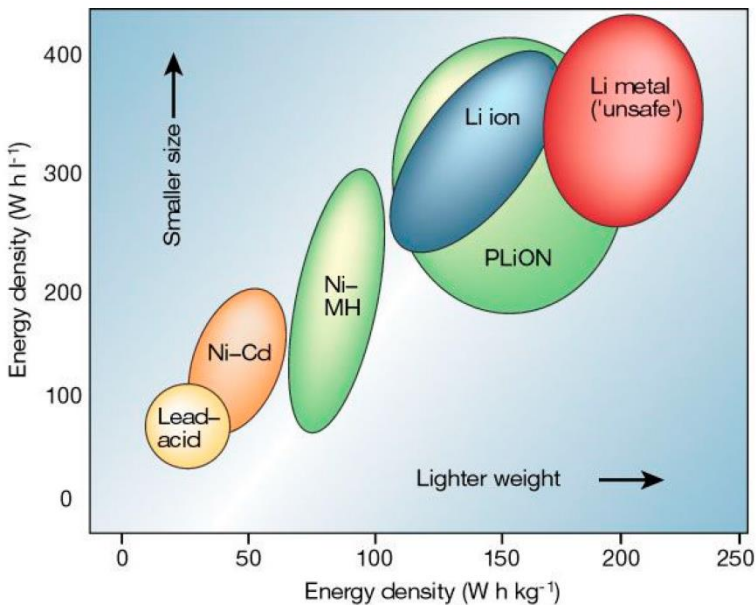
Batteries can be classified into two major categories; primary batteries and secondary batteries.

Primary batteries are disposable devices that cannot be recharged and, as a consequence, they cannot be used for storing the energy generated in any power source. They are supplied fully charged and disposed once discharged [7]. Among this type of batteries zinc-air, zinc-carbon, alkaline, mercury and lithium metal can be found.

Secondary batteries are rechargeable devices that can be recharged many times when they have been discharged. Rechargeable batteries are devices able to reversibly convert the chemical energy into electric energy by electrochemical oxidation/reduction reactions. Some of the technologies that can be found among this type of batteries are: lead acid (Pb-acid), nickel-cadmium (Ni-Cd), nickel-metal

hydride (Ni-MH), metal air, (M-air), redox flow, sodium-sulphur (Na-S), lithium sulphur (Li-S), lithium-ion (LIBs) and now sodium-ion batteries (NIBs) [8-10].

Among the rechargeable batteries, lithium-ion batteries (LIBs) have been emerging as promising candidates due to fast charge/discharge rates, long cycle life and, most importantly, their superior specific energy density compared to other energy storage technologies, as it can be observed in **Figure 1.2** [8, 11-15]. These features make them suitable for mobile electronics where they gradually replace the nickel-type batteries since their commercialization, representing 60% of the total energy storage for portable applications. In the last years they have also been implemented in electric vehicle market [16, 17].



**Figure 1.2.** Comparison of the different rechargeable battery technologies in terms of gravimetric and volumetric energy density. Reproduced with permission from Ref. [18].

### 1.2.2. Rechargeable lithium batteries

The first commercial rechargeable lithium batteries were launched in the late 1970s to early 1980s, one manufactured by the Exxon Company in the USA with a titanium disulphide ( $\text{TiS}_2$ ) cathode and one by at that time Moli Energy in Canada with a molybdenum disulphide ( $\text{MoS}_2$ ) cathode, both using liquid organic

electrolytes. However, their commercialization was suddenly interrupted due to the safety hazards derived from the use of metallic Li as anode [19].

Since then, tremendous effort has been dedicated to the development of secondary “rocking-chair” batteries, which became the so-called-Li-ion batteries [10]. LIBs were first commercialized by Sony Corporation in 1991 and owe their success to proper electrode materials, identified with graphite ( $\text{Li}_x\text{C}_6$ ) as the “lithium sink” anode and in lithium cobalt oxide ( $\text{LiCoO}_2$ ) as the “lithium source” cathode. These characteristics were provided by  $\text{LiCoO}_2$ , a material disclosed by Goodenough in 1980 [20]. Although most of the commercial production of lithium rocking chair batteries still relies on  $\text{LiCoO}_2$  as cathode, an intensive research of new materials for LIBs has been carried out with success.

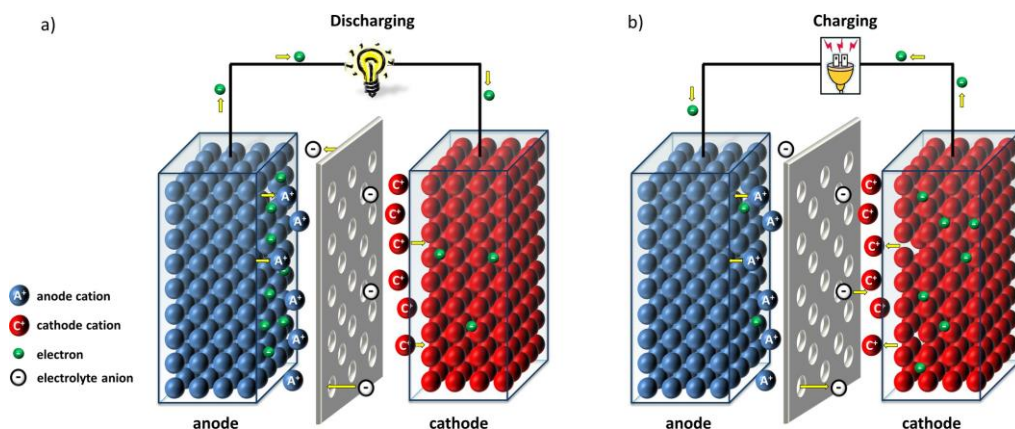
A battery consists of more than one basic electrochemical unit, named as cell, connected in series. However, although the appropriate term for the basic electrochemical unit is “cell”, the term “battery” is often used for simplicity and refers to a reversible electrochemical cell [7].

As it has been mentioned before, rechargeable batteries are devices able to reversibly convert the chemical energy into electric energy by electrochemical oxidation/reduction reactions. The energy density of the batteries depends on the specific capacity of the negative and positive electrodes and the average voltage between them. During the discharge process, the negative electrode is oxidized while the positive electrode is reduced. On the other hand, during the charge process the opposite redox reactions take place. In the field of LIBs, positive and negative electrodes are also known as cathode and anode, respectively. Although this terminology is only correct during the discharge process, for the sake of simplicity, these terms will be used to refer to the positive and negative electrodes [7, 21].

**Figure 1.3** illustrates a representation of the discharge and charge processes of a rechargeable metal-organic battery. The typical cell configuration consists of two electrodes separated by a Li-ion conducting electrolyte which can behave as a simple medium for ion flow between the cathode and the anode or as active participant in the electrochemical reaction [7]. An electrolyte is a chemical compound that dissociates into ions and hence is capable of transporting electric charge. During the discharge process the anode is oxidized and, as a consequence,



the electrons migrate from the anode to the cathode, which is reduced, through the external circuit. At the same time, electroactive cations from the electrolyte migrate to the cathode and anions to the anode in order to ensure the charge balance. During the charge process the opposite behaviour is observed. It has to be mentioned that while discharge is a spontaneous process, a current flow in the opposite direction should be applied during the charge process [22, 23].



**Figure 1.3.** Schematic illustration of **a)** discharge and **b)** charge processes of a metal secondary battery. Reproduced with permission from Ref. [21].

### 1.2.3. The role of polymers in batteries

Polymer materials play a pivotal role in batteries due to their use as porous separators between electrodes, as binder in composite electrode materials and/or as electrolyte in particular cell configuration.

Although the binder is an electrochemically inactive component in the cell, it plays an important role in the performance of Li-ion cells [23]. The cathode processing in Li-ion cells involves the mixing of insulating active materials with conductive additives, usually nanostructured carbon materials that could ensure the good electronic conductivity, combined by a polymer binder [24]. The binder needs also to have a strong adhesion with the current collector which is in charge of the electrons transportation between the electrode and the external circuit [25]. The polymers used as binder in electrodes need to fulfil some requirements such as; 1) chemical and electrochemical stability, 2) high thermal stability, 3) low

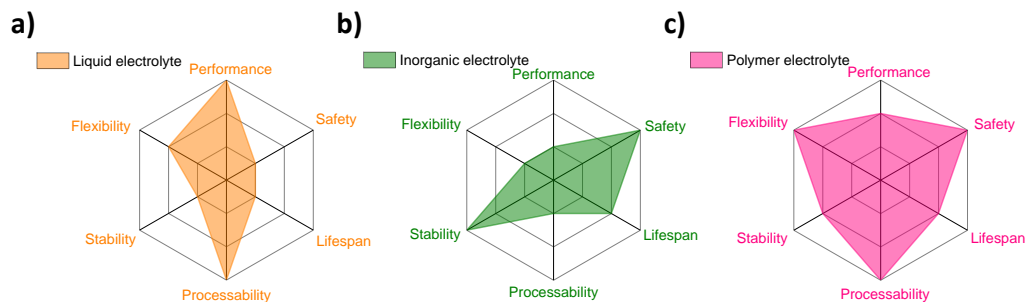
swelling in the electrolyte, and 4) good mechanical properties and ease in processing [23].

In order to improve the capacity of the cell a major research and development effort has been devoted to reduce the concentration of binders in cathode materials. Poly(vinylidene fluoride) (PVDF) has been one of the most commonly used polymer as binder material because of its electrochemical stability and binding capability. However, the requirement of toxic solvents such as *N*-methyl-2-pyrrolidone (NMP) to dissolve the PVDF lead to seek for more environmentally friendly substitutes, like water-soluble carboxy-methyl-cellulose (CMC).

Polymers are also used as separators to prevent the direct contact between electrodes, hence avoiding internal short-circuits, while allowing the migration of electrolyte ions. Conventional separators for LIBs are based on microporous polymers (*e.g.*, Celgard®) able to contain sufficient amount of liquid electrolyte in order to assure lithium-ion conductivity between the electrodes [26, 27]. Nevertheless, the use of flammable liquid electrolytes rises strong safety issues such as leakage and ignition of the gas produced [28].

Solid state batteries (SSBs) have emerged as one of the most promising candidates to replace unstable liquid electrolytes due to their lower flammability, thermal stability and low toxicity [29]. Moreover, the mechanical strength of the so-called dry electrolytes is of great importance to allow the simplification of the cell assembly.

Among dry electrolytes, polymer electrolyte (PE)-based SSBs have better processability and flexibility than inorganic electrolyte-based ones as it can be observed in **Figure 1.4**. Moreover, they allow to Li metal instead of graphite as anode and they can be used as binder in the positive electrode composite. However, the room temperature (RT) operation of the PE-based SSBs remains as one of the most critical issues [30-35].



**Figure 1.4.** Radar chart of different features for **a)** liquid, **b)** inorganic and **c)** polymer electrolytes.

### 1.3. Fundamentals of polymer electrolytes

The ionic conductivity of poly(ethylene oxide) (PEO) complexes with various sodium and potassium salts was discovered in the 1970s by Wright *et al.* [36] at the same time of the discovery of the electronic conductivity of doped conjugated polymers. Polymer lithium salt complexes became promising candidates as ionic conductor materials in energy storage devices. However, it was not until the 1980s that the importance of its technological application was recognized [37]. In the past four decades, the development of new PEs has received attention from many researchers due to their potential applications in electro-chemical/electrical power generation, storage and conversion systems [38].

PEs are based on a low dissociation energy salt dissolved in a high molecular weight polymer matrix, sometimes including low-molecular-weight plasticizers and/or solid additives [29, 39]. Due to their good mechanical properties, PEs can act as separator between electrodes. For this purpose they must present sufficient mechanical integrity to withstand the pressure and stress caused by the dimensional changes of the electrodes during the charge and discharge processes [23, 26].

#### 1.3.1. Why polymer electrolytes

The use of lithium ion-conducting PEs could eliminate some of the safety problems encountered when liquid electrolytes are used due to their reduced flammability and relatively high mechanical strength and good adhesion properties

that could prevent the dendrite formation [40]. However, they are hampered by their conductivities that are typically much lower than the ones obtained with their liquid counterparts at RT [35].

Dendrites are thin, finger like projections of the metal that start to build from the lithium electrode and have the potential to extend all the way across the electrolyte material and reach the other electrode. If these dendrites reach the other electrode, they cause short-circuit and permanent damage to the battery and the device equipping it.

The dendrite formation in ceramic solid electrolyte material follows the next process; the lithium from one of the electrodes begins to deposit through an electrochemical reaction into any defect such as pits, cracks or scratches that exist on the electrode/electrolyte surface leading to the initiation of dendrite formation by providing a toehold for the metallic deposits. This deposition continues to build up and extend towards the other electrode over time causing catastrophic consequences [41].

PEs overcome many drawbacks faced by liquid electrolytes in terms of efficiency and capacity retention capability [42]. Moreover, they present many other advantages such as high energy density, improved compatibility with metallic Li, solvent-free condition, structural stability, low volatility, wide electrochemical stability window and ease of formation [40].

As PEs operate both as separator and electrolyte in a solid-state configuration, they must possess many essential properties as listed below [32, 43, 44]:

a) Good mechanical strength. This feature is of great importance in the large-scale manufacture of LIBs. PEs need to be able to elastically relax when stress arises in the process of manufacture, cell assembly and usage.

b) High chemical and thermal stability. PEs should be inert to lithium anode and cathode and other battery components such as current collectors, additives and cell packaging materials. Moreover, the thermal stability ensures the safe use of a battery in the case of thermal or electrical misuse.

c) Wide electrochemical stability window. The primary requirement for an electrolyte is to be inert to both electrodes, which means that the oxidation potential must be higher than the operating potential of the cathode and the reduction potential must be lower than that of the Li in the anode [45]. Consequently, the electrochemical window for PEs should reach from 0 to 4–5 V vs. Li/Li<sup>+</sup> in order to be compatible with both electrodes.

d) High Li<sup>+</sup> transference number ( $T_{\text{Li}^+}$ ). This parameter represents the contribution of the charged species present in the electrolyte to the overall charge transport. Decreasing the mobility of anions can greatly increase  $T_{\text{Li}^+}$ . As a consequence, the concentration polarization of electrolytes during charge/discharge processes can be reduced, hence obtaining higher power density and reducing the nucleation of dendrites [46].

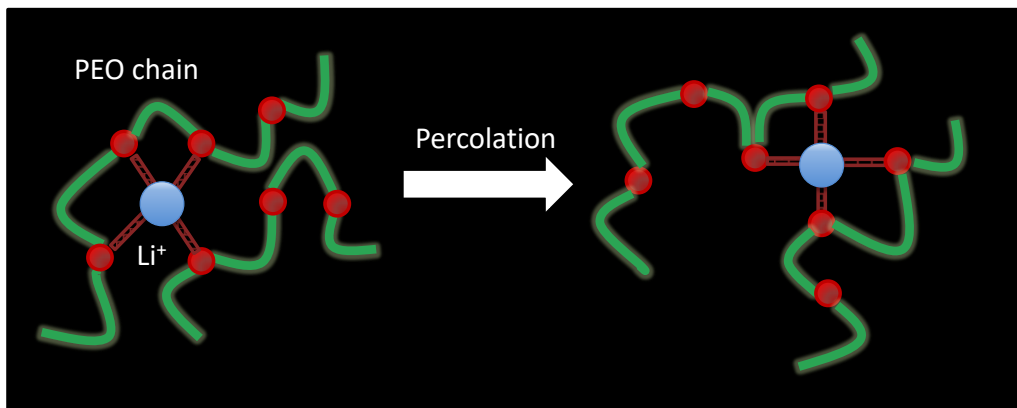
e) High ionic conductivity. Ionic conductivity is the determining factor of the internal impedance and electrochemical performance at different charge/discharge rates. Good ionic conduction and electronic insulation are required so that ion transport can be facilitated and self-discharge minimized. PEs should present conductivities that approach  $10^{-4}$  S cm<sup>-1</sup> at RT to achieve rapid charge/discharge of the cell.

### 1.3.2. Ionic conduction

Ion transport in PEs constitutes a complex field where theoretical modelling has met considerable challenges due to the nature of these materials [47]. Polymers possess complex phase diagrams where crystallinity is temperature dependent [48–50]. As a consequence, an important ion pairing in the conducting amorphous phase is temperature dependent, and the complexation of ions to the polymer matrix depends on the anion and cation type and the functionalities provided by the polymer. In addition, features like the polymer structure and molecular weight have a great impact on the polymer dynamics [51].

The detailed microscopic mechanism of ionic conduction can be explained by the segmental motion of the polymer chains [50, 52, 53]. The glass transition temperature ( $T_g$ ) is the temperature that marks the boundary between the glassy, rigid state and the soft, flexible state of a polymer. Above the  $T_g$ , local segmental motion of the polymer chains takes place facilitating the motion of ion through the

polymer, likewise the transport of voids through amorphous polymers above  $T_g$ . Lithium ions (Lewis-acidic species) are coordinated by polar atoms of the polymer chain (*e.g.*  $-O-$  in poly(ethylene oxide) or  $-CN$  in poly(acrylonitrile)). The local segmental motion of the polymer chains originating from conformational change of polymer segments results in the appearance of free volume. When an electric field is applied, lithium ions migrate in the direction of external electric field from one coordination site to new sites along the polymeric chains or hop from one chain to another through these free volumes. One of the most sophisticated models describing this process is known as the dynamic bond percolation model [54].



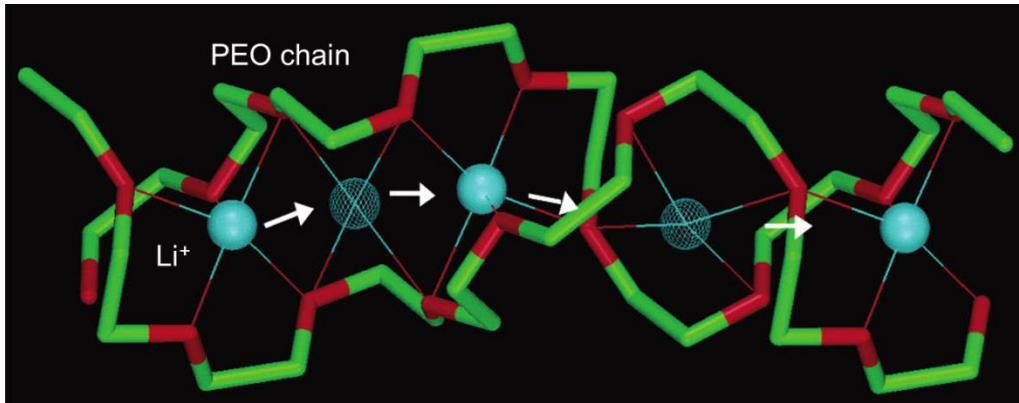
**Figure 1.5.** Schematic diffusion pathway of the  $\text{Li}^+$  cations based on the dynamic percolation model proposed by Ratner *et al.* [54].

Macroscopic studies of ionic conduction upon variations in temperature may provide valuable information on the ion transfer mechanism. Two main conducting mechanisms have been proposed for the temperature dependence ionic conductivity: the Arrhenius behaviour and the Vogel-Tamman-Fulcher (VTF) behaviour [29, 43, 54]. The Arrhenius equation can be expressed by **Equation 1.1**:

$$\sigma = \sigma_0 \exp\left(\frac{-E_a}{kT}\right)$$

**Equation 1.1** wherein,  $\sigma_0$  is the pre-exponential factor related to the number of charge carriers,  $E_a$  is the activation energy and  $k$  is the Boltzmann constant.

Thermal activated Arrhenius type law has been widely used for the expression of temperature dependent ionic conductivity in inorganic electrolytes with ordered rigid structures as well as in crystalline polymer electrolytes [48, 55]. Materials that exhibit linear Arrhenius variations present a microscopic mechanism in which the ion transport occurs by a simple hopping of ionic species from currently occupied sites to vacant sites, as it can be observed in **Figure 1.6** [54].



**Figure 1.6.** Schematic diffusion pathway of the  $\text{Li}^+$  cations based on the structures of lithium hexafluoroarsenate ( $\text{LiAsF}_6$ )/PEO. Reproduced with permission from [48].

In the case of polymer electrolytes, the ionic conductivity vs. temperature differs from the typical Arrhenius behaviour. In this case, the VTF equation is adopted. VTF behaviour can be expressed by **Equation 1.2**.

$$\sigma = \sigma_0 T^{-\frac{1}{2}} \exp\left(-\frac{B}{T - T_0}\right)$$

**Equation 1.2** wherein,  $\sigma_0$  is the pre-exponential factor related to the number of charge carriers,  $B$  is the pseudo-activation energy for the conductivity, and  $T_0$  is the ideal glass transition temperature.

The VTF equation was devised in order to describe the diffusion process in disordered materials. For PEs,  $\sigma$ - $T$  dependences in Arrhenius coordinates deviate from linearity, which is indicative of a mechanism of conductivity that involves migration by redistribution of free volume coupled with segmental motion of polymer chains, as depicted in **Figure 1.5** [43]. This behaviour is usually observed

above  $T_g$ , in gel polymer electrolytes, ionic liquids and completely amorphous PEs [29].

### 1.3.3. Electrode/electrolyte interfacial chemistry and compatibility

One of the requirements of PEs is that they have to be chemically and electrochemically stable versus electrodes in broad potential range [56]. Li batteries generally operate between 2.5 and 4 V vs. Li/Li<sup>+</sup>. For this reason, the electrochemical stability of the PEs is desired within this potential range [57]. The cycling of PEs in the electrochemical window beyond their stability leads to the degradation of the electrolyte and/or active material in the cathode resulting in a passive film. This process, also called “solid electrolyte interphase” (SEI) formation, will have a profound effect in the performance of all-solid-state lithium metal batteries (ASSLMBs) [58-61]. This film will keep fresh lithium away from the electrolyte, stopping further reactions, and stabilizing the interface.

PEs present a solid-electrolyte interphase in which the intimate contact between the electrolyte and the electrode are extremely important to improve the electrochemical performance of the battery because the contacted areas are the sites where the charge-transfer reactions will take place. Moreover, fast ion charge and mechanical stability are required.

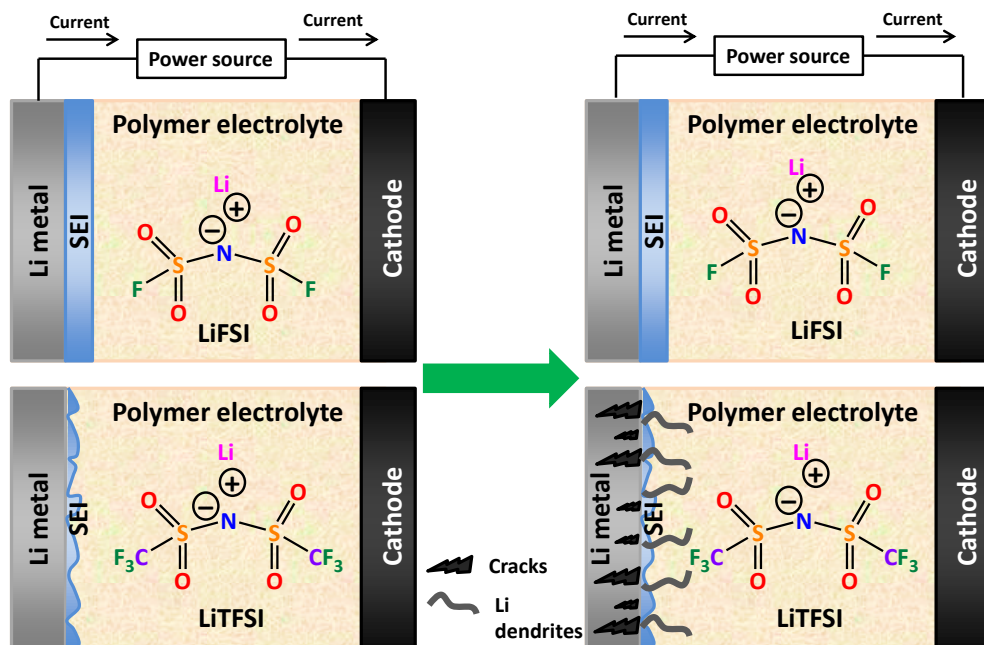
In comparison with liquid electrolytes, the SEI for PEs can be considered more stable due to the limited number of redox active sites and the absence of convection. Moreover, their SEI layer is dynamic enough and, as a consequence, enables a good cycle performance of the battery without losing additional capacity ascribed to the reformation of the passivating layer [62].

Apart from the electrochemical side reactions, several factors affect the interfacial stability of the SEI such as: 1) physical delamination due to volume expansion/contraction during charge/discharge processes; 2) non-uniform current density distribution due to the changeable morphology of Li metal during the cycling and 3) interfacial reactions on composite cathodes.

The nature of the salt used in the electrolyte preparation is also proven to affect the stability of the SEI [63, 64]. In **Figure 1.7** the schematic illustrations for the SEI formation using lithium bis(trifluoromethanesulfonyl)imide (LiTFSI) and lithium bis(fluorosulfonyl)imide (LiFSI) are compared. As it can be observed, a



stable and uniform SEI is formed on the Li|PE interphase in the case of LiFSI. This fact can be ascribed to the inorganic F–SO<sub>2</sub> group in LiFSI instead of the organic CF<sub>3</sub>–SO<sub>2</sub>– group in LiTFSI. This fact leads to the formation of a robust SEI film in the surface of the Li metal electrode avoiding the soft dendrite formation observed in the case of LiTFSI [63, 65].



**Figure 1.7.** Schematic illustration of SEI evolution after charge/discharge processes for a) LiFSI-based electrolytes and b) LiTFSI-based electrolytes.

## 1.4 Type of polymer electrolytes

Among the PEs, two groups have gained special attention in the last decades as safer replacement for liquid electrolytes in LIBs: 1) solid polymer electrolytes (SPEs) [33, 45, 66], representing a lithium salt associated with an ion-conducting polymer matrix and 2) gel polymer electrolytes (GPEs) [67-69], based on a polymer matrix swollen by a liquid electrolyte [34].

### 1.4.1. Gel polymer electrolytes (GPEs)

GPEs are based on an inert polymer matrix in which a salt and a liquid plasticizer and/or solvent are dissolved. This concept was first introduced in 1970s

by Feuillade *et al.*, who studied the process of plasticizing a polymer matrix with an aprotic solution containing an alkali metal salt [70].

This kind of electrolytes combine the diffusive properties of liquids (high conductivity) while the polymer matrix holds the electrolyte to provide mechanical strength [71]. In this case, due to the introduction of a liquid plasticizer or solvent constituent, the transport of lithium ions occurs in the swollen gelled phase, thus is not dominated by the segmental motion of polymer chains.

GPEs present several advantages that make them very attractive to substitute their liquid counterparts such as: a high ionic conductivity, wide electrochemical stability window, and chemical, mechanical and electrochemical stabilities. Moreover, the absence of leakage enhance the safety of this kind of batteries compared to the liquid ones, but the volatility and reactivity of the imbibing solvent remains the same [72, 73]. If the plasticizer is an ionic liquid or an oligomer, the volatility can be much reduced.

Several polymer matrices such as PEO [74-76], poly(vinyl chloride) (PVC) [77, 78], poly(acrylonitrile) (PAN) [79, 80], poly(vinylidene fluoride) (PVDF) [81] and poly(vinylidene fluoride-co-hexafluoropropylene) (PVDF-HFP) [82] have been widely used in gel polymer electrolytes. However, GPEs based on a single polymer matrix cannot fulfill all the above mentioned requirements and, as a consequence, modifications such as crosslinking, blending or addition of inorganic particles are needed. Moreover, drawbacks such as poor mechanical properties, toxicity of low molecular weight solvent and the reactivity of the added plasticizer with electrode materials that leads to shorter life span prevent their wide use in practical applications except in niche market, the so-called “polymer lithium batteries” for high power applications [83].

#### **1.4.2. Solid polymer electrolytes (SPEs)**

SPEs are considered as one of the viable solutions to replace their liquid counterparts due to their superior advantages [33]. The high chemical/electrochemical stability against Li anode [9], the absence of the safety hazards caused by the highly volatile and flammable organic solvents utilized in liquid electrolytes [44, 84], the low cost in design and easy processability for a wide variety of fabrication methods make them suitable candidates for

commercial applications. Moreover, SPEs also outperform inorganic solid electrolytes in terms of processability and electrode/electrolyte interface compatibility due to the flexible nature of polymer network [65]. This feasibility of the technological application of SPEs has been well demonstrated by the expansion of Bluecar<sup>®</sup> commercialized by Bolloré, equipped with a  $\text{Li}^+|\text{SPE}|\text{LiFePO}_4$  battery [85].

The development of SPEs has been a pursuit of a compromise between good mechanical properties and high ionic conductivity. Several attempts to improve both properties at the same time have been conducted based on different polymer architectures. However, SPEs with low  $T_g$  and low crystallinity, essential to speed up the ionic transport, can barely form self-standing membranes [86, 87].

SPEs, which comprise a salt dissolved in a polymer matrix, are now also called dry solid polymer electrolytes. The discovery of SPEs dates back to 1973 when Wright *et al.* reported the conductivity in complexes formed by sodium (Na) and potassium (K) salts and PEO [36, 88]. PEO presents electrochemical stability and high ability to dissolve salts due to its flexible ethylene oxide segments and oxygen atoms, which have a strong electron donor character and thus readily solvate  $\text{Li}^+$  cations [45].

In 1979 Armand *et al.* proposed the application of these PEO-based SPEs in electrochemical devices based on all-solid-state Li batteries [89-91]. Since then great efforts have been dedicated to the development of large families of PEs.

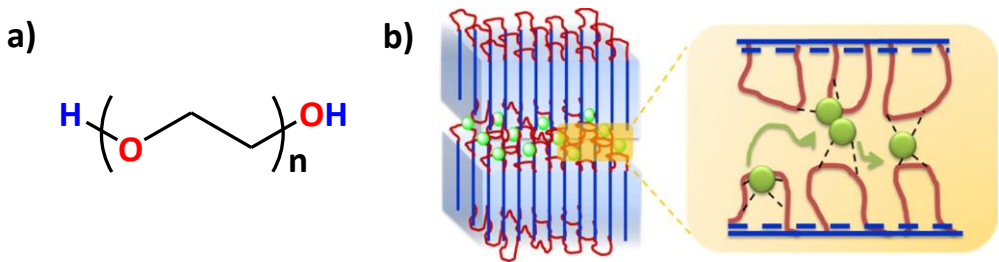
#### **a) Poly(ethylene oxide) (PEO)-based polymer electrolytes**

Among all the investigated polymer hosts for SPEs, PEO has by far received more attention and the subject of extensive research. PEO is a polyether compound with a chemical structure in which  $(-\text{CH}_2\text{CH}_2\text{O}-)_n$  is the repeating unit, as it can be observed in **Figure 1.8** [92].

As it has been mentioned above, PEO can complex with lithium salts to form polymer electrolytes. The repeating units of PEO are properly spaced ether solvating units which have strong solvation abilities. As a consequence, the formation of lithium salt/PEO complex is favoured and a sufficient concentration

of charge carriers is provided [56]. Moreover, it presents a high dielectric constant, optimal  $\text{Li}^+$  dissociation condition and high chain flexibility resulting in a rapid ion transport [91].

However, PEO-based SPEs present several drawbacks. On the one hand, PEO presents low anodic stability ( $\leq 4.0 \text{ V vs. Li}^0/\text{Li}^+$ ) at elevated temperature. Moreover, high molecular weight PEO is a semi-crystalline polymer in which ionic transport occurs mainly in the amorphous phase, leading to a low ionic conductivity at temperatures below the melting point ( $T_m$ , ca.  $65 \text{ }^\circ\text{C}$ ) and resulting in PEO-based ASSLMs operating at elevated temperatures ( $70\text{--}90 \text{ }^\circ\text{C}$ ) [93-95]. Although a few questionable reports indicated that crystalline PEO can offer even greater ion conductivity than amorphous one, prevailing, the crystallization of PEO is considered to be detrimental to ion transport owing to the slowed down polymer chain dynamics upon crystallization, as it can be observed in **Figure 1.8** [96-98].



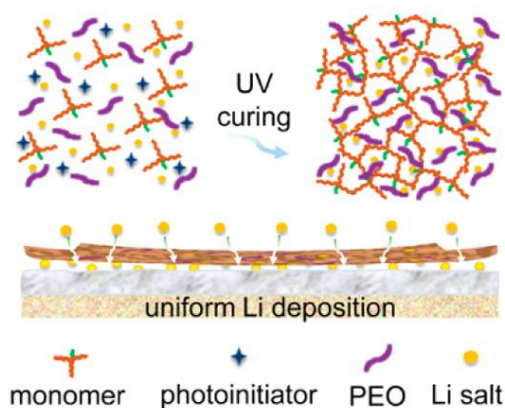
**Figure 1.8.** a) Structure of PEO and b) schematic illustration of PEO crystalline stems (blue) and amorphous loops (red) in which ions are confined and the ionic conductivity occurs.

Reproduced with permission from Ref. [98].

Trying to overcome these drawbacks, numerous efforts have been dedicated to the design and synthesis of non-crystalline and low  $T_g$  polymer matrices with improved mechanical properties and higher stability against Li anode in order to suppress the dendrite formation. Among these molecular level modifications architecture alteration by branching polymer segments [99], crosslinking of polymer network [100], random [101], comb [102] and/or block polymerization [103] can be found in the literature. Other strategies such as the addition of plasticizers [104-106] or nanofillers [107] and polymer blends [108-110] have also been studied by several groups.

### b) Modified PEO-based polymer electrolytes

One strategy to overcome the above mentioned challenges involves the cross-linking of PEO with other polymers [111]. The cross-linked semi-interpenetrated PEs exhibit fully amorphous nature keeping sufficient ionic conductivity at ambient temperature. Thereby, the crosslinking of PEO with branched acrylate was found to create a completely amorphous polymer matrix with lower  $T_g$  than pure PEO [112]. **Figure 1.9** illustrates the preparation of this kind of electrolyte. The high ionic conductivity and lithium transference number at RT allowed for the evaluation of these SPEs in a Li | SPE | LiFePO<sub>4</sub> full cell.

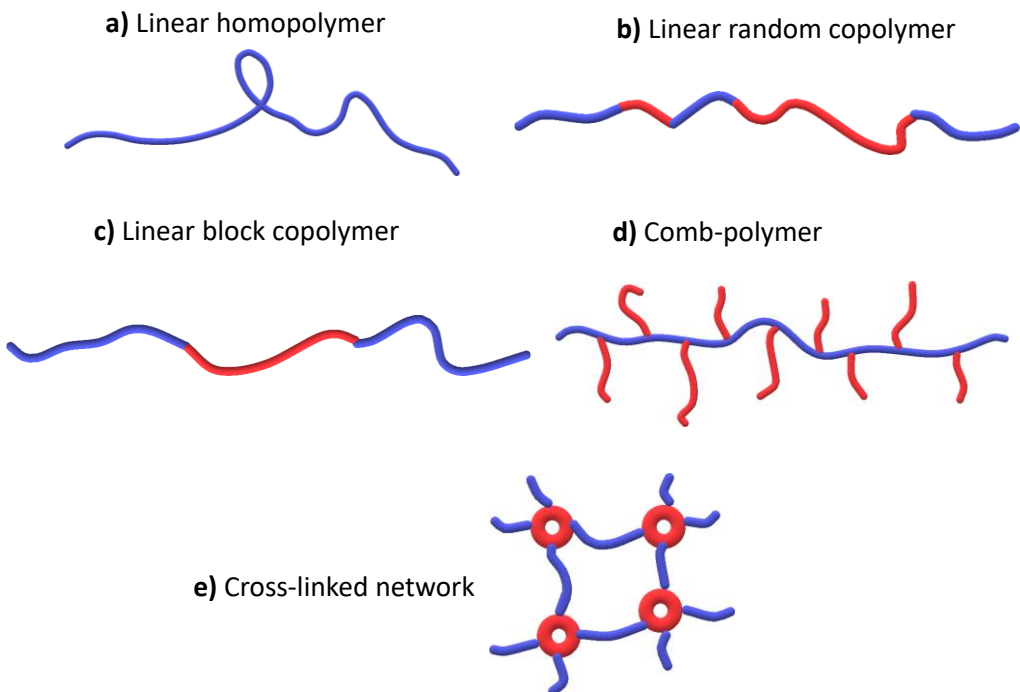


**Figure 1.9.** Schematic illustration of cross-linked PEO and branched acrylate. Reproduced with permission from Ref. [112].

Block copolymers (BCPs) are considered as an interesting class of polymeric materials owing to their ability to self-assemble into ordered supramolecular structures [92]. BCPs are composed of two or more different covalently bound polymers that provide to the matrix with a combination of their own properties. In general, one block is usually an ethylene oxide (EO) based polymer responsible of the ionic conductivity, whereas the other block provides other functionalities such as mechanical stiffness [113, 114].

In 1980s Passiniemi *et al.* studied a new linear copolymer based on PEO and poly(propylene oxide) (PPO). The introduction of PPO resulted in a decrease of the crystallinity, though a depression of the ionic conductivity was observed [115].

Among all the studied BCPs, one of the most representative example is poly(styrene-*b*-ethylene oxide) (PS-PEO). Balsara *et al.* synthesized polymer electrolytes based on PS-PEO and LiTFSI as salt. These polymers showed high modulus, due to the PS block, and high ionic conductivity due to the PEO block [113, 114, 116-119]. The maximum ionic conductivity of this copolymer with high salt content was about twice that of the corresponding PEO-based one [117]. On the other hand, Bouchet *et al.* evaluated the performance of different block copolymers by varying the molecular weight of PEO segment, the composition, as well as the architecture [103]. They evidenced a negative correlation between the thermal and mechanical properties; as the PS block content increases, the  $T_m$  and crystallinity decrease regardless the length of the PEO chain, while the Young's modulus increases. The decreased melting transition compared to PEO allowed the operation of these cells at relatively low temperatures.



**Figure 1.10.** Schematic illustration of polymer architectures; **a)** linear homopolymer, **b)** linear random copolymer, **c)** linear block copolymer, **d)** comb-polymer and **e)** cross-linked network.

Another strategy that is gaining attention in recent years is the development of comb-like polymers. In this kind of materials PEO-based moieties are grafted to a polymeric backbone. In 2017, a comb-like polymer based on a polynorbornene backbone and PEO conductive side chains was synthesized by Ping *et al.* [120]. The introduction of rigid side chains resulted in the suppression of the crystallinity of PEO, giving rise to a completely amorphous polymer matrix. **Figure 1.10** summarizes some of the main polymer architectures that have been described in this section.

Despite the recent progress in the performance of PEO-based batteries, the poor stability of these polymer electrolytes with Li anode urges the research on alternative polymer matrices.

### c) Non PEO-based polymer electrolytes

In later years, poly(acrylonitrile) (PAN) has been widely studied as polymer host due to its high thermal stability and flame retardant behaviour [121]. PEs based on PAN present decent ionic conductivities and the lithium transference number  $T_{Li}^+$  is higher than in PEO-based electrolytes. However, severe passivation of lithium anode occurs when in contact with PAN. Poly(vinylidene fluoride) (PVDF) is also emerging as a host polymer due to the high dielectric constant. Moreover, the presence of strong electron-withdrawing functional groups ( $-C-F$ ) helps for better dissolution of lithium salts [122]. Nevertheless, although they present suitable electrochemical properties, the presence of fluorinated groups makes it unstable against lithium anode. Poly(methyl methacrylate) (PMMA) presents enhanced interface stability than other polymer hosts. However, their poor mechanical flexibility restricts their use as electrolytes in energy storage systems [123]. Despite the above mentioned drawbacks, these three polymer matrices can be applied in order to enhance the mechanical properties of other materials as well as to improve the stability towards electrochemical oxidation [124-126].

Among the variety of polymers to replace PEO, polycarbonates (PCs) have been emerging as promising candidates. This can be ascribed to the fact that carbonates are extensively used in conventional LIBs. PCs can coordinate to Li ions by means of the carbonyl group oxygen although some coordination by the ester oxygens adjacent to the carbonyl group has also been implicated in carbonate solvents [127-129]. Due to the weaker interaction between the carbonyl group and

$\text{Li}^+$ , this kind of PEs present higher  $T_{\text{Li}^+}$  than PEO-based ones. However, their ionic conductivities at RT are much lower than the ones obtained for their PEO counterparts. This effect can be suppressed by the addition of large amount of salt that results in a strong plasticizing effect and therefore in a fast Li-ion conduction ("polymer in salt" configuration) [130]. Moreover, a good cell performance at RT can be obtained for  $\text{Li} \parallel \text{LiFePO}_4$  cells based on PCs as recently proven by Kimura *et al.* [131] and Mindemark *et al.* [132]. However, PCs have a limited stability in contact with lithium [133]

#### **d) Blend polymer electrolytes**

Among the approaches that can be applied to improve the properties and performance of PEs blending is a commonly used one. Polymer blending is a physical mixture of two or more polymers in which the final properties are superior to those of the component polymers.

This technique has been widely used in order to increase the ionic conductivity. Blend-based PEs may show improved ionic conductivities or mechanical strength and better lithium/electrolyte interfacial performance than PEO-based ones. These systems can overcome the drawbacks from other PEs by improving the physical and electrochemical properties. Nicotera *et al.* demonstrated that a PMMA/PVDF blend-based polymer electrolyte can remarkably improve the lithium conduction properties [134]. On the other hand, Howlett *et al.* proved that the blending of ionic plastic crystals with PVDF greatly improved both the mechanical and electrochemical properties of the electrolyte [135, 136].

#### **e) Salts**

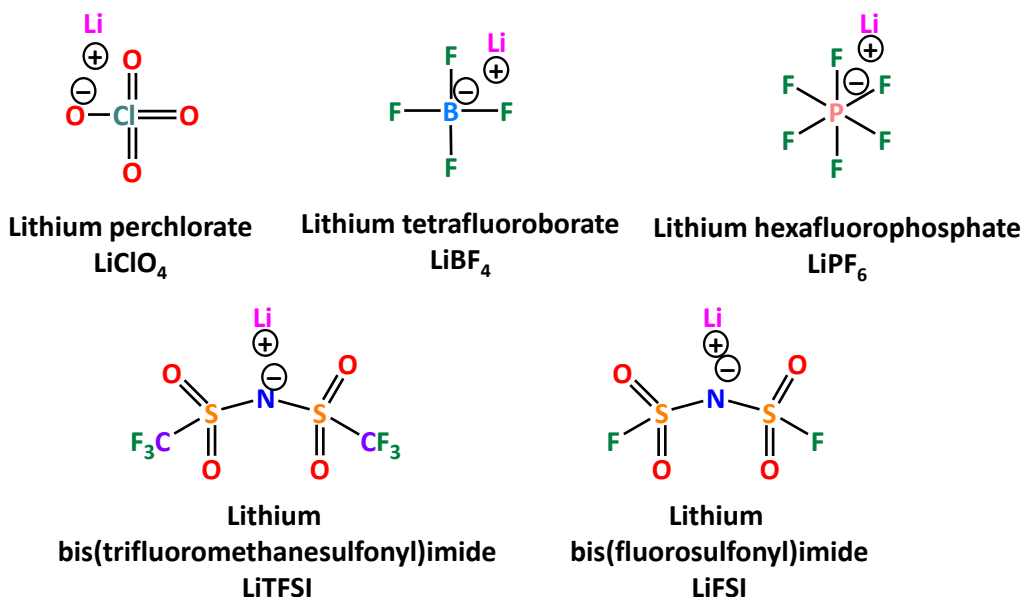
The overall performance of SPEs does not only depend on the polymer host, but also on the election of the Li salt. In general, in order to enhance the amorphicity and ionic conductivity of the polymer matrix, anions with highly delocalized negative charge are selected [137].

The incorporation of different type of salts can drastically improve the transport properties of SPEs [90, 91]. To date numerous lithium salts with weak coordinating character have been studied including perchlorate ( $\text{ClO}_4^-$ ) [97, 138], tetrafluoroborate ( $\text{BF}_4^-$ ) [139], hexafluorophosphate ( $\text{PF}_6^-$ ) [140], and



bis(trifluoromethanesulfonyl) imide ( $[\text{N}(\text{SO}_2\text{CF}_3)_2]^-$ , TFSI $^-$ ) [93, 141, 142]. Among the above mentioned salts, LiTFSI has been the most widely studied as conducting salt owing to the sulfonimide group  $-\text{SO}_2-\text{N}-\text{SO}_2-$ . The high flexibility of this group enhances the ionic conductivity by reducing the crystallinity of the polymer host due to the plasticizing effect. Moreover, the excellent thermal and electrochemical stability of this salt, as well as the highly delocalized charge distribution (5 oxygens and one nitrogen) promoting the dissociation of  $\text{Li}^+$  cations, make this salt suitable for developing SPEs for Li-based batteries [64].

In recent years, lithium bis(fluorosulfonyl)imide ( $\text{Li}[\text{N}(\text{SO}_2\text{F})_2]$ , LiFSI), an analogue of LiTFSI, has been widely studied due to the improved compatibility with various electrodes, such as lithium iron phosphate ( $\text{LiFePO}_4$ , LFP) cathodes and  $\text{Li}^0$  electrode [143, 144]. **Figure 1.11** shows the chemical structure of the most commonly used Li salts.



**Figure 1.11.** Chemical structures of commonly used lithium salts for SPEs.

## 1.5. Towards room temperature solid-state batteries

### 1.5.1. Basic requirements

The main barriers for developing SPEs-based ASSLMBs operational at ambient temperatures are the low ionic conductivity and poor interfacial compatibility with electrode materials, especially vs. Li anode.

As mentioned before, the ionic transportation is coupled with segmental motion of polymer matrices in the amorphous phase. For this reason, tremendous efforts have been dedicated to the design and synthesis of novel amorphous polymer matrices with low  $T_g$  values. The lower crystallinity and  $T_g$ , the higher ionic conductivity can be expected [145-147].

On the other hand, good electrochemical compatibility with electrode materials is required for obtaining good cycling performance of ASSLMBs. This is supported by the fact that due to the lack of good electrochemical compatibility of electrolyte/electrode interface at RT SPEs-based cells exhibit efficient cycling only at elevated temperatures.

Finally, the polymer binders in the cathode composite material need to present high ionic conductivity, thermal and electrochemical stability, mechanical strength and good adhesive properties. When the cell is cycled at RT, the cell resistance increases and, as a consequence, the internal contact of active material within the cathode is decreased. This effect may result in local cell polarization. Moreover, the high polarization can lead to the decomposition of lithium salt and/or polymer matrix and even pulverize active materials in the cathode [148]. For this reason, the role of the polymer binder is crucial for improving the cycle life of ASSLMBs.

### 1.5.2. State-of-the-art

Polycarbonates have been the polymers capturing much attention towards RT operation ASSLMBs recently. In 2015, Brandell *et al.* described a highly conductive polymer electrolyte based on LiTFSI/poly(trimethylene carbonate-co-caprolactone) [P(TMC-co-CL)]. This copolymer presented a high ionic conductivity (*ca.*  $4.1 \times 10^{-5} \text{ S cm}^{-1}$  at 25 °C) and the Li|SPE|LFP based cell could be run at RT at different charge/discharge capacities with good specific capacity and Coulombic

efficiency [132]. One year later, Kimura *et al.* reported a high ionic conductivity (*ca.*  $1.6 \times 10^{-5} \text{ S cm}^{-1}$  at  $30 \text{ }^\circ\text{C}$ ) and good cycling performance of Li|SPE|LFP cells at RT by using highly concentrated poly(ethylene carbonate) (PEC)/LiFSI electrolytes [131].

In 2019, a new type of polymer-polymer solid-state electrolyte design has been proposed by Cui *et al.* [149]. In this work,  $8.6 \text{ }\mu\text{m}$  thick nanoporous polyimide film is filled with PEO/LiTFSI electrolyte and used as safe solid polymer electrolyte. The vertical channels of this innovative membrane enhance the ionic conductivity of the infused polymer electrolyte (*ca.*  $2.3 \times 10^{-4} \text{ S cm}^{-1}$  at  $30 \text{ }^\circ\text{C}$ ). Moreover, the polyimide film is nonflammable and mechanically strong, preventing the batteries from short-circuiting even after more than 1000 h of cycling. The Li|SPE|LFP cells can be run at  $30 \text{ }^\circ\text{C}$  under a C rate of 0.5/0.5C showing good specific capacity (*ca.*  $100 \text{ mAh g}^{-1}$ ) and good Coulombic efficiency.

## 1.6. General objectives of the present work

Nowadays, electrochemical energy storage systems play an important role in order to move away from non-renewable fossil fuels towards more sustainable renewable energy sources. In this context, lithium-ion batteries (LIBs) are suitable candidates to face this challenge due to their high energy density, fast charge/discharge rates and long cycle life. However, they contain toxic metals and the use of conventional liquid electrolytes derives in strong safety issues.

In the past years, solid polymer electrolytes (SPEs) were proposed to replace their liquid counterparts owing to their easy processing, good electrochemical properties and low flammability, which accounts for safer LIBs. However, the development of SPEs has been largely hindered by the trade-off between high ionic conductivity and good mechanical properties, since SPEs with low glass transition temperature ( $T_g$ ), which are crucial for facilitating fast ion transport, can hardly form self-standing membranes.

Poly(ethylene oxide) (PEO) is the most commonly used polymer matrix as it contains ether coordination sites that facilitate lithium salt dissociation. Ionic transport in PEO depends on the chain flexibility and occurs mainly in the amorphous phase, leading to a low ionic conductivity due to the presence of crystalline phase at temperatures below the melting point ( $T_m = 65$  °C). Consequently, PEO-based LIBs need to operate above the  $T_m$ . Under this condition, PEO is extremely soft and weak, and do not guarantee a suitable interfacial layer able to prevent the lithium dendrite growth.

Trying to overcome these drawbacks, tremendous efforts have been devoted to the design of non-crystalline and low  $T_g$  polymer matrices, such as structural alteration by random, comb and/or block-copolymerization.

Within this scope, the main objective of this work is the synthesis of new polymer electrolytes that present low crystallinity and high ionic conductivity in order to decrease the operational temperature of all-solid-state lithium metal batteries (ASSLMBS). This thesis work has been divided in five different parts.

1. A new type of comb-like polymer matrices based on imide ring and Jeffamine® side chains comprising of ethylene oxide (EO) and propylene oxide (PO) units will be synthesized. The influence of the

molecular weight of the side chains and the ratio between EO/PO units will be studied in order to ensure low  $T_g$  and high amorphicity to favour the high mobility of Li ions even at room temperature (RT). Among the synthesized matrices the most suitable candidate will be selected as base material for the next chapters.

2. Previously synthesized polymer matrix with different sulfonimide salts and different EO/Li ratios will be compared. The aim is to obtain fully amorphous and highly conductive SPEs with improved interfacial compatibility with electrode in order to decrease the operational temperature of polymer-based ASSLMs.
3. A new type of tailor-made block copolymer where the structural block is made of amine terminated polystyrene (PS), while the conducting block is made of comb polymer containing polyether side moieties (Jeffamine®) will be synthesized. The purpose is to improve the mechanical properties of the above mentioned new polymer backbones without high detriment of the ionic conductivity.
4. A new flowable polymer electrolyte (FPE) obtained by controlling the chain entanglement of above mentioned base material will be prepared in order to study the influence of the physical properties of the electrolytes on the electrochemical performance of the cells. Moreover, the application of this innovative material as buffer layer will be analysed in order to improve the performance of PEO-based Li<sup>+</sup> || LiFePO<sub>4</sub> cells.
5. Finally, a nanofiber-reinforced polymer electrolyte comprising of poly(vinylidene fluoride) (PVDF) fibers along with FPE will be prepared with the aim of obtaining a SPE that presents a good compromise between high ionic conductivity and good mechanical properties even at RT in order to decrease the operational temperature of ASSLMs.

## References

- [1] International energy outlook 2015 [Online].  
<https://www.iea.org/publications/freepublications/publication/WEO2015.pdf>.
- [2] Statistical review of world energy 2019 [Online]  
<https://www.bp.com/en/global/corporate/energy-economics/statistical-review-of-world-energy.html>.
- [3] D. J. Wuebbles, A. K. Jain. Concerns about climate change and the role of fossil fuel use. *Fuel Process. Technol.* 2001; **71**(1), 99-119.
- [4] 1997 Kyoto Protocol to the United Nations Framework Convention on Climate Change (UNFCCC).
- [5] O. Morton. A new day dawning?: Silicon Valley sunrise. *Nature*. 2006; **443**(7107), 19-22.
- [6] M. Lei, L. Shiyan, J. Chuanwen, L. Hongling, Z. Yan. A review on the forecasting of wind speed and generated power. *Renew. Sust. Energ. Rev.* 2009; **13**(4), 915-920.
- [7] D. Linden, T. Reddy. *Handbook of Batteries*: McGraw-Hill Education. 2001.
- [8] X.Luo, J. Wang, M. Dooner, J. Clarke. Overview of current development in electrical energy storage technologies and the application potential in power system operation. *Appl. Energ.* 2015; **137**, 511-536.
- [9] J.W. Choi, D. Aurbach. Promise and reality of post-lithium-ion batteries with high energy densities. *Nat. Rev. Mater.* 2016; **1**, 16013.
- [10] M. Armand, J.M. Tarascon. Building better batteries. *Nature*. 2008; **451**, 652-657.
- [11] Z. Yang, J. Zhang, M. C. W. Kintner-Meyer, X. Lu, D. Choi, J.P. Lemmon, J. Liu. Electrochemical energy storage for green grid. *Chem. Rev.* 2011; **111**(5), 3577-3613.
- [12] H. Ibrahim, A. Ilinca, J. Perron. Energy storage systems—Characteristics and comparisons. *Renew. Sust. Energ. Rev.* 2008; **12**(5), 1221-1250.

- [13] L. Jabbour, R. Bongiovanni, D. Chaussy, C. Gerbaldi, D. Beneventi. Cellulose-based Li-ion batteries: a review. *Cellulose*. 2013; **20**(4), 1523-1545.
- [14] Y. Miao, P. Hynan, A. Von Jouanne, A. Yokochi. Current Li-ion battery technologies in electric vehicles and opportunities for advancements. *Energies*. 2019; **12**(6), 1074-1094.
- [15] H.D. Yoo, E. Markevich, G. Salitra, D. Sharon, D. Aurbach. On the challenge of developing advanced technologies for electrochemical energy storage and conversion. *Mater. Today*. 2014; **17**(3), 110-121.
- [16] D. Andre, S.J. Kim, P. Lamp, S.F. Lux, F. Maglia, O. Paschos, B. Stiaszny. Future generations of cathode materials: an automotive industry perspective. *J. Mater. Chem. A*. 2015; **3**(13), 6709-6732.
- [17] T.H. Kim, J.S. Park, S.K. Chang, S. Choi, J.H. Ryu, H. K. Song. The current move of lithium ion batteries towards the next phase. *Adv. Energy Mater.* 2012; **2**(7), 860-872.
- [18] J.M. Tarascon, M. Armand. Issues and challenges facing rechargeable lithium batteries. *Nature*. 2001; **414**(6861), 359-367.
- [19] J.B. Goodenough, Y. Kim. Challenges for rechargeable Li batteries. *Chem. Mater.* 2010; **22**(3), 587-603.
- [20] K. Mizushima, P.C. Jones, P.J. Wiseman, J.B. Goodenough.  $\text{Li}_x\text{CoO}_2$  ( $0 < x \leq 1$ ): A new cathode material for batteries of high energy density. *Solid State Ion.* 1981; **3-4**, 171-174.
- [21] S. Muench, A. Wild, C. Friebe, B. Häupler, T. Janoschka, U.S. Schubert. Polymer-based organic batteries. *Chem. Rev.* 2016; **116**(16), 9438-9484.
- [22] D. Deng. Li-ion batteries: basics, progress, and challenges. *Energy Sci. Eng.* 2015; **3**(5), 385-418.
- [23] B. John, G. Cheruvally. Polymeric materials for lithium-ion cells. *Polym. Adv. Technol.* 2017; **28**(12), 1528-1538.
- [24] M. Yoshio, R.J. Brodd, A. Kozawa. Lithium-ion batteries: science and technologies: *Springer New York*. 2010

- [25] S.L. Chou, Y. Pan, J.Z. Wang, H.K. Liu, S.X. Dou. Small things make a big difference: binder effects on the performance of Li and Na batteries. *Phys. Chem. Chem. Phys.* 2014; **16**(38), 20347-20359.
- [26] P. Arora, Z. Zhang. Battery separators. *Chem. Rev.* 2004; **104**(10), 4419-4462.
- [27] S.S. Zhang. A review on the separators of liquid electrolyte Li-ion batteries. *J. Power Sources.* 2007; **164**(1), 351-364.
- [28] E.P. Roth, C. J. Orendorff. How electrolytes influence battery safety. *J. Electrochem. Soc.* 2012; **21**(2), 45-49.
- [29] E. Quartarone, P. Mustarelli. Electrolytes for solid-state lithium rechargeable batteries: recent advances and perspectives. *Chem. Soc. Rev.* 2011; **40**(5), 2525-2540.
- [30] H. Zhang, C. Li, M. Piszcz, E. Coya, T. Rojo, L.M. Rodriguez-Martinez, M. Armand, Z. Zhou. Single lithium-ion conducting solid polymer electrolytes: advances and perspectives. *Chem. Soc. Rev.* 2017; **46**(3), 797-815.
- [31] D.T. Hallinan Jr., N.P. Balsara. Polymer electrolytes. *Annu. Rev. Mater. Res.* 2013; **43**(1), 503-525.
- [32] M. Marcinek, J. Syzdek, M. Marczewski, M. Piszcz, L. Niedzicki, M. Kalita, A. Plewa-Marczewska, A. Bitner, P. Wieczorek, T. Trzeciak, M. Kasprzyk, P. Łęzak, Z. Zukowska, A. Zalewska, W. Wieczorek. Electrolytes for Li-ion transport – Review. *Solid State Ion.* 2015; **276**, 107-126.
- [33] V. Di Noto, S. Lavina, G.A. Giffin, E. Negro, B. Scrosati. Polymer electrolytes: present, past and future. *Electrochim. Acta.* 2011; **57**, 4-13.
- [34] J. Kalhoff, G.G. Eshetu, D. Bresser, S. Passerini. Safer electrolytes for lithium-ion batteries: state of the art and perspectives. *ChemSusChem.* 2015; **8**(13), 2154-2175.
- [35] J. Muldoon, C.B. Bucur, N. Boaretto, T. Gregory, V. di Noto. Polymers: opening doors to future batteries. *Polym. Rev.* 2015; **55**(2), 208-246.
- [36] D.E. Fenton, J.M. Parker, P.V. Wright. Complexes of alkali metal ions with poly(ethylene oxide). *Polymer.* 1973; **14**(11), 589.
- [37] P.G. Bruce. *Solid State Electrochemistry*: Cambridge University Press. 1997



- [38] K.S. Ngai, S. Ramesh, K. Ramesh, J.C. Juan. A review of polymer electrolytes: fundamental, approaches and applications. *Ionics*. 2016; **22**(8), 1259-1279.
- [39] W.H. Meyer. Polymer electrolytes for lithium-ion batteries. *Adv. Mater.* 1998; **10**(6), 439-448.
- [40] A. Arya, A.L. Sharma. Polymer electrolytes for lithium ion batteries: a critical study. *Ionics*. 2017; **23**(3), 497-540.
- [41] L. Porz, T. Swamy, B.W. Sheldon, D. Rettenwander, T. Frömling, H.L. Thaman, S. Berendts, R. Uecker, W.C. Carter, Y.M. Chiang. Mechanism of lithium metal penetration through inorganic solid electrolytes. 2017; **7**(20), 1701003.
- [42] P. Barai, K. Higa, V. Srinivasan. Lithium dendrite growth mechanisms in polymer electrolytes and prevention strategies. *Phys. Chem. Chem. Phys.* 2017; **19**(31), 20493-20505.
- [43] R.C. Agrawal, G.P. Pandey. Solid polymer electrolytes: materials designing and all-solid-state battery applications: an overview. *J. Phys. D*. 2008; **41**(22), 223001.
- [44] B. Scrosati, C.A. Vincent. Polymer electrolytes: the key to lithium polymer batteries. *MRS Bull.* 2000; **25**(3), 28-30.
- [45] L. Long, S. Wang, M. Xiao, Y. Meng. Polymer electrolytes for lithium polymer batteries. *J. Mater. Chem. A*. 2016; **4**(26), 10038-10069.
- [46] J.Y. Song, Y.Y. Wang, C.C. Wan. Review of gel-type polymer electrolytes for lithium-ion batteries. *J. Power Sources*. 1999; **77**(2), 183-197.
- [47] A. Nitzan, M.A. Ratner. Conduction in polymers: dynamic disorder transport. *J. Phys. Chem.* 1994; **98**(7), 1765-1775.
- [48] Z. Stoeva, I. Martin-Litas, E. Staunton, Y.G. Andreev, P.G. Bruce. Ionic conductivity in the crystalline polymer electrolytes  $\text{PEO}_6:\text{Li}_x\text{F}_6$ ,  $X = \text{P, As, Sb}$ . *J. Am. Chem. Soc.* 2003; **125**(15), 4619-4626.
- [49] J. Sun, X. Liao, A.M. Minor, N.P. Balsara, R.N. Zuckermann. Morphology-conductivity relationship in crystalline and amorphous sequence-defined peptoid block copolymer electrolytes. *J. Am. Chem. Soc.* 2014; **136**(42), 14990-14997.

[50] C. Berthier, W. Gorecki, M. Minier, M.B. Armand, J.M. Chabagno, P. Rigaud. Microscopic investigation of ionic conductivity in alkali metal salts-poly(ethylene oxide) adducts. *Solid State Ion.* 1983; **11**(1), 91-95.

[51] O. Borodin, G.D. Smith. Mechanism of ion transport in amorphous poly(ethylene oxide)/LiTFSI from molecular dynamics simulations. *Macromolecules.* 2006; **39**(4), 1620-1629.

[52] F.M. Gray. *Polymer electrolytes*: Cambridge: Royal Society of Chemistry. 1997.

[53] M.C. Wintersgill, J.J. Fontanella, J.P. Calame, D.R. Figueroa, C.G. Andeen. Dielectric relaxation in poly(ethylene oxide) complexed with alkali metal perchlorates. *Solid State Ion.* 1983; **11**(2), 151-155.

[54] M.A. Ratner, P. Johansson, D.F. Shriver. Polymer electrolytes: ionic transport mechanisms and relaxation coupling. *MRS Bull.* 2000; **25**(3), 31-37.

[55] J. Gao, Y.S. Zhao, S.Q. Shi, H. Li. Lithium-ion transport in inorganic solid state electrolyte. *Chin. Phys. B.* 2016; **25**(1), 018211.

[56] G.G. Eshetu, X. Judez, C. Li, M. Martinez-Ibañez, E. Sánchez-Diez, L.M. Rodriguez-Martinez, H. Zhang, M. Armand. Solid electrolytes for lithium metal and future lithium-ion batteries: Future Lithium-ion Batteries-The Royal Society of Chemistry. 2019.

[57] Y. Zhu, X. He, Y. Mo. Origin of outstanding stability in the lithium solid electrolyte materials: insights from thermodynamic analyses based on first-principles calculations. *ACS Appl. Mater. Interfaces.* 2015; **7**(42), 23685-23693.

[58] K. Edström, M. Herstedt, D.P. Abraham. A new look at the solid electrolyte interphase on graphite anodes in Li-ion batteries. *J. Power Sources.* 2006; **153**(2), 380-384.

[59] A.C. Luntz, J. Voss, K. Reuter. Interfacial challenges in solid-state Li ion batteries. *J. Phys. Chem. Lett.* 2015; **6**(22), 4599-4604.

[60] Y. Li, W. Zhou, X. Chen, X. Lü, Z. Cui, S. Xin, L. Xue, Q. Jia, J.B. Goodenough. Mastering the interface for advanced all-solid-state lithium rechargeable batteries. *PNAS.* 2016; **113**(47), 13313.

[61] Y. Zhu, X. He, Y. Mo. Strategies based on nitride materials chemistry to stabilize Li metal anode. *Adv. Sci.* 2017; **4**(8), 1600517.

- [62] Y. Tian, T. Shi, W.D. Richards, J. Li, J.C. Kim, S.H. Bo, G. Ceder. Compatibility issues between electrodes and electrolytes in solid-state batteries. *Energy & Environ. Sci.* 2017; **10**(5), 1150-1166.
- [63] X. Judez, H. Zhang, C. Li, J.A. González-Marcos, Z. Zhou, M. Armand, L.M. Rodriguez-Martinez. Lithium bis(fluorosulfonyl)imide/poly(ethylene oxide) polymer electrolyte for all solid-state Li-S cell. *J. Phys. Chem. Lett.* 2017; **8**(9), 1956-1960.
- [64] H. Zhang, C. Liu, L. Zheng, F. Xu, W. Feng, H. Li, X. Huang, M. Armand, J. Nie, Z. Zhou. Lithium bis(fluorosulfonyl)imide/poly(ethylene oxide) polymer electrolyte. *Electrochim. Acta.* 2014; **133**, 529-538.
- [65] X. Judez, M. Piszcz, E. Coya, C. Li, I. Aldalur, U. Oteo, Y. Zhang, W. Zhang, L.M. Rodriguez-Martinez, H. Zhang, M. Armand. Stable cycling of lithium metal electrode in nanocomposite solid polymer electrolytes with lithium bis(fluorosulfonyl)imide. *Solid State Ion.* 2018; **318**, 95-101.
- [66] F. Croce, G.B. Appetecchi, L. Persi, B. Scrosati. Nanocomposite polymer electrolytes for lithium batteries. *Nature.* 1998; **394**(6692), 456-458.
- [67] S. Liang, W. Yan, X. Wu, Y. Zhang, Y. Zhu, H. Wang, Y. Wu. Gel polymer electrolytes for lithium ion batteries: fabrication, characterization and performance. *Solid State Ion.* 2018; **318**, 2-18.
- [68] Y. Aihara, G.B. Appetecchi, B. Scrosati. A new concept for the formation of homogeneous, poly(ethylene oxide) based, gel-type polymer electrolyte. *J. Electrochem. Soc.* 2002; **149**(7), A849-A854.
- [69] F. Groce, F. Gerace, G. Dautzemberg, S. Passerini, G.B. Appetecchi, B. Scrosati. Synthesis and characterization of highly conducting gel electrolytes. *Electrochim. Acta.* 1994; **39**(14), 2187-2194.
- [70] G. Feuillade, P. Perche. Ion-conductive macromolecular gels and membranes for solid lithium cells. *J. Appl. Electrochem.* 1975; **5**(1), 63-69.
- [71] A. Manuel Stephan. Review on gel polymer electrolytes for lithium batteries. *Eur. Polym. J.* 2006; **42**(1), 21-42.
- [72] D. Saikia, Y.W. Chen-Yang, Y.T. Chen, Y.K. Li, S.I. Lin. Investigation of ionic conductivity of composite gel polymer electrolyte membranes based on P(VDF-

HFP), LiClO<sub>4</sub> and silica aerogel for lithium ion battery. *Desalination*. 2008; **234**(1), 24-32.

[73] S. Ramesh, C.W. Liew, K. Ramesh. Evaluation and investigation on the effect of ionic liquid onto PMMA-PVC gel polymer blend electrolytes. *J. Non-Cryst. Solids*. 2011; **357**(10), 2132-2138.

[74] A. Chakrabarti, R. Filler, B.K. Mandal. Synthesis and properties of a new class of fluorine-containing dilithium salts for lithium-ion batteries. *Solid State Ion*. 2010; **180**(40), 1640-1645.

[75] H. Kim, B. Oh, Y. Kang. Preparation and electrochemical properties of nonwoven reinforced solid polymer electrolytes. *Polym. Bull*. 2000; **44**(5), 509-515.

[76] Y.T. Kim, E.S. Smotkin. The effect of plasticizers on transport and electrochemical properties of PEO-based electrolytes for lithium rechargeable batteries. *Solid State Ion*. 2002; **149**(1), 29-37.

[77] S. Rajendran, R. Babu, P. Sivakumar. Optimization of PVC– PAN-based polymer electrolytes. *J. Appl. Polym. Sci*. 2009; **113**(3), 1651-1656.

[78] P. Vickraman, S. Ramamurthy. A study on the blending effect of PVDF in the ionic transport mechanism of plasticized PVC–LiBF<sub>4</sub> polymer electrolyte. *Mater. Lett*. 2006; **60**(28), 3431-3436.

[79] H.S. Min, J.M. Ko, D.W. Kim. Preparation and characterization of porous polyacrylonitrile membranes for lithium-ion polymer batteries. *J. Power Sources*. 2003; **119-121**, 469-472.

[80] P. Carol, P. Ramakrishnan, B. John, G. Cheruvally. Preparation and characterization of electrospun poly(acrylonitrile) fibrous membrane based gel polymer electrolytes for lithium-ion batteries. *J. Power Sources*. 2011; **196**(23), 10156-10162.

[81] X. Wang, C. Gong, D. He, Z. Xue, C. Chen, Y. Liao, X. Xie. Gelled microporous polymer electrolyte with low liquid leakage for lithium-ion batteries. *J. Membrane Sci*. 2014; **454**, 298-304.

[82] Z.H. Li, C. Cheng, X.Y. Zhan, Y.P. Wu, X.D. Zhou. A foaming process to prepare porous polymer membrane for lithium ion batteries. *Electrochim. Acta*. 2009; **54**(18), 4403-4407.

- [83] G.B. Appetecchi, G.T. Kim, M. Montanino, M. Carewska, R. Marcilla, D. Mecerreyes, I. De Meatza. Ternary polymer electrolytes containing pyrrolidinium-based polymeric ionic liquids for lithium batteries. *J. Power Sources*. 2010; **195**(11), 3668-3675.
- [84] G.B. Appetecchi, Y. Aihara, B. Scrosati. Investigation of swelling phenomena in PEO-based polymer electrolytes: II. Chemical and electrochemical characterization. *Solid State Ion*. 2004; **170**(1), 63-72.
- [85] Bluecar. <https://www.bluecar.fr/>.
- [86] F.B. Dias, L. Plomp, J.B.J. Veldhuis. Trends in polymer electrolytes for secondary lithium batteries. *J. Power Sources*. 2000; **88**(2), 169-191.
- [87] J. Rolland, E. Poggi, A. Vlad, J.F. Gohy. Single-ion diblock copolymers for solid-state polymer electrolytes. *Polymer*. 2015; **68**, 344-352.
- [88] P.V. Wright. Electrical conductivity in ionic complexes of poly(ethylene oxide). *Br. Polym. J.* 1975; **7**(5), 319-327.
- [89] P. Vashishta, J.N. Mundy, G.K. Shenoy. Fast ion transport in solids: electrodes, and electrolytes : proceedings of the international conference on fast ion transport in solids, electrodes, and electrolytes. North Holland. 1979.
- [90] M. Armand. Polymer solid electrolytes - an overview. *Solid State Ion*. 1983; **9-10**, 745-754.
- [91] M.B. Armand. Polymer Electrolytes. *Annu. Rev. Mater. Res.* 1986; **16**(1), 245-261.
- [92] Z. Xue, D. He, X. Xie. Poly(ethylene oxide)-based electrolytes for lithium-ion batteries. *J. Mater. Chem. A*. 2015; **3**(38), 19218-19253.
- [93] S. Lascaud, M. Perrier, A. Vallee, S. Besner, J. Prud'homme, M. Armand. Phase diagrams and conductivity behavior of poly(ethylene oxide)-molten salt rubbery electrolytes. *Macromolecules*. 1994; **27**(25), 7469-7477.
- [94] M. Armand. The history of polymer electrolytes. *Solid State Ion*. 1994; **69**(3), 309-319.
- [95] S.J. Kwon, D.G. Kim, J. Shim, J.H. Lee, J.H. Baik, J.C. Lee. Preparation of organic/inorganic hybrid semi-interpenetrating network polymer electrolytes

based on poly(ethylene oxide-co-ethylene carbonate) for all-solid-state lithium batteries at elevated temperatures. *Polymer*. 2014; **55**(12), 2799-2808.

[96] Z. Gadjourova, Y.G. Andreev, D.P. Tunstall, P.G. Bruce. Ionic conductivity in crystalline polymer electrolytes. *Nature*. 2001; **412**(6846), 520-523.

[97] S.K. Fullerton-Shirey, J.K. Maranas. Effect of LiClO<sub>4</sub> on the structure and mobility of PEO-based solid polymer electrolytes. *Macromolecules*. 2009; **42**(6), 2142-2156.

[98] S. Cheng, D.M. Smith, C.Y. Li. How does nanoscale crystalline structure affect ion transport in solid polymer electrolytes? *Macromolecules*. 2014; **47**(12), 3978-3986.

[99] T. Zheng, Q. Zhou, Q. Li, L. Zhang, H. Li, Y. Lin. A new branched copolyether-based polymer electrolyte for lithium batteries. *Solid State Ion*. 2014; **259**, 9-13.

[100] Z. Wen, T. Itoh, T. Uno, M. Kubo, T. Wen, O. Yamamoto. Polymer electrolytes based on poly(ethylene oxide) and cross-linked poly(ethylene oxide-co-propylene oxide). *Solid State Ion*. 2004; **175**(1), 739-742.

[101] C.P. Fonseca, S. Neves. Characterization of polymer electrolytes based on poly(dimethyl siloxane-co-ethylene oxide). *J. Power Sources*. 2002; **104**(1), 85-89.

[102] K.M. Abraham, M. Alamgir. Ambient temperature rechargeable polymer-electrolyte batteries. *J. Power Sources*. 1993; **43**(1), 195-208.

[103] D. Devaux, L. Liénafa, E. Beaudoin, S. Maria, T.N.T. Phan, D. Gigmes, E. Giroud, P. Davidson, R. Bouchet. Comparison of single-ion-conductor block-copolymer electrolytes with polystyrene-TFSI and polymethacrylate-TFSI structural blocks. *Electrochim. Acta*. 2018; **269**, 250-261.

[104] Y. Kumar, S.A. Hashmi, G.P. Pandey. Lithium ion transport and ion-polymer interaction in PEO based polymer electrolyte plasticized with ionic liquid. *Solid State Ion*. 2011; **201**(1), 73-80.

[105] M. Wetjen, M.A. Navarra, S. Panero, S. Passerini, B. Scrosati, J. Hassoun. Composite poly(ethylene oxide) electrolytes plasticized by *N*-alkyl-*N*-butylpyrrolidinium bis(trifluoromethanesulfonyl)imide for lithium batteries. *ChemSusChem*. 2013; **6**(6), 1037-1043.

- [106] K. Vignarooban, M.A.K.L. Dissanayake, I. Albinsson, B.E. Mellander. Effect of TiO<sub>2</sub> nano-filler and EC plasticizer on electrical and thermal properties of poly(ethylene oxide) (PEO) based solid polymer electrolytes. *Solid State Ion.* 2014; **266**, 25-28.
- [107] A. Manuel Stephan, K.S. Nahm. Review on composite polymer electrolytes for lithium batteries. *Polymer.* 2006; **47**(16), 5952-5964.
- [108] D. Brandell, H. Kasemägi, T. Tamm, A. Aabloo. Molecular dynamics modeling the Li-polystyrene TFSI/PEO blend. *Solid State Ion.* 2014; **262**, 769-773.
- [109] S. Wang, K. Min. Solid polymer electrolytes of blends of polyurethane and polyether modified polysiloxane and their ionic conductivity. *Polymer.* 2010; **51**(12), 2621-2628.
- [110] C.H. Park, Y.K. Sun, D.W. Kim. Blended polymer electrolytes based on poly(lithium 4-styrene sulfonate) for the rechargeable lithium polymer batteries. *Electrochim. Acta.* 2004; **50**(2), 375-378.
- [111] A. Nishimoto, K. Agehara, N. Furuya, T. Watanabe, M. Watanabe. High ionic conductivity of polyether-based network polymer electrolytes with hyperbranched side chains. *Macromolecules.* 1999; **32**(5), 1541-1548.
- [112] X.X. Zeng, Y.X. Yin, N.W. Li, W.C. Du, Y.G. Guo, L.J. Wan. Reshaping lithium plating/stripping behavior via bifunctional polymer electrolyte for room-temperature solid Li metal batteries. *J. Amer. Chem. Soc.* 2016; **138**(49), 15825-15828.
- [113] E.D. Gomez, A. Panday, E.H. Feng, V. Chen, G.M. Stone, A.M. Minor, C. Kisielowski, K.H. Downing, O. Borodin, G.D. Smith, N.P. Balsara. Effect of ion distribution on conductivity of block copolymer electrolytes. *Nano Lett.* 2009; **9**(3), 1212-1216.
- [114] M. Singh, O. Odusanya, G.M. Wilmes, H.B. Eitouni, E.D. Gomez, A.J. Patel, V.L. Chen, M.J. Park, P. Fragouli, H. Iatrou, N. Hadjichristidis, D. Cookson, N.P. Balsara. Effect of molecular weight on the mechanical and electrical properties of block copolymer electrolytes. *Macromolecules.* 2007; **40**(13), 4578-4585.
- [115] P. Passiniemi, S. Takkumäki, J. Kankare, M. Syrjämä. Ionic conduction in ethylene oxide-propylene oxide copolymers containing LiClO<sub>4</sub>. *Solid State Ion.* 1988; **28-30**, 1001-1003.

- [116] A. Panday, S. Mullin, E.D. Gomez, N. Wanakule, V.L. Chen, A. Hexemer, J. Pople, N.P. Balsara. Effect of molecular weight and salt concentration on conductivity of block copolymer electrolytes. *Macromolecules*. 2009; **42**(13), 4632-4637.
- [117] M. Chintapalli, X.C. Chen, J.L. Thelen, A.A. Teran, X. Wang, B.A. Garetz, N.P. Balsara. Effect of grain size on the ionic conductivity of a block copolymer electrolyte. *Macromolecules*. 2014; **47**(15), 5424-5431.
- [118] R. Yuan, A.A. Teran, I. Gurevitch, S.A. Mullin, N.S. Wanakule, N.P. Balsara. Ionic conductivity of low molecular weight block copolymer electrolytes. *Macromolecules*. 2013; **46**(3), 914-921.
- [119] W.S. Young, T.H. Epps. Ionic conductivities of block copolymer electrolytes with various conducting pathways: sample preparation and processing considerations. *Macromolecules*. 2012; **45**(11), 4689-4697.
- [120] J. Ping, H. Pan, P.P. Hou, M.Y. Zhang, X. Wang, C. Wang, J. Chen, D. Wu, Z. Shen, X.H. Fan. Solid polymer electrolytes with excellent high-temperature properties based on brush block copolymers having rigid side chains. *ACS Appl. Mater. Interfaces*. 2017; **9**(7), 6130-6137.
- [121] B.K. Choi, Y.W. Kim, H.K. Shin. Ionic conduction in PEO–PAN blend polymer electrolytes. *Electrochim. Acta*. 2000; **45**(8), 1371-1374.
- [122] Z. Jiang, B. Carroll, K.M. Abraham. Studies of some poly(vinylidene fluoride) electrolytes. *Electrochim. Acta*. 1997; **42**(17), 2667-2677.
- [123] S. Ramesh, K.H. Leen, K. Kumutha, A.K. Arof. FTIR studies of PVC/PMMA blend based polymer electrolytes. *Spectrochim. Acta A*. 2007; **66**(4), 1237-1242.
- [124] A.L. Sharma, A.K. Thakur. Plastic separators with improved properties for portable power device applications. *Ionics*. 2013; **19**(5), 795-809.
- [125] A.L. Sharma, A.K. Thakur. Improvement in voltage, thermal, mechanical stability and ion transport properties in polymer-clay nanocomposites. *J. Appl. Polym. Sci*. 2010; **118**(5), 2743-2753.
- [126] P. Tamilselvi, M. Hema. Structural, thermal, vibrational, and electrochemical behavior of lithium ion conducting solid polymer electrolyte based on poly(vinyl alcohol)/poly(vinylidene fluoride) blend. *Polym. Sci. Ser. A*. 2016; **58**(5), 776-784.



- [127] J. Mindemark, M.J. Lacey, T. Bowden, D. Brandell. Beyond PEO—Alternative host materials for Li<sup>+</sup>-conducting solid polymer electrolytes. *Prog. Polym. Sci.* 2018; **81**, 114-143.
- [128] M.T. Ong, O. Verners, E.W. Draeger, A.C.T. van Duin, V. Lordi, J.E. Pask. Lithium ion solvation and diffusion in bulk organic electrolytes from first-principles and classical reactive molecular dynamics. *J. Phys. Chem. B.* 2015; **119**(4), 1535-1545.
- [129] X. Bogle, R. Vazquez, S. Greenbaum, A.V.W. Cresce, K. Xu. Understanding Li<sup>+</sup>-solvent interaction in nonaqueous carbonate electrolytes with <sup>17</sup>O NMR. *J. Phys. Chem. Lett.* 2013; **4**(10), 1664-1668.
- [130] Y. Tominaga, K. Yamazaki. Fast Li-ion conduction in poly(ethylene carbonate)-based electrolytes and composites filled with TiO<sub>2</sub> nanoparticles. *Chem. Commun.* 2014; **50**(34), 4448-4450.
- [131] K. Kimura, M. Yajima, Y. Tominaga. A highly-concentrated poly(ethylene carbonate)-based electrolyte for all-solid-state Li battery working at room temperature. *Electrochem. Commun.* 2016; **66**, 46-48.
- [132] J. Mindemark, B. Sun, E. Törmä, D. Brandell. High-performance solid polymer electrolytes for lithium batteries operational at ambient temperature. *J. Power Sources.* 2015; **298**, 166-170.
- [133] C. Wang, H. Zhang, J. Li, J. Chai, S. Dong, G. Cui. The interfacial evolution between polycarbonate-based polymer electrolyte and Li-metal anode. *J. Power Sources.* 2018; **397**, 157-161.
- [134] I. Nicotera, L. Coppola, C. Oliviero, M. Castriota, E. Cazzanelli. Investigation of ionic conduction and mechanical properties of PMMA–PVdF blend-based polymer electrolytes. *Solid State Ion.* 2006; **177**(5), 581-588.
- [135] X. Wang, H. Zhu, G.W. Greene, J. Li, N. Iranipour, C. Garnier, J. Fang, M. Armand, M. Forsyth, J.M. Pringle, P.C. Howlett. Enhancement of ion dynamics in organic ionic plastic crystal/PVDF composite electrolytes prepared by co-electrospinning. *J. Mater. Chem. A.* 2016; **4**(25), 9873-9880.
- [136] Y. Zhou, X. Wang, H. Zhu, M. Yoshizawa-Fujita, Y. Miyachi, M. Armand, M. Forsyth, G.W. Greene, J.M. Pringle, P.C. Howlett. Solid-state lithium conductors for lithium metal batteries based on electrospun nanofiber/plastic crystal composites. 2017; **10**(15), 3135-3145.

[137] M. Armand, P. G. Bruce, M. Forsyth, B. Scrosati, W. Wieczorek. Polymer Electrolytes. *Energy Materials*. 2011

[138] W. Gorecki, R. Andreani, C. Berthier, M. Armand, M. Mali, J. Roos, D. Brinkmann. NMR, DSC, and conductivity study of a poly(ethylene oxide) complex electrolyte : PEO(LiClO<sub>4</sub>)<sub>x</sub>. *Solid State Ion*. 1986; **18-19**, 295-299.

[139] M. Kalita, M. Bukat, M. Ciosek, M. Siekierski, S.H. Chung, T. Rodríguez, S.G. Greenbaum, R. Kovarsky, D. Golodnitsky, E. Peled, D. Zane, B. Scrosati, W. Wieczorek. Effect of calixpyrrole in PEO–LiBF<sub>4</sub> polymer electrolytes. *Electrochim. Acta*. 2005; **50**(19), 3942-3948.

[140] A. Magistris, P. Mustarelli, E. Quartarone, C. Tomasi. Transport and thermal properties of (PEO)<sub>n</sub>–LiPF<sub>6</sub> electrolytes for super-ambient applications. *Solid State Ion*. 2000; **136-137**, 1241-1247.

[141] W. Gorecki, M. Jeannin, E. Belorizky, C. Roux, M. Armand. Physical properties of solid polymer electrolyte PEO(LiTFSI) complexes. *J. Phys.: Condens. Mat*. 1995; **7**(34), 6823-6832.

[142] M. Marzantowicz, J.R. Dygas, F. Krok, A. Łasińska, Z. Florjańczyk, E. Zygadło-Monikowska, A. Affek. Crystallization and melting of PEO:LiTFSI polymer electrolytes investigated simultaneously by impedance spectroscopy and polarizing microscopy. *Electrochim. Acta*. 2005; **50**(19), 3969-3977.

[143] H.B. Han, J. Nie, K. Liu, W.K. Li, W.F. Feng, M. Armand, H. Matsumoto, Z.B. Zhou. Ionic liquids and plastic crystals based on tertiary sulfonium and bis(fluorosulfonyl)imide. *Electrochim Acta*. 2010; **55**(3), 1221-1226.

[144] T. Sugimoto, M. Kikuta, E. Ishiko, M. Kono, M. Ishikawa. Ionic liquid electrolytes compatible with graphitized carbon negative without additive and their effects on interfacial properties. *J. Power Sources*. 2008; **183**(1), 436-440.

[145] D. Golodnitsky, E. Strauss, E. Peled, S. Greenbaum. Review—on order and disorder in polymer electrolytes. *J. Electrochem. Soc*. 2015; **162**(14), A2551-A2566.

[146] Y. Ikeda, Y. Wada, Y. Matoba, S. Murakami, S. Kohjiya. Characterization of comb-shaped high molecular weight poly(oxyethylene) with tri(oxyethylene) side chains for a polymer solid electrolyte. *Electrochim. Acta*. 2000; **45**(8), 1167-1174.

**[147]** N.A. Stolwijk, C. Heddier, M. Reschke, M. Wiencierz, J. Bokeloh, G. Wilde. Salt-concentration dependence of the glass transition temperature in PEO–NaI and PEO–LiTFSI polymer electrolytes. *Macromolecules*. 2013; **46**(21), 8580-8588.

**[148]** M. Nakayama, S. Wada, S. Kuroki, M. Nogami. Factors affecting cyclic durability of all-solid-state lithium polymer batteries using poly(ethylene oxide)-based solid polymer electrolytes. *Energ. Environ. Sci.* 2010; **3**(12), 1995-2002.

**[149]** J. Wan, J. Xie, X. Kong, Z. Liu, K. Liu, F. Shi, A. Pei, H. Chen, W. Chen, J. Chen, X. Zhang, L. Zong, J. Wang, L.Q. Chen, J. Qin, Y. Cui. Ultrathin, flexible, solid polymer composite electrolyte enabled with aligned nanoporous host for lithium batteries. *Nature Nanotechnol.* 2019; **14**, 705-711.



## Chapter 2

---

# Experimental framework





## Chapter 2:

### EXPERIMENTAL FRAMEWORK

2.1.	Introduction.....	49
2.2.	Synthesis methods and sample preparation.....	49
2.2.1.	Materials.....	49
2.2.2.	Synthesis of new polymer backbones.....	50
2.2.3.	Electrolyte preparation.....	51
2.2.4.	Poly(vinylidene fluoride) nanofiber preparation.....	52
2.3.	Cell preparation.....	53
2.3.1.	Electrode preparation.....	53
2.3.2.	Cell assembly .....	54
2.4.	Characterization techniques.....	55
2.4.1.	Chemical characterization.....	55
2.4.2.	Morphological and elemental characterization.....	56
2.4.3.	Mechanical characterization.....	56
2.4.4.	Thermal characterization .....	57
2.4.5.	Electrochemical characterization .....	58
	References.....	61





## 2.1. Introduction

The aim of this chapter is to describe the synthesis methods, the sample preparation and the experimental techniques that have been used during this thesis work. First, a general overview on the synthesis mechanism that has been followed for the polymer preparation is presented. Then, the processing of the polymers for their use as electrolytes or polymer binder in cathode materials in batteries is described. In this section special emphasis is given to the description of the cell assembly.

Finally, a brief description of the equipment and the experimental conditions at which the different techniques were used is provided. In this section, a summary of all the chemical, morphological and mechanical techniques required for determining the chemical and structural properties is presented at a first stage. Then, the techniques deployed for testing the thermal stability and phase transitions are detailed. At last, the techniques utilized for evaluating the electrochemical properties of the materials are provided.

## 2.2. Synthesis methods and sample preparation

### 2.2.1. Materials

All the starting materials were purchased from commercial suppliers and were dried in a Schlenk line or in a vacuum oven prior to their use.

#### *a) Synthesis of Jeffamine-based homopolymer*

All starting materials and reagents were purchased from commercial suppliers and were used after purification. Jeffamine M-2070, Jeffamine M-1000 and Jeffamine M-600 were a generous gift of Huntsman Corporation and were dried in a Schlenk line at room temperature (RT) prior to use. Poly(ethylene-*alt*-maleic) anhydride [(PEaMA), average molecular weight ( $M_w$ ) =  $1 \times 10^5$  to  $5 \times 10^5$  g mol<sup>-1</sup>], *N,N*-dimethylformamide (DMF,  $\geq 99.8\%$ ),  $\alpha, \alpha', \alpha''$ -trifluorotoluene (TFT,  $\geq 99.5\%$  anhydrous), triethylamine (Et<sub>3</sub>N,  $\geq 99\%$ ) and 1-methyl-2-pyrrolidinone (NMP,  $\geq 99.5\%$ ) were purchased from Sigma-Aldrich and used as received.

**b) Synthesis of Jeffamine-Polystyrene block-copolymer**

Amine terminated polystyrene (PS,  $M_w = 5 \times 10^3 \text{ g mol}^{-1}$ ), 1,1-carbonyldiimidazole (CDI) and dimethyl sulfoxide (DMSO, 99.5 %), were supplied by Sigma-Aldrich

**c) Poly(vinylidene fluoride) nanofiber preparation**

Commercial poly(vinylidene fluoride) (PVDF) powder, *N,N*-dimethylformamide (DMF) and acetone were from Sigma-Aldrich and kindly provided by Deakin University.

**d) Electrolyte preparation**

Poly(ethylene oxide) (PEO,  $M_w = 5 \times 10^6 \text{ g mol}^{-1}$ ) was purchased from Sigma-Aldrich. Acetonitrile (ACN, synthesis grade) and tetrahydrofuran (THF  $\geq 99.5\%$ ) were supplied by Scharlab. Battery grade lithium bis (trifluoromethanesulfonyl) imide (LiTFSI) and lithium bis (fluorosulfonyl) imide (LiFSI) were supplied by Solvionic (France) and Suzhou Fluolyte (China), respectively.

**e) Electrode preparation**

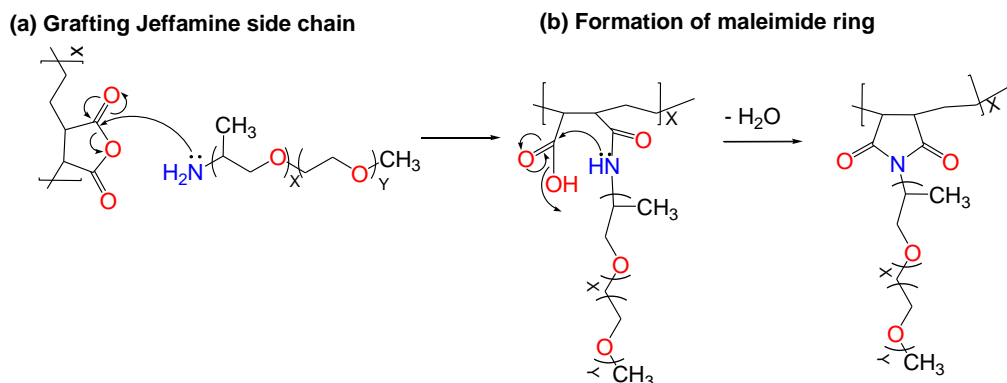
Lithium metal disks, conductive carbon (C65), and lithium iron phosphate [ $\text{LiFePO}_4$  (LFP)] powder were received from China Energy Lithium, TIMCAL, and a generous gift from Aleees (Taiwan), respectively.

**2.2.2. Synthesis of new polymer backbones**

As mentioned before, the main objective of this thesis work is the synthesis of new polymer backbones for their use as electrolytes in all-solid-state lithium batteries. With this aim, different synthesis were carried out in order to obtain comb-like polymer matrices based on imide ring formation with highly conductive chains based on ethylene oxide units.

Throughout this thesis work, several modifications will be carried out on the starting polymer material in order to improve the mechanical and/or ion-conducting properties. However, although more specific synthesis methods will be

explained in next chapters, all these materials are based on imide ring formation following the synthesis mechanism described in **Scheme 2.1**.

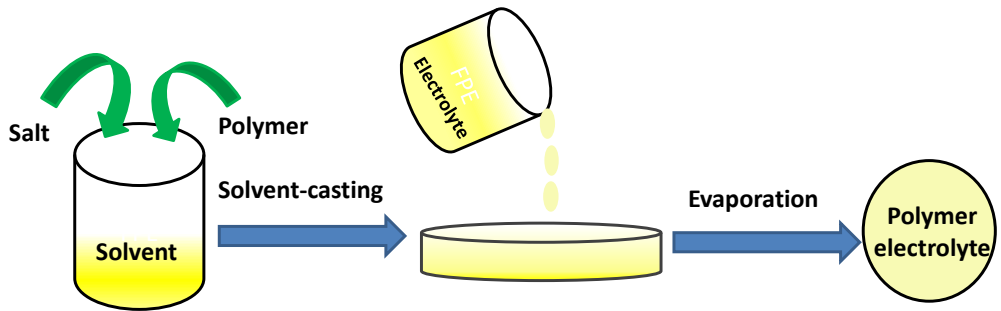


**Scheme 2.1.** Imide ring formation synthesis mechanism.

The mechanism can be explained in two steps; **a)** the grafting of Jeffamine side chain and **b)** the formation of maleimide ring. In the first step the nucleophilic addition ( $N_A$ ) of the Jeffamine ending amine to the anhydride carbonyl group takes place, with the subsequent ring opening. In the second step a condensation reaction occurs, where the addition of the amide group on the carbonyl of the acid leads to the ring closing with overall loss of a water molecule.

### 2.2.3. Electrolyte preparation

All the electrolytes used in this work were prepared by the solvent casting method, as schematically shown in **Figure 2.1**. A pre-weighted amount of polymer matrix (*i.e.*, Jeffamine-based polymers or PEO) and the corresponding amount of lithium salt (LiTFSI or LiFSI) were dissolved into a certain amount of ACN. For Jeffamine-Polystyrene block-copolymers, a mixture of ACN:THF (50:50 by volume) was used in order to increase the solubility.



**Figure 2.1.** Schematic illustration of polymer electrolyte preparation by solvent casting method.

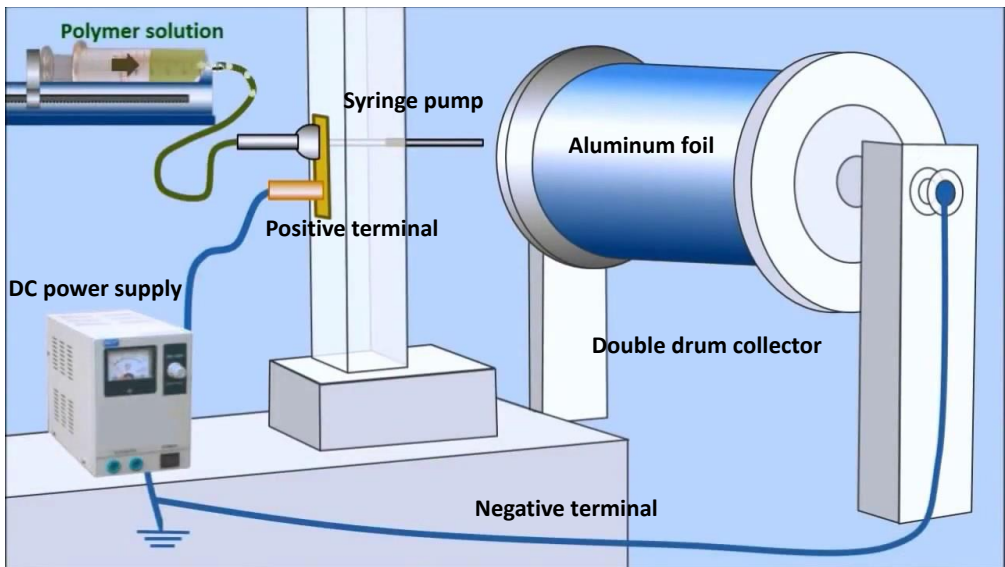
In the case of Jeffamine-based homopolymers, elastic and sticky electrolytes are obtained, being impossible to obtain as self-standing membranes. In the case of the block-copolymer, self-standing membranes with good ductility are obtained. In all cases, after solvent evaporation the electrolytes were dried in a vacuum oven at 80 °C over 12 h in order to remove solvent traces.

In the case of PEO based reference membranes, hot-pressing was used after solvent casting. This technique is based on a manual hydraulic press equipped with a temperature controller that allows obtaining homogeneous self-standing membranes with a determined thickness. The samples were pressed over 1 minute at 70 °C under pressure (*ca.* 2 tons/cm<sup>2</sup>). The membranes were obtained with an average thickness of 100 μm and they were dried under dynamic vacuum at 50 °C over 12h.

#### **2.2.4. Poly(vinylidene fluoride) nanofiber preparation**

To obtain the electrospun porous membranes, typical electrospinning procedure was followed. First, the PVDF powder was dissolved in a mixture of DMF/acetone (1:1 by weight) at RT for at least 12 h. Once the polymer was completely dissolved, the solution was fed into a plastic syringe ending with a stainless steel needle (Terumo, 20 G × 1<sup>1/2</sup>”) connected to a high voltage power supply (0–30 kV, 350 μA, Gamma High Voltage Research, USA) and the applied voltage was kept at 15 kV. The syringe pump flow was set at 0.5 ml h<sup>-1</sup>. A grounded rotating drum collector (100 r/min) was used in order to obtain a uniform membrane and the distance from the needle tip to the drum was fixed at

15 cm. The resultant electrospun mats, with an average thickness of 50  $\mu\text{m}$ , were collected and dried in a vacuum oven for 48 h at 55  $^{\circ}\text{C}$  before use [1-3].



**Figure 2.2.** Schematic illustration of electrospinning method for the preparation of PVDF fibers.

## 2.3. Cell preparation

### 2.3.1. Electrode preparation

The electrode preparation was carried out using carbon-coated aluminium foil as current collector. The composition of the electrodes was set as 63 wt% LFP active material, 30 wt% polymer binder and 7 wt% C65 conductive carbon.

In order to prepare the slurry, first the polymer electrolyte was dissolved in a certain amount of ACN under vigorous stirring overnight at RT. Then a mixture of active material (LFP) and conducting carbon (C65) was obtained by grinding them in a mortar with a small amount of NMP, and slowly added in the polymer solution. In order to obtain a homogeneous mixture, IKA stirrer was used at 16.2 rpm for 20 minutes. The obtained solution was degassed in an ultrasonic bath and later in a roller mixer for 1 h in order to avoid air bubbles. Finally, the viscous solution was dropped to the carbon coated aluminium foil and casted by Doctor Blade with a desired thickness ( $\sim 1500 \mu\text{m}$ ). The laminates were left for drying in

the fume hood for 24 h and when most of the solvent was evaporated the electrodes were dried in a vacuum oven at 50 °C for at least 12 h.

Once the laminates were fully dried, 12 mm diameter discs were punched and dried again at 50 °C for 12 h and directly transferred into the glovebox, avoiding the exposure to the air. The loading of active mass of the electrodes was set between 5.5–6.5 mg cm<sup>-2</sup>. However, this value was decreased in some cases to analyse the effect of the active mass loading in the battery performance (**Chapter 4 ca. 3.1 mg**)

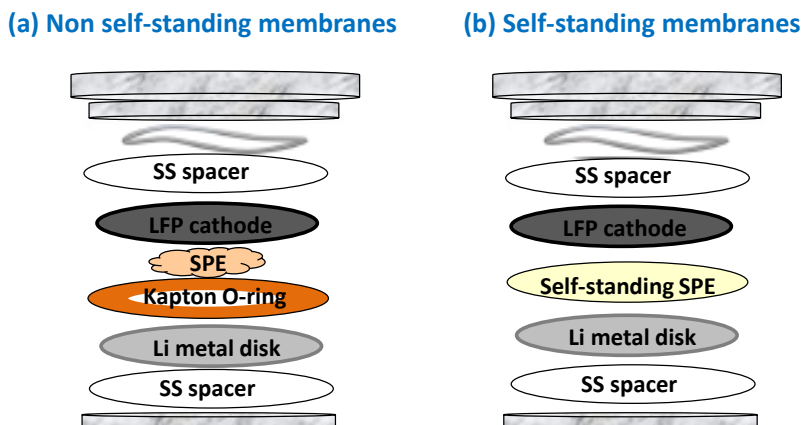


**Figure 2.3.** Casting of the LFP based laminate in the Doctor Blade.

### 2.3.2. Cell assembly

All the electrochemical measurements in this thesis work were carried out in CR2032 type coin cells. In all cases, metallic lithium (Li) was used as anode, and LFP-based electrodes were used as cathodes when required. Due to the fact that metallic Li and the electrolytes are sensitive to the moisture and O<sub>2</sub> from the air, the coin cells were assembled in an argon-filled (Ar) glovebox.

Different cell configurations were used depending on the physical properties of the electrolyte. For full cells, lithium foil used as anode electrode is separated from the LFP-based cathode by the polymer electrolyte and sandwiched between two stainless steel (SS) electrodes. However, the mechanical properties of several polymers synthesized in this work did not allow the obtainment of self-standing membranes. In this case, a Kapton® O-ring spacer (10 mm in diameter) was used in order to avoid the contact between the anode and the cathode. The schematic illustration is shown in **Figure 2.4**.



**Figure 2.4.** Schematic illustration of the cell configuration for **a)** electrolytes presenting poor mechanical properties and **b)** self-standing membranes.

## 2.4. Characterization techniques

This section is divided into five parts; chemical ( $^1\text{H}$  NMR, ATR-FTIR), morphological (SEM) and elemental (EDX), mechanical (rheology and DMA), thermal (DSC, TGA) and electrochemical characterization. The acronyms will be spelled out in the next sections.

### 2.4.1. Chemical characterization

Chemical characterization was carried out by hydrogen-1 nuclear magnetic resonance ( $^1\text{H}$  NMR) and attenuated total reflectance Fourier-transform infrared spectroscopy (ATR-FTIR).

#### **a) Liquid nuclear magnetic resonance (NMR)**

The structure characterization of the polymer matrices was accomplished using liquid nuclear magnetic resonance (NMR). The measurements were performed using deuterium oxide ( $\text{D}_2\text{O}$ , 99.9%) or deuterated dimethyl sulfoxide ( $(\text{CD}_3)_2\text{SO}$ , 99.8%) as solvent on a Bruker 300 Ultrashield NMR instrument (300 MHz).

***b) Attenuated total reflectance Fourier-transform infrared spectroscopy (ATR-FTIR)***

Attenuated total reflectance-Fourier-transform infrared spectroscopy (ATR-FTIR) spectra were collected using a Vertex-70 Bruker spectrometer. The spectrum was averaged from 64 scans with a spectral range spanning 4000–450  $\text{cm}^{-1}$  and a resolution of 2  $\text{cm}^{-1}$ . In the case of moisture-sensitive samples, the ATR-FTIR spectra were collected using an Agilent Technologies Cary 630 spectrometer setup inside an Ar filled glovebox.

**2.4.2. Morphological and elemental characterization**

***a) Scanning electron microscopy (SEM)***

Surface and cross-section morphologies of the as-prepared polymer electrolytes and cathodes were studied by a Field Emission Gun Quanta 200 FEG (FEI) scanning electron microscope (SEM). The micrographs from the scanning electron microscope (FEI-Quanta 200 FEG) were obtained using the back-scattered electron detector (BSE) and secondary electron detector (ETD). The operation voltage for polymer electrolytes and cathodes were fixed at 5 and 10 kV, respectively.

***b) Energy dispersive X-ray spectroscopy (EDX)***

Elemental chemical identification of a specimen and its quantification is fundamental to obtain information related to the composition of the materials. Energy dispersive X-ray spectroscopy (EDX), allows obtaining information concerning the elemental chemical composition using the EDX spectrometer. The analysis is based in the detection of the characteristic X-rays produced by the electron beam-specimen interaction. Same settings as in the SEM were used for the data acquisition.

**2.4.3. Mechanical characterization**

***a) Rheology***

Viscoelastic behavior of the polymer matrices was investigated with a rotational rheometer Physica MCR301 equipped with a Peltier device for precise temperature control, and the TrueGap option. Measurements were performed in



an oscillatory mode using measuring cell of parallel plate geometry (25 mm diameter and 0.5 or 0.8 mm gap for liquid-like samples and solid samples, respectively). To reveal the viscoelastic properties of the prepared polymers, dynamic mechanical analysis tests involving oscillatory tests at constant frequency (1 Hz) and variable shear stress amplitude ( $0.1\text{--}10^3$  Pa) were performed at 20 °C and 70 °C. Temperature-dependent behavior at constant dynamic mechanical conditions (frequency of 1 Hz and amplitude 10 Pa) were studied. Tests were performed at temperatures ranging from 10 to 100 °C, at a heating rate of 2 °C  $\text{min}^{-1}$ . For thermal studies the gaps between measuring plates were of 0.4 and 0.7 mm for liquid-like materials and solid materials, respectively.

### ***b) Differential mechanical analysis (DMA)***

Differential mechanical analysis (DMA) is a frequency response analysis that uses a constant, non-destructive oscillatory strain (or stress) at selected frequencies and temperatures while recording the resulting stress (or strain) response of the sample material [4]. The DMA is used to measure the glass transition temperature ( $T_g$ ) and viscoelastic properties of polymeric materials.

DMA testing was performed with a METTLER TOLEDO DMA/SDTA861e dynamic mechanical analyzer. A tension system was employed, where a rectangular specimen is clamped at both extremes and stretched in a dynamic mode. Testing was performed in the force scan mode in the range 0 – 0.1 N. For the analysis a heating scan in the temperature range from –150 °C to 120 °C at a heating rate of 10 °C  $\text{min}^{-1}$  was carried out. A frequency of 1 Hz was used.

## **2.4.4. Thermal characterization**

### ***a) Thermogravimetric analysis (TGA)***

Thermogravimetric analysis (TGA) was carried out on a NETZSCH simultaneous thermal analyser (STA) 449 F3 Jupiter from RT up to 600 °C at a heating rate of 10 °C  $\text{min}^{-1}$  under synthetic air or Ar atmosphere.

### ***b) Differential scanning calorimeter (DSC)***

The phase transitions of the polymer electrolytes were measured on a differential scanning calorimeter (DSC, Q2000, TA instruments). For the analysis two consecutive scans at a cooling and heating rate of 10 °C  $\text{min}^{-1}$  in the

temperature range from  $-80$  to  $150$  °C (for polymer electrolytes) or  $200$  °C (for polymer matrices) were carried out under Ar atmosphere.

#### 2.4.5. Electrochemical characterization

##### a) Ionic conductivity ( $\sigma$ )

The ionic conductivity was determined by electrochemical impedance spectroscopy (EIS) analysis of CR2032 type cells assembled by sandwiching the polymer electrolyte between two stainless steel (SS) blocking electrodes (SS | SPE | SS) in an Ar filled glove box. The measurement was carried out in a VMP3 potentiostat (Biologic) and the frequency ranged from  $10^{-1}$  to  $10^6$  Hz with a signal amplitude of 10 mV. In order to ensure a good contact between the electrolyte and the electrodes, the cells were heated up to  $70$  °C prior to the measurement. The conductivities were analysed in a temperature range from  $30$  to  $100$  °C using a Vötsch VT 7004 temperature chamber and allowing the cells to reach the thermal equilibrium for at least 1 h before each test.

##### b) Li-ion transference number

The Li-ion transference number ( $T_{Li^+}$ ) of the polymer electrolyte at different temperatures was measured by a combined measurement of AC impedance and DC polarization method proposed by Bruce *et al.* and Watanabe *et al.* [5, 6] using a symmetric  $Li^+|SPE|Li^+$  cell. The temperature of the cell was controlled by a temperature chamber (Lan technics, Model DHG). The cell was firstly heated to  $70$  °C during 24 h to ensure a good contact between the electrolyte and electrodes. Then, a DC voltage was applied until a steady current was obtained. The impedance spectra of the cell were recorded in the frequency range from  $10^{-2}$  to  $10^6$  Hz with an oscillation voltage of 10 mV, before and after the DC polarization. The value of  $T_{Li^+}$  was calculated by the **Equation 2.1** below:

$$T_{Li^+} = \frac{I_s R_b^s (\Delta V - I_0 R_i^0)}{I_0 R_b^0 (\Delta V - I_s R_i^s)}$$

**Equation 2.1.** Wherein,  $I_0$  and  $I_s$  are the respective initial and steady-state currents,  $R_b^0$  and  $R_b^s$  are the respective initial and final resistances of the bulk electrolytes,  $R_i^0$  and  $R_i^s$  are the respective initial and final resistances of the interfacial layers of the  $Li^+$  electrode/electrolyte and  $\Delta V$  is the applied DC voltage.

### c) Diffusion coefficient

Same procedure as for the Li-ion transference number test was followed. The diffusion coefficient ( $D$ ) of the polymer electrolyte was calculated from the relaxation profile of polarized cells by the **Equation 2.2** proposed by Newman *et al.* [7].

$$a = - \frac{\pi^2}{L^2} D$$

**Equation 2.2.** Wherein,  $a$  is the slope calculated from representing the Napierian logarithm of the voltage vs. time,  $L$  is the thickness of the electrolyte and  $D$  the diffusion coefficient.

### d) Electrochemical stability toward oxidation

The anodic stability of the polymer electrolytes was determined by linear sweep voltammetry (LSV). The measurement was performed in a VMP3 potentiostat (Biologic) using a two electrode cell at 70 °C. Stainless steel was used as working electrode, and Li<sup>o</sup> disk served as both counter and reference electrode. The LSV measurements were performed between the open circuit voltage (OCV) and 6.0 V vs. Li<sup>o</sup>/Li<sup>+</sup> at a scan rate of 1 mV s<sup>-1</sup>.

### e) Electrochemical stability of electrolyte/Li<sup>o</sup> electrode

Li<sup>o</sup> symmetrical coin cells (Li<sup>o</sup>|SPE|Li<sup>o</sup>) were assembled in an argon-filled glove box to investigate the electrochemical stability of electrolyte/Li<sup>o</sup> electrode interphase. For the electrochemical stability test, the Li<sup>o</sup> symmetric cells were kept at 70 °C for 24 h and then cycled galvanostatically at a current density of 0.1 or 0.2 mA cm<sup>-2</sup>, wherein the duration of each half-cycle was 2 h.

### f) Cycling of Li<sup>o</sup> || LiFePO<sub>4</sub> cell performance

The cells were assembled in an argon-filled glovebox using the prepared LFP-based electrodes as cathode, Jeffamine-based or PEO-based membranes as polymer electrolytes and Li metal disk as anode, using a Kapton<sup>®</sup> O-ring spacer when required.

The cycling performances of the Li || LiFePO<sub>4</sub> cells were evaluated using a Maccor or Neware<sup>®</sup> battery testing system. The cells were charged and discharged

in a potential range between 2.5 and 3.7 V at different temperatures using a Vötsch VT 7004 temperature chamber.

## References

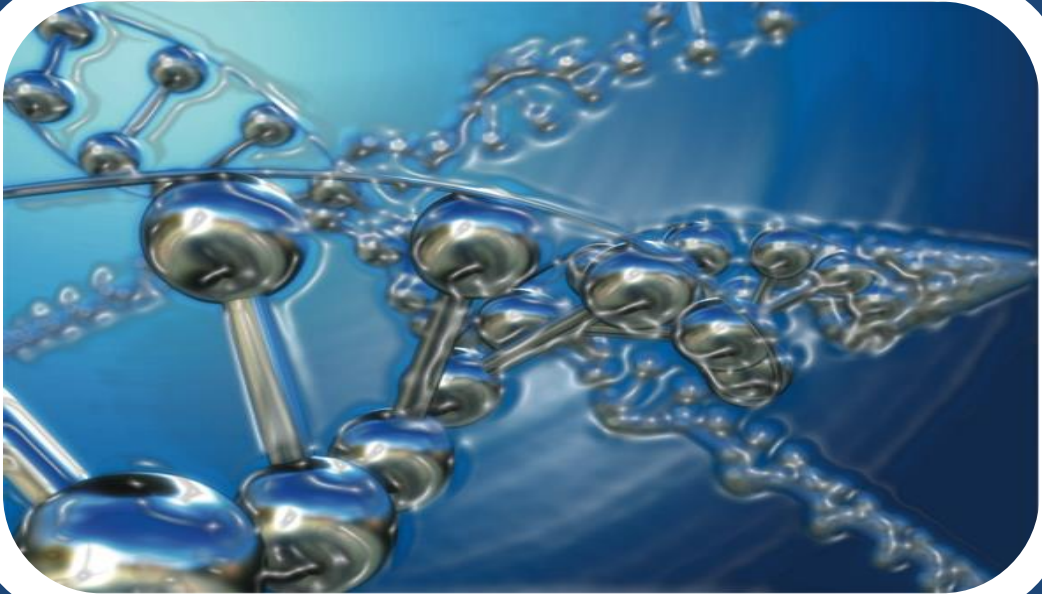
- [1] Y. Zhou, X. Wang, H. Zhu, M. Armand, M. Forsyth, G.W. Greene, J.M. Pringle, P.C. Howlett. *N*-ethyl-*N*-methylpyrrolidinium bis(fluorosulfonyl)imide-electrospun polyvinylidene fluoride composite electrolytes: characterization and lithium cell studies. *Phys. Chem. Chem. Phys.* 2017; **19**(3), 2225-2234.
- [2] X. Wang, H. Zhu, G.W. Greene, Y. Zhou, M. Yoshizawa-Fujita, Y. Miyachi, M. Armand, M. Forsyth, J.M. Pringle, P.C. Howlett. Organic ionic plastic crystal-based composite electrolyte with surface enhanced ion transport and its use in all-solid-state lithium batteries. *Adv. Mater. Technol.* 2017; **2**(7), 1700046.
- [3] Y. Zhou, X. Wang, H. Zhu, M. Yoshizawa-Fujita, Y. Miyachi, M. Armand, M. Forsyth, G.W. Greene, J.M. Pringle, P.C. Howlett. Solid-state lithium conductors for lithium metal batteries based on electrospun nanofiber/plastic crystal composites. *ChemSusChem.* 2017; **10**(15), 3135-3145.
- [4] J.J.L. Brent, S.J. Mulvaney, C. Cohen, J.A. Bartsch. Thermomechanical glass transition of extruded cereal melts. *J. Cereal Sci.* 1997; **26**(3), 301-312.
- [5] J. Evans, C.A. Vincent, P.G. Bruce. Electrochemical measurement of transference numbers in polymer electrolytes. *Polymer.* 1987; **28**(13), 2324-2328.
- [6] M. Watanabe, S. Nagano, K. Sanui, N. Ogata. Estimation of  $\text{Li}^+$  transport number in polymer electrolytes by the combination of complex impedance and potentiostatic polarization measurements. *Solid State Ion.* 1988; **28-30**, 911-917.
- [7] Y. Ma, M. Doyle, T.F. Fuller, M.M. Doeff, L.C. De Jonghe, J. Newman. The measurement of a complete set of transport properties for a concentrated solid polymer electrolyte solution. *J. electrochem. Soc.* 1995; **142**(6), 1859-1868.



## Chapter 3

---

# Jeffamine<sup>®</sup>-based highly conductive solid polymer electrolytes



*I. Aldalur, H. Zhang , M. Piszcz, U. Oteo, L.M. Rodriguez-Martinez, D.Shanmukaraj,T. Rojo, M. Armand, , Journal of Power Sources, 347 (2017) 37-46.*





## Chapter 3:

### JEFFAMINE<sup>®</sup>-BASED HIGHLY CONDUCTIVE SOLID POLYMER ELECTROLYTES

3.1.	Introduction.....	67
3.2.	Synthesis of Jeffamine-based polymer matrix.....	69
3.3.	Chemical characterization.....	71
5.3.1.	Hydrogen-1 nuclear magnetic resonance ( <sup>1</sup> H NMR).....	71
5.3.2.	Attenuated total reflectance-Fourier-transform infrared spectroscopy (ATR-FTIR).....	72
3.4.	Thermal characterization.....	73
3.4.1.	Thermogravimetric analysis (TGA).....	73
3.4.2.	Differential scanning calorimetry (DSC).....	74
3.5.	Ionic conductivity.....	76
3.6.	Conclusions.....	77
	References.....	79



### 3.1. Introduction

The field of lithium-ion batteries (LIBs) is rapidly expanding due to the growing demand of new technologies such as portable electronics, electric vehicles, and stationary large-scale energy storage [1-4]. Despite the lightweight, long lifetime and rapid charge/discharge of this kind of batteries, the use of flammable liquid electrolytes raises strong safety issues. Moreover, the use of graphite electrode results in much lower energy density than the Li metal anode. For this reason the search for rechargeable all-solid-state lithium metal ( $\text{Li}^\circ$ ) batteries (ASSLMBs) has been incentivized [5, 6].

Solid polymer electrolytes (SPEs) are considered as one of the most viable solutions to replace their liquid counterparts [7]. This is mainly motivated by their superior advantages when compared to the liquid electrolytes: 1) the absence of the safety hazards caused by the highly flammable organic solvents utilized in conventional liquid electrolytes [8, 9]; 2) low cost in design and easy processability, being available for a wide variety of fabrication methods in desirable sizes and shapes; and 3) high chemical/electrochemical stability against  $\text{Li}^\circ$ , allowing a stable operation of rechargeable ASSLMBs which theoretically will increase the energy density of the state-of-art LIBs [5, 10]. Moreover, SPEs also outperform inorganic solid electrolytes (ISEs) in terms of processability and electrode/electrolyte interface compatibility due to the flexible nature of polymer network [11-15].

The development of SPEs has been interfered with the pursuit of a compromise between good mechanical properties and high ionic conductivity. Several attempts to improve both properties at the same time have been conducted based on different polymer architectures. However, SPEs with low glass transition temperature ( $T_g$ ) and low crystallinity, essential for high ionic conductivity, can barely form self-standing membranes [16, 17]. The ionic conductivity of salts in poly(ethylene oxide) (PEO) was first reported by Wright in 1973 [18]. Since then, PEO has been one of the most widely used polymer matrices due to its good mechanical properties and the high solvation power provided by ether coordination sites [19, 20]. It has to be mentioned that high molecular weight PEO is a semi-crystalline polymer in which ionic transport occurs mainly in the amorphous phase, where conformational changes of the polymer are thermally restricted. This leads to a low ionic conductivity at temperatures below the melting point ( $T_m$ , *ca.* 65 °C) [21] resulting in PEO-based ASSLMBs operating at

elevated temperatures (70–90 °C) [22, 23]. Besides, the poor quality of the solid electrolyte interphase (SEI) layers formed between PEO-based SPEs and Li metal (Li<sup>o</sup>) electrode leads to an inferior electrochemical performance (*e.g.*, low Coulombic efficiency and short cycle life) of the corresponding ASSLMBs [24].

In order to overcome above-mentioned drawbacks, tremendous efforts have been dedicated to the design and synthesis of novel non-crystalline polymer matrices with low  $T_g$  value [25].

Among numerous chemical modifications, extensive research has been dedicated to copolymers based on poly(ethylene oxide)/poly(propylene oxide) (PEO/PPO) units [26, 27]. It was shown that the incorporation of propylene oxide units (PO) prevents the crystallization of the polymer chains while the good ion solvation properties are not affected. Moreover, the glass transition temperature ( $T_g$ ) is decreased and, as a consequence, the ionic conductivity is increased compared with the electrolytes based only in ethylene oxide (EO) units. On the contrary, polymer electrolytes based mainly on PPO exhibit lower ionic conductivity than PEO based ones [28]. For this reason, the architecture of the copolymer needs to be set with a low fraction of PO units *vs.* EO units in order to prevent the crystallization but at the same time keeping the good solvation power of  $-\text{[OCH}_2\text{CH}_2\text{]}-$  (EO) group.

In 1992, Benrabah *et al.* proposed the use of diamine-poly(oxyethylene-co-oxypropylene) (Jeffamine<sup>®</sup>) compounds as polymer electrolytes, obtaining a fully amorphous PE with low  $T_g$  value and presenting an ionic conductivity in the range of  $10^{-6}$  S cm<sup>-1</sup> at room temperature (RT) [29]. In 2006, completely amorphous polymer matrices based on diamine-terminated Jeffamine<sup>®</sup> with molecular weight  $M_w = 2000$  g/mol were synthesized by Kao *et al.* [30]. In 2010, Brandell *et al.* used Jeffamine T3000 (a trifunctional polyether amine oligomer) to synthesize a polymer electrolyte destined to micro 3D batteries, obtaining a good cell performance as a result [31].

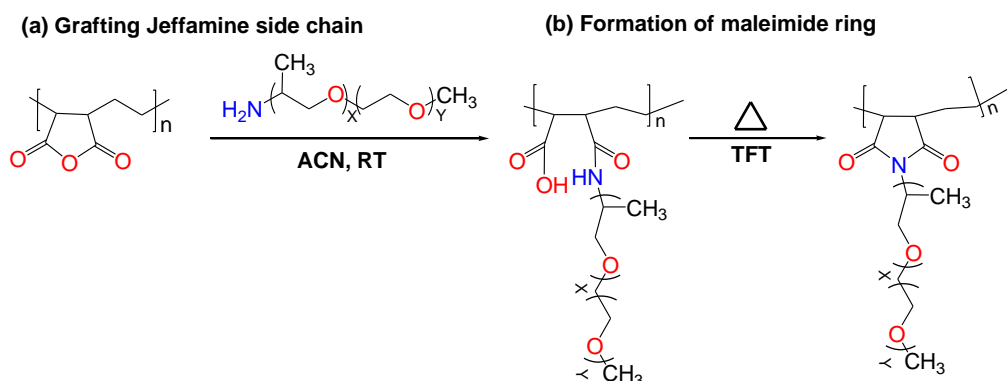
Jeffamine<sup>®</sup> compounds enable the possibility for relatively easy modification of polymer matrices due to their reactive NH<sub>2</sub> end group. Moreover, their low cost and commercial accessibility make them suitable candidates for large-scale synthesis.

In this chapter, a new type of comb-like polymer matrices based on imide ring and Jeffamine® side chains comprising blocks of EO and PO units are reported. The influence of the molecular weight of the side chains and the ratio between EO/PO units in the final products will be studied. Finally, the most suitable polymer matrix for the purpose of this thesis will be selected and defined as the base material for the next chapters. The selection of the best matrix will be conceived in the basis of the following considerations:

- 1) The ratio PO/EO unit needs to ensure low  $T_g$  and high amorphicity in order to favour the high mobility of  $\text{Li}^+$  ions.
- 2) Remarkable adhesion properties to provide a good contact between the electrolyte and the electrode.

### 3.2. Synthesis of Jeffamine-based polymer matrices

#### Reaction for synthesizing Jeffamine based comb-polymer



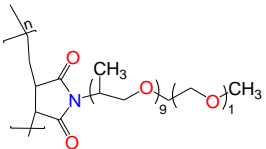

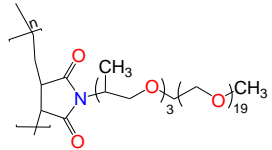

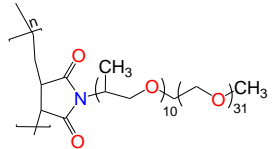

**Scheme 3.1.** Reaction mechanism for synthesizing Jeffamine-based homopolymers.

The solid polymer (SP) matrices were easily obtained by the reaction shown in **Scheme 3.1**. A two steps reaction was followed in an inert atmosphere in order to obtain the polymer matrices. In the first step, 5 mmol of Jeffamine® side chain with amine group as an ending moiety were dissolved in dry acetonitrile (ACN) (mass ratio 1:25). The solution was added dropwise into an equimolar suspension of poly(ethylene-*alt*-maleic anhydride) (PEaMA) in 20 mL of dry ACN. A highly viscous solution was obtained as intermediate product and, for this reason, it was kept under vigorous stirring over 24 h to ensure a good conversion. In the second step, the formation of maleimide ring by thermal treatment was carried

out with a Dean-Stark extraction system using triethylamine (0.3 mL) as catalyst and 50 mL of  $\alpha,\alpha',\alpha''$ -trifluorotoluene (TFT) as solvent.

3 different Jeffamine<sup>®</sup> compounds were used for the synthesis of the polymer matrices; 1) Jeffamine M-600, 2) Jeffamine M-1000 and 3) Jeffamine-M2070 where the number represents the approximate molecular weight of the compound. Each Jeffamine<sup>®</sup> compound is comprised of a different ratio of EO/PO units, giving 3 different polymer matrices with different physical, mechanical and electrochemical properties as a result. These differences are summarized in **Table 3.1**.

**Table 3.1.** Acronyms and corresponding EO/PO units,  $M_w$ , structure and optical image of the as-prepared polymer matrices.

Jeffamine <sup>®</sup> type	Acronym <sup>[a]</sup>	EO/PO <sup>[b]</sup> units	$M_w$ <sup>[c]</sup> / g/mol	Structure after reaction with PEaMA <sup>[d]</sup>	Optical image <sup>[e]</sup>
Jeffamine M-600	SP-600	1/9	600		
Jeffamine M-1000	SP-1k	19/3	1000		
Jeffamine M-2070	SP-2k	31/10	2000		

[a] Acronyms; [b] corresponding EO/PO units ratio; [c] molecular weight of different Jeffamine<sup>®</sup> compounds (g/mol); [d] structure and [e] optical image of the as-prepared polymer matrices.

As it can be observed, Jeffamine M-600 is mainly composed by PO units (EO/PO=1/9), whereas for Jeffamine M-1000 and Jeffamine M-2070 the number of EO units is much higher than PO units. On the other hand, the molecular weight has a great impact on the physical and mechanical properties of the obtained polymer matrices. In the case of Jeffamine M-600 the molecular weight is lower than for the other Jeffamine<sup>®</sup> compounds, obtaining a liquid-like and highly

viscous polymer matrix soluble in different type of organic solvents. On the other hand, for Jeffamine M-2070 and Jeffamine M-1000 rubber-like polymer matrices presenting poor solubility in any kind of solvent are obtained. Polar solvents such as ACN, acetic acid (Ac) or *N,N*-dimethylformamide (DMF) give extensive swelling though. This behaviour could be ascribed to entanglement or internal cross-linking among side chains. However, entanglement seems to be more realistic due to the fact that the shortest chains (SP-600) do not indicate this problem, giving a fully soluble polymer matrix.

### 3.3. Chemical characterization

In order to study the efficiency of imide ring formation and analyse the differences between the 3 polymer matrices, the chemical structures of the Jeffamine-based SP matrices are characterized by <sup>1</sup>H NMR and ATR-FTIR measurements.

#### 3.3.1. Hydrogen-1 Nuclear Magnetic Resonance (<sup>1</sup>H NMR)

The <sup>1</sup>H NMR spectra obtained for the 3 polymer matrices are depicted in **Figure 3.1**. The imide ring closing reaction can be followed by this technique by changes in the signals related to –NH and –OH groups. The imide ring is obtained as final product. This is confirmed by the absence of peaks related to –NH (6–8 ppm) and –OH (13–15 ppm) groups in the final spectra, proving the completion of the reaction between Jeffamine<sup>®</sup> and PEaMA. The peaks at 1.2 and 3.6 ppm, named as **A** and **C** in the spectra, correspond to the protons from –CH<sub>3</sub> and –CH groups of the PO units in Jeffamine<sup>®</sup> side chains, respectively. The peak at 3.4 ppm, marked as **B**, corresponds to the terminal –CH<sub>3</sub> of the EO units of the Jeffamine<sup>®</sup> side chains. Finally, the peak at 3.7 ppm, designated as **D**, corresponds to the protons from –CH groups from the polymer backbone and –CH<sub>2</sub> group from Jeffamine<sup>®</sup> side chains. The spectrum for intermediate product is shown in **Figure A.3.1** as an example.

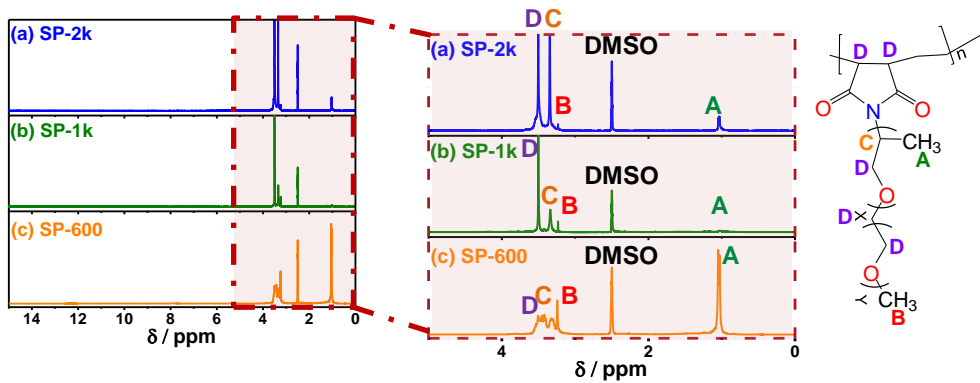
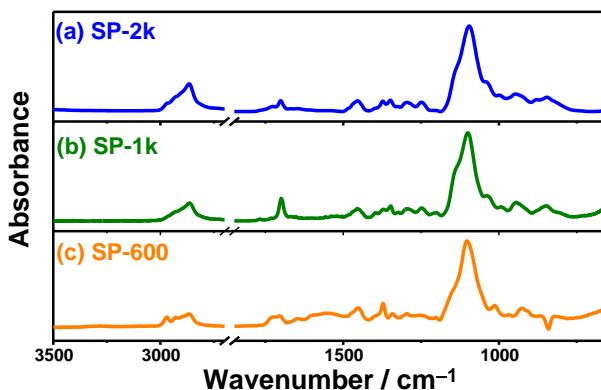


Figure 3.1.  $^1\text{H}$  NMR spectra for the as-prepared polymer matrices.

### 3.3.2. Attenuated total reflectance-Fourier-transform infrared spectroscopy (ATR-FTIR)

The ATR-FTIR spectra for the SP matrices where typical peaks related to polyether chains can be observed in **Figure 3.2**. The imide ring formation cannot be followed by infrared spectroscopy as the stretching and deformation modes from the ring are not detected due to their low intensity and/or because they are overlapped with other signals. However, PO and EO units from Jeffamine<sup>®</sup> side chains give relatively strong bands. The vibration modes originating from C–H<sub>x</sub> bonds are detected in the spectra: stretching mode 2800–3000  $\text{cm}^{-1}$ ; scissoring mode of C–H<sub>2</sub> at 1450  $\text{cm}^{-1}$ ; wagging mode at 1350  $\text{cm}^{-1}$ ; twisting mode at 1250  $\text{cm}^{-1}$  and rocking mode at 950  $\text{cm}^{-1}$ . As it can be observed, with lower molecular weight Jeffamine<sup>®</sup> side chains, which means fewer amount of PO and EO unit content, the intensity of the signals at 2800–3000  $\text{cm}^{-1}$  decreases. The intense peak at 1100  $\text{cm}^{-1}$  is a result from the superposition of C–O–C stretching and C–H<sub>2</sub> bending modes. Finally, the signals at 1700  $\text{cm}^{-1}$  correspond to the carbonyl stretching absorption (C=O) from the poly(maleimide) polymer backbone. The absence of peaks related to –NH and –OH groups at 3400  $\text{cm}^{-1}$  in the final spectra proves the completion of the reaction between Jeffamine<sup>®</sup> and PEaMA.





**Figure 3.2.** ATR-FTIR spectra for the as-prepared polymer matrices.

### 3.4. Thermal characterization

The study of properties such as phase transitions and thermal stability are important to select suitable polymer electrolytes, as these parameters are associated with the Li-ion conductivity and, as a consequence, with the operational temperature of ASSLMs.

#### 3.4.1. Thermogravimetric analysis (TGA)

**Figure 3.3** presents the TGA traces for the as-prepared SP matrices measured under synthetic air flow. All studied polymers are thermally stable up to 250 °C with a 5% mass loss, whereas rapid decomposition appears at around 350 °C. It is known, that thermal stability for polymer chains based on EO and PO units is around 300 °C, showing a dramatic decomposition between 300–350 °C under argon (Ar), and around 220 °C under synthetic air atmosphere [32, 33]. The increase in thermal stability of the synthesized SPs compared to those described in the literature can be attributed to the presence of the imide ring in the polymer backbone, preventing the thermal degradation.

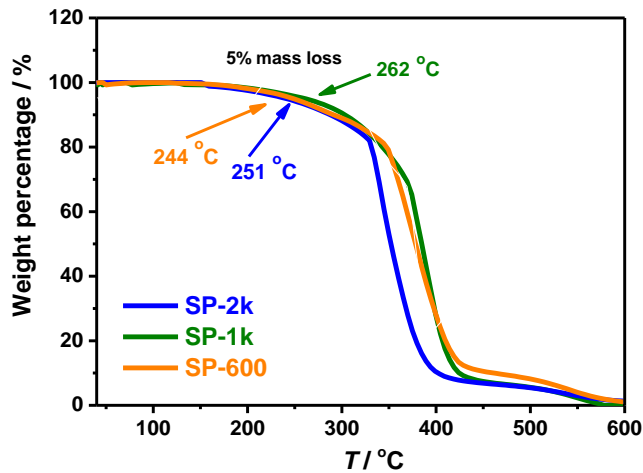


Figure 3.3. Thermal gravimetric analysis (TGA) traces for the as-prepared SP matrices.

### 3.4.2. Differential scanning calorimetry (DSC)

Figure 3.4 compares the obtained DSC traces for the as-prepared SP matrices. The type of Jeffamine<sup>®</sup> has a strong impact in the thermal properties of the polymer matrix, as it can be observed in the thermograms curves. For SP-600 completely amorphous polymer matrix is obtained, whereas SP-2k and SP-1k present a semicrystalline nature. This is attributed to the EO chain blocks crystallizing despite the freedom given by the PO blocks.

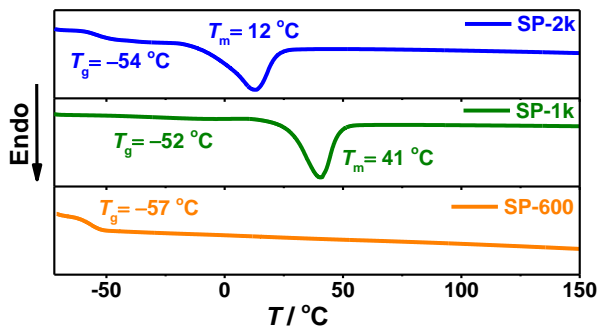


Figure 3.4. Differential scanning calorimetry (DSC) traces for the 3 SP matrices.

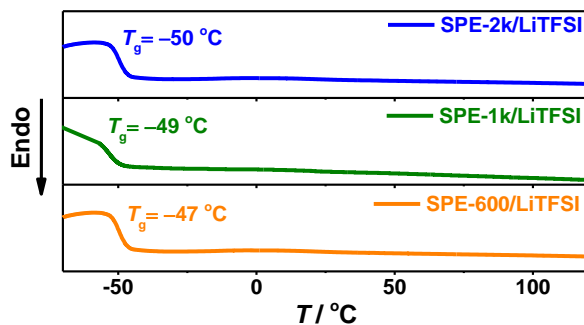
**Table 3.2** summarizes the thermal transitions obtained for the different matrices. All the SPs present low  $T_g$  values between  $-50$  °C and  $-60$  °C, being SP-600 the one presenting the lowest value (*ca.*  $-57$  °C). More interestingly, regarding the melting temperature ( $T_m$ ) of the semicrystalline matrices, the SP-1k presents higher  $T_m$  value [ $40$  °C vs.  $12$  °C] than the SP-2k. Moreover, the quantification of the melting enthalpy proves a higher fraction of crystalline phase in the case of SP-1k than in SP-2k [*e.g.*,  $81.0$  J g $^{-1}$  vs.  $43.5$  J g $^{-1}$ , respectively]. This strongly indicates that the presence of PO block units hinders the crystallization and decreases the melting point of the polymer matrix.

**Table 3.2.** Data summary for the phase behaviour for the as-prepared polymer matrices.

Matrix	EO/PO units	$T_g^a$	$T_m^d$ ( $\Delta H_m^e$ )
SP-2k	31/10	$-54$	$12$ (43.5)
SP-1k	19/3	$-52$	$41$ (81.0)
SP-600	1/9	$-57$	—

[a] Glass transition temperature (°C) taken as the midpoint of the inflexion; [b] Crystallization point (°C) taken as the maximum value of the crystallization peak; [c] Enthalpy of crystallization (J g $^{-1}$ ); [d] Melting point (°C) taken as the maximum value of the melting peak; [e] Enthalpy of melting (J g $^{-1}$ ).

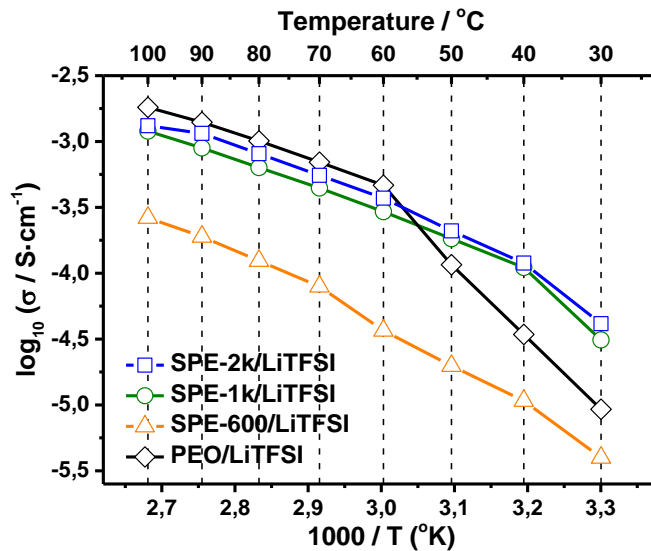
The addition of LiTFSI salt with a molar ratio of EO/LiX = 20 entails amorphism to the SPEs, obtaining fully amorphous electrolytes at RT. **Figure 3.5** presents the thermograms of the measured SPEs, presenting similar  $T_g$  values (*e.g.*,  $-50$  °C for SPE-2k vs.  $-49$  °C for SPE-1k and  $-47$  °C for SPE-600). The suppression of the crystallinity enhances the flexibility of polymer segments, thus facilitating the ionic motion in SPEs.



**Figure 3.5.** Differential scanning calorimetry (DSC) traces for the LiTFSI-based polymer electrolytes with the EO/Li ratio of 20.

### 3.5 Ionic conductivity

The analysis of ionic conductivity is essential as it is one of the key parameters in order to determine the suitability of the polymer electrolytes for their application in ASSLMBs. For this study, LiTFSI was chosen as Li conducting salt and a molar ratio of EO/LiX = 20 was used. **Figure 3.6** shows the temperature dependence of ionic conductivity ( $\sigma$ ) for TFSI-based SPEs and PEO reference electrolyte.



**Figure 3.6.** Temperature dependence of ionic conductivity for the LiTFSI-based polymer electrolytes with the EO/Li ratio of 20.

The reference PEO-based electrolyte displays a non-linear ionic conductivity behaviour due to the melting of the crystalline phase in the temperature ranging from 60 to 70 °C. On the other hand, all the Jeffamine-based SPEs follow a continuous Vogel-Tamman-Fulcher (VTF) behaviour. This performance indicates a fully amorphous nature of the electrolyte in the measured temperature range resulting in a much higher ionic conductivity for SPE-2k and SPE-1k at lower temperatures compared to the reference electrolyte. At an elevated temperature of 70 °C, the ionic conductivities are  $5.2 \times 10^{-4} \text{ S cm}^{-1}$  and  $5.6 \times 10^{-4} \text{ S cm}^{-1}$  for SPE-1k and SPE-2k, respectively, being close to the value for PEO/LiTFSI electrolyte. At a lower temperature of 40 °C, SPE-1k and SPE-2k still

remain highly conductive (*ca.*  $2 \times 10^{-4} \text{ S cm}^{-1}$ ); whereas the conductivity of PEO/LiTFSI drops significantly (*ca.*  $< 10^{-5}$ ), which is ascribed to the crystallization of PEO matrix thereby reducing the conducting amorphous fraction and restricting the conformational changes of EO segments [20].

It can be observed that SPE-2k is slightly more conductive than SPE-1k. This can be ascribed to two facts: 1) SPE-2k presents longer chain obtaining a more flexible side chain and 2) SPE-2k presents lower crystallinity due to the presence of more PO units separating the EO segments from the main chain, decreasing the melting point of the polymer matrix and, as a consequence, increasing the ionic conductivity.

It can be noted that SPE-600 shows lower ionic conductivity than standard PEO/LiTFSI in all measured temperature range. This is in agreement with literature data where PPO based electrolytes exhibit lower conductivity than the ones based on PEO [28]. This behaviour proves that the presence of PO units restricts the mobility of ions due to the steric hindrance of the side methyl group, preventing full solvation of  $\text{Li}^+$ .

### 3.6. Conclusions

A new family of comb-like polymer matrices are presented, where the final product can be easily obtained by a two-steps reaction from cheap and commercially available materials. The comb-like structure guarantees great mechanical properties as elastomer material, whereas the formation of the imide ring improves the thermal stability of the polymer matrix.

The influence of the molecular weight and the number of EO and PO units on the thermal properties and ionic conductivity of the final product has been studied. The synthesized polymer matrices present different mechanical properties depending on the molecular weight of the Jeffamine side chains moving from the liquid-like SP-600 to the elastic and sticky SP-2k matrix. This latter behaviour is ascribed to the entanglement of the chains when increasing the molecular weight and also to the presence of PO units that prevents the crystallization.

It has been proven that a good compromise between EO and PO units is required to obtain a suitable polymer matrix for its application as polymer electrolyte in ASSLMBS. On the one side, when the number of PO is much higher than that of EO units (SP-600), a fully amorphous material is obtained in detriment of the ionic conductivity. On the other side, if the number of EO units is much higher than PO units (SP-1k), a highly conductive polymer matrix is obtained but with an increased crystallinity.

For all these reasons, in this chapter it was concluded that the polymer matrix based on Jeffamine M-2070 is the most suitable for application as polymer electrolyte in ASSLMBS. The good compromise between EO and PO units allows obtaining a polymer matrix with low fraction of crystallinity and a completely amorphous material when a Li salt is added. Moreover, a high ionic conductivity is achieved even at RT due to the high flexibility of the Jeffamine-based side chain. Taking this into account, in the following chapters of this thesis Jeffamine M-2070 will be used as reference material.

## References

- [1] J.M. Tarascon, M. Armand. Issues and challenges facing rechargeable lithium batteries. *Nature*. 2001; **414**(6861), 359-367.
- [2] M. Armand, J.M. Tarascon. Building better batteries. *Nature*. 2008; **451**, 652.
- [3] J.B. Goodenough, Y. Kim. Challenges for rechargeable Li batteries. *Chem. Mater*. 2010; **22**(3), 587-603.
- [4] G.L. Soloveichik. Battery technologies for large-scale stationary energy storage. *Annu. Rev. Chem. Biomol. Eng.* 2011; **2**(1), 503-527.
- [5] J.W. Choi, D. Aurbach. Promise and reality of post-lithium-ion batteries with high energy densities. *Nat. Rev. Mater.* 2016; **1**, 16013.
- [6] J. Janek, W.G. Zeier. A solid future for battery development. *Nat. Energy*. 2016; **1**, 16141.
- [7] V. Di Noto, S. Lavina, G.A. Giffin, E. Negro, B. Scrosati. Polymer electrolytes: present, past and future. *Electrochim. Acta*. 2011; **57**, 4-13.
- [8] G.B. Appetecchi, Y. Aihara, B. Scrosati. Investigation of swelling phenomena in PEO-based polymer electrolytes: II. Chemical and electrochemical characterization. *Solid State Ion*. 2004; **170**(1), 63-72.
- [9] B. Scrosati, J. Garche. Lithium batteries: status, prospects and future. *J. Power Sources*. 2010; **195**(9), 2419-2430.
- [10] W. Xu, J. Wang, F. Ding, X. Chen, E. Nasybulin, Y. Zhang, J.-G. Zhang. Lithium metal anodes for rechargeable batteries. *Energ. Environ. Sci.* 2014; **7**(2), 513-537.
- [11] S.Y. Shen, R.X. Dong, P.T. Shih, V. Ramamurthy, J.J. Lin, K.C. Ho. Novel polymer gel electrolyte with organic solvents for quasi-solid-state dye-sensitized solar cells. *ACS Appl. Mater. Interfaces*. 2014; **6**(21), 18489-18496.
- [12] X. Judez, G.G. Eshetu, C. Li, L.M. Rodriguez-Martinez, H. Zhang, M. Armand. Opportunities for rechargeable solid-state batteries based on Li-intercalation cathodes. *Joule*. 2018; **2**(11), 2208-2224.

[13] H. Huo, N. Zhao, J. Sun, F. Du, Y. Li, X. Guo. Composite electrolytes of polyethylene oxides/garnets interfacially wetted by ionic liquid for room-temperature solid-state lithium battery. *J. Power Sources*. 2017; **372**, 1-7.

[14] H. Huo, J. Sun, C. Chen, X. Meng, M. He, N. Zhao, X. Guo. Flexible interfaces between Si anodes and composite electrolytes consisting of poly(propylene carbonates) and garnets for solid-state batteries. *J. Power Sources*. 2018; **383**, 150-156.

[15] H. Huo, B. Wu, T. Zhang, X. Zheng, L. Ge, T. Xu, X. Guo, X. Sun. Anion-immobilized polymer electrolyte achieved by cationic metal-organic framework filler for dendrite-free solid-state batteries. *Energy Storage Mater.* 2019; **18**, 59-67.

[16] F.B. Dias, L. Plomp, J.B.J. Veldhuis. Trends in polymer electrolytes for secondary lithium batteries. *J. Power Sources*. 2000; **88**(2), 169-191.

[17] J. Rolland, E. Poggi, A. Vlad, J.F. Gohy. Single-ion diblock copolymers for solid-state polymer electrolytes. *Polymer*. 2015; **68**, 344-352.

[18] D.E. Fenton, J.M. Parker, P.V. Wright. Complexes of alkali metal ions with poly(ethylene oxide). *Polymer*. 1973; **14**(11), 589.

[19] M.B. Armand. Polymer electrolytes. *Annu. Rev. Mater. Sci.* 1986; **16**(1), 245-261.

[20] H. Zhang, C. Liu, L. Zheng, F. Xu, W. Feng, H. Li, X. Huang, M. Armand, J. Nie, Z. Zhou. Lithium bis(fluorosulfonyl)imide/poly(ethylene oxide) polymer electrolyte. *Electrochim. Acta*. 2014; **133**, 529-538.

[21] S.J. Kwon, D.G. Kim, J. Shim, J.H. Lee, J.H. Baik, J.C. Lee. Preparation of organic/inorganic hybrid semi-interpenetrating network polymer electrolytes based on poly(ethylene oxide-co-ethylene carbonate) for all-solid-state lithium batteries at elevated temperatures. *Polymer*. 2014; **55**(12), 2799-2808.

[22] S. Lascaud, M. Perrier, A. Vallee, S. Besner, J. Prud'homme, M. Armand. Phase diagrams and conductivity behavior of poly(ethylene oxide)-molten salt rubbery electrolytes. *Macromolecules*. 1994; **27**(25), 7469-7477.

[23] M. Armand. The history of polymer electrolytes. *Solid State Ion*. 1994; **69**(3), 309-319.

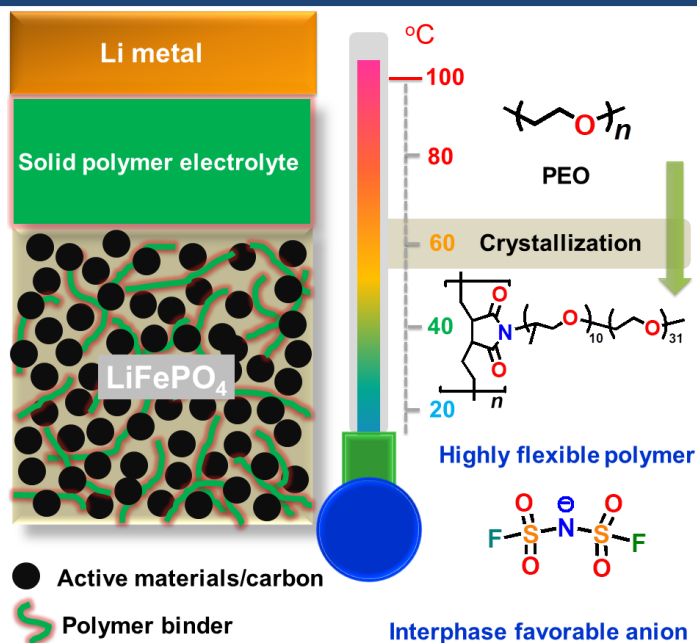


- [24] X. Judez, M. Piszcz, E. Coya, C. Li, I. Aldalur, U. Oteo, Y. Zhang, W. Zhang, L.M. Rodriguez-Martinez, H. Zhang, M. Armand. Stable cycling of lithium metal electrode in nanocomposite solid polymer electrolytes with lithium bis(fluorosulfonyl)imide. *Solid State Ion.* 2018; **318**, 95-101.
- [25] N.A. Stolwijk, C. Heddiar, M. Reschke, M. Wiencierz, J. Bokeloh, G. Wilde. Salt-concentration dependence of the glass transition temperature in PEO–NaI and PEO–LiTFSI polymer electrolytes. *Macromolecules.* 2013; **46**(21), 8580-8588.
- [26] G.G. Cameron, M.D. Ingram, G.A. Sorrie. The mechanism of conductivity of liquid polymer electrolytes. *J. Chem. Soc. Faraday Trans.* 1987; **83**(11), 3345-3353.
- [27] X. Andrieu, J.F. Fauvarque, A. Goux, T. Hamaide, R. M'Hamdi, T. Vicedo. Solid polymer electrolytes based on statistical poly (ethylene oxide-propylene oxide) copolymers. *Electrochim. Acta.* 1995; **40**(13), 2295-2299.
- [28] C. Roux, W. Gorecki, J.Y. Sanchez, M. Jeannin, E. Belorizky. Physical properties of polymer electrolytes: nuclear magnetic resonance investigation and comparison with (PEO)<sub>n</sub>(LiTFSI). *J. Phys. Condens. Matter.* 1996; **8**(38), 7005-7017.
- [29] D. Benrabah, J.Y. Sanchez, M. Armand. New polyamide-ether electrolytes. *Electrochim. Acta.* 1992; **37**(9), 1737-1741.
- [30] H.M. Kao, S.W. Chao, P.C. Chang. Multinuclear solid-state NMR, self-diffusion coefficients, differential scanning calorimetry, and ionic conductivity of solid organic–inorganic hybrid electrolytes based on PPG–PEG–PPG diamine, siloxane, and lithium perchlorate. *Macromolecules.* 2006; **39**(3), 1029-1040.
- [31] S. Tan, S. Walus, J. Hilborn, T. Gustafsson, D. Brandell. Poly(ether amine) and cross-linked poly(propylene oxide) diacrylate thin-film polymer electrolyte for 3D-microbatteries. *Electrochem. Commun.* 2010; **12**(11), 1498-1500.
- [32] T. Shodai, B.B. Owens, H. Ohtsuka, J.I. Yamaki. Thermal stability of the polymer electrolyte (PEO)<sub>8</sub>LiCF<sub>3</sub>SO<sub>3</sub>. *J. Electrochem. Soc.* 1994; **141**(11), 2978-2981.
- [33] S. Han, C. Kim, D. Kwon. Thermal/oxidative degradation and stabilization of polyethylene glycol. *Polymer.* 1997; **38**(2), 317-323.



## Chapter 4

# Lowering the operational temperature of all-solid-state lithium metal batteries with highly conductive solid polymer electrolytes



I. Aldalur, M. Martinez-Ibañez, M. Piszcz, L.M. Rodriguez-Martinez, H. Zhang, M. Arman. Lowering the operational temperature of all-solid-state lithium metal batteries with highly conductive and interfacially robust solid polymer electrolytes. *Journal of Power Sources*, 383(2018) 144-149.

The first part of the document discusses the importance of maintaining accurate records of all transactions. This includes not only sales and purchases but also any other financial activities that may occur. It is essential to ensure that all entries are properly documented and supported by appropriate evidence.

In addition, the document emphasizes the need for regular reconciliation of accounts. This process involves comparing the company's internal records with the bank statements to identify any discrepancies. By doing so, the company can ensure that its financial statements are accurate and reliable.

Another key aspect of financial management is the timely payment of bills and invoices. Failure to do so can result in late fees, penalties, and damage to the company's credit rating. Therefore, it is crucial to establish a system for tracking and paying all obligations on time.

Finally, the document highlights the importance of maintaining a clear and concise record of all financial transactions. This record should be easily accessible and understandable to all relevant parties. By doing so, the company can ensure that its financial information is transparent and trustworthy.

## Chapter 4:

# LOWERING THE OPERATIONAL TEMPERATURE OF ALL-SOLID-STATE LITHIUM METAL BATTERIES WITH HIGHLY CONDUCTIVE SOLID POLYMER ELECTROLYTES

4.1.	Introduction.....	87
4.2.	Solid polymer electrolyte preparation.....	89
4.3.	Chemical characterization.....	90
4.4.	Morphological characterization.....	91
4.5.	Thermal characterization.....	92
4.5.1.	Thermogravimetric analysis (TGA).....	92
4.5.2.	Differential scanning calorimetry (DSC).....	93
4.6.	Electrochemical characterization.....	95
4.6.1.	Ionic conductivity.....	95
4.6.2.	Li-ion transference number.....	97
4.6.3.	Diffusion coefficient.....	98
4.6.4.	Electrochemical stability toward oxidation.....	99
4.6.5.	Compatibility with Li <sup>o</sup> electrode.....	100
4.6.6.	Cycling of Li <sup>o</sup>   LiFePO <sub>4</sub> cell performance.....	104
4.6.6.1.	LiTFSI-based cells.....	104
4.6.6.2.	LiFSI-based cells.....	107
4.7.	Conclusions.....	111
	References.....	112



## 4.1. Introduction

Currently there is no commercial solution of solvent free all-solid-state lithium metal batteries (ASSLMBs) operating at room temperature (RT). The main reasons are: low ionic conductivity of solid polymer electrolytes (SPEs) and poor interfacial compatibility with electrode materials, especially vs. lithium ( $\text{Li}^\circ$ ) anode. In this regards, tremendous efforts have been devoted to the design and synthesis of polymer matrices, aiming at preparing non-crystalline and low glass transition polymers [1-3]. Ionic transportation of SPEs is generally coupled with segmental motion of polymer segments in the amorphous phases, *i.e.*, the lower crystallinity and glass transition temperature ( $T_g$ ), results in higher ionic conductivity [4]. However, as it was shown in **Chapter 3**, it is not always a guarantee of high ionic conductivity. Other factors such as high dielectric constant, optimal  $\text{Li}^+$  dissociation and fast interchain transfer are fundamental for rapid ion transport [5].

The role of polymers in solid-state batteries is essential for their proper operation not only as electrolyte, but also as the binder of the positive electrode in  $\text{Li}^\circ$  based cells. As it is known, the compatibility of the cathode with the electrolyte is critical for the good electrochemical performance of the battery in order to guarantee the free movement of the migrating ions between them. For this reason, polymer electrolytes have been implemented as binders in cathode materials for all-solid-state batteries. Polymers used as binders in cathode materials need to provide distinctive features: 1) high bonding strength between the current collector and cathode components, 2) broad range of physical and electrochemical stability, 3) low resistance and, finally, 4) volume buffering properties for expansion/shrinkage of active material [6, 7].

As it was discussed in **Chapter 1**, the incorporation of different type of salts is critical for improving transport properties of SPEs [5, 8]. Lithium bis(trifluoromethanesulfonyl)imide ( $\text{LiTFSI}$ ) has been one of the most widely studied conducting salt owing to the sulfonimide  $-\text{[SO}_2\text{-N-SO}_2\text{]}-$  group [4, 9, 10]. The high flexibility of this group enhances the ionic conductivity by reducing the crystallinity of the polymer matrix due to the plasticizing effect. Moreover, the outstanding thermal and electrochemical stability of this salt, as well as the highly delocalized charge distribution promoting the dissociation of  $\text{Li}^+$  cation due to the flexible S-N bond make this salt suitable for developing reliable SPEs for  $\text{Li}^\circ$ -based

batteries [11]. In recent years, lithium bis(fluorosulfonyl)imide (LiFSI), a lighter analogue of LiTFSI, has been widely studied due to the improved compatibility with various electrodes, *e.g.*, lithium iron phosphate (LiFePO<sub>4</sub>, LFP) cathodes [12] and Li<sup>o</sup> electrode [13, 14]. This enhanced stability with Li<sup>o</sup> anode is attributed to the formation of LiF-rich solid electrolyte interphase (SEI) layer resulting in a stable cycling performance [11, 15].

Highly conductive, electronic insulating, and stable interfacial layers on both Li<sup>o</sup> and cathode sides are desired for obtaining good cycling performance of ASSLMs [16-18]. This implies that SPEs should afford not only high ionic conductivity but also good electrochemical compatibility with electrode materials, which is supported by the fact that most of the SPEs-based cells exhibit efficient cycling only at elevated temperatures (*e.g.*, 70 °C) due to the lack of good chemical /electrochemical compatibility of electrolyte/electrode interphases at RT. In addition, the problem of internal contact of the active materials within composite cathode will be magnified when operating the SPEs-based ASSLMs at lower temperature even at low C-rates, due to the increased cell resistance upon decreasing the temperature. The high polarization of the cell can result in the decomposition of the polymer matrix and/or the lithium salt, ruining the binding properties and losing the active material from the cathode [19]. Thus, the binders herein SPEs themselves with good ionic conductivity, stability, mechanical strength and good adhesive properties in a broad temperature range are crucial for improving the cycle life of lithium-ion batteries (LIBs) [19, 20].

In this chapter, synthesized Jeffamine M-2070 based super soft polymer matrix and sulfonimide salts (*i.e.*, LiTFSI and LiFSI) are presented with the aim of improving the interfacial compatibility with electrodes and decrease the operational temperature of polymer-based ASSLMs. For this purpose, different concentrations of Li salt were used in order to determine the optimum ethylene oxide (EO)/Li ratio in order to obtain fully amorphous, highly conductive and electrochemically stable SPEs for battery application.



## 4.2. Solid polymer electrolyte preparation

In order to prepare the SPEs, the polymer matrix SP-2k described in **Chapter 3**, which contains 31 units of EO and 10 units of propylene oxide (PO), was used.

A set of different SPEs were prepared using LiTFSI and LiFSI as lithium salts with different EO/Li molar ratios and compared with poly(ethylene oxide) (PEO)-based reference electrolytes. All the materials are summarized in **Table 4.1**.

**Table 4.1.** Abbreviations and corresponding composition of the as-prepared polymer matrices and electrolytes.

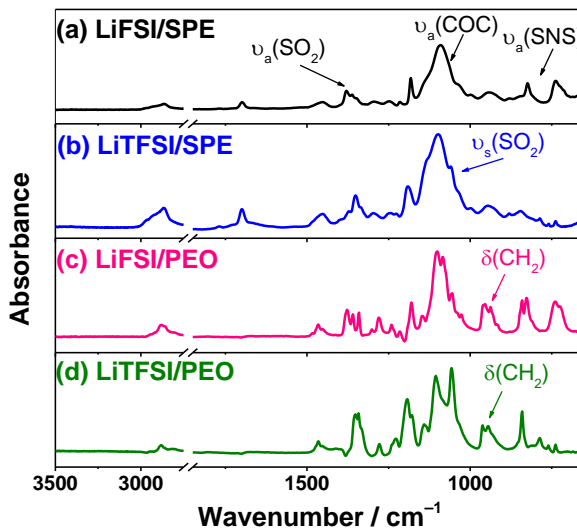
Acronym	Polymer matrix <sup>[a]</sup>	EO/Li <sup>[b]</sup>
<b>SP</b>	<b>Solid Jeffamine homopolymer</b>	–
<b>LiFSI/SPE</b>	<b>Solid Jeffamine homopolymer</b>	<b>20</b>
LiFSI/SPE(1#)	Solid Jeffamine homopolymer	10
LiFSI/SPE(2#)	Solid Jeffamine homopolymer	15
LiFSI/SPE(3#)	Solid Jeffamine homopolymer	20
LiFSI/SPE(4#)	Solid Jeffamine homopolymer	30
LiFSI/SPE(5#)	Solid Jeffamine homopolymer	50
<b>LiTFSI/SPE</b>	<b>Solid Jeffamine homopolymer</b>	<b>20</b>
LiTFSI/SPE(1#)	Solid Jeffamine homopolymer	10
LiTFSI/SPE(2#)	Solid Jeffamine homopolymer	15
LiTFSI/SPE(3#)	Solid Jeffamine homopolymer	20
LiTFSI/SPE(4#)	Solid Jeffamine homopolymer	30
LiTFSI/SPE(5#)	Solid Jeffamine homopolymer	50
<b>LiFSI/PEO</b>	<b>PEO</b>	<b>20</b>
<b>LiTFSI/PEO</b>	<b>PEO</b>	<b>20</b>

[a] Synthesized new polymer matrix based on Jeffamine M-2070 has been named as solid Jeffamine homopolymer. [b] The molar ratio of EO/Li.

### 4.3. Chemical characterization

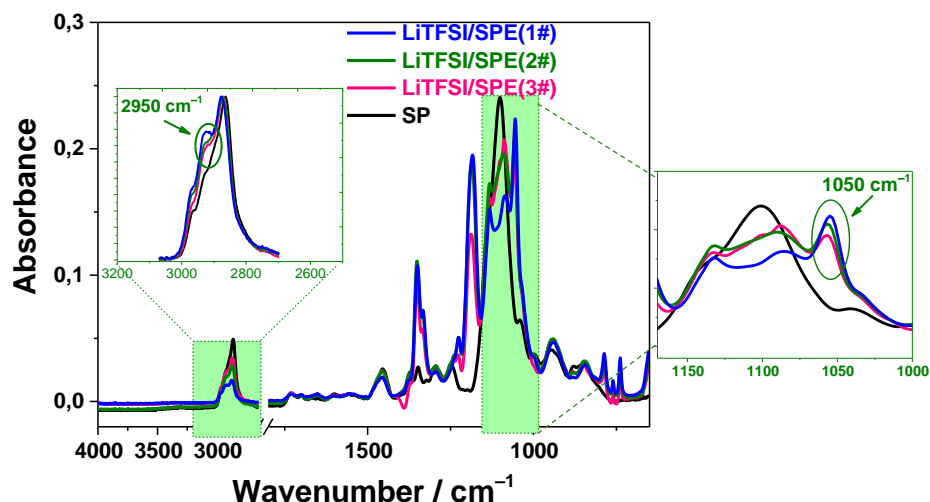
Infrared spectroscopy was used to determine the interaction between the Li ion and the polymer matrix.

The attenuated total reflectance-Fourier-transform infrared spectroscopy (ATR-FTIR) spectra obtained for Jeffamine-based SPEs and PEO reference electrolytes with a salt ratio EO/Li = 20 are shown in **Figure 4.1**. Characteristic signals assigned to TFSI<sup>-</sup> appear at  $\sim 1380\text{ cm}^{-1}$  and  $\sim 1130\text{ cm}^{-1}$  (asymmetric ( $\nu_a$ ) and symmetric ( $\nu_s$ ) stretching of SO<sub>2</sub>), respectively;  $1060\text{ cm}^{-1}$  and  $761\text{ cm}^{-1}$  ( $\nu_a$  and  $\nu_s$  (SNS)), respectively [21]. Signals assigned to FSI<sup>-</sup> appear at  $\sim 1370\text{ cm}^{-1}$  ( $\nu_a$  (SO<sub>2</sub>)),  $1235\text{--}1150\text{ cm}^{-1}$  ( $\nu_s$ (SO<sub>2</sub>)),  $890\text{--}850\text{ cm}^{-1}$  ( $\nu_a$  (SNS)), and  $\sim 740\text{ cm}^{-1}$  ( $\nu_s$  (SNS) and  $\nu_s$  (SF)) [22]. On the other hand, the characteristic signals for PEO-based electrolytes appear at  $1470\text{--}1450\text{ cm}^{-1}$  (CH<sub>2</sub> scissoring deformation ( $\delta_s$ )),  $1270\text{ cm}^{-1}$  (CH<sub>2</sub> twisting ( $\tau$ )),  $\sim 1100\text{ cm}^{-1}$  ( $\nu_a$  (COC)), and  $980\text{--}990\text{ cm}^{-1}$  (CH<sub>2</sub> rocking ( $\rho$ )) [23]. The sharp nature of these peaks indicates the presence of crystalline phase in PEO-based electrolytes. However, the broad signals in the ATR-FTIR spectra of Jeffamine based SPEs suggest the amorphous nature of the electrolytes. The characteristic signals for the Jeffamine-based polymer matrices were discussed in **Chapter 3**.



**Figure 4.1.** ATR-FTIR spectra of the prepared four electrolytes: **a)** LiFSI/SPE, **b)** LiTFSI/SPE, **c)** LiFSI/PEO and **d)** LiTFSI/PEO.

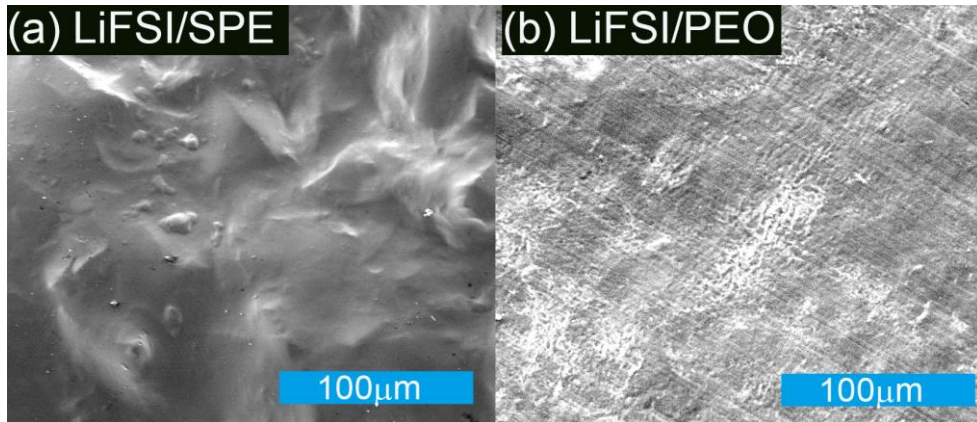
On the other hand, the interaction between Li ions and the polymer matrix can be followed by this technique, as it has been displayed in **Figure 4.2** where the electrolytes ranging from EO/Li= 10 to EO/Li= 20 have been compared with the SP matrix. This interaction can be studied observing the changes in the peak at  $2950\text{ cm}^{-1}$  and  $1100\text{ cm}^{-1}$ . As it can be observed, with increasing salt concentration the intensity of these peaks increase, proving the wrapping of Li ions by polymer chain.



**Figure 4.2.** ATR-FTIR spectra of some of the as-prepared electrolytes using LiTFSI as lithium salt.

#### 4.4. Morphological characterization

The polymer electrolytes were prepared by conventional solvent casting method, obtaining a self-standing membrane in the case of LiFSI/PEO electrolyte and a very elastic and sticky polymer in the case of LiFSI/SPE. Scanning electron microscopy (SEM) imaging was carried out in order to study the morphology of both polymer electrolytes. As it can be observed in **Figure 4.3**, LiFSI/PEO membrane shows a more homogeneous surface, whereas LiFSI/SPE based electrolyte presents higher roughness which could be ascribed to lumps due to the entanglement of the polymer chains.



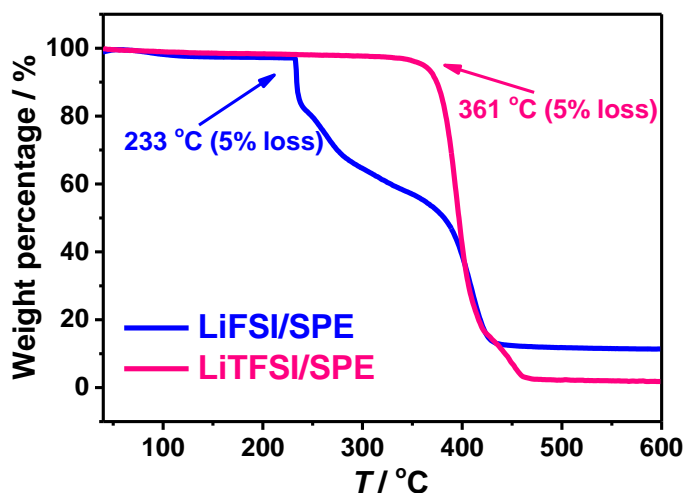
**Figure 4.3.** SEM images of the surface morphology for **a)** LiFSI/SPE and **b)** LiFSI/PEO electrolytes.

#### 4.5. Thermal characterization

The study of the phase transitions is of great importance in order to establish the operational temperature of ASSLMBs. Moreover, phase transitions, including  $T_g$ , allow to determine the materials that will present high ionic motion in solid polymer electrolytes. This feature is crucial for screening the suitability of the electrolytes for their application in ASSLMBs.

##### 4.5.1. Thermogravimetric analysis (TGA)

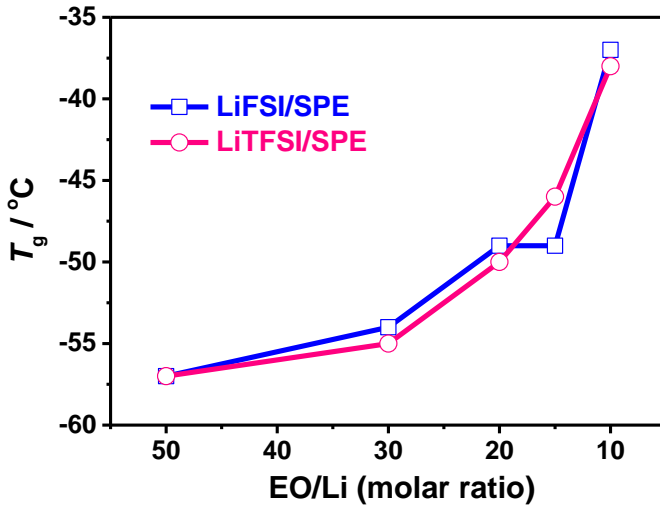
**Figure 4.4** shows the TGA traces of LiFSI/SPE and LiTFSI/SPE samples. Both electrolytes are thermally stable up to 200 °C, which is much higher than the operational temperature of ASSLMBs. Compared to LiTFSI/SPE, the LiFSI/SPE one shows a lower value of decomposition temperature ( $T_d$ ), and presents two distinct steps of degradation. The first one is associated with the decomposition of FSI<sup>-</sup> anion at *ca.* 230 °C that releases fluorinated residues leading to the decomposition of Jeffamine-side chains and, the second one, related to the polymer matrix at *ca.* 350 °C. This is in accordance with lower thermal stability of the neat LiFSI salt [*i.e.*,  $T_d = 200$  °C (without mass loss) and  $T_d = 312$  °C (5% mass loss) for LiFSI [24] vs.  $T_d = 384$  °C (5% mass loss) for LiTFSI [23, 25]].



**Figure 4.4.** Thermogravimetric analysis traces for the LiFSI/SPE and LiTFSI/SPE with the EO/Li ratio of 20.

#### 4.5.2. Differential scanning calorimetry (DSC)

**Figure 4.5** shows the  $T_g$  of LiFSI/SPEs and LiTFSI/SPEs with various salt concentrations. Phase transition temperatures are summarized in **Table 4.2** and DSC traces are shown in **Figure A.4.1**. The values of  $T_g$  for both LiFSI/SPE and LiTFSI/SPE are slightly lower than those of PEO-based ones (e.g.,  $T_g = -49$  °C (LiTFSI/SPE) vs.  $T_g = -45$  °C (LiTFSI/PEO) [15] for the molar ratio of EO/Li = 20), suggesting a higher degree of flexibility for Jeffamine-based matrices. The neat Jeffamine-based polymer matrix shows a glass transition at  $-54$  °C and a melting point at  $12$  °C, as it was shown in **Chapter 3**. The addition of an even low amount of lithium salt (*i.e.*, EO/Li above 20) entails amorphism of the SPEs, obtaining a fully amorphous matrix at RT (**Figure A.4.1**). This is ascribed to the plasticizing effect of the lithium salt into the polymer matrix. The salt breaks the crystalline phase of the polymer host by the interaction of Li cations with EO units. This interaction restricts the freedom of conformational movements and can lead to an increase of  $T_g$ . However the S–N–S bond in the anion is able to rotate and provides a high plasticizing effect. Comparing the effect of the type of Li salt added, no differences are found, the same tendency is obtained for both LiFSI and LiTFSI.



**Figure 4.5.** Glass transition temperature ( $T_g$ ) of the prepared electrolytes with various salt concentrations.

**Table 4.2.** The characterization data for the phase behavior for the as-prepared electrolytes.

Samples	EO/Li	$T_g$ [a]	$T_c$ [b] ( $\Delta H_c$ ) [c]	$T_m$ [d] ( $\Delta H_m$ ) [e]
LiFSI/SPE	50	-58	-26 (21.9)	4 (22.4)
	30	-54	-13 (5.5)	7 (4.6)
	20	-49		
	15	-48		
	10	-37		
LiTFSI/SPE	50	-58	-28 (21.9)	4 (25.6)
	30	-56	-14 (3.3)	6 (3.8)
	20	-50		
	15	-46		
	10	-38		
LiFSI/PEO	20	-47	3 (0.8)	63 (67)
LiTFSI/PEO	20	-45		65 (50)

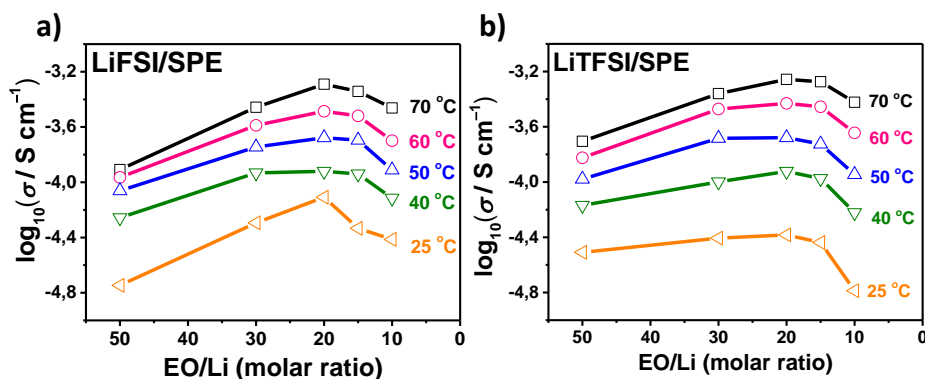
[a] Glass transition temperature ( $^{\circ}\text{C}$ ) taken as the midpoint of the inflexion. [b] Crystallization point ( $^{\circ}\text{C}$ ) taken as the maximum value of the crystallization peak. [c] Enthalpy of crystallization ( $\text{J g}^{-1}$ ). [d] Melting point ( $^{\circ}\text{C}$ ) taken as the maximum value of the melting peak. [e] Enthalpy of melting ( $\text{J g}^{-1}$ ).

## 4.6 Electrochemical characterization

The study of properties such as ionic conductivity, Li-ion transference number, diffusion coefficient, electrochemical stability toward oxidation and compatibility with  $\text{Li}^\circ$  electrode is essential as these parameters will determine the suitability of the polymer electrolytes for their application in ASSLMBs.

### 4.6.1 Ionic conductivity

**Figure 4.6** presents the logarithm of ionic conductivity ( $\sigma$ ) at different temperatures vs. the concentration of lithium salt (EO/Li ratio). Both LiFSI/SPE and LiTFSI/SPE show the same dependency upon increasing the salt concentration, and the highest ionic conductivities are obtained with a molar ratio of EO/Li = 20 in all the measured temperatures.



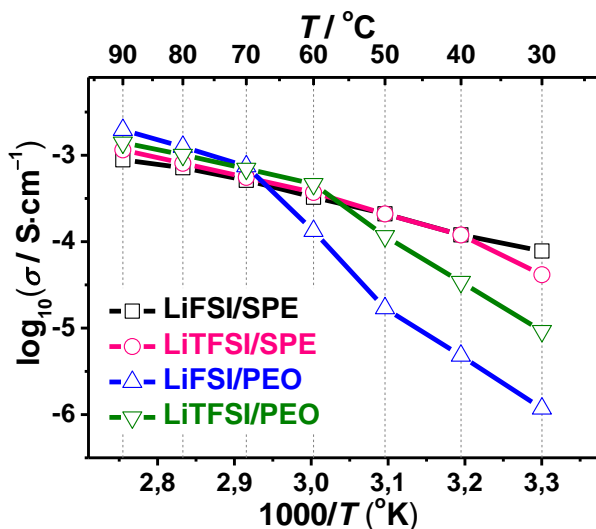
**Figure 4.6.** Conductivity dependence of salt concentration at different temperatures for **a)** LiFSI/SPE and **b)** LiTFSI/SPE.

**Figure 4.7** shows the temperature dependence of ionic conductivity ( $\sigma$ ) for both the TFSI<sup>-</sup> and FSI<sup>-</sup> based SPEs, as well as for PEO-based reference electrolytes. In all cases a molar ratio of EO/Li(X) = 20 (X = TFSI, FSI) was used as both LiFSI/SPE and LiTFSI/SPE show the same dependency upon increasing the salt concentration, and the highest ionic conductivities are obtained with this molar ratio. This is ascribed to the optimal transient interaction between  $\text{Li}^+$  and ether units, where higher number of ions does not result in higher ionic conductivity. When high amount of salt is added (*ca.* EO/LiX = 10), there is an increase in the viscosity and, as a consequence, the ionic mobility decreases due to the local

restriction of conformational movements of EO units. This is supported by the increase in the  $T_g$  value, as it was observed in **Figure 4.5**.

The reference PEO-based electrolytes display non-linear ionic conductivity behaviour due to the melting of the crystalline phase in the temperature ranging from 60 to 70 °C, whereas all the Jeffamine-based SPEs follow a continuous Vogel-Tamman-Fulcher (VTF) behaviour, indicating a fully amorphous nature of the electrolytes in the measured temperature range. This is in accordance with the results obtained for the DSC study where Jeffamine-based electrolytes are free from thermal changes in the temperature range of the conductivity test.

At an elevated temperature of 70 °C, the ionic conductivities are  $5.3 \times 10^{-4}$  S cm<sup>-1</sup> and  $5.6 \times 10^{-4}$  S cm<sup>-1</sup> for LiFSI/SPE and LiTFSI/SPE, respectively, being close to the values for PEO/LIFSI and PEO/LiTFSI electrolytes. At a lower temperature of 40 °C, Jeffamine-based SPEs still remain highly conductive (*ca.*  $2 \times 10^{-4}$  S cm<sup>-1</sup>); whereas the conductivity of PEO-based electrolytes drops significantly ( $<10^{-5}$  S cm<sup>-1</sup> for LiTFSI/PEO and  $<10^{-6}$  S cm<sup>-1</sup> for LiFSI/PEO), which is ascribed to the crystallization of PEO matrix and thereby reducing the fraction of highly conducting amorphous phase and the conformational changes of EO segments in close vicinity of the crystalline phase [11].



**Figure 4.7.** Arrhenius plots for the LiFSI/SPE and LiTFSI/SPE, as well as for the reference electrolytes LiFSI/PEO and LiTFSI/PEO with the EO/Li(X) = 20 (X = TFSI, FSI).



#### 4.6.2 Li-ion transference number

The Li-ion transference number ( $T_{Li}^+$ ) of the TFSI- and FSI-based SPEs and PEO reference electrolytes were measured and the calculated values have been summarized in **Table 4.3**. The contribution of Li-ion to the total ionic conductivity is quantified by the  $T_{Li}^+$  value and was measured using the method described in **Chapter 2** section 2.4.5 [21, 26]. In order to study the dependency of  $T_{Li}^+$  with the temperature, LiFSI/SPE was selected as an example. The results suggest a negligible difference with the variation of temperature (*e.g.*,  $T_{Li}^+ = 0.16$  at both 70 °C and 40 °C).

**Table 4.3.** The calculated values of Li-ion transference number ( $T_{Li}^+$ ) of various electrolytes with the same EO/Li ratio of 20 at different temperatures.

Electrolyte	EO/Li	$T_C^{[a]}$	$I_0^{[b]}$ μA	$I_S^{[c]}$ μA	$R_{b[d]}^0$ Ω	$R_{b[e]}^s$ Ω	$R_{i[f]}^0$ Ω	$R_{i[g]}^s$ Ω	$\Delta V^{[h]}$ mV	$T_{Li}^{+[i]}$
<b>LiFSI/SPE</b>										
	20	70	13	3	452	445	785	848	10	0.16
	20	60	28	5	410	392	281	271	10	0.15
	20	50	7	2	1510	1550	750	760	10	0.16
	20	40	4	1	2875	2920	1150	1180	10	0.16
<b>LiTFSI/SPE</b>										
	20	70	43	8	101	92	61	81	10	0.14
	15	70							10	0.25
	10	70							10	0.38
<b>LiFSI/PEO</b>										
	20	70	32	15	33	33	257	258	10	0.13
<b>LiTFSI/PEO</b>										
	20	70	23	12	30	31	360	364	10	0.17

[a] Temperature at which the measurement was performed; [b] Initial and [c] steady-state current obtained by dc polarization; [d] initial and [e] final resistances of the electrolytes measured by ac impedance method before and after polarization, respectively; [f] initial and [g] final resistances of interfacial layer between electrode/electrolyte measured by ac impedance method before polarization and after polarization, respectively; [h] the dc voltage subjected to the  $Li^+$  symmetric cell; [i] calculated values of Li-ion transference number.

In terms of salt type, the obtained results (*ca.* 0.15) suggest an insignificant difference between the measured samples with the same EO/Li ratio for both LiTFSI and LiFSI, presenting typical  $T_{\text{Li}}^+$  values for salt-in-polymer systems.

Regarding the salt concentration, the  $T_{\text{Li}}^+$  value increases with increasing salt concentration, indicating a lower interaction between the Li cation and the polymer matrix. However, reverse tendency can be found in literature for polymers containing EO and PO units where lower  $T_{\text{Li}}^+$  values are obtained for higher salt concentrations [27]. This behaviour can be attributed to the polymer structure where PO units are bonded to the rigid polymer backbone based on imide rings. At low salt concentrations, Li-ions are selectively coordinated with EO units. However, when the salt loading is increased all EO units are saturated by Li salt and, as a consequence, PO units bonded to rigid polymer backbone are not able to distribute the salt groups due to their low dielectric constant and steric hindrance.

#### 4.6.3 Diffusion coefficient

**Table 4.4.** The calculated values of diffusion coefficient ( $D$ ) of various electrolytes with EO/Li ratio of 20 at different temperatures.

Electrolyte	EO/Li	T / °C <sup>[a]</sup>	D / cm <sup>2</sup> s <sup>-1</sup> <sup>[b]</sup>
LiFSI/SPE	20	70	$4.1 \times 10^{-7}$
	20	60	$3.6 \times 10^{-7}$
	20	50	$3.1 \times 10^{-7}$
	20	40	$2.9 \times 10^{-7}$
LiTFSI/SPE	20	70	$3.7 \times 10^{-7}$
LiFSI/PEO	20	70	$5.2 \times 10^{-8}$
LiTFSI/PEO	20	70	$4.3 \times 10^{-8}$

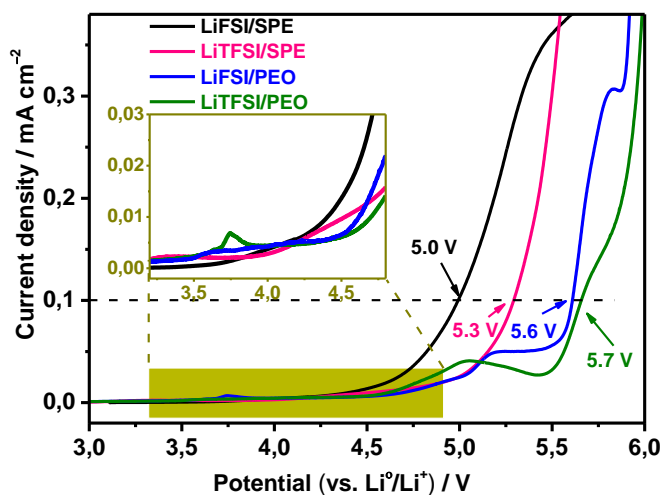
[a] Temperature at which the measurement was performed; [b] calculated values of diffusion coefficient.

The diffusion coefficient ( $D$ ) of the TFSI- and FSI-based SPEs and PEO reference electrolytes were measured and the calculated values have been summarized in **Table 4.4**. As it can be observed, the  $D$  values obtained for LiFSI-based electrolytes are slightly higher than the corresponding  $D$  values for TFSI-based ones. This can be ascribed to the lower resistivity of the interfacial layer vs. Li electrode. Even though it decreases slightly with decreasing temperature,

LiFSI/SPE can retain the value of  $2.9 \times 10^{-7} \text{ cm}^2 \text{ s}^{-1}$  at  $40^\circ\text{C}$ . Moreover,  $D$  values for Jeffamine-based SPEs are one order of magnitude higher than the ones for PEO, proving that the ion mobility is higher when the viscosity of the polymer is lower.

#### 4.6.4 Electrochemical stability toward oxidation

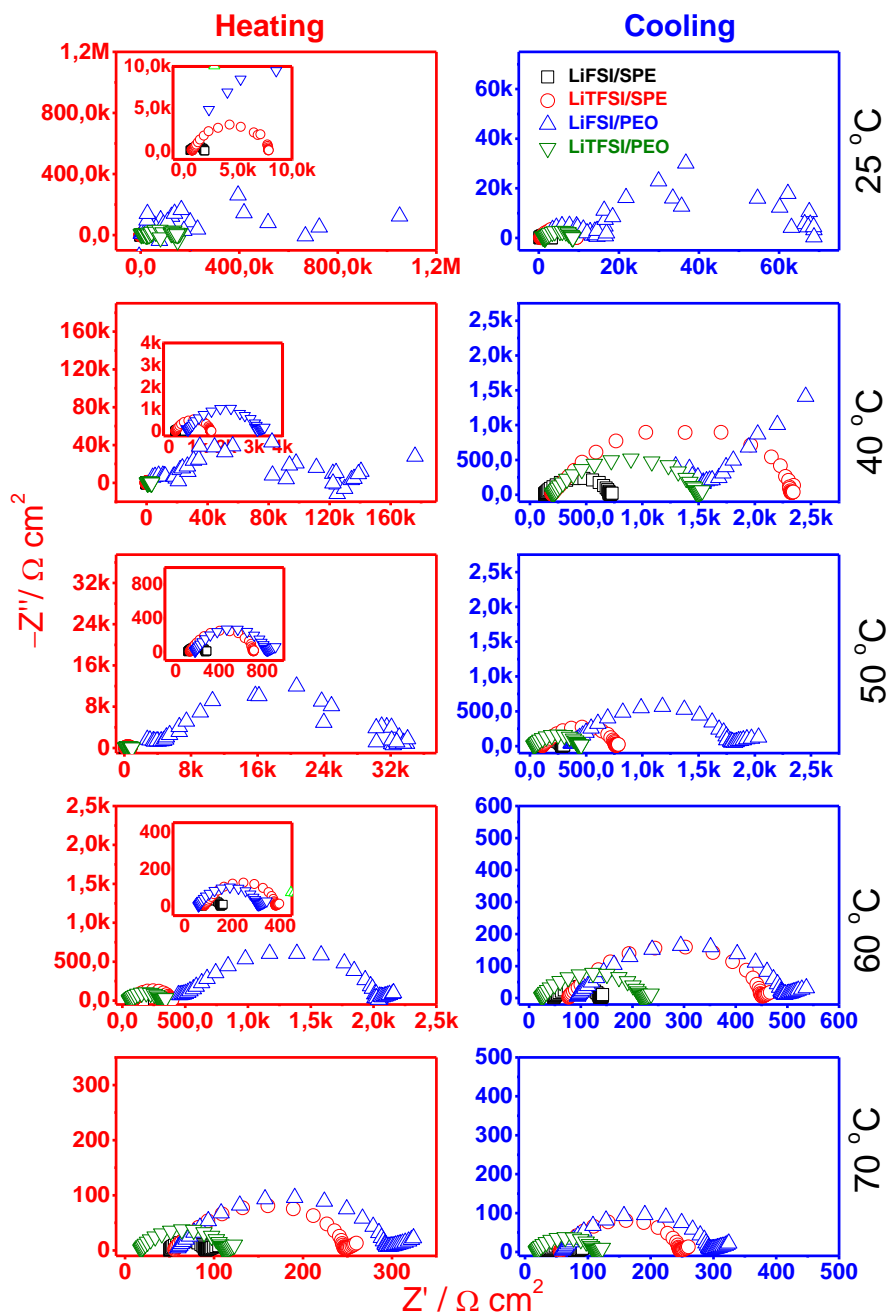
The anodic stability of polymer electrolytes is generally limited by the nature of polymer matrix when a perfluorinated anion is chosen as conducting salt [28] and it is determined by linear sweep voltammetry (LSV). This method follows the oxidation reactions on the electrode by an imposed increase of potential in the working electrode (WE). The LSV profiles depicted in **Figure 4.8** indicate that the anodic stabilities for Jeffamine-based SPEs are slightly lower than those of the corresponding PEO-based ones. This can be attributed to the greater sensitivity of the PO segment to oxidation. However, one may notice that the electrochemical stabilities for all the studied electrolytes are limited by the degradation of ether chains  $-\text{[CH}_2\text{CH}_2\text{O]}-$  with a characteristic value at *ca.* 4 V vs.  $\text{Li}^\circ/\text{Li}^+$ . Nevertheless, the stability of Jeffamine-based electrolytes can meet the requirement of the extensively used lithium iron phosphate ( $\text{LiFePO}_4$ ) composite polymer cathode, which has a working voltage at 3.5 V vs.  $\text{Li}^\circ/\text{Li}^+$ .



**Figure 4.8.** Linear sweeping voltammetry (LSV) profiles of the as-prepared four electrolytes with EO/Li = 20 at  $70^\circ\text{C}$ .

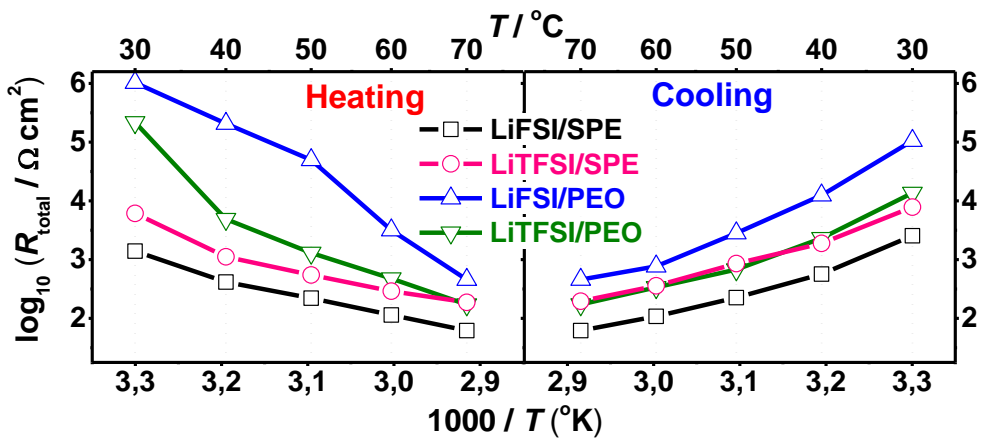
#### 4.6.5 Compatibility with Li<sup>o</sup> electrode

The interphase formed between the electrolyte and the Li metal electrode plays pivotal role in order to determine the cycling performance of ASSLMBs. The properties of the SEI are highly dependent on the identity of the anion of lithium salt. For this reason, the stability of the interphase of Li metal electrode with FSI- and TFSI-based PEO and SPEs were analysed. The SEI growth can be easily followed by electrochemical impedance spectroscopy (EIS) where resistivity of the cell, including the SEI layer, can be detected. EIS plots of Li<sup>o</sup> symmetric cells for Jeffamine-based SPEs and PEO-based cells with EO/Li = 20 at different temperatures are presented in **Figure 4.9**. The simplified equivalent circuit used to fit collected EIS data is given in **Figure A.4.2** and the best fitted-results are summarized in **Table A.4.1**.



**Figure 4.9.** Electrochemical impedance spectra of  $\text{Li}^+$  symmetric cell for Jeffamine-based SPEs and PEO reference electrolyte with  $\text{EO}/\text{Li}(\text{X}) = 20$  ( $\text{X} = \text{TFSI}, \text{FSI}$ ) at various temperatures.

**Figure 4.10** shows the effect of temperature on the total resistance ( $R_{\text{total}}$ ) of the  $\text{Li}^{\circ}$  symmetric cells using Jeffamine-based SPEs and PEO reference electrolytes. Interestingly, the temperature dependence of  $R_{\text{total}}$  for Jeffamine-based SPEs shows a linear behaviour continuously throughout the measured temperature range (30–70 °C), being different from the non-linear behaviour for the PEO-based ones showing high  $R_{\text{total}}$  values below 60 °C. The tendency of  $R_{\text{total}}$  vs.  $T$  is well in line with the conductivity and DSC results, where the melting transition of PEO at *ca.* 65 °C could be observed. For Jeffamine-based electrolytes a smooth dependency of  $\log(R_{\text{total}})$  is observed in the measured temperature range.



**Figure 4.10.** Total resistance ( $R_{\text{total}}$ ) of the  $\text{Li}^{\circ}$  symmetric cells using various electrolytes at heating and cooling scans.

**Table 4.5** summarizes the calculated values of Arrhenius fitting for the  $R_{\text{total}}$  for the Jeffamine-based  $\text{Li}^{\circ}$  symmetric cells. These values were calculated by **Equation 4.1**.

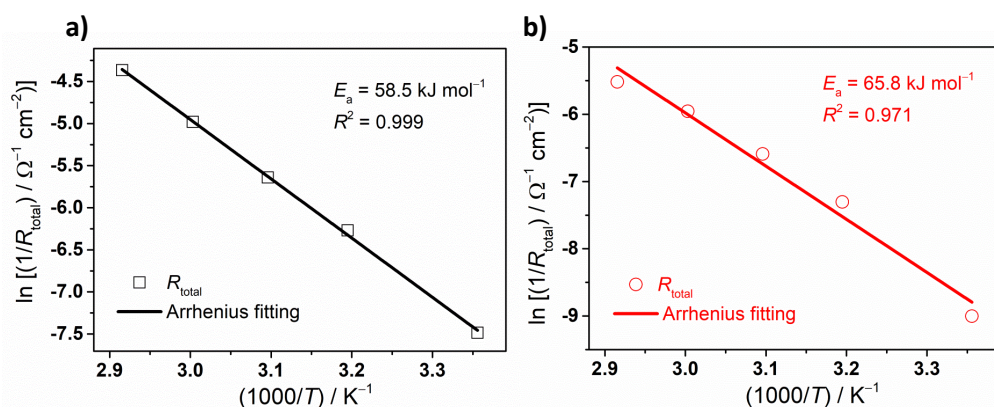
**Table 4.5.** The calculated values of Arrhenius fitting for the total resistance ( $R_{\text{total}}$ ) obtained from  $\text{Li}^{\circ}$  symmetric cells using LiFSI/SPE and LiTFSI/SPE.

Electrolyte	$E_a / \text{kJ mol}^{-1}$	$A / \Omega^{-1} \text{cm}^{-2}$	Adjusted R-square
LiFSI/SPE	58.5	$1.0 \times 10^7$	0.999
LiTFSI/SPE	65.8	$5.1 \times 10^7$	0.972

$$\sigma(T) = Ae^{-\frac{E_a}{RT}}$$

**Equation 4.1** wherein,  $A$  is pre-exponential factor,  $E_a$  is the activation energy and  $R$  is the gas constant [29].

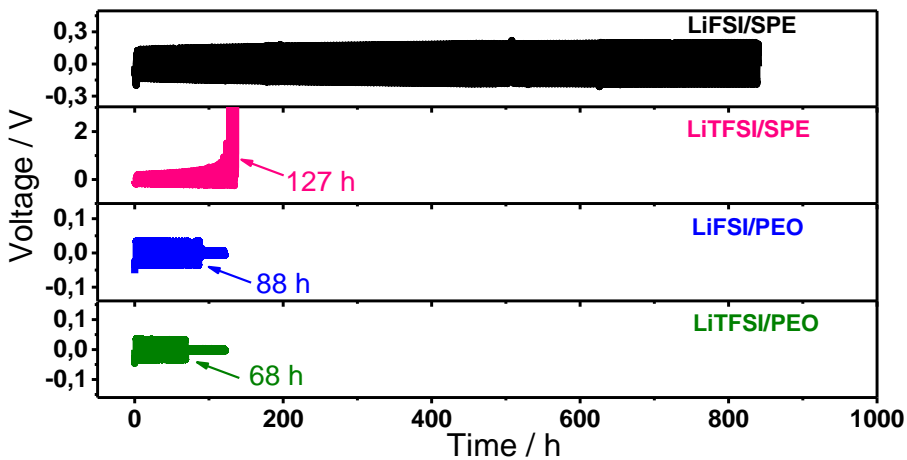
As it can be observed in **Table 4.5**, the activation energy of  $R_{\text{total}}$  is lower for LiFSI/SPE than that for LiTFSI/SPE one, *i.e.*,  $49.3 \text{ kJ mol}^{-1}$  (LiFSI/SPE) vs.  $65.8 \text{ kJ mol}^{-1}$  (LiTFSI/SPE). This further suggests that the amorphous nature of the polymer matrix not only enhances the ionic transportation of SPEs, but also greatly regulates the chemical compatibility of SPEs with  $\text{Li}^\circ$  electrode. Surprisingly, the values of  $R_{\text{total}}$  for LiFSI/SPE are maintained as low as *ca.*  $10^3 \Omega \text{ cm}^2$  at ambient temperature range (25–40 °C), suggesting a superior chemical compatibility of LiFSI/SPE with  $\text{Li}^\circ$  electrode. **Figure 4.11** shows the Arrhenius fitting for the temperature dependence of the  $R_{\text{total}}$  obtained from Li symmetric cell for Jeffamine-based electrolytes.



**Figure 4.11.** Arrhenius fitting for the temperature dependence of the total resistance ( $R_{\text{total}}$ ) obtained from  $\text{Li}^\circ$  symmetric cells using **a)** LiFSI/SPE and **b)** LiTFSI/SPE electrolytes.

**Figure 4.12** presents the voltage profiles for the Li plating/stripping test using  $\text{Li}^\circ$  symmetric cell at a current density of  $0.2 \text{ mA cm}^{-2}$ . This chronoamperometry test displays the electrode/electrolyte interface behaviour under cycling conditions simulating the battery operation. The cell based on LiFSI/SPE sustains more than 800 h (corresponding to  $160 \text{ mAh cm}^{-2}$  charge passing through each  $\text{Li}^\circ$  electrode) continuous cycling without any visible side reaction, whereas the analogous one using LiTFSI/SPE, as well as those using

LiFSI/PEO and LiTFSI/PEO encounter short-circuiting after less than 150 h. This can be attributed to the fully amorphous nature and good adhesive properties of Jeffamine-based electrolytes, allowing a better contact between  $\text{Li}^\circ$  electrode and solid polymer electrolytes, thus retarding the formation of dendritic lithium in the  $\text{Li}^\circ$  symmetric cell. This observation strongly implies that the synergetic effect of Jeffamine-based polymer matrix and SEI-favourable FSI anion can significantly improve the electrochemical performance of  $\text{Li}^\circ$  electrode with SPEs mitigating the growth of  $\text{Li}^\circ$  dendrites.



**Figure 4.12.** Galvanostatic cycling of the  $\text{Li}^\circ$  symmetric cells at  $70\text{ }^\circ\text{C}$  with a current density of  $0.2\text{ mA cm}^{-2}$ , and a half-duration of 2h.

#### 4.6.6 Cycling of $\text{Li}^\circ$ || $\text{LiFePO}_4$ cell performance

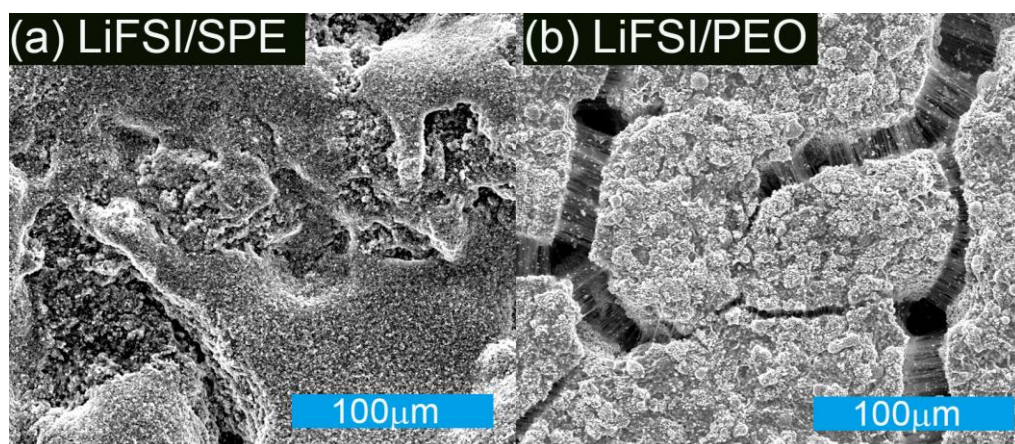
##### 4.6.6.1 LiTFSI-based electrolytes

The possibility of implementing the Jeffamine-based SPEs in rechargeable ASSLMBs is further evaluated by the cycling performance of  $\text{Li}^\circ$  ||  $\text{LiFePO}_4$  cells.

$\text{LiFePO}_4$  based cathodes were prepared using 63 wt% LFP active material, 7 wt% C65 conductive carbon and 30 wt% SPE/LiX [(SPE = Jeffamine-based SPE, PEO) and (X = TFSI, FSI)] as polymer binder following the method reported in **Chapter 2** section **2.3.1**.



Firstly, the surface morphology of the composite LFP cathode was investigated by SEM, as it can be observed in **Figure 4.13**. The Jeffamine-based SPE LFP cathode shows a continuous layer which can effectively bind the active material and conductive carbon, being a characteristic of good adhesive properties of Jeffamine-based polymer. In contrast, isolated aggregates are observed in the PEO-based cathode, due to the semicrystalline nature and lesser degree of entanglement for PEO matrix.

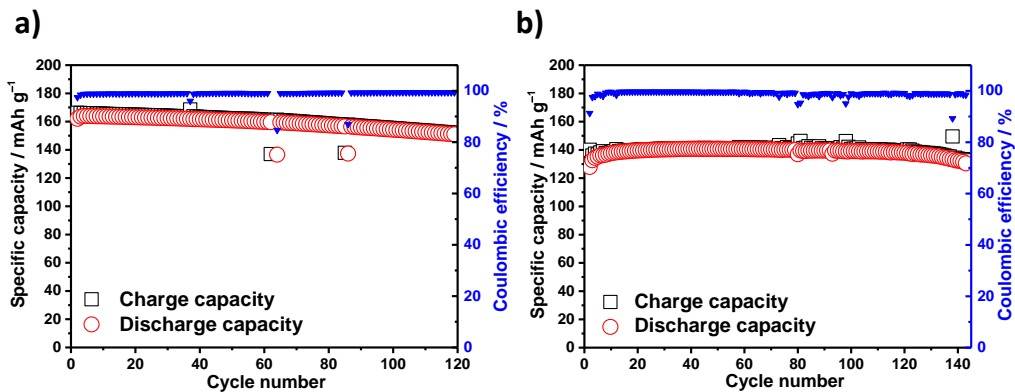


**Figure 4.13.** SEM images of the surface morphology for **a)** LiFSI/SPE and **b)** LiFSI/PEO based LFP cathodes.

In the first stage of the study, Jeffamine-based SPE was used as binder electrolyte in LFP based cathode and PEO was used as polymer electrolyte. As it has been presented in this chapter, Jeffamine-based electrolyte presents outstanding electrochemical properties. However, in order to study its feasibility as polymer binder a well-known polymer electrolyte (*e.g.*, LiTFSI/PEO) was chosen. **Figure 4.14** shows the specific capacity and Coulombic efficiency (CE) vs. cycle number of two cells with different loading of active material [*e.g.*, **a)**  $3.1 \text{ mg cm}^{-2}$  ( $0.53 \text{ mAh cm}^{-2}$ ) and **b)**  $5.6 \text{ mg cm}^{-2}$  ( $0.95 \text{ mAh cm}^{-2}$ )] at  $70^\circ\text{C}$  at a constant charge/discharge rate of 0.1/0.1C. As it can be observed, both cells can be cycled for at least 120 cycles with low capacity fading and good Coulombic efficiency (CE). In the case of lower active material loading (**Figure 4.14a**), in the first cycles the cell delivers a discharge capacity of  $165 \text{ mAh g}^{-1}$ , while after 120 cycles the discharge capacity decays to  $151 \text{ mAh g}^{-1}$  with a CE close to 100%. For higher

active material loading (**Figure 4.14b**), the discharge capacity varies from 141 mAh g<sup>-1</sup> in the first cycles to 130 mAh g<sup>-1</sup> after 140 cycles.

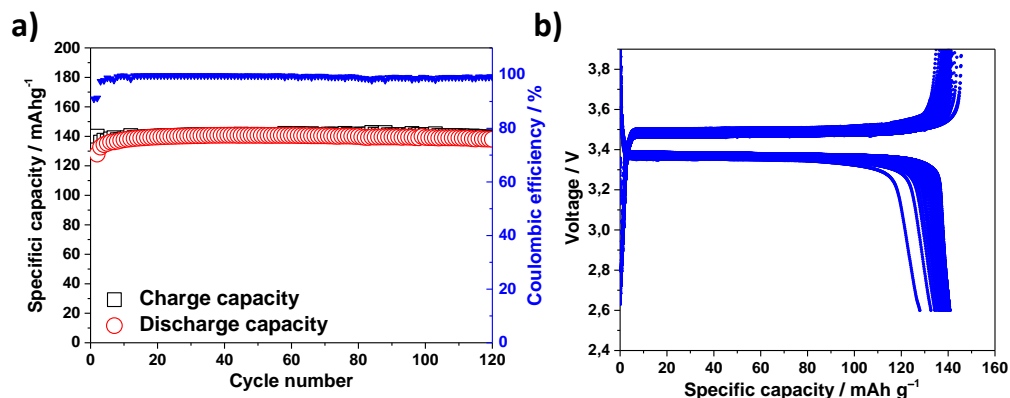
As it can be observed, higher areal mass loading results in lower specific capacity values. This behaviour can be attributed to the higher current density that needs to be applied that can also favour the soft dendrite formation.



**Figure 4.14.** Specific capacity and Coulombic efficiency vs. cycle number for the cells using LiTFSI/PEO as electrolyte and Jeffamine-based SPE as binder in LFP cathode cycled at 70 °C at a constant charge/discharge rate of 0.1/0.1C for an active material loading of **a)** 3.1 mg cm<sup>-2</sup> and **b)** 5.6 mg cm<sup>-2</sup>.

After this study, it can be concluded that good electrochemical performance can be achieved by the implementation of Jeffamine-based SPEs as polymer binders in cathode materials. This could be ascribed to the high ionic conductivity, fast ion mobility and volume-compliant mechanical properties of the polymer.

In the next step of the study Jeffamine-based SPE with LiTFSI was utilized as both electrolyte and binder in LFP based ASSLMs. **Figure 4.15a** depicts the specific capacity and Coulombic efficiency vs. cycle number and **Figure 4.15b** the charge/discharge profiles for the as-prepared cell at 70 °C under a constant C rate of 0.1/0.1C. As it can be observed, the cell shows good long-term cycling stability and a high discharge capacity of 140 mAh g<sup>-1</sup> after 120 cycles. Moreover, the smooth voltage profiles shown in **Figure 4.15b** indicate that there is no dendrite growth during the cycling of the cell, probably due to the good contact between the electrolyte and Li anode.



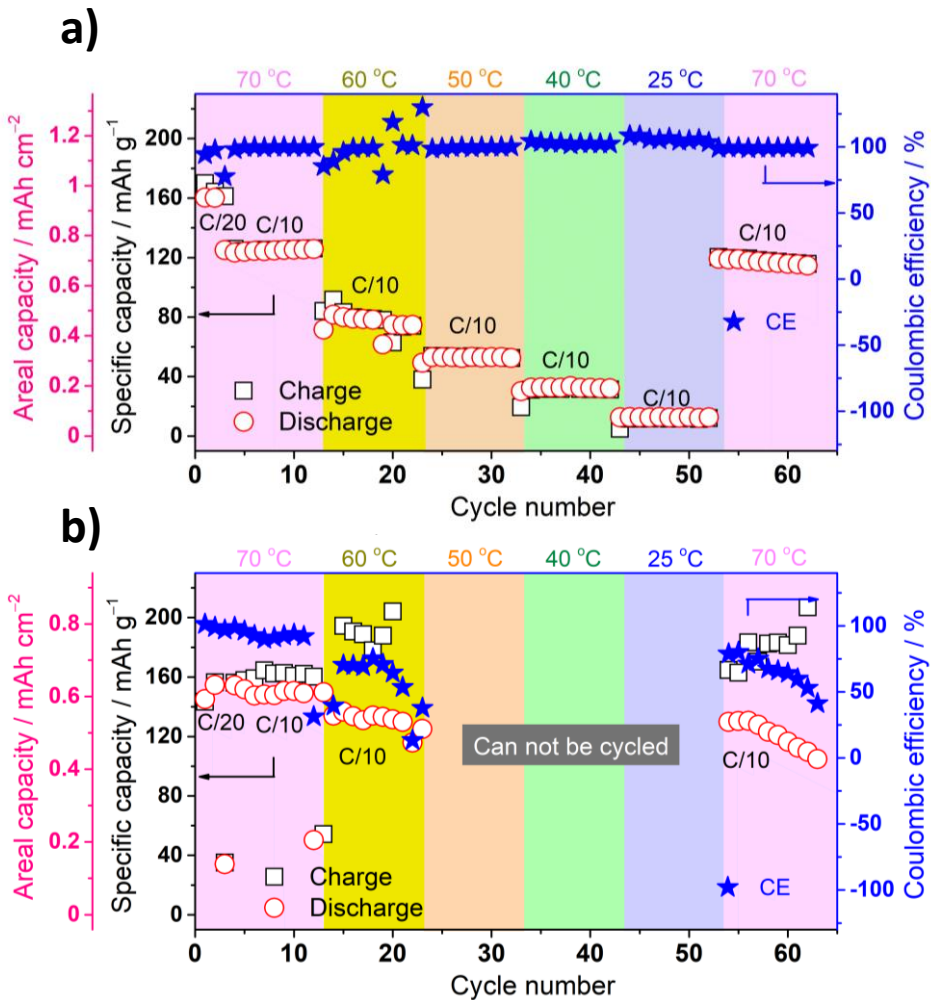
**Figure 4.15.** a) Specific capacity and Coulombic efficiency vs. cycle number and b) charge/discharge profiles for the cells using LiTFSI/SPE as both electrolyte and binder in LFP cathode cycled at 70 °C under a constant C rate of 0.1/0.1C.

#### 4.6.6.2 LiFSI-based electrolytes

Inspired by the previously mentioned advantageous chemical and electrochemical properties of LiFSI/SPE, such as higher ionic conductivity at low temperatures and higher stability against Li<sup>o</sup> electrode than the LiTFSI counterparts, and the suitability of Jeffamine-based polymer as both electrolyte and binder material in LFP-based cells, this electrolyte was chosen in order to decrease the operational temperature of ASSLMBs.

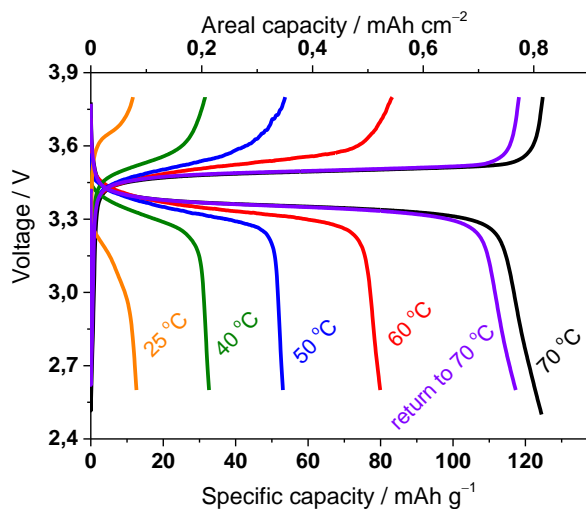
**Figure 4.16** shows the specific/areal capacities and Coulombic efficiency vs. cycle number at various temperatures for both a) Li<sup>o</sup> | LiFSI/SPE | LFP and b) Li<sup>o</sup> | LiFSI/PEO | LFP cells. At an elevated temperature of 70 °C, where most of the solid polymer electrolytes-based Li<sup>o</sup> | LFP cells being cycled, the Li<sup>o</sup> | LFP cell using LiFSI/PEO delivers discharge capacities around 140 mAh g<sup>-1</sup> at a current rate of C/10, which are close to the theoretical value of LFP cathode. The cell using LiFSI/SPE has an initial capacity of 160 mAh g<sup>-1</sup> at C/20 and then decreases to 120 mAh g<sup>-1</sup> at a current rate of C/10. This could be attributed to the higher loading of active material in the LiFSI/SPE-based cell [*ca.* 6.0 mg cm<sup>-2</sup> (1.02 mAh cm<sup>-2</sup>)] than that in the LiFSI/PEO-based cell [*ca.* 4.5 mg cm<sup>-2</sup> (0.77 mAh cm<sup>-2</sup>)]. This fact causes a slightly higher polarization during both charge and discharge processes in the former cell, thus resulting in a slightly lower utilization of LFP. Notwithstanding,

the LiFSI/SPE cell outperforms LiFSI/PEO-based one in terms of areal capacities at 70 °C being benefited from its higher LFP loading, *e.g.*, 0.75 mAh cm<sup>-2</sup> (LiFSI/SPE) vs. 0.63 mAh cm<sup>-2</sup> (LiFSI/PEO).



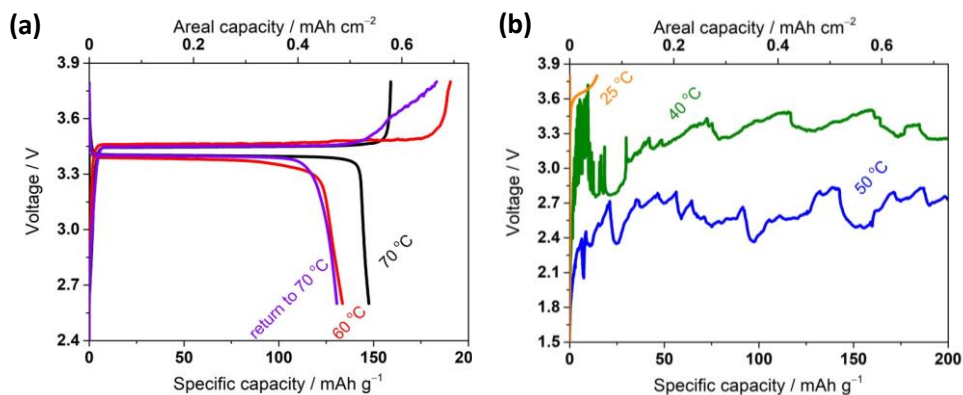
**Figure 4. 16.** Specific/areal capacity and Coulombic efficiency vs. cycle number for the Li<sup>+</sup>||LiFePO<sub>4</sub> cells using **a)** Jeffamine-based LiFSI/SPE and **b)** LiFSI/PEO at various temperatures.

As it can be observed in **Figure 4.16a**, the LiFSI/SPE cell exhibits specific capacities of *ca.* 50 mA h g<sup>-1</sup> with good Coulombic efficiency at 50 °C though with a significant increase in polarization, as depicted in **Figure 4.17**.



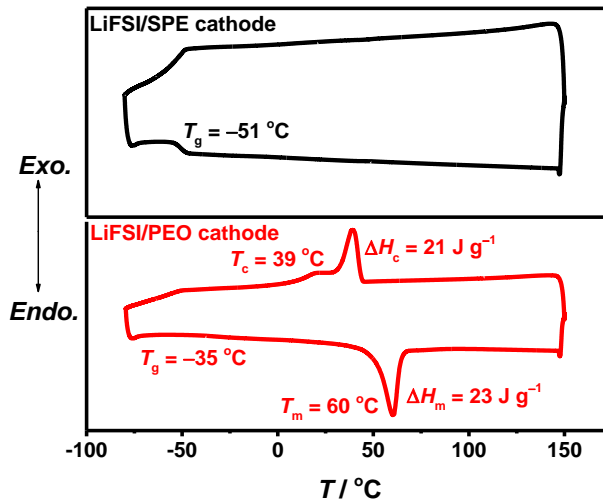
**Figure 4. 17.** Charge/discharge profiles of the  $\text{Li}^\circ || \text{LiFePO}_4$  cells using LiFSI/SPE at various temperatures under a constant C rate of 0.1/0.1C (Cycle number: the third cycle in each temperature).

As it can be observed in **Figure 4.18**, the LiFSI/PEO cell does not work successfully at the same temperature. This is in accordance with the drastic decrease of ionic conductivity for LiFSI/PEO electrolyte at 50 °C due to the crystallization of PEO in the electrolyte.



**Figure 4. 18.** Charge/discharge profiles of the  $\text{Li}^\circ || \text{LiFePO}_4$  cells using LiFSI/PEO at **a)** elevated temperatures and **b)** ambient temperatures under a constant C rate of 0.1/0.1C (Cycle number: the third cycle in each temperature).

Besides, the formation of crystallized PEO phases within the cathode material is confirmed by the DSC measurement for the composite cathode, where a sharp exothermic peak for crystallization of PEO is observed for LiFSI/PEO-based composite cathode instead of the amorphous LiFSI/Jeffamine-SPE-based one (Figure 4.19).



**Figure 4. 19.** DSC traces of the respective LiFSI/SPE and LiFSI/PEO composite  $\text{LiFePO}_4$  cathodes.

Remarkably, at room temperature region (25–40 °C), the areal capacities of 0.1–0.2 mAh  $\text{cm}^{-2}$  are achieved by using LiFSI/SPE. These results are comparable to those reported recently by Mindemark [30] and Tominaga *et al.* [31], where either LiTFSI/poly(ethylene carbonate-*co*-caprolactone) or highly concentrated LiFSI/poly(ethylene carbonate) (PEC) electrolytes were employed for  $\text{Li}^+ | \text{LFP}$  cells (*e.g.*, 0.19 mAh  $\text{cm}^{-2}$  for the cell using LiFSI/PEC at 30 °C under a constant C rate of 0.1/0.1C). In addition, the capacity for LiFSI/SPE cell can be reversibly regained with good Coulombic efficiency after cycling at various temperatures for 50 cycles. This could be again ascribed to the high ionic conductivity, superior electrochemical compatibility with  $\text{Li}^+$  electrode, as well as good adhesive properties for LiFSI/SPE.

#### 4.7. Conclusions

The application of Jeffamine<sup>®</sup> compounds with PO and EO units makes polymer matrices more elastic and resistant to crystallization, obtaining completely amorphous electrolytes after mixing them with LiTFSI or LiFSI salts. The Li(X)/SPE (X = TFSI,FSI) electrolytes show high ionic conductivity at the temperature ranging from 70 °C to room temperature region, due to the amorphicity of the polymer matrix with soft and disordered polyether moieties. The high ionic conductivity at low temperatures is ascribed to the low energy value for conformational changes of flexible EO units.

The chemical and electrochemical stability of solid polymer electrolytes against Li<sup>o</sup> electrode can be remarkably enhanced by the implementation of Jeffamine-based SPEs, especially when mixed with LiFSI salt. The suitability of the new as-prepared polymer electrolyte as binder materials in LFP based cathodes has been demonstrated. The Li<sup>o</sup>|LiTFSI/SPE|LFP cell shows good cycling stability and high Coulombic efficiency at 70 °C. The Li<sup>o</sup>|LiFSI/SPE|LFP cell delivers decent specific/areal capacity with good Coulombic efficiency when decreasing the operational temperature close to RT. Those results suggest that LiFSI/SPE could be promising candidates for enhancing the cycling performance of ASSLMs at ambient temperature region, thus further improving their energy efficiency and energy density.

**References**

- [1] D. Golodnitsky, E. Strauss, E. Peled, S. Greenbaum. Review—on order and disorder in polymer electrolytes. *J. Electrochem. Soc.* 2015; **162**(14), A2551-A2566.
- [2] Y. Ikeda, Y. Wada, Y. Matoba, S. Murakami, S. Kohjiya. Characterization of comb-shaped high molecular weight poly(oxyethylene) with tri(oxyethylene) side chains for a polymer solid electrolyte. *Electrochim. Acta.* 2000; **45**(8), 1167-1174.
- [3] N.A. Stolwijk, C. Heddier, M. Reschke, M. Wiencierz, J. Bokeloh, G. Wilde. Salt-concentration dependence of the glass transition temperature in PEO–NaI and PEO–LiTFSI polymer electrolytes. *Macromolecules.* 2013; **46**(21), 8580-8588.
- [4] S. Lascaud, M. Perrier, A. Vallee, S. Besner, J. Prud'homme, M. Armand. Phase diagrams and conductivity behavior of poly(ethylene oxide)-molten salt rubbery electrolytes. *Macromolecules.* 1994; **27**(25), 7469-7477.
- [5] M.B. Armand. Polymer Electrolytes. *Annu. Rev. Mater. Sci.* 1986; **16**(1), 245-261.
- [6] J. Wang, Z. Yao, C.W. Monroe, J. Yang, Y. Nuli. Carbonyl- $\beta$ -cyclodextrin as a novel binder for sulfur composite cathodes in rechargeable lithium batteries. *Adv. Funct. Mater.* 2013; **23**(9), 1194-1201.
- [7] A. Guerfi, M. Kaneko, M. Petitclerc, M. Mori, K. Zaghib. LiFePO<sub>4</sub> water-soluble binder electrode for Li-ion batteries. *J. Power Sources.* 2007; **163**(2), 1047-1052.
- [8] M. Armand. Polymer solid electrolytes - an overview. *Solid State Ion.* 1983; **9-10**, 745-754.
- [9] W. Gorecki, M. Jeannin, E. Belorizky, C. Roux, M. Armand. Physical properties of solid polymer electrolyte PEO(LiTFSI) complexes. *J. Phys. Condens. Matter.* 1995; **7**(34), 6823-6832.
- [10] M. Marzantowicz, J.R. Dygas, F. Krok, A. Łasińska, Z. Florjańczyk, E. Zygadło-Monikowska, A. Affek. Crystallization and melting of PEO:LiTFSI polymer electrolytes investigated simultaneously by impedance spectroscopy and polarizing microscopy. *Electrochim. Acta.* 2005; **50**(19), 3969-3977.
- [11] H. Zhang, C. Liu, L. Zheng, F. Xu, W. Feng, H. Li, X. Huang, M. Armand, J. Nie, Z. Zhou. Lithium bis(fluorosulfonyl)imide/poly(ethylene oxide) polymer electrolyte. *Electrochim. Acta.* 2014; **133**, 529-538.



- [12] H.B. Han, J. Nie, K. Liu, W.K. Li, W.F. Feng, M. Armand, H. Matsumoto, Z.B. Zhou. Ionic liquids and plastic crystals based on tertiary sulfonium and bis(fluorosulfonyl)imide. *Electrochim. Acta.* 2010; **55**(3), 1221-1226.
- [13] H.B. Han, K. Liu, S.W. Feng, S.S. Zhou, W.F. Feng, J. Nie, H. Li, X.J. Huang, H. Matsumoto, M. Armand, Z.B. Zhou. Ionic liquid electrolytes based on multi-methoxyethyl substituted ammoniums and perfluorinated sulfonimides: preparation, characterization, and properties. *Electrochim. Acta.* 2010; **55**(23), 7134-7144.
- [14] T. Sugimoto, M. Kikuta, E. Ishiko, M. Kono, M. Ishikawa. Ionic liquid electrolytes compatible with graphitized carbon negative without additive and their effects on interfacial properties. *J. Power Sources.* 2008; **183**(1), 436-440.
- [15] X. Judez, M. Piszcz, E. Coya, C. Li, I. Aldalur, U. Oteo, Y. Zhang, W. Zhang, L.M. Rodriguez-Martinez, H. Zhang, M. Armand. Stable cycling of lithium metal electrode in nanocomposite solid polymer electrolytes with lithium bis(fluorosulfonyl)imide. *Solid State Ion.* 2018; **318**, 95-101.
- [16] K.M. Abraham, M. Alamgir. Ambient temperature rechargeable polymer-electrolyte batteries. *J. Power Sources.* 1993; **43**(1), 195-208.
- [17] G.B. Appetecchi, S. Scaccia, S. Passerini. Investigation on the stability of the lithium-polymer electrolyte interface. *J. Electrochem. Soc.* 2000; **147**(12), 4448-4452.
- [18] K. Xu. Electrolytes and interphases in Li-ion batteries and beyond. *Chem. Rev.* 2014; **114**(23), 11503-11618.
- [19] M. Nakayama, S. Wada, S. Kuroki, M. Nogami. Factors affecting cyclic durability of all-solid-state lithium polymer batteries using poly(ethylene oxide)-based solid polymer electrolytes. *Energy Environ. Sci.* 2010; **3**(12), 1995-2002.
- [20] J.K. Kim, J. Manuel, M.H. Lee, J. Scheers, D.H. Lim, P. Johansson, J.H. Ahn, A. Matic, P. Jacobsson. Towards flexible secondary lithium batteries: polypyrrole-LiFePO<sub>4</sub> thin electrodes with polymer electrolytes. *J. Mater. Chem.* 2012; **22**(30), 15045-15049.
- [21] J. Evans, C.A. Vincent, P.G. Bruce. Electrochemical measurement of transference numbers in polymer electrolytes. *Polymer.* 1987; **28**(13), 2324-2328.

[22] M. Piszcz, H. Zhang, M. Marczewski, G.Z. Żukowska, K. Lemańska, M. Sukiennik, M. Siekierski. Vibrational spectroscopic studies combined with viscosity analysis and VTF calculation for hybrid polymer electrolytes. *Solid State Ion.* 2017; **303**, 78-88.

[23] M. Kerner, N. Pylahan, J. Scheers, P. Johansson. Thermal stability and decomposition of lithium bis(fluorosulfonyl)imide (LiFSI) salts. *RSC Adv.* 2016; **6**(28), 23327-23334.

[24] H.B. Han, S.S. Zhou, D.J. Zhang, S.W. Feng, L.F. Li, K. Liu, W.F. Feng, J. Nie, H. Li, X.J. Huang, M. Armand, Z.B. Zhou. Lithium bis(fluorosulfonyl)imide (LiFSI) as conducting salt for nonaqueous liquid electrolytes for lithium-ion batteries: Physicochemical and electrochemical properties. *J. Power Sources.* 2011; **196**(7), 3623-3632.

[25] R. Hagiwara, K. Tamaki, K. Kubota, T. Goto, T. Nohira. Thermal properties of mixed alkali bis(trifluoromethylsulfonyl)amides. *J. Chem. Eng. Data.* 2008; **53**(2), 355-358.

[26] M. Watanabe, S. Nagano, K. Sanui, N. Ogata. Estimation of Li<sup>+</sup> transport number in polymer electrolytes by the combination of complex impedance and potentiostatic polarization measurements. *Solid State Ion.* 1988; **28-30**, 911-917.

[27] T. Itoh, K. Fujita, T. Uno, M. Kubo. Polymer electrolytes based on vinyl ethers with various EO chain length and their polymer electrolytes cross-linked by electron beam irradiation. *Ionics.* 2017; **23**(2), 257-264.

[28] G.G. Eshetu, X. Judez, C. Li, M. Martinez-Ibañez, I. Gracia, O. Bondarchuk, J. Carrasco, L.M. Rodriguez-Martinez, H. Zhang, M. Armand. Ultrahigh performance all solid-state lithium sulfur batteries: salt anion's chemistry-induced anomalous synergistic effect. *J. Am. Chem. Soc.* 2018; **140**(31), 9921-9933.

[29] M.A. Ratner, D.F. Shriver. Ion transport in solvent-free polymers. *Chem. Rev.* 1988; **88**(1), 109-124.

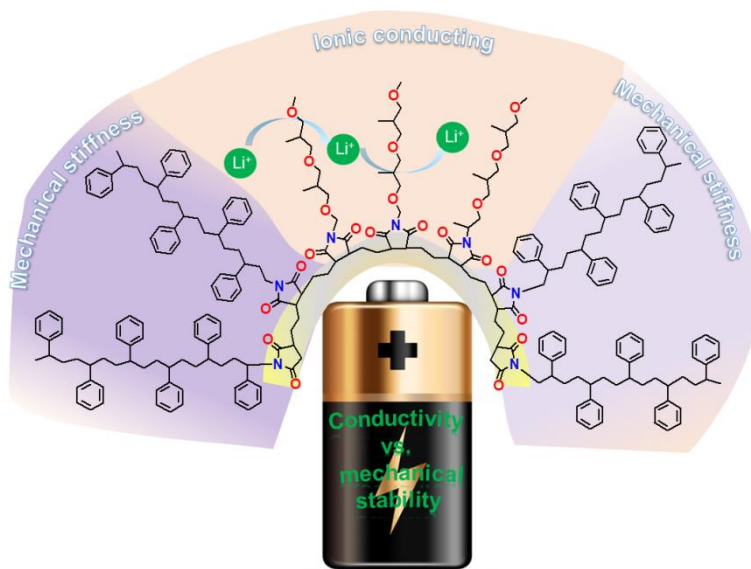
[30] J. Mindemark, B. Sun, E. Törmä, D. Brandell. High-performance solid polymer electrolytes for lithium batteries operational at ambient temperature. *J. Power Sources.* 2015; **298**, 166-170.

[31] K. Kimura, M. Yajima, Y. Tominaga. A highly-concentrated poly(ethylene carbonate)-based electrolyte for all-solid-state Li battery working at room temperature. *Electrochem. Commun.* 2016; **66**, 46-48.

## Chapter 5

# Self-standing highly conductive block copolymer electrolytes for lithium metal batteries

Towards robust solid polymer electrolytes



I. Aldalur, M. Martínez-Ibañez, M. Piszcz, H. Zhang, M. Armand. Self-standing highly conductive solid electrolytes based on block copolymers for rechargeable all-solid-state lithium-metal batteries. *Batteries & Supercaps*. 2018; 1(4), 149-159.



## Chapter 5:

### SELF-STANDING HIGHLY CONDUCTIVE BLOCK COPOLYMER ELECTROLYTES FOR LITHIUM METAL BATTERIES

5.1.	Introduction.....	119
5.2.	Synthesis of polymer matrices.....	121
5.3.	Selection of the best block copolymer matrix.....	123
5.3.1.	Chemical characterization of polymer matrices.....	124
5.3.1.1.	Hydrogen-1 nuclear magnetic resonance ( $^1\text{H}$ NMR).....	124
5.3.1.2.	Attenuated total reflectance-Fourier-transform infrared spectroscopy (ATR-FTIR).....	125
5.3.2.	Mechanical properties.....	126
5.3.3.	Thermal characterization.....	127
5.3.4.	Ionic conductivity.....	128
5.4.	Characterization of BCP70 polymer matrix and electrolytes.....	129
5.4.1.	Chemical characterization.....	129
5.4.2.	Thermal characterization.....	130
5.4.2.1.	Thermogravimetric analysis (TGA).....	130
5.4.2.2.	Differential scanning calorimetry (DSC).....	131
5.4.3.	Electrochemical characterization.....	134
5.4.3.1.	Ionic conductivity.....	134
5.4.3.2.	Li-ion transference number.....	136
5.4.3.3.	Electrochemical stability toward oxidation.....	138

5.4.3.4.	Compatibility with Li° electrode .....	139
5.4.3.5.	Cycling of Li°    LiFePO <sub>4</sub> cell performance.....	140
5.5.	Conclusions.....	141
	References.....	143

## 5.1. Introduction

The development of solid polymer electrolytes (SPEs) has been largely hindered by the trade-off between high ionic conductivity and good mechanical properties, since the SPEs with low glass transition temperature ( $T_g$ ) and suppressed crystallinity, which are crucial for facilitating fast ionic transport, can hardly form self-standing membranes.

As it was mentioned in previous chapters, among the different macromolecular hosts, poly(ethylene oxide) (PEO) is one of the most widely used polymer matrices as it contains ether coordination sites that facilitates lithium salt dissociation [1, 2]. Ionic transport in PEO depends on the chain flexibility and occurs mainly in the amorphous phase, leading to a low ionic conductivity at temperatures below its melting point (*ca.* 65 °C). Thus, PEO-based all-solid-state lithium metal batteries (ASSLMBs) have to operate at temperatures above the PEO melting temperature ( $T_m$ ) [3, 4]. Under this condition, PEO is too soft microscopically to prevent the growth of lithium metal soft dendrites upon cycling despite the high molecular weight ( $M_w$ ) giving solid-state mechanical properties in macroscopic scale [5, 6].

Trying to overcome above mentioned drawbacks of PEO-based SPEs, tremendous efforts have been devoted to the design of non-crystalline and low  $T_g$  polymer matrices [7-9], such as structural alteration by random [10], comb [11, 12] and/or block copolymerization [13-16]. Block-copolymer-based SPEs are a promising solution that combines both good mechanical properties and high ionic conductivity. They are composed of two or more different covalently bound block of polymers that provide to the matrix with a combination of their own properties. In general, one block is usually an ethylene oxide (EO) based polymer responsible of the ionic conductivity, whereas the other block provides other functionalities such as mechanical stiffness [17, 18].

It has been proven by different groups that higher conductivities are obtained when the conducting block is attached to a rubbery block instead of a glassy block [19, 20]. However, the blocks based on phosphazenes or siloxanes are not ensuring good mechanical properties. Glassy kind of blocks presenting high values of  $T_g$ , such as polystyrene (PS) play the role of a scaffold for polymer matrices where highly conducting amorphous phase can be placed in between [21-

23]. Balsara *et al.* studied a series of SPEs based on poly(ethylene oxide)-block-polystyrene (PEO-*b*-PS). Their results showed that the molecular weight of each block [18, 23], thermal history [24] and concentration of lithium salt [22] have a pivotal impact on the ionic conductivity and mechanical properties of the SPEs. The optimized electrolyte, with a high mechanical strength (modulus, 50 MPa) and acceptable ionic conductivity, suppressed significantly the lithium (Li<sup>0</sup>) dendrite growth and afforded a long-term cycling of Li<sup>0</sup> | LiFePO<sub>4</sub> cell at 90 °C [25, 26].

Bouchet *et al.* reported the difference between a large series of SPEs where the structural block was made of PS and the conductive block was made of either linear PEO or comb PEO based on poly(ethylene-glycol) methyl ether methacrylate [27, 28]. The comb structure was expected to increase the dynamics of the polymeric chains, thus preventing their crystallization. It was proved that the ionic motion was improved and a better ionic conductivity around room temperature (RT) was obtained (*ca.* 10<sup>-5</sup> S cm<sup>-1</sup> at 30 °C). It is worthy to point out that the ionic conductivities of above-mentioned SPEs are still not sufficient for the desirable performance of ASSLMBs [23]. Hence, further modifications of the polymer matrices with customized functional moieties, being advantageous for achieving good mechanical properties and high ionic conductivities, are highly appreciated.

In this chapter a new type of self-standing and highly conductive SPEs based on tailor-made block copolymers (*i.e.*, Jeffamine-PS, **Scheme 5.1**) are reported. The structural block of these copolymers is made of amine terminated PS, while the conducting block is made of comb polymer containing polyether side moieties (so-called Jeffamine<sup>®</sup>) doped with lithium bis(fluoromethanesulfonylimide) (LiTFSI). The structure was conceived on the basis of the following considerations:

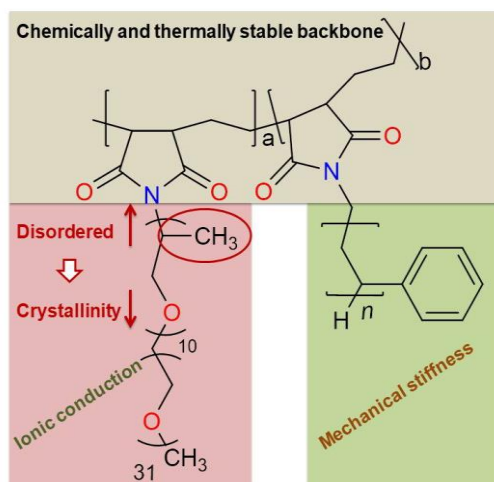
**1)** The conducting block, Jeffamine-side chain polymer is a polyether based on propylene oxide (PO), ethylene oxide (EO) units ensuring low  $T_g$  and high amorphicity, presenting remarkable adhesion properties, high mobility of Li<sup>+</sup> ions and good compatibility with Li<sup>0</sup> electrode. However, the matrix suffers from weak mechanical properties and, as a result, self-standing membranes are impossible to obtain, as it was discussed in **Chapter 3** and **Chapter 4** [12, 29].



2) The PS block is favourable for providing mechanical stiffness, acting as scaffolding, in order to obtain self-standing membranes. This feature was well proven by previous work of Balsara [23] and Bouchet [27, 28].

3) Poly(ethylene-*alt*-maleimide) backbone is easy to modify in clean reactions where both side chains contain the same amine terminated moieties able to react in the same manner.

4) LITFSI is chosen due to its highly delocalized negative charge, structural flexibility (plasticizing), and chemical and electrochemical stabilities [2].



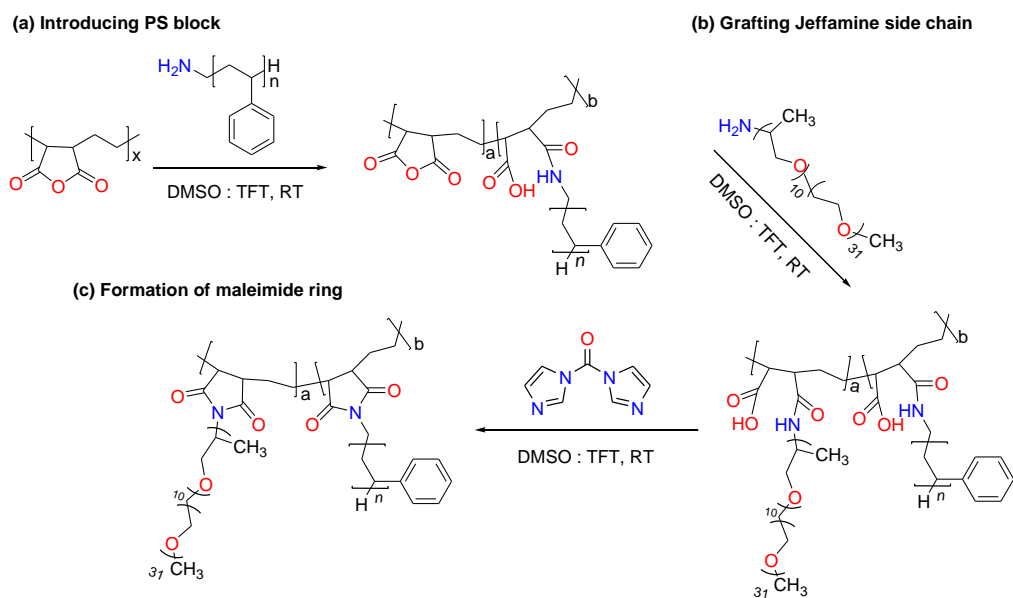
**Scheme 5.1.** Schematic illustration of the tailor-made block copolymer.

## 5.2. Synthesis of polymer matrices

The block copolymer matrices, hereafter BCPs, were readily accessible via one-pot reaction in a mixture of dimethyl sulfoxide (DMSO) and  $\alpha,\alpha',\alpha''$ -trifluorotoluene (TFT) at RT, as shown in **Scheme 5.2**. The selection of the solvent was made considering the features of the reaction. As for the solubility of the starting polymer backbone, DMSO was chosen as the best candidate, whereas TFT was compatible with the PS moieties favouring the dissolution of the polymer. Also, TFT has been proved to be an efficient solvent in the preparation of Jeffamine-based homopolymers, as seen in **Chapter 3**.

BCPs were synthesized in a three-step reaction (**Scheme 5.2**). Firstly, a given amount of poly(ethylene-*alt*-maleic anhydride) (PEaMA) was dissolved in

DMSO/TFT (50:50 by volume), followed by the addition of a pre-determined amount of amine-terminated PS dissolved in DMSO/TFT (same ratio) in order to obtain a homogeneous distribution of PS block via the linkage of *N*-substituted alkenamides. This also ensured a good conversion of the high-cost amine-terminated PS. Secondly, corresponding amount of Jeffamine<sup>®</sup> side chain with amine group as an ending moiety was grafted readily to the polymer backbone in a similar manner as the first step. In the last step, the formation of maleic imide ring was successfully made in the presence of carbonyldiimidazole (CDI) under mild conditions (*i.e.*, RT, 24 hours). This is in line with the work where CDI can act as an efficient agent for converting amine to amide and amic acid to imide [30]. After vigorous stirring over 24 h, the solvent was rotary evaporated and unreacted compounds and by-product imidazole were removed by water dialysis.



**Scheme 5.2.** One-pot reaction for synthesizing the block copolymers.

A set of block copolymers with different Jeffamine<sup>®</sup>/PS composition have been prepared and compared with the Jeffamine M-2070 based homopolymer (SP) shown in **Chapter 3** and **Chapter 4** and PEO-based reference electrolyte. For the electrolyte preparation LiTFSI has been used as lithium salt with different EO/Li molar ratios. All the materials are summarized in **Table 5.1**.

**Table 5.1.** Abbreviations and corresponding composition of the as-prepared copolymers and electrolytes.

Acronym	Polymer matrix <sup>[a]</sup>	EO/Li <sup>[b]</sup>	Salt content / wt% <sup>[c]</sup>
<b>Polymer matrices</b>			
BCP70	Jeffamine-PS copolymer (70:30)		
BCP60	Jeffamine-PS copolymer (60:40)		
BCP50	Jeffamine-PS copolymer (50:50)		
SP	Solid Jeffamine homopolymer		
<b>Electrolytes</b>			
BCP70-1#	Jeffamine-PS copolymer (70:30)	20	13
BCP70-2#	Jeffamine-PS copolymer (70:30)	10	23
BCP70-3#	Jeffamine-PS copolymer (70:30)	8	27
BCP70-4#	Jeffamine-PS copolymer (70:30)	4	43
BCP70-5#	Jeffamine-PS copolymer (70:30)	3	50
BCP60-3#	Jeffamine-PS copolymer (60:40)	8	24
BCP50-3#	Jeffamine-PS copolymer (50:50)	8	21
SPE-1#	Solid Jeffamine homopolymer	50	8
SPE-2#	Solid Jeffamine homopolymer	30	12
SPE-3#	Solid Jeffamine homopolymer	20	18
SPE-4#	Solid Jeffamine homopolymer	15	22
SPE-5#	Solid Jeffamine homopolymer	10	30
RE	PEO	20	25

[a] The number in parentheses refers to the weight ratio of Jeffamine® vs. PS blocks. [b] The molar ratio of EO/Li. [c] The weight percentage of the added lithium salt in the SPEs.

### 5.3. Selection of the best block copolymer matrix

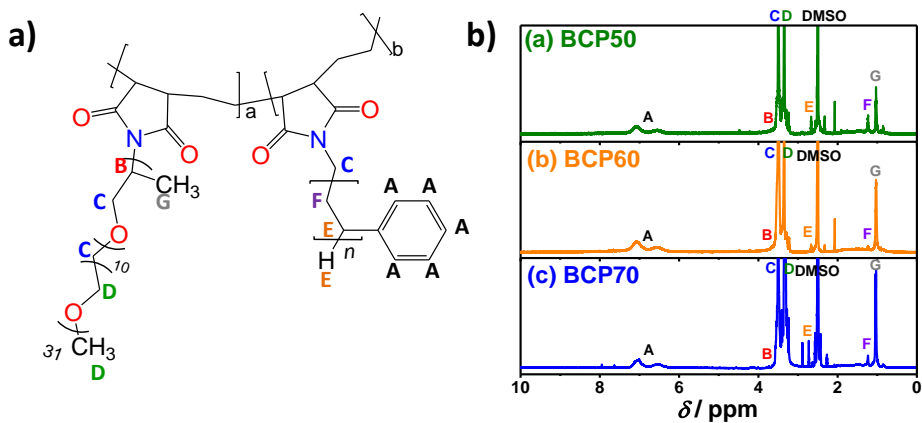
In order to determine the best copolymer matrix different properties of the materials were analysed. First, the chemical structures were analysed to confirm the reaction of the reagents. Then, the phase transitions were studied to

ensure the suitability of these polymers as electrolytes since this parameter is associated with the operational temperature of ASSLMs and Li-ion conductivity. On the other hand, the mechanical properties and stability are important in order to obtain self-standing membranes. Finally, the ionic conductivities of the three different block copolymers were compared.

### 5.3.1. Chemical characterization of polymer matrices

The structures of the resulting BCPs were characterized by hydrogen-1 nuclear magnetic resonance ( $^1\text{H}$  NMR) and attenuated total reflectance-Fourier-transform infrared spectroscopy (ATR-FTIR).

#### 5.3.1.1. Hydrogen-1 nuclear magnetic resonance ( $^1\text{H}$ NMR)



**Figure 5.1.** a) Structure of the as-prepared block-copolymer and b)  $^1\text{H}$  NMR spectra of copolymer matrices with three different compositions.

As it can be observed in **Figure 5.1b**, the absence of  $-\text{NH}_2$  and  $-\text{OH}$  signals in the range of 8–10 ppm in  $^1\text{H}$  NMR confirms the dehydration reaction of amine and carboxyl groups, thus the imide ring is formed. The broad peaks in the 6–8 ppm range, named as **A** in the spectra, correspond to  $-\text{CH}$  groups from the phenyl group of the PS. The doublet at 1 ppm and the singlet at 3.6 ppm, marked as **G** and **B**, correspond to the protons from  $-\text{CH}_3$  and  $-\text{CH}$  groups of the propylene oxide (PO) units in Jeffamine<sup>®</sup> side chains, respectively. The peaks at 1.2 ppm and 3.5 ppm, designated as **F** and **C**, correspond to the protons from  $-\text{CH}_2$  groups from the polymer backbone and PS and Jeffamine<sup>®</sup> side chains. The signal at 3.35 ppm,

named as **D**, corresponds to the protons from  $-CH_2$  and terminal  $-CH_3$  groups from Jeffamine<sup>®</sup> side chains. Finally, the signal at 2.7 ppm, marked as **E**, correspond to the  $-CH$  groups from the polymer backbone and terminal  $-CH_2$  group from PS block.

Taking into account the differentiated signals at 7 ppm and 1 ppm assigned to the respective phenyl group of PS block  $-[CH-CH-C_6H_5]-$  and methyl group  $-[CH_2-CH-(CH_3)-O]-$  of PO units contained in Jeffamine<sup>®</sup> chain, the obtained weight ratios of Jeffamine<sup>®</sup>/PS blocks are quantified and given in **Table 5.2**. The feeding ratios of Jeffamine<sup>®</sup>/PS closely match with the observed ones, and those copolymers have molecular weights in the range of  $2 \times 10^6$  to  $1.4 \times 10^7$  g mol<sup>-1</sup>, estimated from the <sup>1</sup>H-NMR spectra and taking into account the theoretical molecular weights of each component.

**Table 5.2.** Comparison of Jeffamine/PS feeding ratios and observed ratios quantified by <sup>1</sup>H-NMR for the different copolymers and calculated molecular weight.

Matrix	Feeding ratio/ wt%	Observed ratio <sup>[a]</sup> / wt%	$M_w^{[b]}/ \times 10^6$ g mol <sup>-1</sup>
BCP70	70:30	74:26	2–12
BCP60	60:40	59:41	2–13
BCP50	50:50	52:48	2–14

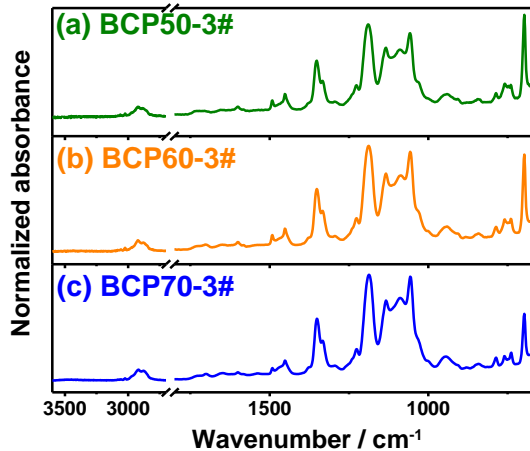
[a] Calculated by the integration of the peaks at 1 and 7 ppm in <sup>1</sup>H-NMR assigned to the methyl group of the PO segment of Jeffamine and the styrene ring of PS, respectively. [b] Estimated molecular weight from <sup>1</sup>H-NMR.

### 5.3.1.2. Attenuated total reflectance-Fourier-transform Infrared Spectroscopy (ATR-FTIR)

In **Figure 5.2** the ATR-FTIR spectra collected for the different block copolymer electrolytes with EO/Li = 8 are shown. The absence of  $-NH_2$  and  $-OH$  signals at the range of  $3500-3200$  cm<sup>-1</sup> in ATR-FTIR confirms, again, the imide ring formation by chemical dehydration treatment. The characteristic signals of Jeffamine<sup>®</sup> side chains appear in the wavenumbers assigned in **Chapter 3**; *i.e.*, stretching mode of C-H<sub>x</sub> at  $3000$  cm<sup>-1</sup>; scissoring mode of C-H<sub>2</sub> at  $1450$  cm<sup>-1</sup>; wagging mode of C-H<sub>x</sub> at  $1350$  cm<sup>-1</sup>; twisting mode of C-H<sub>x</sub> at  $1250$  cm<sup>-1</sup>, rocking mode C-H<sub>x</sub> at  $950$  cm<sup>-1</sup> and C-O-C stretching and C-H<sub>2</sub> bending peak at  $1150$  cm<sup>-1</sup>. Finally, the signal at  $700$  cm<sup>-1</sup> corresponds to C-H bonds from phenyl group of PS.

As it can be observed, this signal decreases with decreasing concentration of PS fraction.

On the other hand, characteristic signals assigned to TFSI<sup>-</sup> appear at  $\sim 1380\text{ cm}^{-1}$  and  $\sim 1130\text{ cm}^{-1}$  (stretching of SO<sub>2</sub>),  $1060\text{ cm}^{-1}$  and  $761\text{ cm}^{-1}$  (stretching SNS) as it was discussed in **Chapter 4** [31].



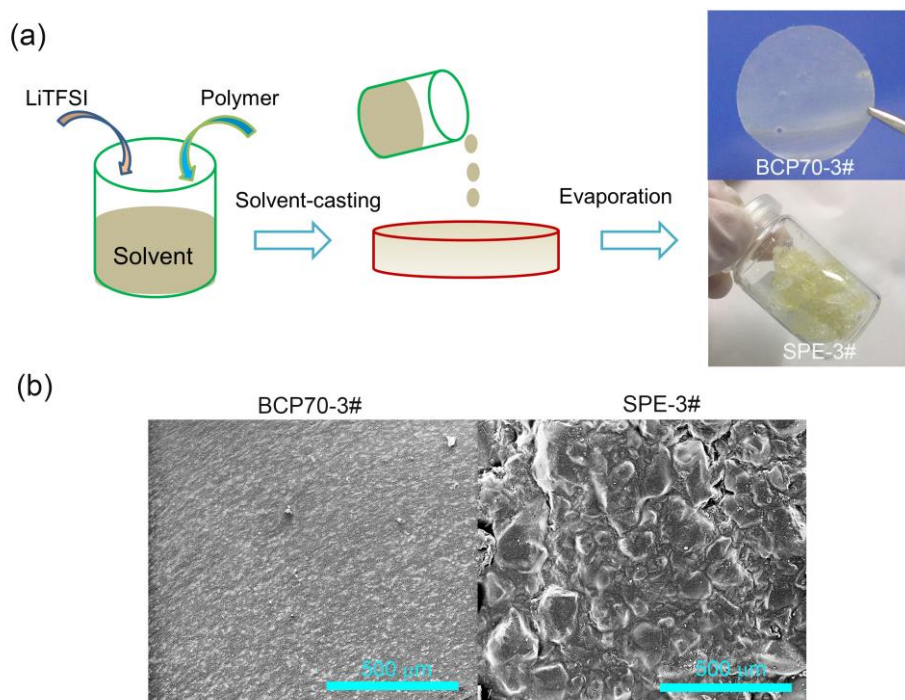
**Figure 5.2.** ATR-FTIR spectra of copolymer matrices with three different compositions.

### 5.3.2. Mechanical properties

The polymer electrolytes based on both copolymer and homopolymer matrices were prepared by conventional solvent casting method using a mixture of acetonitrile (ACN) and tetrahydrofuran (THF) (50:50 by volume), as illustrated in **Figure 5.3**. As it can be observed in **Figure 5.3a**, the introduction of PS block dramatically improves the solubility of Jeffamine-based copolymer in organic solvents, as well as their mechanical stabilities, and thereby a self-standing membrane with good ductility could be obtained. In contrast, the homopolymer-based SPEs appear to be very elastic and sticky as it has been described in **Chapter 3** and **Chapter 4**. As seen from **Figure 5.3b** the comparison of the SEM images for both types of electrolytes clearly shows a better homogeneity for copolymer-based polymer electrolyte.

It has to be mentioned that the mechanical properties of the BCPs were measured by differential mechanical analysis (DMA). However, all the membranes

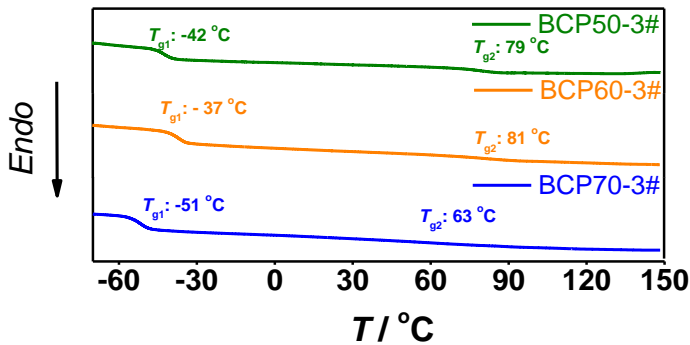
were broken when the measurement started. This can be due to immiscibility between Jeffamine and PS blocks and the high  $T_g$  value (*ca.* 87 °C) of the PS blocks that determine the mechanical properties of copolymer.



**Figure 5.3.** a) Preparation, optical and b) SEM images of the copolymer (BCP70-3#) and homopolymer (SPE-3#).

### 5.3.3. Thermal characterization

**Figure 5.4** gathers the thermograms of copolymer electrolytes with different amount of PS block and same salt concentration of EO/Li = 8. Clearly, the  $T_g$  values of BCP60 and BCP50-based electrolytes are higher than that of the BCP70-based one, suggesting that 70 wt% Jeffamine is an optimal composition that could balance the mechanical properties and flexibility of polymer backbone.



**Figure 5.4.** DSC traces of the copolymer-based electrolytes with different content of PS block.

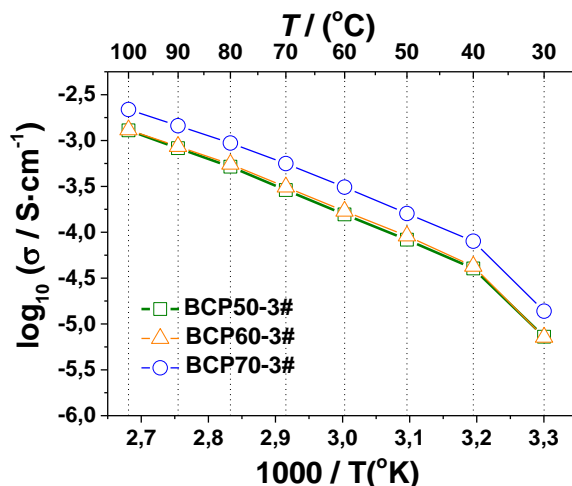
#### 5.3.4. Ionic conductivity

As it was described in the introduction chapter, the limiting factor of practical usage of polymer electrolytes is their ionic conductivity. The drop of ionic conductivity in block copolymers is related with the presence of high fraction of PS chains that are not able to dissociate the salt. As a consequence, the ionic conductivity occurs in the Jeffamine-based block (conductive block).

Jeffamine<sup>®</sup>-based electrolytes and the PS block show sufficient electrochemical stability and compatibility with Li electrode, as it is known from literature [32]. For this reason, the study of ionic conductivity was chosen as the key parameter to determine the most suitable copolymer matrix.

**Figure 5.5** presents the influence of Jeffamine/PS composition for ionic conductivity of BCP-based polymer electrolytes. One may note that the highest values of conductivities are registered for electrolyte BCP70 matrix, and the increase of the amount of PS block in the matrix results in a lower value of ionic conductivity. This can be related to two main factors: 1) lower fraction of conducting volume, and 2) the tortuosity of the resulting material. This is supported by the DSC results where BCP-based electrolytes tend to have a higher  $T_g$  for Jeffamine block with the increase of PS ratio. Thus, among the three analyzed materials, the material comprising BCP70 was selected as the most suitable polymer matrix for the next steps of the study.





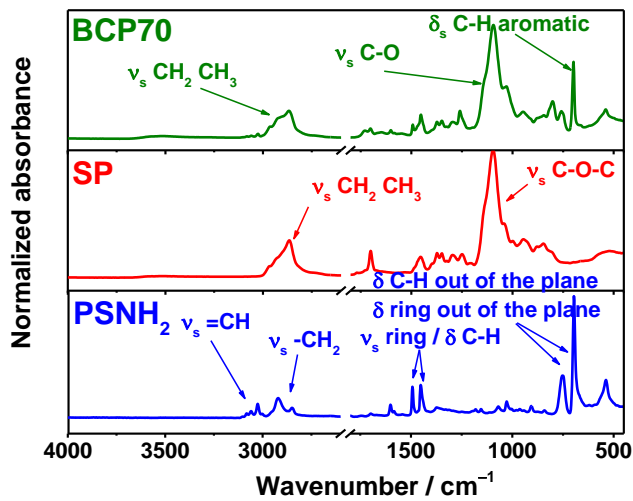
**Figure 5.5.** Arrhenius plot of ionic conductivity of the BCP-based electrolytes with various amount of Jeffamine block.

## 5.4. Characterization of BCP70 polymer matrix and electrolytes

### 5.4.1. Chemical characterization

The ATR-FTIR spectra collected for copolymer matrix BCP70, Jeffamine-based homopolymer (SP) and PS-NH<sub>2</sub> are depicted in **Figure 5.6**. In the case of PS-NH<sub>2</sub>, the stretching modes of =C-H and C-H<sub>2</sub> are detected at 3030 cm<sup>-1</sup> and 2900 cm<sup>-1</sup> respectively. The signals corresponding to the ring appear at the following wavenumber; symmetric stretching of the ring at 1490 cm<sup>-1</sup>, deformation of C-H bond at 1450 cm<sup>-1</sup>, and deformation modes out of the plane at 745 cm<sup>-1</sup> and 700 cm<sup>-1</sup> respectively. As for the SPE, stretching mode of C-H<sub>2</sub> and C-H<sub>3</sub> are detected at 3000 cm<sup>-1</sup>. The intense peak at 1150 cm<sup>-1</sup> is a result from the superposition of C-O-C stretching and C-H<sub>2</sub> bending modes from Jeffamine<sup>®</sup> side chains.

In the case of BCP70, a mixture of the above mentioned signals is detected. At around 3000 cm<sup>-1</sup> the signal corresponding to stretching mode of C-H<sub>2</sub> and C-H<sub>3</sub> is detected. The intense peak at 1150 cm<sup>-1</sup> corresponds to Jeffamine<sup>®</sup> side chains, whereas the intense peak at 700 cm<sup>-1</sup> corresponds to the deformation modes of PS ring.



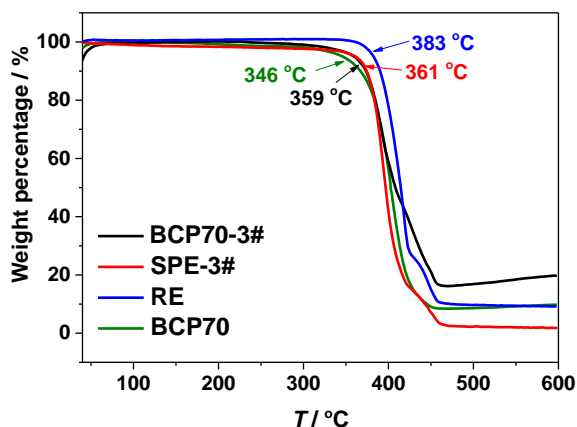
**Figure 5.6.** ATR-FTIR spectra of copolymer matrix, Jeffamine-based homopolymer and PS-NH<sub>2</sub>.

## 5.4.2. Thermal characterization

### 5.4.2.1. Thermogravimetric analysis (TGA)

**Figure 5.7** presents the TGA traces of selected solid polymer electrolytes, as well as the polymer matrix of BCP70. All the materials show decomposition temperatures ( $T_d$ ) higher than 300 °C, which are suitable for ASSLMBs where the stability is limited by the melting point of Li<sup>o</sup> electrode ( $T_m = 180$  °C). The slightly lower value of  $T_d$  for BCP70-3# compared to that for the representative LiTFSI/PEO electrolyte (referred as RE) imposes that the pyrolysis of the electrolytes is dominated by the thermal lability of the Jeffamine-based copolymer matrix. This is in agreement with the nearly overlapped TGA traces between the copolymer electrolyte (BCP70-3#) and its matrix (BCP70), and the reported excellent thermal stability for LiTFSI ( $T_d = 384$  °C)[33].

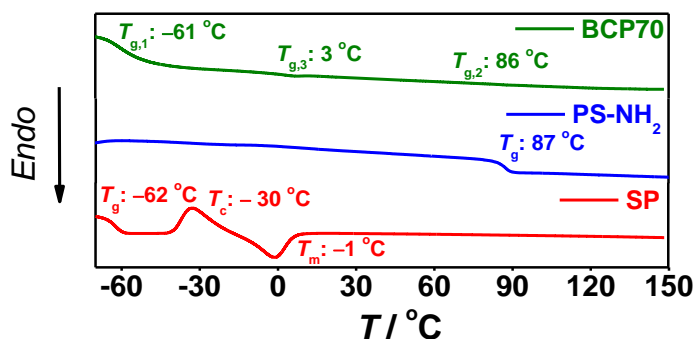
One may also notice that the copolymer electrolyte (BCP70-3#) has a  $T_d$  value very close to the homopolymer electrolyte (SPE-3#), suggesting that the introduction of PS block does not affect the thermal stability of the Jeffamine-based SPEs and thermal degradation is initiated by polyether chain decomposition.



**Figure 5.7.** Thermal gravimetric analysis (TGA) traces of the polymer matrix and electrolytes.

#### 5.4.2.2. Differential scanning calorimetry (DSC)

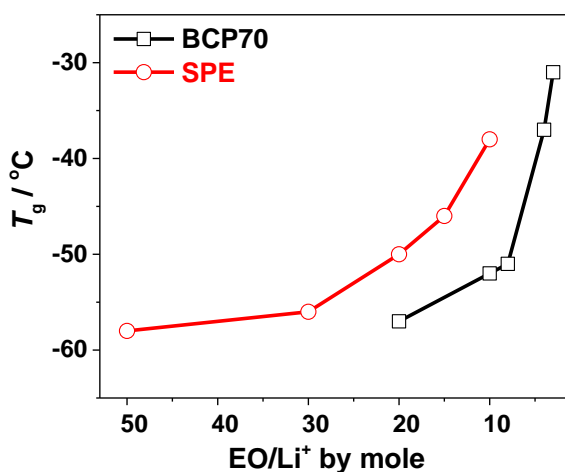
The flexibility of polymer segments is of great importance for facilitating the ionic motion in solid polymer electrolytes. It could be partially revealed by the glass transitions of the electrolytes. **Figure 5.8** presents the thermograms of Jeffamine-based homopolymer (SPE), amine terminated poly(styrene) (PS-NH<sub>2</sub>) and BCP70. The magnified DSC trace is shown in **Figure A.5.1** to make all the glass transitions legible.



**Figure 5.8.** DSC traces of polymer matrices and PS-NH<sub>2</sub> starting product.

PS-NH<sub>2</sub> shows only glass transition at *ca.* 87 °C, which is related to the amorphous fraction within PS having molecular weight below 10<sup>4</sup> g mol<sup>-1</sup> [34]. The polyether fraction in SPE has glass transition at -62 °C, which is typical for Jeffamine side chains as described in **Chapter 3** and **Chapter 4** [12, 29]. The  $T_g$  value for Jeffamine and PS blocks in the copolymer are very close to the respective ones in the homopolymers, *e.g.*, -62 °C (Jeffamine in BCP) *vs.* -61 °C (Jeffamine in homopolymer) and 86 °C (PS in BCP) *vs.* 87 °C (PS in homopolymer). This indicates that Jeffamine and PS blocks are immiscible and separated blocks in the copolymer matrices. However, in addition to the benefit that copolymerization by PS side chains led to an improvement in global mechanical properties (**Scheme 5.1**), the copolymer was free from the crystallization of EO or, of course, PO units which could be ascribed to the presence of rigid PS phase that could block the reorganization of ether units to form crystalline phase.

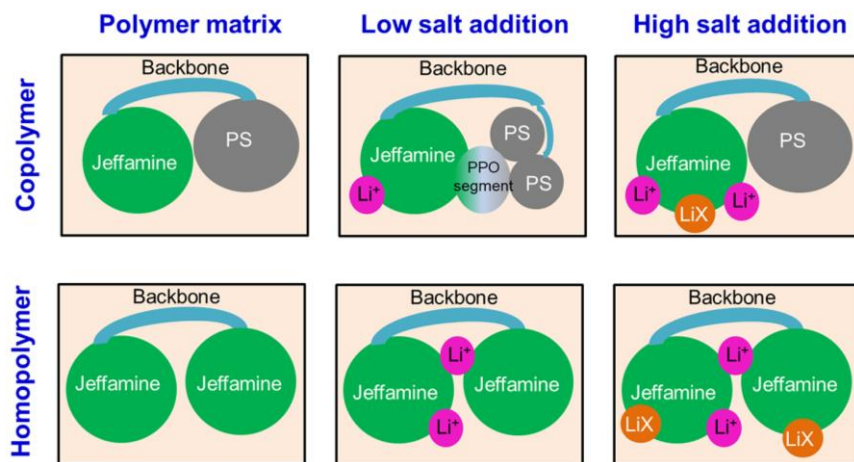
**Figure 5.9** depicts the dependence of  $T_g$  values (for polyether moieties) *vs.* salt concentration for both copolymer and homopolymer-based electrolytes. The corresponding DSC traces of BCP- and SPE-based electrolytes are presented in **Figure A.5.2**.



**Figure 5.9.** The dependence of  $T_g$  values (for polyether moieties) *vs.* salt concentration for both copolymer and homopolymer-based electrolytes.

The value of  $T_g$  for SPE without salt reaches  $-62\text{ }^\circ\text{C}$ , and then increases up to  $-38\text{ }^\circ\text{C}$  ( $\text{EO}/\text{Li} = 10$ ) with the addition of lithium salt. This is a characteristic behaviour of solid polymer electrolytes where salt concentration increases the number of transient crosslinking in bulk polymer resulting in higher energy required for  $T_g$  of polymer [2]. With increasing salt content in copolymer electrolyte,  $T_g$  values of EO segments are increasing but not as significantly as those for the homopolymer samples. The lower value of  $T_g$  in BCP vs. SPE could be the result of the dilution of the ionic interaction in the presence of the PS block. Interestingly, new  $T_g$  values in the range between  $45\text{--}86\text{ }^\circ\text{C}$  are detected for the PS fraction in the copolymer (**Figure A.5.2**).

It is proposed that at low salt concentrations,  $\text{Li}^+$  interacts primarily with the PEO segments from the Jeffamine while the less solvating propylene oxide (PO) segments remain free. This free PPO segments are able to plasticize the PS blocks due to the interaction between them in the contacting surface and, as a consequence, the  $T_g$  value is decreased. At very high salt concentration (BCP70–5#) the PPO itself becomes involved in the solvation, and the PS blocks regain their original  $T_g$  as illustrated in **Figure 5.10**.



**Figure 5.10.** Schematic illustration of the phase transition in copolymer and homopolymer-based electrolytes.

In particular, a dramatic increase of  $T_g$  in BCP-based electrolytes appears for salt concentrations higher than EO/Li = 8. This behaviour indicates that there is a preferential salt/EO-PO interaction, thus leaving less PO segments free to plasticize the PS block and giving higher  $T_g$  values corresponding to PS fraction.

### 5.4.3. Electrochemical characterization

#### 5.4.3.1. Ionic conductivity

Figure 5.11 shows the ionic conductivity ( $\sigma$ ) of the polymer matrix BCP70 with different salt concentration. The temperature dependence of ionic conductivities for all the BCP-based samples follows a continuous Vogel-Tamman-Fulcher (VTF) behaviour, indicating a fully amorphous nature of the electrolyte in the measured temperature range. This is supported by the DSC results where low glass transitions of  $-60$  to  $-30$  °C are observed for those BCP-based polymer electrolytes without any other thermal change before reaching the  $T_g$  of the styrene blocks (Figure A.5.2).

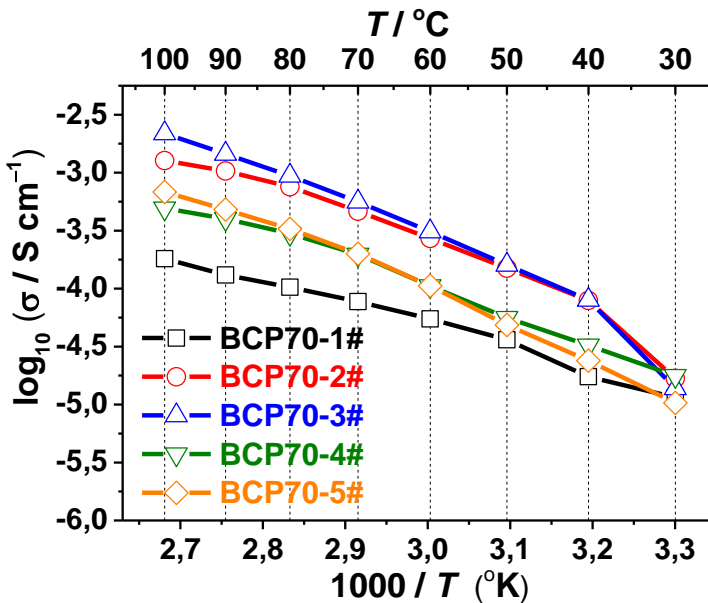
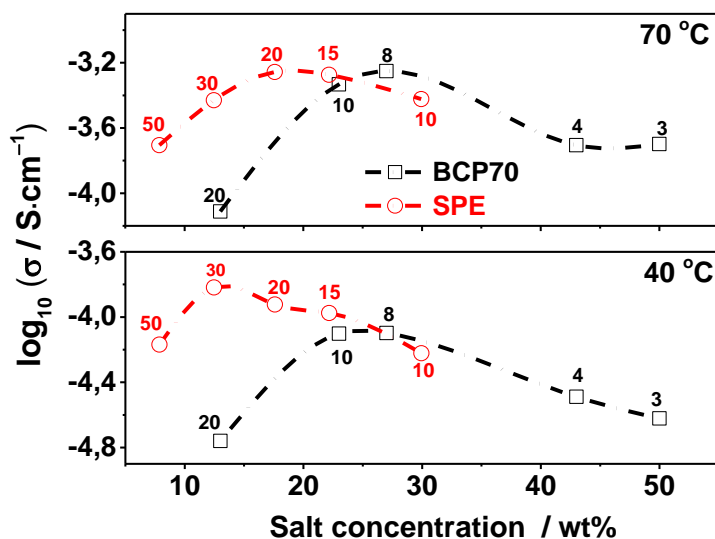


Figure 5.11. Arrhenius plot of ionic conductivity for the polymer matrix BCP70 with different salt concentration.

The effect of salt concentration on ionic conductivity for the BCP-based electrolytes is comparatively displayed with SPE-based electrolytes in **Figure 5.12**. For both type of electrolytes, an optimal amount of lithium salt is observed, due to the trade-off between ion species and ion mobility, *i.e.*, the increase of salt concentration provides more ionic species but at the expense of a decreased flexibility of the polymer backbone. For example, the highest ionic conductivities are registered with 27 wt% (EO/Li = 8) and 18 wt% LiTFSI (EO/Li = 20) for the BCP-3# and SPE-3# electrolytes, respectively

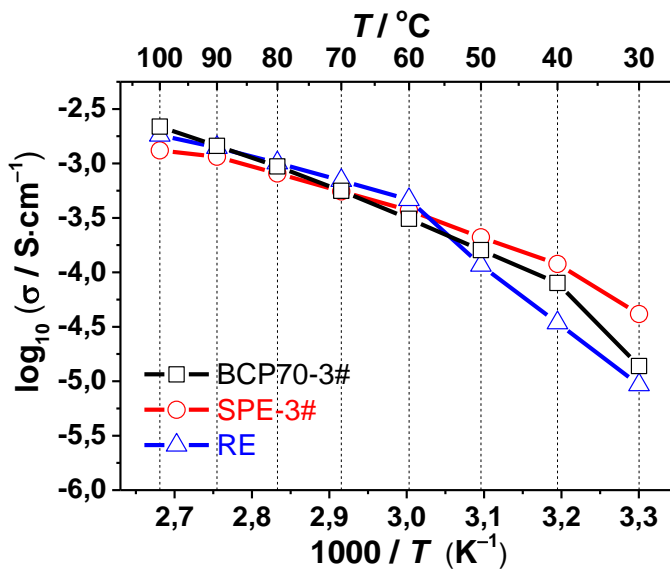


**Figure 5.12.** Dependence of the ionic conductivity on the salt concentration for the BCP-based and SPE-based electrolytes.

Effectively, the ionic conductivity of BCP70-3# is very close to that of the SPE-3# and reaches a high value of  $5 \times 10^{-4} \text{ S cm}^{-1}$  at 70 °C. It suggests that the incorporation of immiscible PS block into Jeffamine-based polymers improves remarkably the mechanical properties but with minimal impact on the ionic conductivity, a feature that has not been observed before for other block copolymers.

**Figure 5.13** compares further the ionic conductivity of BCP70-3#, SPE-3# and RE. Though the ionic conductivity decreases slightly at RT for BCP70-3#, is still higher than that of RE. This is due to the flexible PO/EO units within the Jeffamine

block, which could ensure the high mobility of polymer backbone, and thereby resulting in higher ionic conductivities.



**Figure 5.13.** Comparison of the ionic conductivity of BCP70-3#, SPE-3# and reference electrolyte.

#### 5.4.3.2. Li-ion transference number

The lithium-ion transference number ( $T_{Li}^+$ ) was measured by the method described in **Chapter 2** section 2.4.5. **Table 5.3** summarizes the measured results of the parameters used to calculate the value of  $T_{Li}^+$  for the three solid polymer electrolytes. As an example, the EIS spectra and polarization profile of a Li | BCP70-3# | Li cell is presented in **Figure 5.14**.

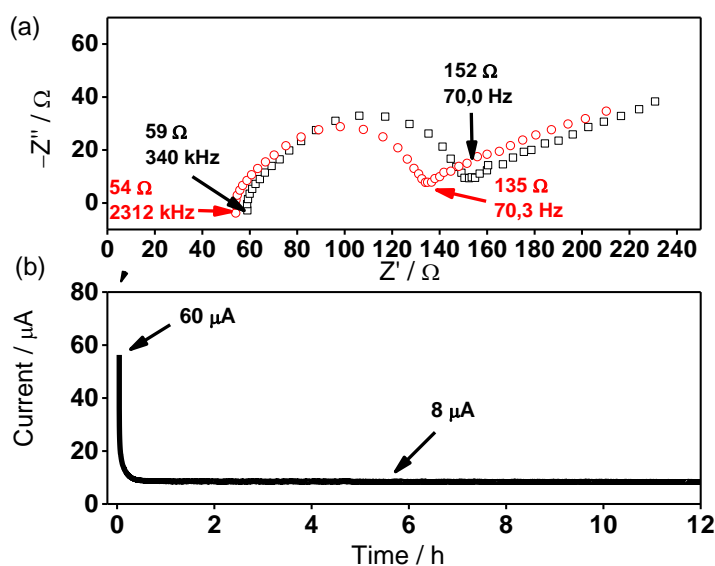
In general, the ion transport of coupled polymer electrolyte systems is facilitated by the segmental motion of flexible polymer backbones (*e.g.*, Jeffamine® chains). The transport of  $Li^+$  cations is demonstrated to be more difficult than that of anions in the coupled polymer electrolyte systems (*i.e.*, low  $T_{Li}^+$  of  $< 0.5$ ), due to the strong interactions between  $Li^+$  cation and electron donating ethylene oxide units.



**Table 5.3.** The calculated values of Li-ion transference number ( $T_{Li^+}$ ) of various electrolytes at 70 °C.

Electrolyte	$I_0$ [a] / $\mu\text{A}$	$I_s$ [b] / $\mu\text{A}$	$R_b^0$ [c] / $\Omega$	$R_b^s$ [d] / $\Omega$	$R_i^0$ [e] / $\Omega$	$R_i^s$ [f] / $\Omega$	$\Delta V$ [g] / mV	$T_{Li^+}$
BCP70-3#	60	8	59	54	92	81	10	0.08
SPE-3#	8	2	435	442	966	812	10	0.16
RE	23	12	30	31	360	364	10	0.17

[a] Initial and [b] steady-state current obtained by dc polarization; [c] initial and [d] final resistances of the electrolytes measured by ac impedance method before and after polarization, respectively; [e] initial and [f] final resistances of interfacial layer between electrode/electrolyte measured by ac impedance method before and after polarization, respectively; [g] the dc voltage subjected to the  $Li^+$  symmetrical cell.



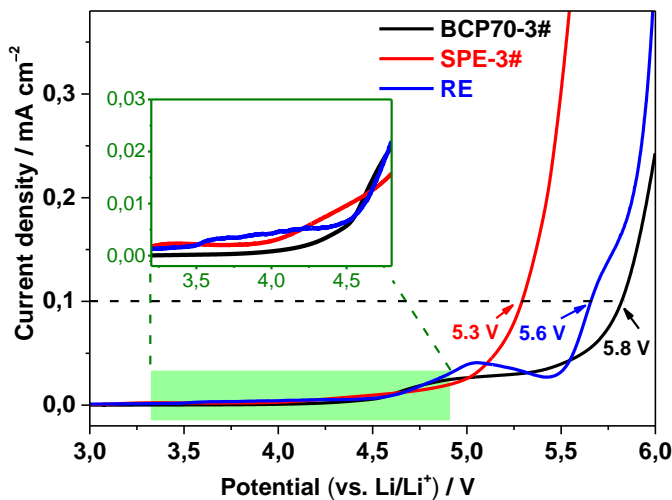
**Figure 5.14.** a) Impedance spectra and b) time-dependence response of current to 10 mV dc polarization for the BCP70-3# obtained on the  $Li^+$  symmetric cell at 70 °C.

As seen from **Table 5.3** and **Figure 5.14**, all these three electrolytes show low  $T_{Li^+}$  values of  $< 0.2$ , characteristic of dual-ion conducting electrolytes where lithium salts with discrete anions are employed [35]. The value of  $T_{Li^+}$  for BCP70-3# is 0.08 at 70 °C, which is lower than those of SPE-3# and RE. This implies that the motion of  $Li^+$  cation is more significantly retarded compared to that of the corresponding anions upon the introduction of PS blocks. Knowing that the PPO segments which are brought by the Jeffamine are also immiscible with the PEO

when salt-laden, this lower  $T_{Li^+}$  can be likely ascribed to the increased tortuosity of the lithium path in the Jeffamine chains due to the PS and PPO domains, as the  $Li^+$  cations are “bound” to polymer backbones and their transport relies heavily on the properties of polymer host. However, unsolvated  $TFSI^-$  anions are less sensitive to these phase separations and may diffuse at least in the PPO phase.

### 5.4.3.3. Electrochemical stability toward oxidation

The choice of cathode materials for ASSLMBs is generally governed by the anodic stability of SPEs. **Figure 5.15** exhibits the linear sweeping voltammetry (LSV) profiles of the  $Li^+ ||$  stainless steel (SS) cells using BCP70-3#, SPE-3# and RE at 70 °C.



**Figure 5.15.** Linear sweeping voltammetry profiles of  $Li^+ ||$  stainless steel (SS) cells using the as-prepared BCP70-3#, SPE-3# and RE at 70 °C.

As a reference, the conventional PEO-based electrolytes suffer from severe oxidative decomposition at a potential above *ca.* 3.8 V vs.  $Li/Li^+$ , due to the presence of the electrochemically liable C–O bond in the polymer backbone. The Jeffamine homopolymer-based electrolyte shows slightly higher onset of oxidation at 4.0 V vs.  $Li/Li^+$ , which is responsible for the cleavage of C–O linkage for EO and PO units in Jeffamine side moieties. However, this electrochemical degradation could be suppressed after introducing the PS blocks and enhanced anodic stability up to 4.2 V vs.  $Li/Li^+$  is detected, as shown in **Figure 5.15**. This could be rationalized by the better electrochemical stability of PS; this segment adsorbs on the surface

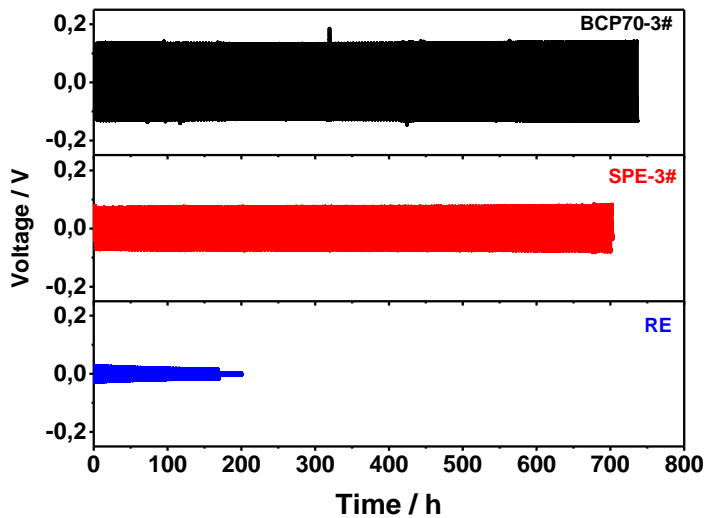
of the electrode and prevent access of the ether-containing chains to the electrode.

It is worthy to point out that the oxidation potential of those three electrolytes could be marked to be higher than 5 V vs. Li/Li<sup>+</sup>, if one overwhelms the minor oxidation of EO-containing matrices around 4 V vs. Li/Li<sup>+</sup>. However, it may not be significant for the implementation of those electrolytes in ASSLMs, since the active materials such as lithium cobalt oxide (LCO) or lithium nickel manganese cobalt oxide (NMC) can strongly oxidize catalytically the PEO matrices at a potential *ca.* 4 V vs. Li/Li<sup>+</sup>. Therefore, the BCP-based solid polymer electrolytes are better suited for the cathode having a working potential lower than 4 V vs. Li/Li<sup>+</sup>, such LFP (< 4.5 vs. Li/Li<sup>+</sup>), sulphur (S<sub>8</sub>) and oxygen (O<sub>2</sub>) (< 3.0 vs. Li/Li<sup>+</sup>) cathode materials.

#### 5.4.3.4. Compatibility with Li<sup>0</sup> electrode

The operation of ASSLMs requires a highly reversible, dendrite-free cycling of the Li<sup>0</sup> electrode. This could be assessed by the plating/stripping measurements under galvanostatic mode. **Figure 5.16** shows the voltage profiles of Li<sup>0</sup> symmetric cells after applying a constant current density of 0.1 mA cm<sup>-2</sup>.

The cell using LiTFSI/PEO reference electrolyte lasts only 160 hours before the occurrence of internal short-circuit. In contrast, the replacement of PEO with Jeffamine-based homopolymer and copolymer improves remarkably the cycle life of Li<sup>0</sup> symmetric cells (> 700 hours), which is attributed to the good contact between electrolyte/electrode inherited from the extremely flexible and elastic properties of the Jeffamine block. Therefore, the BCP-based electrolyte would be a safe and stable electrolyte against the use of Li<sup>0</sup> electrode.



**Figure 5.16.** Galvanostatic cycling performance for the  $\text{Li}^\circ$  symmetrical cells using the as-prepared BCP70-3#, SPE-3# and RE at a constant current density of  $0.1 \text{ mA cm}^{-2}$ , each half-cycle lasts 2 h at  $70^\circ\text{C}$ .

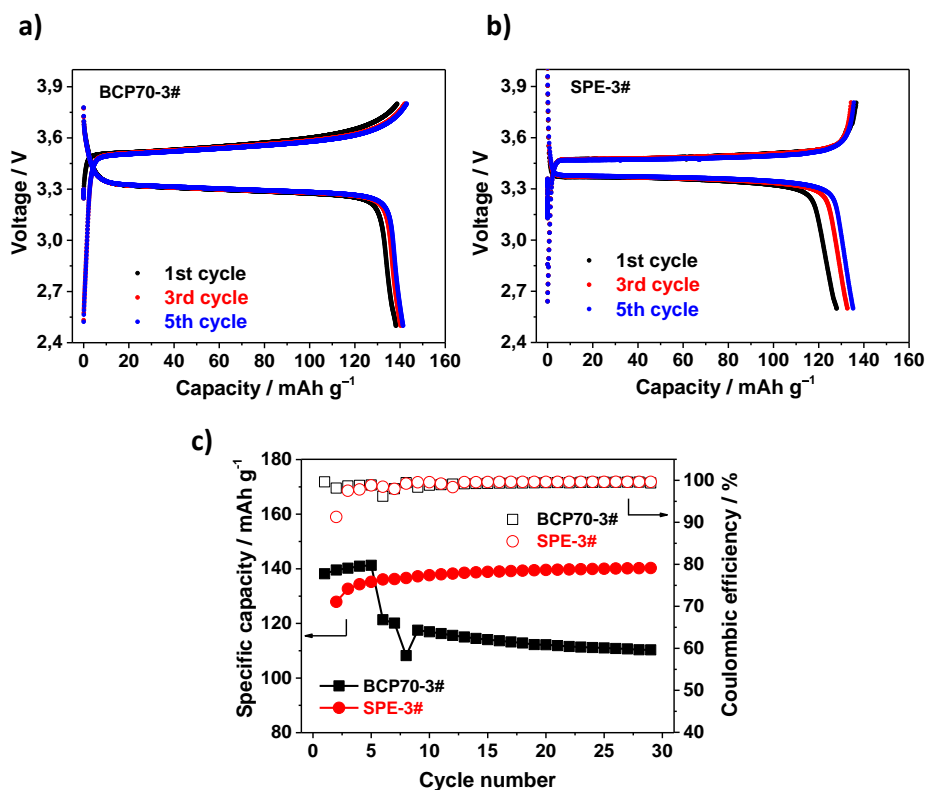
#### 5.4.3.5. Cycling of $\text{Li}^\circ$ | $\text{LiFePO}_4$ cell performance

In view of above mentioned good chemical and electrochemical properties, the feasibility of employing the prepared BCPs as solid electrolytes for ASSLMBs is demonstrated by the galvanostatic cycling of the  $\text{Li}^\circ|\text{BCPs}|\text{LFP}$  cells. **Figure 5.17** shows the cycling performance of the cells using BCP70-3# and SPE-3# electrolytes at  $70^\circ\text{C}$ .

As it can be observed in **Figure 5.17 a)** and **b)**, both the BCP70-3# and SPE-3# cells could deliver a high specific discharge capacity of *ca.*  $140 \text{ mAh g}^{-1}$  at the first cycle and maintains it stable after three formation cycles. This is attributable to the high ionic conductivity of both electrolytes and the good compatibility of Jeffamine-based polymer matrices with  $\text{Li}^\circ$  electrode.

Note that the charge/discharge plateau of BCP-based cell deviates more from the theoretical values ( $3.45 \text{ V vs. Li/Li}^+$ ) compared with that of the SPE-based one, indicating a higher polarization for the former cell. This would be attributed to: 1) the relatively lower Li-ion conductivity resulted from the decreased  $T_{\text{Li}^+}$  of the copolymer electrolyte, 2) the inferior binding properties of BCP matrix in the

composite LFP cathode, thus leading to an increased cell resistance. Nevertheless, BCP-based cell could be cycled with good Coulombic efficiency for 30 cycles, whereas the RE-based cell encounters deteriorated stability for charging process due to the formation of soft Li dendrites, as shown in recent publication from the group [36].



**Figure 5.17.** Charge/discharge profiles of the Li<sup>o</sup>|SPEs|LFP cells using **a)** BCP70-3# and **b)** SPE-3# as electrolyte at 70 °C. Charge/discharge rate 0.05/0.05C. **c)** Specific discharge capacity and Coulombic efficiency vs. cycle number for the cells using BCP70-3# and SPE-3# electrolytes cycled at 70 °C. Charge/discharge rate: 0.05/0.05C (the first five cycles) and 0.1/0.1C (the following cycles).

## 5.5. Conclusions

A new family of self-standing and highly conductive solid polymer electrolytes based on tailor-made block copolymers was prepared and characterized. The polymer matrices, comprising an ionic conducting block (*i.e.*,

comb polymer containing polyether side moieties, Jeffamine®) and a structural block (*i.e.*, amine terminated PS), could be used as a scaffold to build solid polymer electrolytes with a well-balanced ionic conductivity and mechanical properties.

The improved mechanical properties of the Jeffamine-based copolymer electrolytes at a very small expense of the ionic conductivity are crucial for processing solid polymer electrolytes in large-format polymer batteries, since they could allow the adaptation of Li-ion battery production line by using those self-standing electrolyte membranes like conventional separators (~25  $\mu\text{m}$ ). Moreover, with continuous effort on developing lithium salt with less mobile anions, the Li-ion conductivities of the Jeffamine-based copolymer electrolytes could be further improved.

The incorporation of the PS block into the Jeffamine-based polymer could also improve the electrochemical stability of BCP-based solid polymer electrolytes vs.  $\text{Li}^\circ$  electrode. The  $\text{Li}^\circ \mid \mid \text{LFP}$  cell using BCP-based electrolytes shows good cycling stability and high Coulombic efficiency. However, despite the promising properties of these novel BCPs, the  $\text{Li}^\circ \mid \mid \text{LFP}$  cell could not be cycled for more than 30 cycles with good cycling stability. As a consequence, further modifications are required in order to obtain promising candidates for designing safe and high-performance all-solid-state lithium metal batteries.

## References

- [1] M.B. Armand. Polymer Electrolytes. *Annu. Rev. Mater. Sci.* 1986; **16**(1), 245-261.
- [2] H. Zhang, C. Liu, L. Zheng, F. Xu, W. Feng, H. Li, X. Huang, M. Armand, J. Nie, Z. Zhou. Lithium bis(fluorosulfonyl)imide/poly(ethylene oxide) polymer electrolyte. *Electrochim. Acta.* 2014; **133**, 529-538.
- [3] M. Armand. The history of polymer electrolytes. *Solid State Ion.* 1994; **69**(3), 309-319.
- [4] S. Lascaud, M. Perrier, A. Vallee, S. Besner, J. Prud'homme, M. Armand. Phase diagrams and conductivity behavior of poly(ethylene oxide)-molten salt rubbery electrolytes. *Macromolecules.* 1994; **27**(25), 7469-7477.
- [5] M. Rosso, C. Brissot, A. Teyssot, M. Dollé, L. Sannier, J.M. Tarascon, R. Bouchet, S. Lascaud. Dendrite short-circuit and fuse effect on Li/polymer/Li cells. *Electrochim. Acta.* 2006; **51**(25), 5334-5340.
- [6] M. Dollé, L. Sannier, B. Beaudoin, M. Trentin, J.M. Tarascon. Live scanning electron microscope observations of dendritic growth in lithium/polymer cells. *Electrochem. Solid State Lett.* 2002; **5**(12), A286-A289.
- [7] D. Golodnitsky, E. Strauss, E. Peled, S. Greenbaum. Review—on order and disorder in polymer electrolytes. *J. Electrochem. Soc.* 2015; **162**(14), A2551-A2566.
- [8] Y. Ikeda, Y. Wada, Y. Matoba, S. Murakami, S. Kohjiya. Characterization of comb-shaped high molecular weight poly(oxyethylene) with tri(oxyethylene) side chains for a polymer solid electrolyte. *Electrochim. Acta.* 2000; **45**(8), 1167-1174.
- [9] N.A. Stolwijk, C. Heddier, M. Reschke, M. Wiencierz, J. Bokeloh, G. Wilde. Salt-concentration dependence of the glass transition temperature in PEO-NaI and PEO-LiTFSI polymer electrolytes. *Macromolecules.* 2013; **46**(21), 8580-8588.
- [10] C.P. Fonseca, S. Neves. Characterization of polymer electrolytes based on poly(dimethyl siloxane-co-ethylene oxide). *J. Power Sources.* 2002; **104**(1), 85-89.
- [11] K.M. Abraham, M. Alamgir. Ambient temperature rechargeable polymer-electrolyte batteries. *J. Power Sources.* 1993; **43**(1), 195-208.

- [12] I. Aldalur, H. Zhang, M. Piszcz, U. Oteo, L.M. Rodriguez-Martinez, D. Shanmukaraj, T. Rojo, M. Armand. Jeffamine® based polymers as highly conductive polymer electrolytes and cathode binder materials for battery application. *J. Power Sources*. 2017; **347**, 37-46.
- [13] W.S. Young, W.F. Kuan, I. Epps, Thomas H. Block copolymer electrolytes for rechargeable lithium batteries. *J. polym. Sci. Pol. Phys.* 2014; **52**(1), 1-16.
- [14] C. Giacomelli, V. Schmidt, K. Aissou, R. Borsali. Block copolymer systems: from single chain to self-assembled nanostructures. *Langmuir*. 2010; **26**(20), 15734-15744.
- [15] D.R. Sadoway. Block and graft copolymer electrolytes for high-performance, solid-state, lithium batteries. *J. Power Sources*. 2004; **129**(1), 1-3.
- [16] W.S. Young, T.H. Epps. Ionic conductivities of block copolymer electrolytes with various conducting pathways: sample preparation and processing considerations. *Macromolecules*. 2012; **45**(11), 4689-4697.
- [17] E.D. Gomez, A. Panday, E.H. Feng, V. Chen, G.M. Stone, A.M. Minor, C. Kisielowski, K.H. Downing, O. Borodin, G.D. Smith, N.P. Balsara. Effect of ion distribution on conductivity of block copolymer electrolytes. *Nano Lett.* 2009; **9**(3), 1212-1216.
- [18] M. Singh, O. Odusanya, G.M. Wilmes, H.B. Eitouni, E.D. Gomez, A.J. Patel, V.L. Chen, M.J. Park, P. Fragouli, H. Iatrou, N. Hadjichristidis, D. Cookson, N.P. Balsara. Effect of molecular weight on the mechanical and electrical properties of block copolymer electrolytes. *Macromolecules*. 2007; **40**(13), 4578-4585.
- [19] S.W. Ryu, P.E. Trapa, S.C. Olugebefola, J.A. Gonzalez-Leon, D.R. Sadoway, A.M. Mayes. Effect of counter ion placement on conductivity in single-ion conducting block copolymer electrolytes. *J. Electrochem. Soc.* 2005; **152**(1), A158-A163.
- [20] P.E. Trapa, Y.Y. Won, S.C. Mui, E.A. Olivetti, B. Huang, D.R. Sadoway, A.M. Mayes, S. Dallek. Rubbery graft copolymer electrolytes for solid-state, thin-film lithium batteries. *J. Electrochem. Soc.* 2005; **152**(1), A1-A5.
- [21] N.S. Wanakule, A. Panday, S.A. Mullin, E. Gann, A. Hexemer, N.P. Balsara. Ionic conductivity of block copolymer electrolytes in the vicinity of order–disorder and order–order transitions. *Macromolecules*. 2009; **42**(15), 5642-5651.



- [22] M. Chintapalli, T.N.P. Le, N.R. Venkatesan, N.G. Mackay, A.A. Rojas, J.L. Thelen, X.C. Chen, D. Devaux, N.P. Balsara. Structure and ionic conductivity of polystyrene-block-poly(ethylene oxide) electrolytes in the high salt concentration limit. *Macromolecules*. 2016; **49**(5), 1770-1780.
- [23] R. Yuan, A.A. Teran, I. Gurevitch, S.A. Mullin, N.S. Wanakule, N.P. Balsara. Ionic conductivity of low molecular weight block copolymer electrolytes. *Macromolecules*. 2013; **46**(3), 914-921.
- [24] S.A. Mullin, A.A. Teran, R. Yuan, N.P. Balsara. Effect of thermal history on the ionic conductivity of block copolymer electrolytes. *J. polym. Sci. Pol. Phys.* 2013; **51**(12), 927-934.
- [25] G.M. Stone, S.A. Mullin, A.A. Teran, D.T. Hallinan, A.M. Minor, A. Hexemer, N.P. Balsara. Resolution of the modulus versus adhesion dilemma in solid polymer electrolytes for rechargeable lithium metal batteries. 2012; **159**(3), A222-A227.
- [26] D.T. Hallinan, S.A. Mullin, G.M. Stone, N.P. Balsara. Lithium metal stability in batteries with block copolymer electrolytes. *J. electrochem. Soc.* 2013; **160**(3), A464-A470.
- [27] D. Devaux, D. Glé, T.N.T. Phan, D. Gignes, E. Giroud, M. Deschamps, R. Denoyel, R. Bouchet. Optimization of block copolymer electrolytes for lithium metal batteries. *Chem. Mater.* 2015; **27**(13), 4682-4692.
- [28] R. Bouchet, T.N.T. Phan, E. Beaudoin, D. Devaux, P. Davidson, D. Bertin, R. Denoyel. Charge transport in nanostructured PS-PEO-PS triblock copolymer electrolytes. *Macromolecules*. 2014; **47**(8), 2659-2665.
- [29] I. Aldalur, M. Martinez-Ibañez, M. Piszcz, L.M. Rodriguez-Martinez, H. Zhang, M. Armand. Lowering the operational temperature of all-solid-state lithium polymer cell with highly conductive and interfacially robust solid polymer electrolytes. *J. Power Sources*. 2018; **383**, 144-149.
- [30] M. Piszcz, O. Garcia-Calvo, U. Oteo, J.M. Lopez del Amo, C. Li, L.M. Rodriguez-Martinez, H.B. Youcef, N. Lago, J. Thielen, M. Armand. New single ion conducting blend based on PEO and PA-LiTFSI. *Electrochim. Acta*. 2017; **255**, 48-54.
- [31] M. Piszcz, H. Zhang, M. Marczewski, G.Z. Żukowska, K. Lemańska, M. Sukiennik, M. Siekierski. Vibrational spectroscopic studies combined with viscosity analysis and VTF calculation for hybrid polymer electrolytes. *Solid State Ion*. 2017; **303**, 78-88.

**[32]** B. Zhang, Y. Zhang, N. Zhang, J. Liu, L. Cong, J. Liu, L. Sun, A. Mauger, C.M. Julien, H. Xie, X. Pan. Synthesis and interface stability of polystyrene-poly(ethylene glycol)-polystyrene triblock copolymer as solid-state electrolyte for lithium-metal batteries. *J. Power Sources*. 2019; **428**, 93-104.

**[33]** H. Zhang, W. Feng, J. Nie, Z. Zhou. Recent progresses on electrolytes of fluorosulfonimide anions for improving the performances of rechargeable Li and Li-ion battery. *J. Fluorine Chem.* 2015; **174**, 49-61.

**[34]** E.Q. Chen, Y. Xia, M.J. Graham, M.D. Foster, Y. Mi, W.L. Wu, S.Z.D. Cheng. Glass transition behavior of polystyrene blocks in the cores of collapsed dry micelles tethered by poly(dimethylsiloxane) coronae in a PS-b-PDMS diblock copolymer. *Chem. Mater.* 2003; **15**(11), 2129-2135.

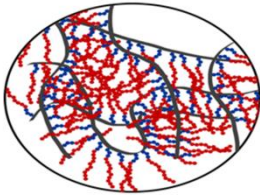
**[35]** H. Zhang, C. Li, M. Piszcz, E. Coya, T. Rojo, L.M. Rodriguez-Martinez, M. Armand, Z. Zhou. Single lithium-ion conducting solid polymer electrolytes: advances and perspectives. *Chem. Soc. Rev.* 2017; **46**(3), 797-815.

**[36]** X. Judez, M. Piszcz, E. Coya, C. Li, I. Aldalur, U. Oteo, Y. Zhang, W. Zhang, L.M. Rodriguez-Martinez, H. Zhang, M. Armand. Stable cycling of lithium metal electrode in nanocomposite solid polymer electrolytes with lithium bis(fluorosulfonyl)imide. *Solid State Ion.* 2018; **318**, 95-101

## Chapter 6

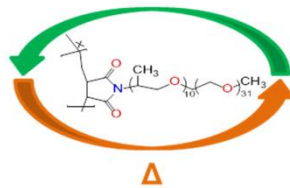
# Flowable polymer electrolytes for lithium metal batteries

Solid polymer (non-soluble)

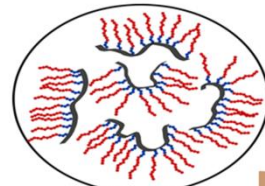


Entanglement between chains

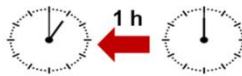
Time



Flowable polymer (soluble)



Free chains



FPE



Flowable polymer electrolytes (FPEs)

I. Aldalur, M. Martinez-Ibañez, A. Krztoń-Maziopa, M. Piszcz, M. Armand, H. Zhang. Flowable polymer electrolytes for lithium metal batteries *Journal of Power Sources*, 423 (2019) 218-226.



## Chapter 6:

### FLOWABLE POLYMER ELECTROLYTES FOR LITHIUM METAL BATTERIES

6.1.	Introduction.....	151
6.2.	Synthesis of Jeffamine-based polymer matrix.....	152
6.3.	Chemical characterization.....	154
6.3.1.	Hydrogen-1 nuclear magnetic resonance ( $^1\text{H}$ NMR).....	154
6.3.2.	Attenuated total reflectance-Fourier-transform infrared spectroscopy (ATR-FTIR).....	155
6.4.	Morphological characterization: Scanning electron microscopy (SEM).....	156
6.5.	Mechanical properties.....	156
6.6.	Thermal characterization.....	159
6.6.1.	Thermogravimetric analysis (TGA).....	159
6.6.2.	Differential scanning calorimetry (DSC).....	160
6.7.	Electrochemical characterization of FPEs.....	162
6.7.1.	Ionic conductivity.....	162
6.7.2.	Li-ion transference number.....	163
6.7.3.	Electrochemical stability toward oxidation.....	164
6.7.4.	Compatibility with $\text{Li}^\circ$ electrode.....	165
6.8.	Application of FPE as buffer layer.....	167
6.8.1.	Formation of buffer layer.....	168
6.8.2.	Electrochemical stability of electrolyte/ $\text{Li}^\circ$ electrode.....	168

6.8.3. Cycling of $\text{Li}^+$    $\text{LiFePO}_4$ cell performance.....	170
6.9. Conclusions.....	172
References.....	174

## 6.1. Introduction

As it has been shown in previous chapters, Jeffamine®-based comb-like homopolymers present several advantages compared to poly(ethylene oxide) (PEO) for their application in all-solid-state lithium metal batteries (ASSLMBs) [1, 2]. These new polymer electrolytes (SPEs) present a completely amorphous nature with low glass transition temperature ( $T_g$ ) values, leading to a high ionic conductivity, especially at room temperature (RT) compared to other SPEs. Moreover the chemical and electrochemical stability against lithium (Li) is remarkably enhanced. The  $\text{Li}^\circ | \text{LiFSI/SPE} | \text{LFP}$  cells show good cyclability even when decreasing the operational temperature close to RT. However, the main barrier for the commercial application of these materials is their poor processability and the impossibility of obtaining self-standing membranes.

In order to overcome the above mentioned drawback related to the mechanical properties, a new type of tailor-made block copolymer (BCP) was synthesized in **Chapter 5** [3]. The introduction of polystyrene (PS) blocks into Jeffamine-based polymer resulted in the improvement of the mechanical properties with no detriment in the ionic conductivity. These BCPs showed improved electrochemical stability vs.  $\text{Li}^\circ$  electrode. However, the  $\text{Li}^\circ | \text{BCP} | \text{LFP}$  cells presented deteriorated performance compared to Jeffamine-based SPEs, possibly linked to the low lithium transference number.

The concept of entanglement assumes that polymer long chains interact with other chains, restricting the motion of an individual chain caused by molecular movements of other chains [4]. Entanglement has a significant impact on the rheological behaviour and mechanical properties of the polymer [5].

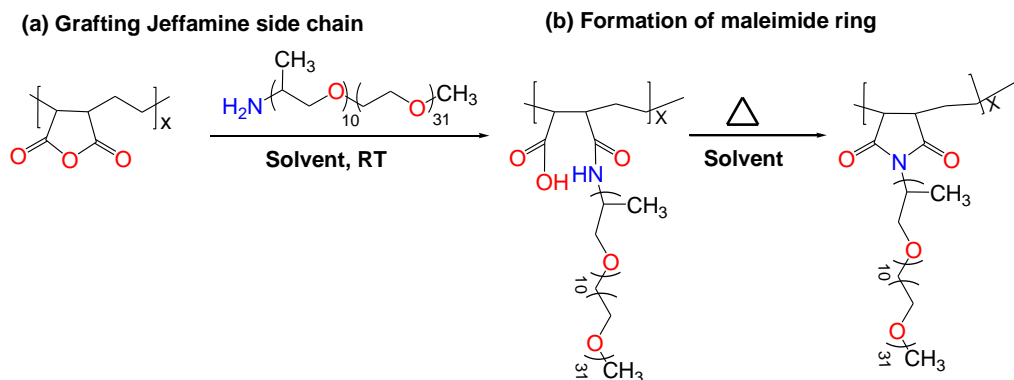
In general, macroscopic mechanical properties of the amorphous polymers depend on chain entanglement. The higher entanglement gives rise to improved mechanical stiffness but restricts the processability of the polymer (*i.e.* good solubility, extrusion...). The ionic conductivity and low temperature performance will be deteriorated due to the restriction of segmental motion of adjacent units in the polymer. The similar effect is observed for high salt concentration electrolytes with high density of transient cross-linking. However, cycle life will probably get better due to rigid mechanical properties [6, 7].

In this chapter, a new type of flowable polymer electrolyte (FPE) comprising of a variation of the super soft polymer matrix containing polyether side moieties (so-called Jeffamine®) and sulphonamide salts (*i.e.*, LiTFSI and LiFSI) presented in **Chapter 4** with the aim of improving the interfacial compatibility with electrode of polymer-based ASSLMs is reported. These new FPEs obtained by tuning the chain entanglement of the polyether side group possess several distinctive features compared to conventional SPEs: 1) high mobility of  $\text{Li}^+$  ions and improved ionic conductivity due to the low  $T_g$  values and high amorphicity of the flowable polymer matrices; and 2) good adhesion properties and improved compatibility against  $\text{Li}^\circ$  anode. These outstanding properties make them suitable as an artificial buffer layer for improving the compatibility of PEO-based SPEs with  $\text{Li}^\circ$  electrode. Notably, the  $\text{Li}^\circ \parallel \text{LiFePO}_4$  cells using Jeffamine-based FPE as buffer layer and PEO as SPE could be cycled with remarkably enhanced electrochemical performance compared with the ones using plain PEO-based SPEs.

## 6.2. Synthesis of Jeffamine-based polymer matrix

The flowable polymer (FP) was easily obtained by one-pot reaction as shown in **Scheme 6.1**. A two steps reaction was carried out in an inert atmosphere in order to obtain the polymer matrix.

### One-pot reaction for synthesizing Jeffamine based comb-polymer



**Scheme 6.1.** One-pot reaction for synthesizing the Jeffamine-based homopolymers.

In the first step, 10 g of Jeffamine M-2070 was reacted with 0.63 g poly(ethylene-*alt*-maleic anhydride) (PEaMA) dissolved in 20 mL of solvent, giving

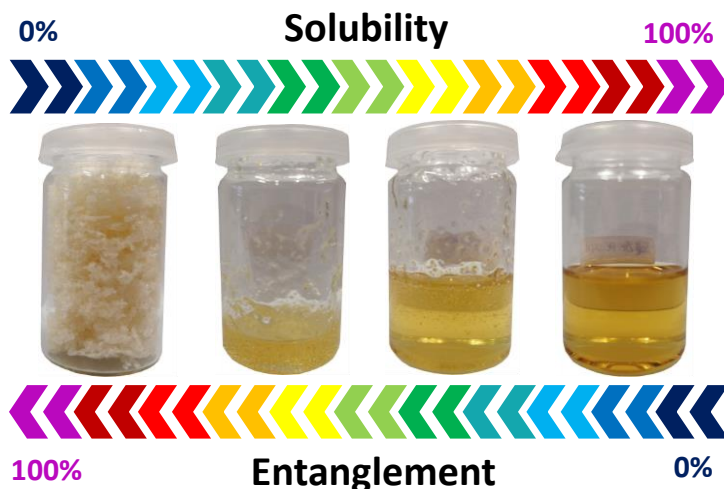


a highly viscous solution as intermediate product. In the second step, the formation of maleimide ring by thermal treatment is carried out. In this step, more solvent is added (mass ratio 1:25) in order to ensure the free movement of the polymer chains and 0.56 g of  $\text{Et}_3\text{N}$  are added as catalyst, resulting in a liquid-like FP matrix (yield 90%).

The amount of solvent and the total dissolution of the reagents are found to tune the physical and mechanical properties of the resulting polymer matrices. Three different solvents were utilized [*i.e.*, *N,N*-dimethylformamide (DMF); 1-methyl-2-pyrrolidinone (NMP) and  $\alpha,\alpha',\alpha''$ -trifluorotoluene (TFT)] resulting in no difference in the final product. The selection of the solvents was conceived on the basis of the next considerations:

- 1) Their high boiling point, requirement to tolerate the high temperatures necessary for the formation of the imide ring.
- 2) The solubility of the reagents.

Depending on the total amount of solvent utilized during the reaction, different polymer matrices with different physical and mechanical properties were obtained as it can be observed in **Figure 6.1**.



**Figure 6.1.** Jeffamine-based polymer matrices synthesized with different degree of entanglement.

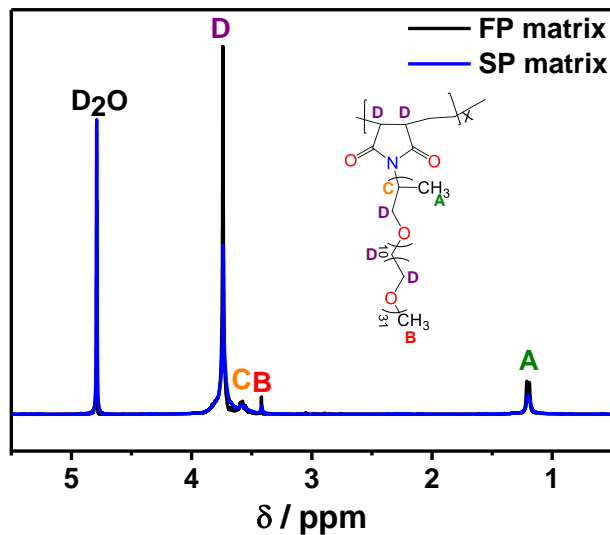
Moreover, these polymer matrices presented distinct solubility in any kind of solvent. This is due to the different degree of entanglement obtained during the reaction as a consequence of the solvent amount. Higher amount of solvent used during the second synthesis step resulted in higher free movement of polymer chains, giving lower entanglement as a result. Although the entanglement is a parameter difficult to quantify, the synthesis was optimized to obtain non-entangled and highly-entangled polymer matrices.

In this chapter two polymer matrices have been chosen; 1) non-soluble polymer matrix (SP) that was described in **Chapter 3** and **Chapter 4** and 2) completely soluble flowable polymer matrix (FP).

### 6.3. Chemical characterization

In order to study if the difference between both matrices could be due to decomposition of the polymer chains attributed to the high temperature reached during the synthesis, the chemical structures of the resulting Jeffamine-based FP and SP matrices are characterized by  $^1\text{H}$  NMR and ATR-FTIR measurements.

#### 6.3.1. Hydrogen-1 nuclear magnetic resonance ( $^1\text{H}$ NMR)

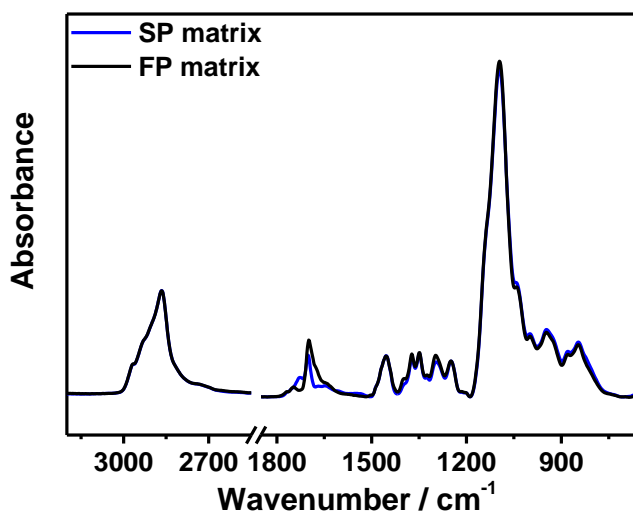


**Figure 6.2.**  $^1\text{H}$  NMR spectra of both FP and SP Jeffamine-based matrices.

**Figure 6.2** shows the  $^1\text{H}$  NMR spectra for Jeffamine-based FP and SP matrices. The doublet at 1.2 ppm and the singlet at 3.6 ppm, named as **A** and **C** in the spectra, correspond to the protons from  $-\text{CH}_3$  and  $-\text{CH}$  groups of the propylene oxide units (PO) in Jeffamine<sup>®</sup> side chains, respectively. The singlet peak at 3.4 ppm, marked as **B**, corresponds to the terminal  $-\text{CH}_3$  of the ethylene oxide (EO) units of the Jeffamine<sup>®</sup> side chains. Finally, the intense peak at 3.7 ppm, designated as **D**, corresponds to the protons from  $-\text{CH}/-\text{CH}_2$  group from the polymer backbone and  $-\text{CH}_2$  group from Jeffamine<sup>®</sup> side chains. These results suggest that the chemical structures of both matrices maintain the same though the physical behaviours are completely different.

### 6.3.2. Attenuated total reflectance-Fourier-transform infrared spectroscopy (ATR-FTIR)

The ATR-FTIR spectra for both polymer matrices where typical peaks related to polyether chain are observed are shown in **Figure 6.3**.



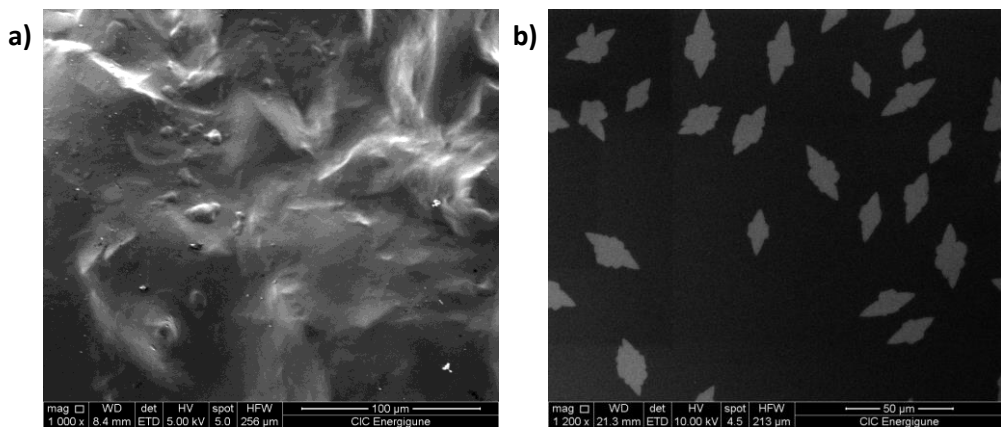
**Figure 6.3.** ATR-FTIR spectra of both FP and SP Jeffamine-based matrices.

The modes originating from  $\text{C}-\text{H}_x$  bonds are detected in the spectra: stretching mode of  $\text{C}-\text{H}_x$  at  $3000\text{ cm}^{-1}$ ; scissoring mode of  $\text{C}-\text{H}_2$  at  $1450\text{ cm}^{-1}$ ; wagging mode of  $\text{C}-\text{H}_x$  at  $1350\text{ cm}^{-1}$ ; twisting mode of  $\text{C}-\text{H}_x$  at  $1250\text{ cm}^{-1}$  and

rocking mode C–H<sub>x</sub> at 950 cm<sup>-1</sup>. The intense peak at 1100 cm<sup>-1</sup> is a result from the superposition of C–O–C stretching and C–H<sub>2</sub> bending modes. Finally, the signals at 1700 cm<sup>-1</sup> correspond to the carbonyl stretching absorption (C=O) from the poly(maleimide) polymer backbone. Clearly, only marginal differences can be observed within both spectra, suggesting that both matrices have the same chemical structure. ATR-FTIR spectra for all the as-prepared electrolytes are summarized in **Figure A.6.1**.

#### 6.4. Morphological characterization: Scanning electron microscopy (SEM)

The morphology of the polymer matrices was analysed by SEM. As it can be observed in **Figure 6.4** the SP matrix appears to be very elastic and sticky presenting a wrinkled surface. In contrast, the suppression of the entanglement dramatically changes the morphology of the polymer matrix. In the case of the FP, some “butterfly” shaped figures can be observed in the SEM image. This phenomenon can be ascribed to the crystallization of the polymer matrix. In the case of SP, it is not able to crystallize due to the movement restriction and rearrangement inability as a consequence of the entanglement domains.



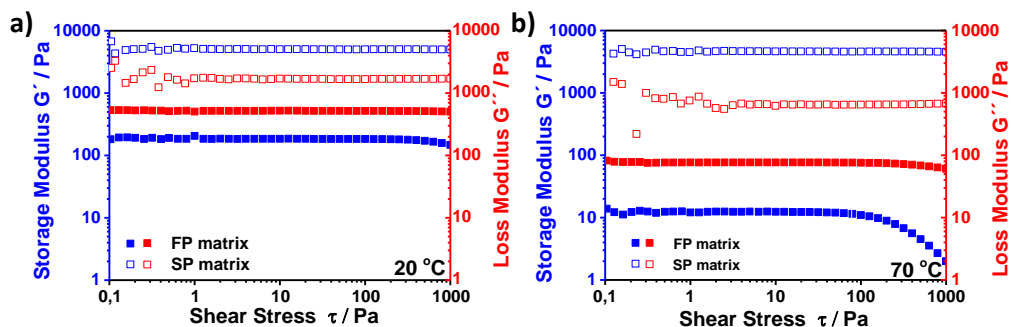
**Figure 6.4.** SEM images of the a) SP and b) FP polymer matrices.

#### 6.5. Mechanical properties

**Figure 6.5** represents the dependency of storage ( $G'$ ) and loss ( $G''$ ) modulus versus shear stress at 20 °C and 70 °C, where  $G'$  and  $G''$  are related to the

elastic and viscous properties of the polymer matrix, respectively. At low stress amplitudes  $G'$  and  $G''$  curves for both materials reveal constant plateau values. For FP polymer a viscous behaviour dominates over elastic one, evidenced by a clear prevalence of  $G''$  modulus over  $G'$ . This behaviour is typical in liquid-like polymer materials. Above 100 Pa material starts to flow, indicating the deviation of both moduli from linearity. SP shows an opposite performance, with a predominance of an elastic component (represented by  $G'$ ) over the viscous one ( $G''$ ) for the whole studied amplitude range. These results evince the hindrance effect of the entanglement in the flowing properties of the SP matrix, blocking the movement of the polymer chains and conferring it certain rigidity. Moreover, the ratio of  $G'/G''$  calculated for SP is much lower than  $10^3$  which can be treated as an evidence of weak physical interactions rather than chemical crosslinking [8].

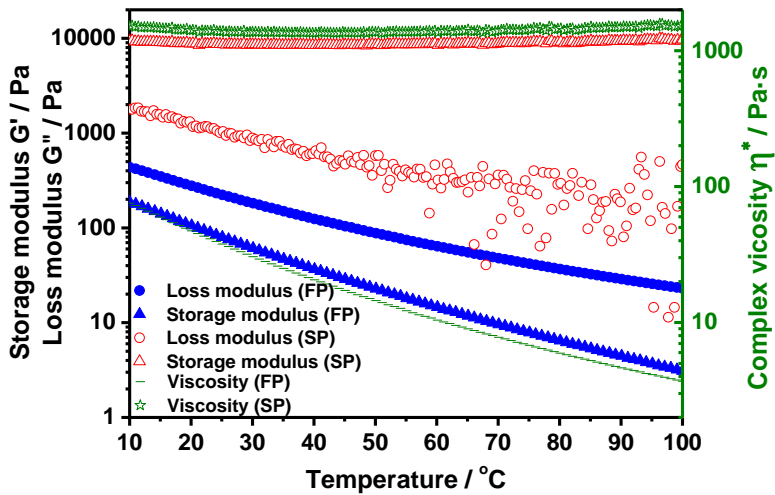
As it can be observed, when the temperature is increased  $G'$  and  $G''$  values for SP do not show a big difference, whereas for FP the decrease in the value of both moduli is obvious and the gap between  $G'$  and  $G''$  is higher. This divergence is due to the different nature of the polymer matrices. SP is a rigid sample where the elastic modulus is not affected by the increase of temperature. On the other hand, FP is a liquid-like polymer, where the increase of temperature means the decrease in viscosity and elastic properties of the material.



**Figure 6.5.** Storage ( $G'$ ) and loss ( $G''$ ) modulus vs. shear stress at **a)** 20 °C and **b)** 70 °C.

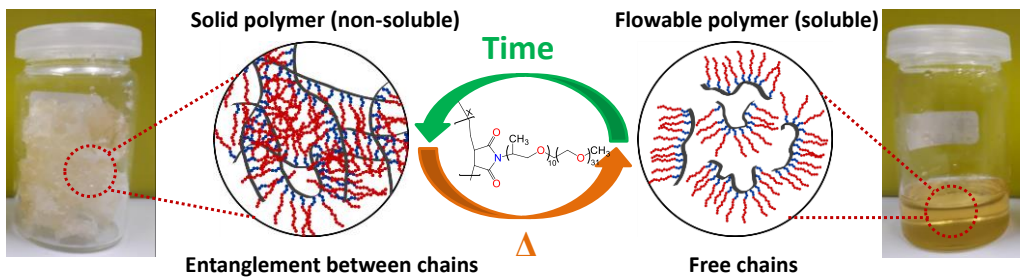
**Figure 6.6** shows broad temperature dependence of complex viscosity ( $\eta^*$ ),  $G'$  and  $G''$  values. For FP, the temperature increase results in lower values of  $\eta^*$  and  $G'$ , which indicates increased mobility of polymer chains and enhanced fluidity of the material at oscillatory conditions. On the contrary, in the SP matrix,

the values of  $\eta^*$  and  $G'$  are temperature independent, which is an additional indication for the high entanglement of polymer chains resulting in solid rubber-like properties at a macroscopic scale.



**Figure 6.6.** Loss ( $G''$ ) and storage ( $G'$ ) modulus and complex viscosity ( $\eta^*$ ) vs. temperature.

As schematically shown in **Figure 6.7**, the as-prepared SP has a solid-like appearance and it could be turned into flowable polymer (FP) upon the disentanglement of the side chains (*e.g.*, heating the polymer in a high boiling point solvent for several hours). Conversely, FP converts to SP slowly at RT.



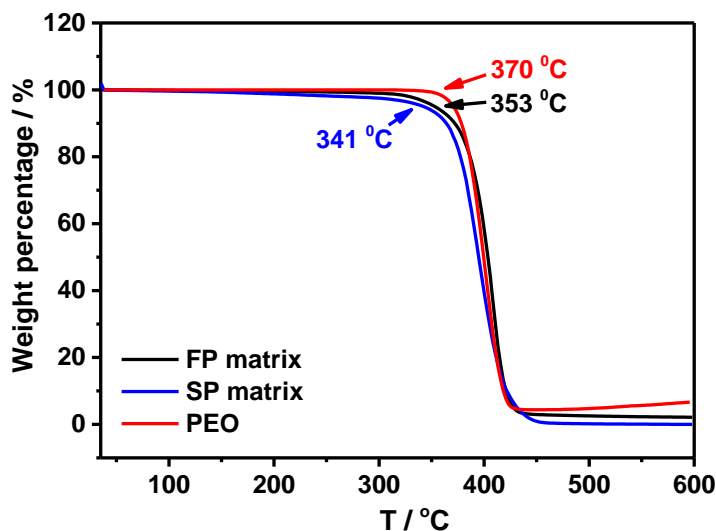
**Figure 6.7.** Schematic illustration of the chain ordering in solid and flowable Jeffamine-based polymer matrices.

## 6.6. Thermal characterization

The evaluation of properties such as thermal stability and phase transition are important for screening the suitable polymer electrolytes, as these two parameters are associated with the operational temperature of ASSLMBs and Li-ion conductivity of the electrolytes respectively.

### 6.6.1. Thermogravimetric analysis (TGA)

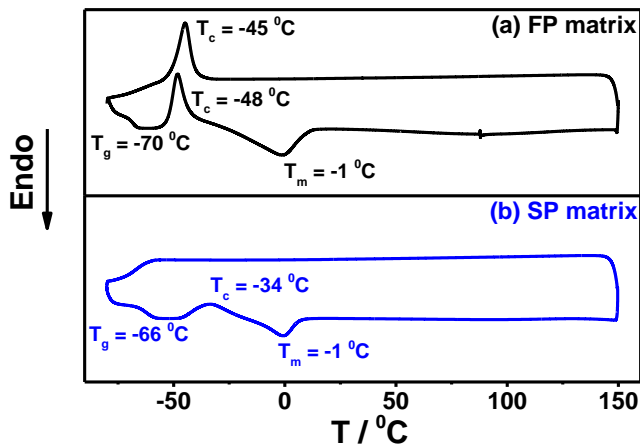
**Figure 6.8** presents the TGA traces for both Jeffamine-based FP and SP matrices, as well as the reference polymer PEO, measured under argon (Ar) flow. All studied polymers are thermally stable above 300 °C, which is much higher than the operational temperature of ASSLMBs. Moreover, nearly overlapped TGA traces are obtained with decomposition temperatures ( $T_d$ ) of 353 and 341 °C for FP and SP, respectively. This result suggests that the different mechanical properties do not affect the thermal stability and evinces that thermal degradation is governed by the chemical composition of the matrix, more concretely by the polyether chain decomposition.



**Figure 6.8.** TGA traces for both Jeffamine-based matrices and PEO reference matrix.

### 6.6.2. Differential scanning calorimetry (DSC)

**Figure 6.9** compares the obtained DSC traces for FP and SP matrices. Comparing the first heating scan for both neat polymers, a slightly lower  $T_g$  value is observed for the Jeffamine-based FP compared to that for the SP one [ $-70\text{ }^\circ\text{C}$  (FP) vs.  $-66\text{ }^\circ\text{C}$  (SP)], indicating a higher flexibility of the former matrix.



**Figure 6.9.** DSC traces of both polymer matrices.

More interestingly, though both polymers present a semicrystalline nature, the quantification of the enthalpy for crystallization and melting transitions prove a higher fraction of crystalline phase in the case of the flowable polymer [e.g.,  $41\text{ J g}^{-1}$  (FP) vs.  $15\text{ J g}^{-1}$  (SP) for melting transition] as it can be observed in **Table 6.1**. This is ascribed to the hindrance effect of the entanglement on the crystallization of the polymer matrix [9, 10]. This effect is even more obvious upon the cooling scan where in the case of FP a prominent exothermic peak is obtained at crystallization temperature ( $T_c = -46\text{ }^\circ\text{C}$ ), while SP is not able to recrystallize at high cooling rates. Both the higher  $T_g$  value and lower  $\Delta H_m$  of SPE can be attributed to the movement limitation and rearrangement inability as a consequence of the entanglement and crystallization susceptibility.

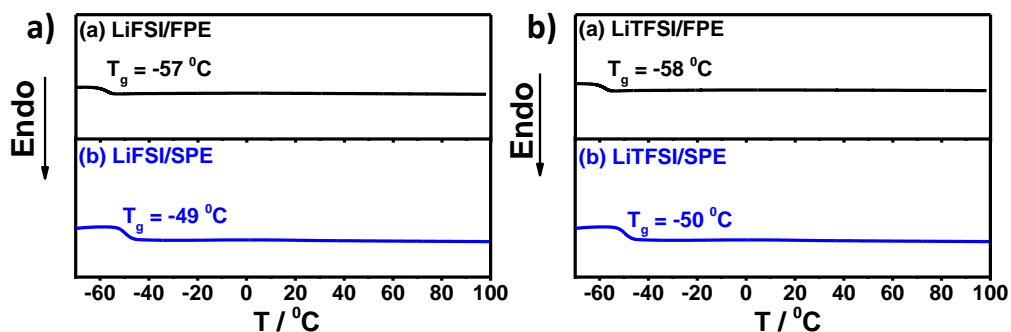


**Table 6.1.** The characterization data for the phase behaviour for the as-prepared polymer matrices.

Matrix	$T_g^a$	$T_c^b (\Delta H_c)^c$ Heating	$T_c^b (\Delta H_c)^c$ Cooling	$T_m^d (\Delta H_m)^e$
FP	-70	-48 (24)	-45 (27)	-1 (41)
SP	-66	-34 (14)		-1 (15)

[a] Glass transition temperature ( $^{\circ}\text{C}$ ) taken as the midpoint of the inflexion; [b] Crystallization point ( $^{\circ}\text{C}$ ) taken as the maximum value of the crystallization peak; [c] Enthalpy of crystallization ( $\text{J g}^{-1}$ ); [d] Melting point ( $^{\circ}\text{C}$ ) taken as the maximum value of the melting peak; [e] Enthalpy of melting ( $\text{J g}^{-1}$ ).

DSC traces and phase transition temperatures for all the as-prepared electrolytes are summarized in **Figure 6.10** and **Table A.6.1** and **Figure A.6.2**, respectively. For both FPE and SPE, the addition of small amount of lithium salt gives rise to amorphism of the polymer electrolyte (PE), obtaining a fully amorphous electrolytes with slightly higher  $T_g$  than bare matrix for EO/Li ratios above 20. Comparing the effect of the type of the Li salt added, no differences are found, the same tendency is observed for both LiFSI and LiTFSI. Nevertheless, the main differences are again ascribed to the Jeffamine-based matrix nature. LiFSI/FPE and LiTFSI/FPE show lower  $T_g$  values compared to that of their LiFSI/SPE and LiTFSI/SPE counterparts [*e.g.*,  $-57^{\circ}\text{C}$  (LiFSI/FPE) vs.  $-49^{\circ}\text{C}$  (LiFSI/SPE) and  $-58^{\circ}\text{C}$  (LiTFSI/FPE) vs.  $-50^{\circ}\text{C}$  (LiTFSI/SPE)], suggesting a higher segmental flexibility for the FP-based electrolytes, and thereby an improved ionic motion.

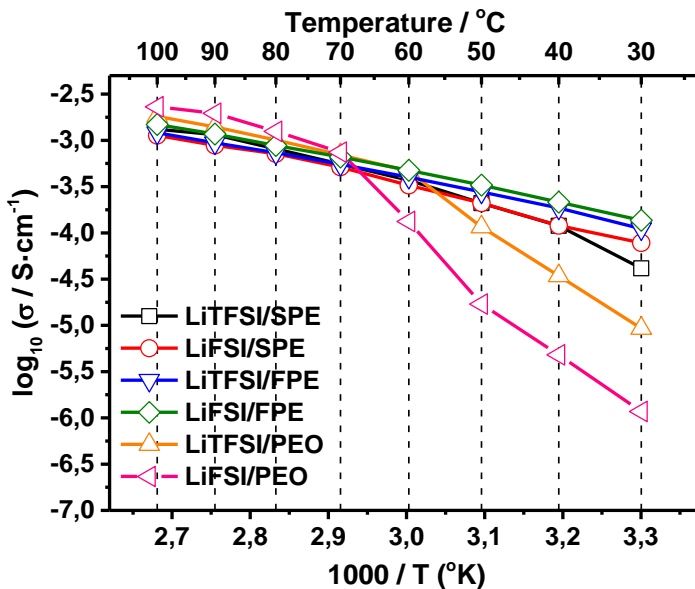
**Figure 6.10.** DSC traces of SPE and FPE **a)** using LiFSI as salt and **b)** using LiTFSI as salt with EO/Li = 20.

## 6.7. Electrochemical characterization of FPEs

The analysis of properties such as ionic conductivity, Li-ion transference number, electrochemical stability toward oxidation and compatibility with Li<sup>o</sup> electrode is essential as these parameters will determine the suitability of the polymer electrolytes for their application in ASSLMBs.

### 6.7.1. Ionic conductivity

**Figure 6.11** shows the Arrhenius plot of ionic conductivity ( $\sigma$ ) vs. temperature for both the TFSI<sup>-</sup> and FSI<sup>-</sup> based FPE and SPE, as well as for PEO based reference electrolytes. In all cases a molar ratio of  $-[\text{CH}_2\text{CH}_2\text{O}]_n\text{EO}/\text{LiX} = 20$  ( $X = \text{TFSI}, \text{FSI}$ ) was used as, in **Chapter 4** it was concluded that this was the optimum salt composition for this kind of electrolytes.



**Figure 6.11.** Temperature dependence of ionic conductivity for the TFSI<sup>-</sup> and FSI<sup>-</sup> based FPEs, SPEs and PEO reference electrolytes with EO/Li = 20.

The reference PEO-based electrolytes display a non-linear ionic conductivity behaviour due to the melting of the crystalline phase in the temperature ranging from 60 to 70 °C, whereas all the Jeffamine-based SPEs and FPEs follow a continuous Vogel-Tamman-Fulcher (VTF) behaviour, indicating a fully

amorphous nature of the electrolyte in the measured temperature range (see **Figure 6.10**) and, as a consequence, giving a much higher ionic conductivity at lower temperatures compared to the reference electrolytes. On the other hand, FPEs present slightly higher ionic conductivity than their SPEs counterparts, regardless the salt content (**Figure A.6.3**). This is due to the flexible PO/EO units within Jeffamine side-chains. In the case of the SPEs the entanglement decreases the free movement of the chains showing a lower conductivity. In the case of FPEs, the complete suppression of the entanglement ensures the high mobility of the polymer chains resulting in higher ionic conductivities. This is in accordance with the results obtained for the DSC study where lower values of  $T_g$  were obtained for the FP and its corresponding electrolytes than for SPEs.

### 6.7.2. Li-ion transference number

The Li-ion transference numbers ( $T_{Li^+}$ ) of the TFSI- and FSI-based FPEs, SPEs and PEO reference electrolytes were measured and the calculated values using the method described in **Chapter 2** section **2.4.5** have been summarized in **Table 6.2**. The obtained values (*ca.* 0.15) suggest a negligible difference between the measured samples, presenting typical  $T_{Li^+}$  values for salt-in-polymer systems [11].

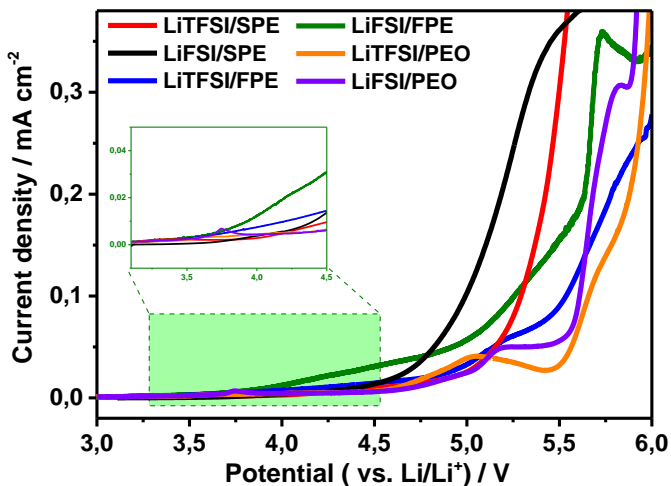
**Table 6.2.** The calculated values of Li-ion transference number ( $T_{Li^+}$ ) of various electrolytes with the same EO/Li ratio of 20 at 70 °C.

Electrolyte	$I_0$ / $\mu A$ <sup>[a]</sup>	$I_s$ / $\mu A$ <sup>[b]</sup>	$R_{\Omega}^b$ / $\Omega$ <sup>[c]</sup>	$R_{\Omega}^s$ / $\Omega$ <sup>[d]</sup>	$R_i^o$ / $\Omega$ <sup>[e]</sup>	$R_i^s$ / $\Omega$ <sup>[f]</sup>	$\Delta V$ / $mV$ <sup>[g]</sup>	$T_{Li^+}$
FPE Jeff2k:TFSI 20:1	43	8	101	92	61	81	10	0.14
FPE Jeff2k:FSI 20:1	43	8	116	116	99	119	10	0.12
SPE Jeff2k:TFSI 20:1	8	2	435	442	966	812	10	0.16
SPE Jeff2k:FSI 20:1	13	3	452	445	785	848	10	0.16
PEO:TFSI 20:1	23	12	30	31	360	364	10	0.17
PEO:FSI 20:1	32	15	33	33	257	258	10	0.13

[a] Initial and [b] steady-state current obtained by dc polarization; [c] initial and [d] final resistances of the electrolytes measured by ac impedance method before and after polarization, respectively; [e] initial and [f] final resistances of interfacial layer between electrode/electrolyte measured by ac impedance method before and after polarization, respectively; [g] dc voltage subjected to the  $Li^+$  symmetrical cell.

### 6.7.3. Electrochemical stability toward oxidation

The anodic stability of polymer electrolytes is generally limited by the nature of polymer matrix and the perfluorinated anion as a conducting counter ion in the salt [2, 12], and it is determined by linear sweep voltammetry (LSV). As shown in **Figure 6.12**, Jeffamine-based FPE and SPE, and the reference PEO electrolytes show minor oxidation peaks at a potential higher than 3.8 V vs. Li/Li<sup>+</sup> at 70 °C, which could be ascribed to the gradual oxidation of EO-containing moieties in the above three matrices.

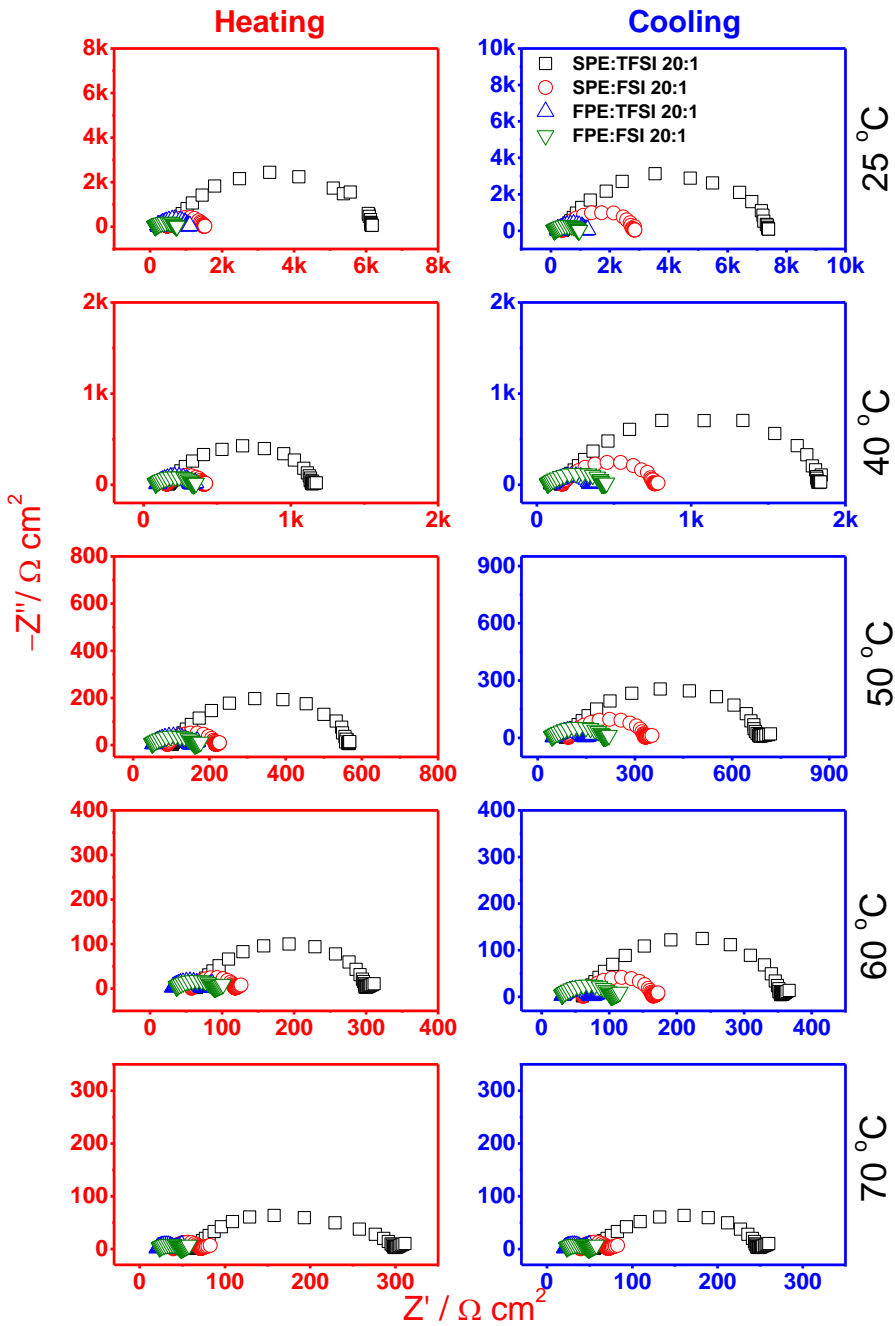


**Figure 6.12.** LSV profiles measured on stainless steel electrode for the TFSI- and FSI-based FPEs, SPEs and PEO-based reference electrolytes with EO/Li = 20.

This is in agreement with previous studies that state EO-based polymers are suitable for < 4 V class LMBs [2, 11]. For both LiFSI and LiTFSI-based electrolytes, the SPE shows better stability towards oxidation than FPE, which might be related to the easier access of polyether chains to the working electrode (WE). In the case of the SPE the chain mobility is restricted due to the entanglement. However, for the FPE, the oxidation reaction is favoured at terminal moieties due to the higher flexibility of the former matrix. In addition, LiFSI-based electrolytes tend to be oxidized more easily compared to LiTFSI-based ones, irrespective of the kind of polymer matrices, which is due to the lower intrinsic oxidation stability of FSI<sup>-</sup> [13].

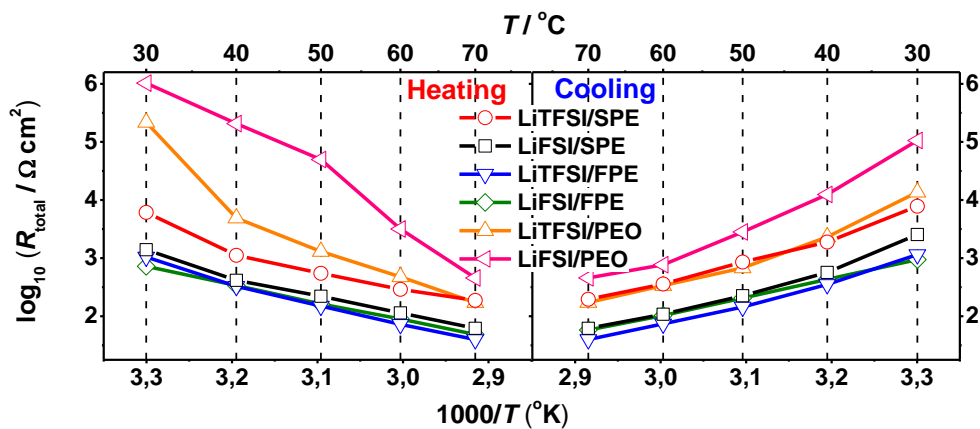
#### 6.7.4. Compatibility with Li<sup>o</sup> electrode

The interphase formed between Li metal electrode and the electrolyte is one of the key parameters in determining the cycling performance of rechargeable ASSLMBs. The properties of the SEI film are highly dependent on the identity of lithium salt, hence, the stability of the interphase of Li metal electrode with the FSI<sup>-</sup> and TFSI<sup>-</sup> based PEO, SPEs and FPEs were investigated. Electrochemical impedance spectroscopy (EIS) plots of Li<sup>o</sup> symmetric cell for SPE and FPE with EO/Li = 20 are presented in **Figure 6.13** (corresponding data for PEO reference cells were presented in **Chapter 4**). The simplified equivalent circuit used to fit collected EIS data is given in **Figure A.6.4** and the best-fitted results are summarized in **Table A.6.2**.



**Figure 6.13.** Electrochemical impedance spectra of  $\text{Li}^+$  symmetric cell for SPE and FPE with  $\text{EO/LiX} = 20$  ( $X = \text{TFSI, FSI}$ ).

**Figure 6.14** shows the temperature effect on the total resistance ( $R_{\text{total}}$ ) of the  $\text{Li}^\circ$  symmetric cells of the studied systems. The tendency of  $R_{\text{total}}$  vs.  $T$  is consistent with the conductivity and DSC results where Jeffamine-based electrolytes present a completely amorphous nature, fitting with Vogel-Tamman-Fulcher (VTF) theory, whereas PEO-based ones present their melting transitions at *ca.* 60 °C. Unlike PEO-based electrolytes, SPEs show a lower  $R_{\text{total}}$  for LiFSI than for LiTFSI; imperceptible differences in the case of FPEs. This performance suggests that the amorphous nature of the polymer matrix not only enhances the ionic transportation, but also regulates the chemical compatibility of the electrolytes with  $\text{Li}^\circ$  electrode. Interestingly, the  $R_{\text{total}}$  for FPEs is lower than that for SPEs. This can be attributed to the good adhesive properties presented by these materials allowing a better contact between  $\text{Li}^\circ$  electrode and the electrolyte, behaviour that may retard the formation of dendritic lithium in the  $\text{Li}^\circ$  symmetric cells.



**Figure 6.14.** Total resistance ( $R_{\text{total}}$ ) of the  $\text{Li}^\circ$  symmetric cells of PEO reference electrolytes and Jeffamine-based FPEs and SPEs using LiTFSI and LiFSI as salt.

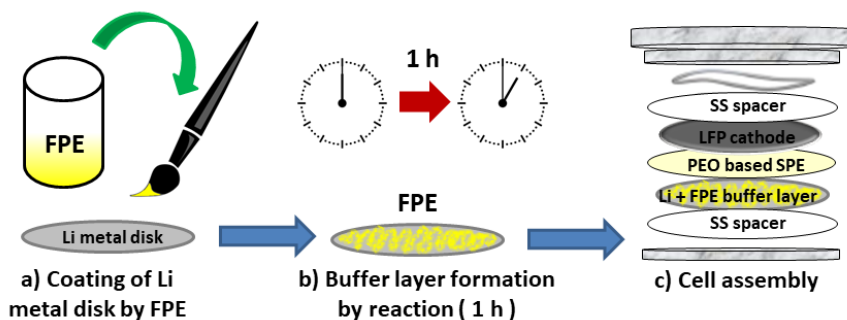
### 6.8. Application of FPE as buffer layer

As it has been previously mentioned, the interphase formed between  $\text{Li}$  metal electrode and the electrolyte is one of the factors that will determine the cycling performance of rechargeable ASSLMBs. PEO-based electrolytes present excellent mechanical properties but inferior electrochemical performance, which urges the search for alternative polymer electrolytes for ASSLMBs. As reported in **Chapter 4** [1, 2], Jeffamine-based SPEs presented outstanding electrochemical

properties, such as high ionic conductivity, good stability against  $\text{Li}^\circ$  anode and good cyclability of  $\text{Li}^\circ \parallel \text{LiFePO}_4$  based batteries; however, the absence of solubility of these SPEs in acetonitrile and other aprotic solvents results in a poor processability. Inspired by the above-mentioned advantageous properties of FPEs, in this chapter we propose the utilization of Jeffamine-based FPEs as an artificial buffer layer for protecting the  $\text{Li}^\circ$  anode in PEO-based ASSLMBs, taking advantage of the good electrochemical stability of Jeffamine-based electrolytes and the mechanical properties of PEO-based ones.

### 6.8.1. Formation of buffer layer

For the formation of FPE buffer layer, Jeffamine-based FP with a molar ratio of  $\text{EO/Li} = 20$  ( $X = \text{TFSI}, \text{FSI}$ ) was homogeneously spread on the top of Li metal anode and kept reacting over 1 h before the cell assembly as shown in **Figure 6.15**. The formation of the buffer layer was controlled by the mass of the FPE (*ca.* 20 mg). In order to study the effect of the Jeffamine-based buffer layer, PEO reference membranes with a molar ratio of  $-\text{[CH}_2\text{CH}_2\text{O]}-\text{EO/Li} = 20$  ( $X = \text{TFSI}, \text{FSI}$ ) were used as both polymer electrolyte and separator.



**Figure 6.15.** Buffer layer of Jeffamine-based FPE formation on top of Li metal disk.

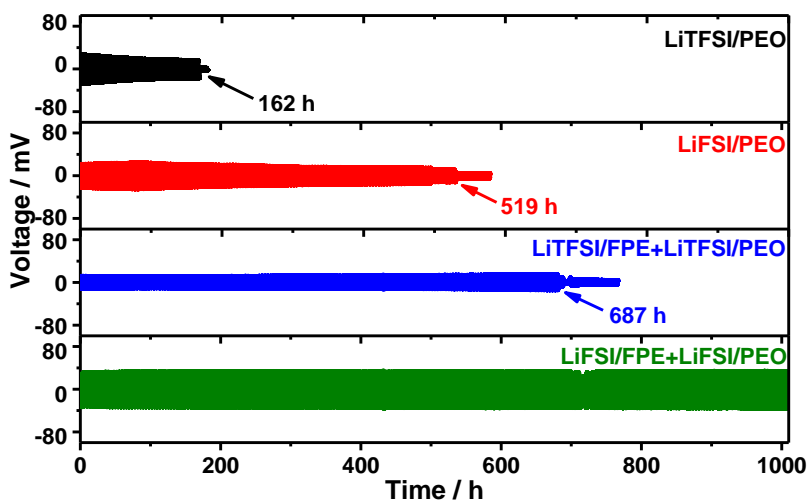
### 6.8.2. Electrochemical stability of electrolyte/ $\text{Li}^\circ$ electrode

**Figure 6.16** presents the voltage profiles of  $\text{Li}^\circ$  symmetric cells after applying a constant current density of  $0.1 \text{ mA cm}^{-2}$  at  $70^\circ \text{C}$  for PEO-based electrolytes with and without buffer layer based on FPEs. The cell based on LiTFSI/PEO reference electrolyte lasts only 160 h before the occurrence of internal



short-circuit, whereas LiFSI/PEO lasts 520 h. This clearly suggests that the  $\text{FSO}_2^-$  functional group can greatly regulate the morphology, composition and mechanical stability of the SEI layer, thus mitigating the growth of  $\text{Li}^\circ$  dendrites in the corresponding electrolytes [2, 13, 14]. In contrast, the application of FPE remarkably improves the cycle life of  $\text{Li}^\circ$  symmetric cells. For the cell comprising of PEO/LiTFSI/FPE the cell was running for 690 h before internal short-circuit, whereas the cell based on PEO/LiFSI/FPE was running for more than 1000 h without any internal short-circuit. This is attributed to the good contact between the FPE and the electrode and the *ad hoc* SEI chemistry from  $\text{FSI}^-$  [12].

One may also notice that the overpotential of LiFSI/FPE+LiFSI/PEO-based  $\text{Li}^\circ$  symmetric cell is higher than that of LiTFSI/FPE+LiTFSI/PEO-based one, which might be ascribed to the following reasons: 1) The S—F bonds in LiFSI are easier to reduce than the C—F bonds in TFSI, resulting in a thicker, but more protective SEI layer of mainly LiF on the  $\text{Li}^\circ$  electrode [12]; 2) the interfacial wettability for LiFSI is lower than that for LiTFSI due to the less amount of fluorine atoms in the former salt, which may lead to an increased resistivity in the interphase between FPE and PEO-based membrane.

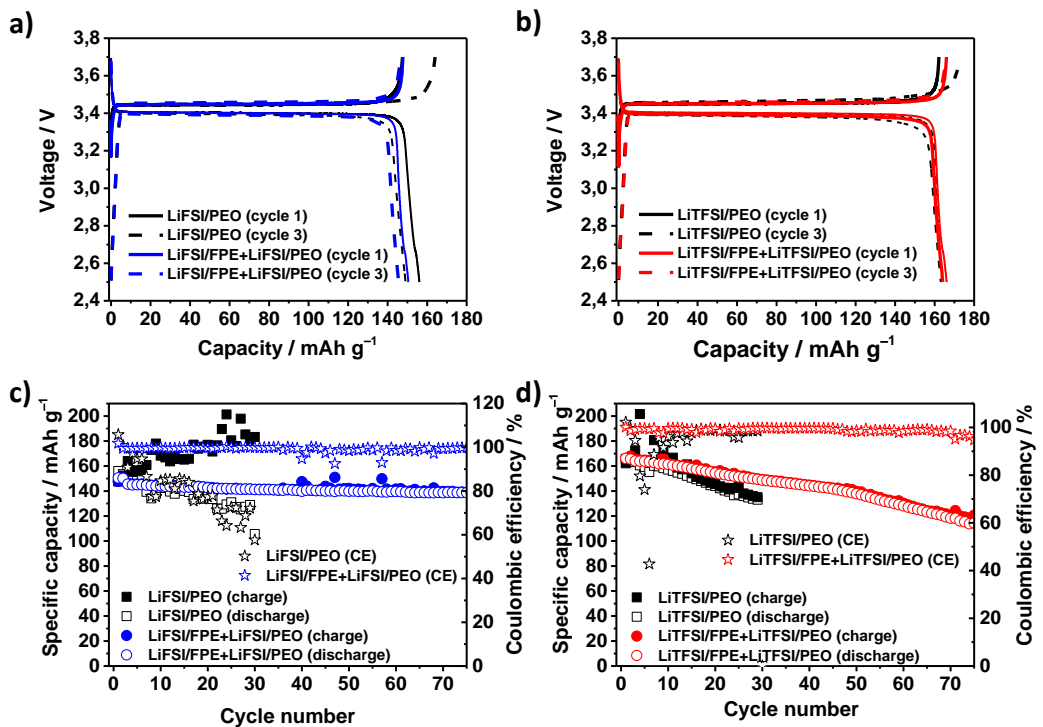


**Figure 6.16.** Galvanostatic cycling of the  $\text{Li}^\circ$  symmetric cells at  $70^\circ\text{C}$  with a current density of  $0.1\text{ mA cm}^{-2}$ , and a half-duration of 2h.

### 6.8.3. Cycling performance of $\text{Li}^\circ \mid \mid \text{LiFePO}_4$ cell

The feasibility of implementing FPE as an artificial buffer layer for rechargeable ASSLMBs was further evaluated by the cycling performance of  $\text{Li}^\circ \mid \mid \text{LiFePO}_4$  cells.

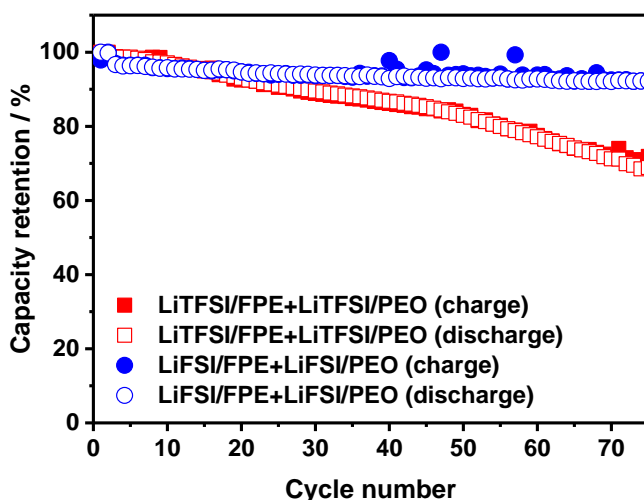
$\text{LiFePO}_4$  based cathodes were prepared with 63 wt% LFP active material, 7 wt% C65 conductive carbon and 30 wt% PEO/LiX (X = TFSl,FSI) as polymer binder. The composite cathodes were prepared following the method reported in **Chapter 2** section 2.3.1.



**Figure 6.17.** Charge/discharge profiles of the  $\text{Li}^\circ \mid \mid \text{SPEs} \mid \mid \text{LFP}$  cells using **a)**  $\text{LiFSI/FPE+LiFSI/PEO}$  and **b)**  $\text{LiTFSI/FPE+LiTFSI/PEO}$  as electrolyte at  $70^\circ\text{C}$  under a constant C-rate of 0.1/0.1C. Specific charge/discharge capacities and Coulombic efficiency vs. cycle number for the cells using **c)**  $\text{LiFSI/FPE+LiFSI/PEO}$  and **d)**  $\text{LiTFSI/FPE+LiTFSI/PEO}$  as electrolyte at  $70^\circ\text{C}$  under a constant C rate of 0.1/0.1C. All the electrolytes were compared with the PEO-based reference electrolyte.

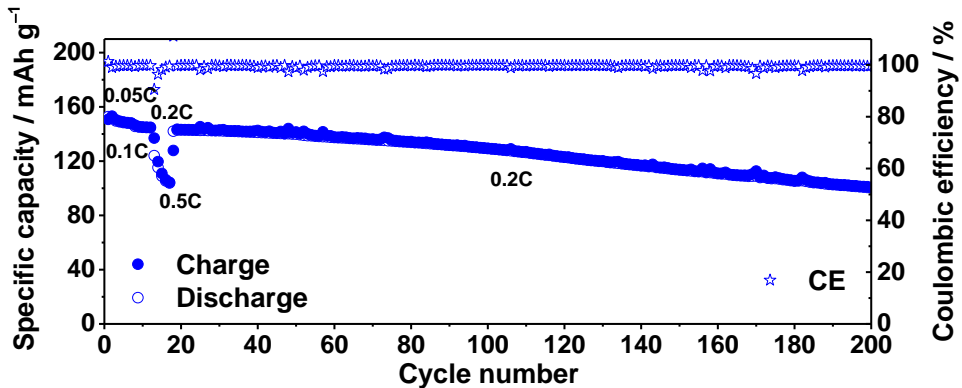
Under a constant charge/discharge rate of 0.1/0.1C, the  $\text{Li}^\circ \parallel \text{LFP}$  cells using FPE/PEO-based electrolytes outperform the ones using conventional PEO-based electrolytes in terms of both Coulombic efficiency (CE) and capacity retention. For example,  $\text{Li}^\circ \parallel \text{LiTFSI/FPE+LiTFSI/PEO} \parallel \text{LFP}$  cell delivers a discharge capacity of  $150 \text{ mAh g}^{-1}$  with a CE close to 100% after 30 cycles (**Figure 6.17 b and d**); while the corresponding LiTFSI/PEO cell attains a low discharge capacity of  $125 \text{ mAh g}^{-1}$  with a CE of 98% even after the first few cycles. This could be attributed to the improved contact between  $\text{Li}^\circ$  anode and PEs in the presence of amorphous and liquid-like FPE layer, which can remarkably facilitate the ionic transport in the vicinity of  $\text{Li}^\circ$  surface. Thus, the soft-dendrite formation is mitigated due to unavoidable current inhomogeneities as a consequence of the semi-crystalline nature of the PEO-based electrolytes.

As it can be observed in **Figure 6.17a and c**, the cells using LiFSI-based FPE and LiFSI/PEO electrolyte show much lower capacity fading than that of the LiTFSI-based one after 50 cycles. This performance can also be noticed in **Figure 6.18** where capacity retention vs. cycle number for both type of electrolytes is shown. This behaviour could be related to better electrochemical compatibility between  $\text{Li}^\circ$  anode and LiFSI-based electrolyte, since the key SEI building specie LiF is one of the main products generated from the electrochemical reduction of LiFSI.



**Figure 6.18.** Capacity retention of the  $\text{Li}^\circ \parallel \text{SPEs} \parallel \text{LFP}$  cells using FPE as buffer layer at  $70^\circ \text{C}$ .

Furthermore, the rate capability of  $\text{Li}^\circ \parallel \text{LFP}$  cells using LiFSI-based FPE is presented in **Figure 6.19**, where the cell shows good long-term cycling stability at 0.2C for 200 cycles and a high discharge capacity of  $110 \text{ mAh g}^{-1}$  at a moderate charge/discharge rate of 0.5/0.5C. Those results suggest that the electrochemical stability of  $\text{Li}^\circ$  electrode towards PEs could be effectively improved in the presence of FPE layer.



**Figure 6.19.** Specific charge/discharge capacities and Coulombic efficiency vs. cycle number for the cell using LiFSI/FPE+LiFSI/PEO as electrolyte at  $70^\circ\text{C}$  and different C-rates.

## 6.9. Conclusions

In this chapter, different synthesis methods for the preparation of a comb-like polymer matrix are described. The one-pot reaction allows obtaining the same polymer matrix with two different mechanical properties due to the control of the entanglement of the side-chains. The suppression of the entanglement on the Jeffamine-based polymers results in higher flexibility of the former matrix, thus giving lower  $T_g$  values and higher ionic conductivities. Moreover, the good adhesive properties presented by these novel materials endow a better contact between  $\text{Li}^\circ$  electrode and the electrolyte, thus retarding the dendrite formation.

This novel FPE is not able to give self-standing membranes by itself, but can be easily processed as buffer layer. Motivated by this fact, and to overcome the inferior electrochemical performance of PEO, FPEs were used as a stable buffer layer between the  $\text{Li}^\circ$  electrode and PEO-based membranes. The stability against  $\text{Li}^\circ$  electrode was significantly improved. The  $\text{Li}^\circ \parallel \text{LFP}$  cell using LiFSI/PEO

membrane and LiFSI/FPE showed good cycling stability and high Coulombic efficiency at different C-rates. Therefore, new FPEs are promising candidates for designing high-performance all-solid-state lithium metal batteries.

## References

- [1] I. Aldalur, H. Zhang, M. Piszcz, U. Oteo, L.M. Rodriguez-Martinez, D. Shanmukaraj, T. Rojo, M. Armand. Jeffamine® based polymers as highly conductive polymer electrolytes and cathode binder materials for battery application. *J. Power Sources*. 2017; **347**, 37-46.
- [2] I. Aldalur, M. Martinez-Ibañez, M. Piszcz, L.M. Rodriguez-Martinez, H. Zhang, M. Armand. Lowering the operational temperature of all-solid-state lithium polymer cell with highly conductive and interfacially robust solid polymer electrolytes. *J. Power Sources*. 2018; **383**, 144-149.
- [3] I. Aldalur, M. Martinez-Ibañez, M. Piszcz, H. Zhang, M. Armand. Self-standing highly conductive solid electrolytes based on block copolymers for rechargeable all-solid-state lithium-metal batteries. *Batteries Supercaps*. 2018; **1**(4), 149-159.
- [4] A.Y. Malkin, A.I. Isayev. *Rheology Concepts, Methods, and Applications*. Oxford: Elsevier. 2012.
- [5] D. Zhang. *Advances in filament yarn spinning of textiles and polymers*. Elsevier Science. 2014.
- [6] J.H. Kiat. *Nanomaterials in energy devices*. CRC Press. 2017.
- [7] K.A. Striebel, K. Zaghib, K. Zaghib, D. Guyomard, E.S. Meeting. *Lithium and lithium-ion batteries: proceedings of the international symposium*. Electrochemical Society. 2004.
- [8] A.V. Shenoy. *Rheology of filled polymer systems*. Springer. 2004.
- [9] X. T. Liu, R. Y. Bao, Y. M. Li, W. Yang, B. H. Xie, M. B. Yang. Effect of chain entanglement on the melt-crystallization behavior of poly(l-lactide) acid. *J. Poly. Res*. 2016; **23**(8), 164.
- [10] C. Luo, J.U. Sommer. Frozen topology: entanglements control nucleation and crystallization in polymers. *Phys. Rev. Lett*. 2014; **112**(19), 195702.

**[11]** J. Mindemark, M.J. Lacey, T. Bowden, D. Brandell. Beyond PEO—Alternative host materials for Li<sup>+</sup>-conducting solid polymer electrolytes. *Prog. Polym. Sci.* 2018; **81**, 114-143.

**[12]** G.G. Eshetu, X. Judez, C. Li, M. Martinez-Ibañez, I. Gracia, O. Bondarchuk, J. Carrasco, L.M. Rodriguez-Martinez, H. Zhang, M. Armand. Ultrahigh performance all solid-state lithium sulfur batteries: salt anion's chemistry-induced anomalous synergistic effect. *J. Amer. Chem. Soc.* 2018; **140**(31), 9921-9933.

**[13]** H. Zhang, C. Liu, L. Zheng, F. Xu, W. Feng, H. Li, X. Huang, M. Armand, J. Nie, Z. Zhou. Lithium bis(fluorosulfonyl)imide/poly(ethylene oxide) polymer electrolyte. *Electrochim. Acta.* 2014; **133**, 529-538.

**[14]** X. Judez, M. Piszcz, E. Coya, C. Li, I. Aldalur, U. Oteo, Y. Zhang, W. Zhang, L.M. Rodriguez-Martinez, H. Zhang, M. Armand. Stable cycling of lithium metal electrode in nanocomposite solid polymer electrolytes with lithium bis(fluorosulfonyl)imide. *Solid State Ion.* 2018; **318**, 95-101.

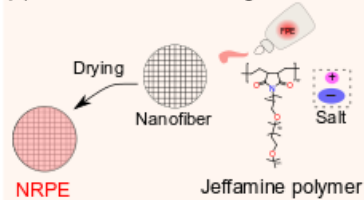




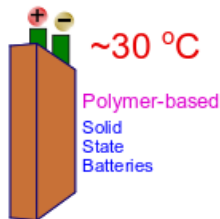
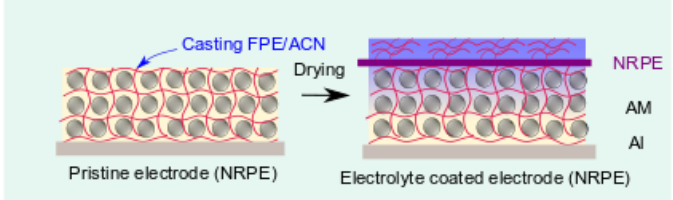
## Chapter 7

# Nanofiber-reinforced polymer electrolytes towards room temperature solid-state lithium batteries

(a) Conductive, self-standing membrane



(b) In-situ coated cathode



I. Aldalur, X. Wang, N. Goujon, M. Echeverria, M. Martinez-Ibañez, M. Piszcz, P. Howlett, M. Forsyth, M. Armand, H. Zhang. Nanofiber reinforced polymer electrolytes toward room temperature solid state lithium batteries. (Submitted)



## Chapter 7:

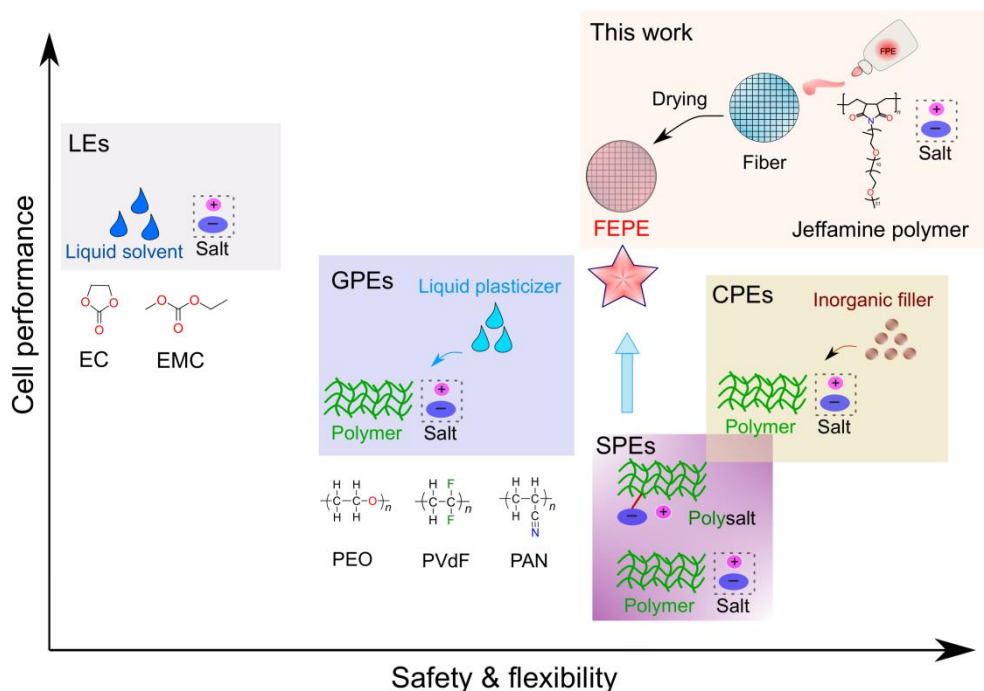
### NANOFIBER-REINFORCED POLYMER ELECTROLYTES TOWARDS ROOM TEMPERATURE SOLID-STATE LITHIUM BATTERIES

7.1.	Introduction.....	181
7.2.	Preparation of NRPEs.....	183
7.3.	Chemical characterization of NRPEs.....	185
7.4.	Morphological characterization.....	186
7.5.	Mechanical characterization.....	188
7.6.	Thermal characterization.....	189
	7.6.1. Thermogravimetric analysis (TGA).....	189
	7.6.2. Differential scanning calorimetry (DSC).....	190
7.7.	Electrochemical characterization.....	192
	7.7.1. Ionic conductivity.....	192
	7.7.2. Li-ion transference number.....	195
	7.7.3. Electrochemical stability toward oxidation.....	196
	7.7.4. Compatibility with Li <sup>o</sup> electrode.....	196
	7.7.5. Cycling of Li <sup>o</sup>    LiFePO <sub>4</sub> cell performance.....	198
	7.7.5.1. Solvent-casting method in LiFePO <sub>4</sub> -based cathodes.....	198
	7.7.5.2. Cycling of Li <sup>o</sup>    LiFePO <sub>4</sub> cell performance at RT.....	201
	7.7.5.3. Cycling of Li <sup>o</sup>    LiFePO <sub>4</sub> cell performance at different temperatures.....	201
7.8.	Conclusions.....	203

References.....	204
-----------------	-----

## 7.1. Introduction

In contrast to conventional liquid electrolytes used in LIBs, solid electrolytes (SEs) possess inherently enhanced safety under abuse conditions due to the absence of flammable liquid components, as well as better chemical and electrochemical compatibility with the 'Holy grail' lithium metal ( $\text{Li}^0$ ) anode [1, 2] and other metallic anodes [3], thereby favouring the stable and reliable operation of rechargeable batteries [4-11]. Currently, there are three families of SEs investigated as solid ionic conductors for SSBs, enlisting polymer electrolytes (PEs) [9-11], inorganic solid electrolytes (ISEs) [4, 7, 8] and composite /hybrid polymer electrolytes (CPEs/HPEs) [5, 6], as it can be observed in **Scheme 7.1**. Among these SEs, PEs containing lithium salts dissolved in electron-donating polymer matrices are the promising candidates to replace their liquid counterparts due to their better processability, flexibility and ease in structural design [11, 12].



**Scheme 7.1.** Comparison of the state-of-the-art electrolytes for rechargeable batteries and the preparation of NRPEs.

In general, PEs are classified into dry solid polymer electrolytes (SPEs, containing only salt and polymer matrix) and gel polymer electrolytes (GPEs, > 70 wt% liquid plasticizers) [11, 13]. Poly(ethylene oxide) (PEO) is one of the most widely used polymer matrices [14, 15]. However, due to its semi-crystalline nature it requires heating accessories for maintaining the temperature of the battery pack, thereby causing decreased overall energy density and efficiency [16, 17]. Alternative polymer matrices such as polycarbonates (PC) [18, 19] have been capturing attention towards room temperature (RT) operation of polymer-based SSBs; however, these polymers have poor compatibility against  $\text{Li}^\circ$  electrode and reverse to their cyclic monomers, leading to the loss of mechanical properties upon cycling [20]. On the other hand, higher ionic conductivity and better interfacial contact are achieved with GPEs which are usually plasticized with flammable liquid solvents or better ionic liquids. Nonetheless, GPEs have poorer mechanical properties and the reactivity of that added plasticizer with electrode materials can be crippling [21-25].

Trying to overcome the drawbacks presented by the above mentioned polymers, Jeffamine-based PEs have been synthesized and characterized in this thesis work. All these PEs presented a completely amorphous nature with low glass transition temperature ( $T_g$ ) and high ionic conductivity at RT. However, the different modifications applied to these materials did not meet the requirements for their application in all-solid-state lithium metal batteries (ASSLMBS) at RT, *i.e.*, high ionic conductivity, good mechanical properties and high stability with Li electrode.

In the case of Jeffamine-based SPE presented in **Chapter 3** and **Chapter 4**, the  $\text{Li}^\circ|\text{LiFSI/SPE}|\text{LFP}$  cell delivered decent specific/areal capacity with good Coulombic efficiency when decreasing the operational temperature close to RT. Nevertheless, the mechanical properties presented by these materials did not allow obtaining self-standing membranes. The introduction of polystyrene blocks in **Chapter 5** dramatically improved the mechanical properties of the PE, but the  $\text{Li}^\circ|\text{BCP70}|\text{LFP}$  cell could not be cycled for more than 30 cycles with good cycling stability. The suppression of the entanglement presented in **Chapter 6** resulted in a high flexible flowable polymer that could be successfully implemented as buffer layer in order to improve the cell performance of PEO-based cells. However,

despite the promising properties presented by this material, the liquid-like mechanical properties prevented the acquisition of self-standing membranes.

Trying to overcome these shortcomings, in this chapter a nanofiber-reinforced polymer electrolyte (NRPE) comprising of poly(vinylidene fluoride) (PVDF) fibers along with flowable polymer electrolyte (presented in **Chapter 6**) and sulfonimide salts (*i.e.*, LiTFSI and LiFSI) is proposed. This work is based on the following considerations:

**1)** The liquid-like PE presents high mobility of Li<sup>+</sup> ions and improved ionic conductivity due to the high amorphicity along with good adhesion properties and improved compatibility against Li<sup>o</sup> electrode [26].

**2)** PVDF nanofibers improve the mechanical properties of PEs, leading to self-standing membranes with good electrochemical performance [27-29], which are essential for the scalable processing of large-format SSBs.

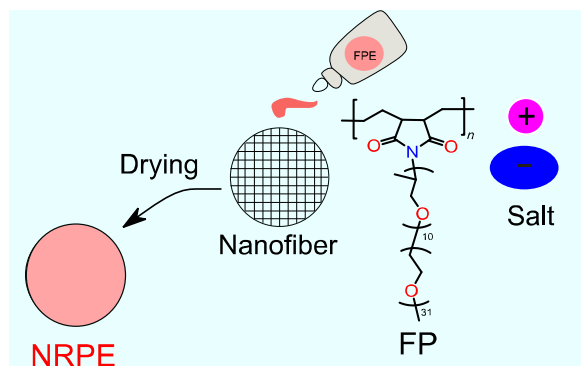
**3)** The sulfonimide anions [*i.e.*, bis(trifluoromethanesulfonyl)imide anion (TFSI<sup>-</sup>) and bis(fluorosulfonyl)imide anion (FSI<sup>-</sup>)] are chemically stable and structurally flexible, enabling the fast motion of ions and good thermal stability of the electrolytes.

As shown in **Scheme 7.1**, the typical solvent casting technique using the Li salt/flowable polymer solution on top of the PVDF fibers yields self-standing membranes with good ductility.

## 7.2. Preparation of NRPEs

Jeffamine M-2070-based flowable polymer matrix (FP) was prepared according to the procedures reported in **Chapter 6**, whereas the PVDF nanofibers were prepared by electrospinning as described in **Chapter 2** section **2.2.4**.

The NRPEs were obtained by a solvent casting method as schematically shown in **Figure 7.1**. First, the polymer matrix was dissolved in acetonitrile (ACN) (mass ratio 1:5) and then a pre-determined amount of Li salt (LiTFSI or LiFSI) was added ( $-\text{[CH}_2\text{CH}_2\text{O]}-\text{EO/Li} = 20$ ). Then, a certain amount of electrolyte solution was casted on the top of the PVDF fibers in order to obtain membranes with different amount of PVDF and an average thickness of 50  $\mu\text{m}$ . The resulting membranes were dried in a vacuum oven for 24 h at 80 °C. All the materials used in this chapter are summarized in **Table 7.1**.



**Figure 7.1.** Schematic illustration of the solvent casting method carried out to obtain the NRPEs.

**Table 7.1.** Abbreviations and corresponding composition of the as-prepared electrolytes.

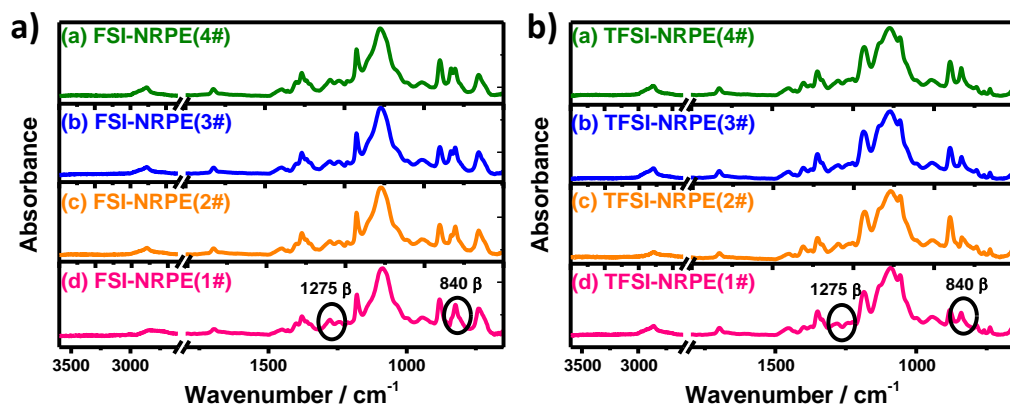
Acronym	Polymer matrix <sup>[a]</sup>	PVDF / wt <sup>[b]</sup>
FSI-NRPE	Jeffamine-based flowable polymer	10
FSI-NRPE(1#)	Jeffamine-based flowable polymer	10
FSI-NRPE(2#)	Jeffamine-based flowable polymer	15
FSI-NRPE(3#)	Jeffamine-based flowable polymer	20
FSI-NRPE(4#)	Jeffamine-based flowable polymer	25
TFSI-NRPE	Jeffamine-based flowable polymer	10
TFSI-NRPE(1#)	Jeffamine-based flowable polymer	10
TFSI-NRPE(2#)	Jeffamine-based flowable polymer	15
TFSI-NRPE(3#)	Jeffamine-based flowable polymer	20
TFSI-NRPE(4#)	Jeffamine-based flowable polymer	25
FSI-RE	PEO	–
TFSI-RE	PEO	–

[a] Type of polymer matrix used for the electrolyte preparation. [b] The weight percentage of the PVDF fibers in the NRPEs.



### 7.3. Chemical characterization of NRPEs

The NRPEs were analysed by attenuated total reflectance-Fourier-transform infrared spectroscopy (ATR-FTIR). The results obtained for FSI-NRPE and TFSI-NRPE-based polymer electrolytes are depicted in **Figure 7.2a** and **b**, respectively.



**Figure 7.2.** ATR-FTIR spectra of the a) FSI-NRPE and b) TFSI-NRPE-based polymer electrolytes with all the studied lithium salt concentrations.

PVDF can present at least four different polymorphs, including three polar phases ( $\beta$ ,  $\gamma$ ,  $\delta$ ) and one non-polar phase ( $\alpha$ ) depending on the chain packing lattices [28]. The  $\beta$  phase has been the most widely studied because of its pyro-, piezo and ferroelectric properties [30]. Infrared spectroscopy can be successfully used for determining the crystalline phases present in the PVDF materials by the analysis of specific absorption bands for different polar or non-polar phases [31, 32].

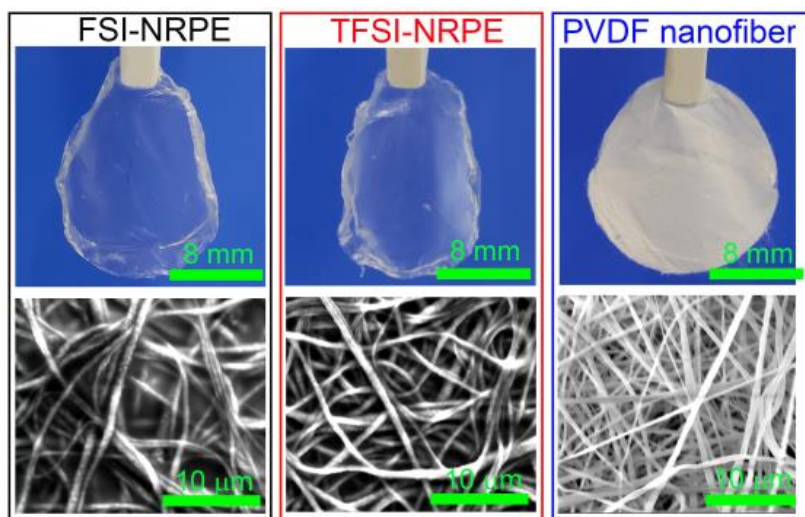
It is known that PVDF powder is rich in non-polar  $\alpha$  phase, presenting absorption peaks at 975, 795, 765 and 614  $\text{cm}^{-1}$ . Nevertheless, after the electrospinning process, the absorption peaks for PVDF fibers confirms the co-existence of  $\beta$ - (1275  $\text{cm}^{-1}$  and 840  $\text{cm}^{-1}$ ) and  $\alpha$  phases (765  $\text{cm}^{-1}$  and 614  $\text{cm}^{-1}$ ) [28]. However, these small peaks disappear when the flowable polymer electrolyte (FPE) is added to the PVDF membranes, indicating that pure  $\beta$  phase NRPEs are obtained and suggesting interaction between the two polymers. These signals can

overlap with the signals corresponding to ethylene oxide units. However, the interaction between Jeffamine-based FPE and PVDF fibers cannot be excluded.

Apart from these characteristic absorption signals and the peaks obtained for the FPE that were previously described in **Chapter 6**, PVDF presents vibration bands at  $1170\text{ cm}^{-1}$  and  $1204\text{ cm}^{-1}$  that can be assigned to the asymmetrical and symmetrical stretching of  $\text{CF}_2$  group, respectively.

#### 7.4. Morphological characterization

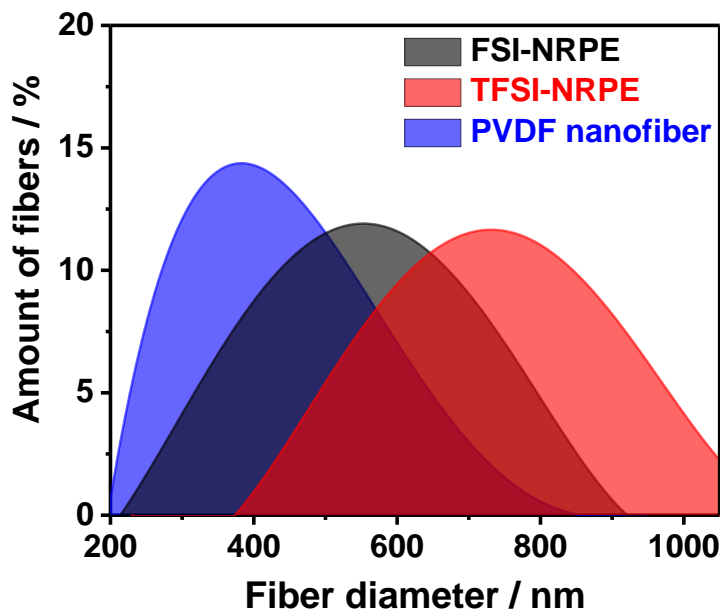
**Figure 7.3** presents the morphological properties of the pristine PVDF fibers and the as-prepared NRPEs. As it can be observed in the optical images, both electrolytes are soft and self-standing membranes with good ductility and the mechanical integrity of PVDF fibers is retained after the addition of Jeffamine-based FPEs. However, from the analysis of the SEM images, it can be concluded that the addition of the FPEs results in the swelling of the PVDF fibers.



**Figure 7.3.** Optical and SEM images of the pristine PVDF fibers and the as-prepared NRPEs.

More interestingly, the micromorphology of the PVDF fibers tends to be influenced by the type of the incorporated salts, as clearly evidenced in **Figure 7.4**, where the diameters of the fibers after the electrolyte addition are represented. The PVDF nanofibers become thicker after blending with Jeffamine-based PEs, due to the partial miscibility between PVDF and ethylene oxide (EO) side moieties but

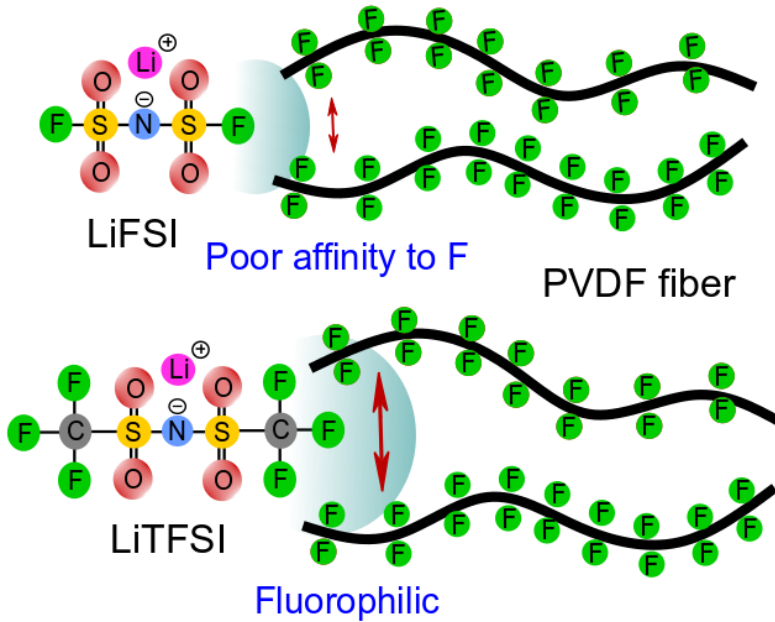
only in the presence of lithium salt [33]. Thus, the average thickness for pristine fibers is  $\sim 350$  nm and increases to  $\sim 550$  nm for FSI-NRPE and  $\sim 750$  nm for TFSI-NRPE.



**Figure 7.4.** Fiber diameter distribution of the as-prepared FSI-NRPE, TFSI-NRPE and pristine PVDF fibers.

Such difference between FSI-NRPE and TFSI-NRPE can be rationalized by the different interactions between these two salts and PVDF. The terminal  $-\text{SO}_2\text{F}$  group of LiFSI presents moderate affinity for the  $-\text{[CH}_2\text{CF}_2\text{]}-$  groups of PVDF impeding the penetration of the Jeffamine-based polymer and salt into the fibers.

However, the  $-\text{CF}_3$  group of LiTFSI exhibits high fluorophilicity due to a larger number of fluorine atoms and thus interacts easily with the  $-\text{CF}_2$  groups of PVDF fibers, and thereby resulting in a higher swelling of the PVDF fibers due to the improved penetration of Jeffamine-based polymers. This behavior is schematically shown in **Figure 7.5**.



**Figure 7.5.** Schematic illustration of the interaction between salt and PVDF fibers.

### 7.5. Mechanical characterization

The mechanical properties of the nanofiber-reinforced polymer matrix (NRP), TFSI-NRPEs and TFSI-PEO reference electrolyte were measured by differential mechanical analysis (DMA). The obtained results are summarized in **Table 7.2**. As it can be observed, all the NRP-based materials present storage modulus values  $\sim 10^9$  MPa and  $\sim 10^5$  MPa before and after the transition, respectively. These values are very similar to the ones obtained for the pristine PEO-based reference electrolyte, which it is well-known for its desirable mechanical properties, concluding that the mechanical properties are highly improved by the addition of the PVDF fibers to the FP matrix.

On the other hand, it is observed that the storage modulus values do not vary with the increasing amount of PVDF. Finally, comparing the results obtained for NRPs and NRPEs, it can be concluded that the addition of the salt does not affect to the mechanical properties of the material. It can be concluded that the global mechanical properties are determined by the PVDF fibers and practically independent from the addition of the FPE.

**Table 7.2.** Differential mechanical analysis results for NRPs, NRPEs and reference PEO electrolyte.

Acronym	PVDF (wt %) <sup>[a]</sup>	Storage Modulus before transition (MPa) <sup>[b]</sup>	Storage Modulus after transition (MPa) <sup>[c]</sup>	$T_g$ (°C) <sup>[d]</sup>
NRP(1#)	10	$1,6 \cdot 10^9$	$1,7 \cdot 10^4$	-54
NRP(2#)	15	$6,9 \cdot 10^8$	$8,7 \cdot 10^5$	-53
NRP(3#)	20	$2,3 \cdot 10^9$	$5,3 \cdot 10^5$	-53
NRP(4#)	25	$4,4 \cdot 10^8$	$5,3 \cdot 10^5$	-52
TFSI-NRPE(1#)	10	$2,9 \cdot 10^9$	$3,5 \cdot 10^5$	-53
TFSI-NRPE(2#)	15	$4,0 \cdot 10^9$	$5,2 \cdot 10^5$	-54
TFSI-NRPE(3#)	20	$2,7 \cdot 10^9$	$3,4 \cdot 10^6$	-53
TFSI-NRPE(4#)	25	$1,8 \cdot 10^9$	$6,8 \cdot 10^5$	-52
TFSI-RE	–	$3,8 \cdot 10^8$	$2,0 \cdot 10^5$	-32

[a] The weight percentage of the PVDF fibers in the NRP and NRPEs. Storage modulus [b] before and [c] after the transition (Mpa). [d] Glass transition temperature (°C).

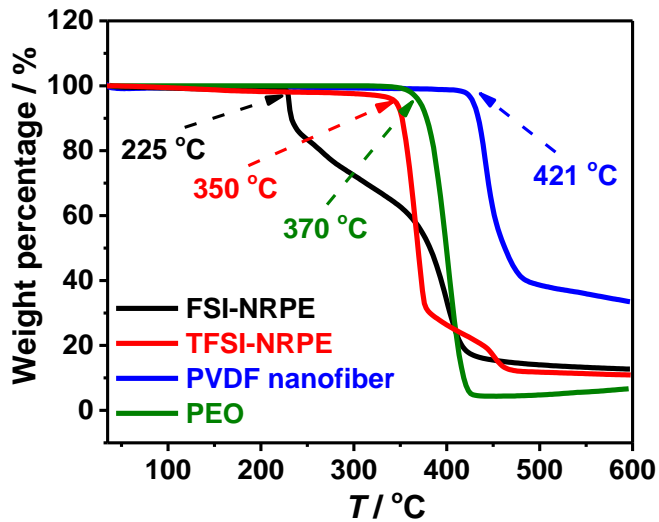
## 7.6. Thermal characterization

The flexibility of polymer segments is of great importance for facilitating the ionic motion in solid polymer electrolytes. For this reason, the study of the phase transition is important for screening the suitability of the electrolytes for their application in ASSLMs. As it is known from **Chapter 6**, FPE presents low  $T_g$  values and good ionic motion. In this chapter, the influence of the PVDF fibers in these properties will be analyzed.

### 7.6.1. Thermogravimetric analysis (TGA)

**Figure 7.6** presents the TGA traces of both types of NRPEs, pristine PVDF fibers and PEO matrix as a reference. All the materials present decomposition temperatures ( $T_d$ ) higher than 200 °C, which are well above the operational

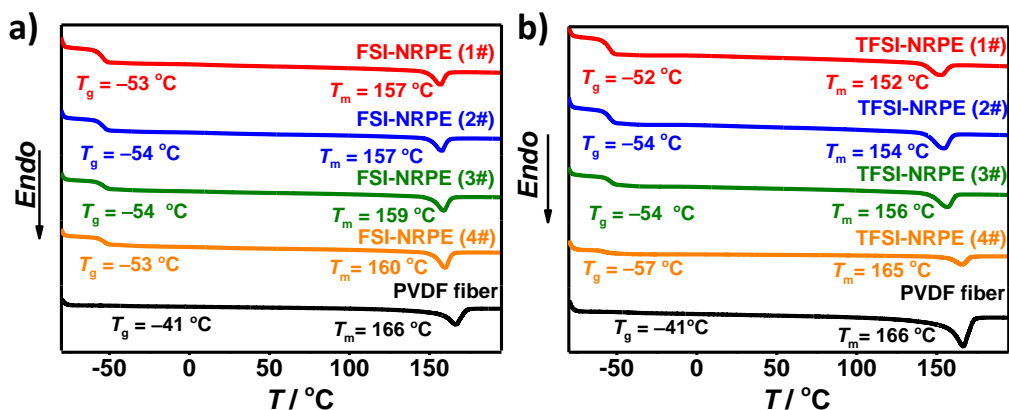
temperature of ASSLMs ( $< 80\text{ }^{\circ}\text{C}$ ). Notice that the lower value of  $T_d$  for FSI-NRPE compared to the other studied materials is attributed to the thermal lability of FSI<sup>-</sup> ( $T_d = 225\text{ }^{\circ}\text{C}$  for FSI-NRPE vs.  $T_d = 350\text{ }^{\circ}\text{C}$  for TFSI-NRPE) [34].



**Figure 7.6.** TGA traces of NRPEs, pristine PVDF fibers and PEO reference.

### 7.6.2. Differential scanning calorimetry (DSC)

The interaction between salt and fibers is further analyzed by DSC study. **Figure 7.7** depicts the DSC traces for **a)** FSI-NRPE and **b)** TFSI-NRPE, respectively, as well as pristine PVDF fibers. As it can be observed, the PVDF melting temperature ( $T_m$ ) of FSI-NRPEs presents small variation for the different measured samples regardless the electrolyte amount. However, in the case of LiTFSI-NRPEs, lower  $T_m$  values are observed with decreasing amount of PVDF fibers. Such behavior testifies the improved fluorophilic nature of LiTFSI vs. LiFSI, *i.e.*, when the fiber concentration is low (TFSI-NRPE (1#)), the salt can easily diffuse between the chains interacting with them and, as a consequence, decreasing the  $T_m$  values.



**Figure 7.7.** DSC traces of pristine PVDF fibers and **a)** FSI-NRPEs and **b)** TFSI-NRPEs.

**Table 7.3** summarizes the thermal transitions and the calculated value of crystallinity for the NRPEs. As it can be observed, both NRPEs show glass transitions at *ca.*  $-55$  °C, signature of the high segmental mobility of hanging EO units in Jeffamine-based polymers [26]. Upon increasing the content of Jeffamine-based PEs, the melting enthalpy at *ca.*  $160$  °C assigned to PVDF decreases monotonically from  $\sim 12$  J g $^{-1}$  to  $\sim 6$  J g $^{-1}$  indicating a higher amorphicity of the electrolytes.

The crystallinity of the measured samples was calculated by **Equation 7.1**. As it is shown in **Table 7.3**, pristine PVDF fibers present a crystallinity value of 45 %, whereas the values for NRPEs range between 41% and 57 %. However, these values do not follow any tendency. This can be ascribed to the errors made when the sample is weighted for electrolyte and DSC sample preparation. A deviation of 0.1 mg when the sample is weighted results in a variation of 5 % in the crystallinity value. For this reason, it can be concluded that the crystallinity values obtained for NRPEs are comparable to that obtained for the pristine PVDF fibers.

$$\chi_c = \frac{\Delta H_m}{\Delta H_{PVDF} \times f_{PVDF}} \times 100$$

**Equation 7.1** wherein,  $\chi_c$  is the crystallinity (%),  $\Delta H_m$  is the melting enthalpy of electrolyte,  $f_{PVDF}$  is the weight fraction of PVDF in the electrolyte, and  $\Delta H_{PVDF}$  is the value of  $104.7$  J g $^{-1}$  for totally crystalline PVDF reported in literature [35].

**Table 7.3.** The characterization data for phase behaviour for the as-prepared electrolytes.

Samples	$T_g$ [a]	$T_m$ [b] ( $\Delta H_m$ ) [c]	$\chi_c$ [d]
PVDF fibers	-41	166 (47.1)	45
<b>FSI-NRPE</b>			
FSI-NRPE(1#)	-54	157 (6.0)	57
FSI-NRPE(2#)	-54	157 (6.5)	41
FSI-NRPE(3#)	-54	159 (9.0)	53
FSI-NRPE(4#)	-53	160 (10.5)	40
<b>TFSI-NRPE</b>			
TFSI-NRPE(1#)	-52	152 (5.5)	52
TFSI-NRPE(2#)	-54	154 (7.6)	48
TFSI-NRPE(3#)	-54	156 (9.8)	47
TFSI-NRPE(4#)	-57	165 (11.5)	44

[a] Glass transition temperature ( $^{\circ}\text{C}$ ) taken as the midpoint of the inflexion. [b] Melting point ( $^{\circ}\text{C}$ ) taken as the maximum value of the melting peak. [c] Enthalpy of melting ( $\text{J g}^{-1}$ ). [d] Crystallinity (%).

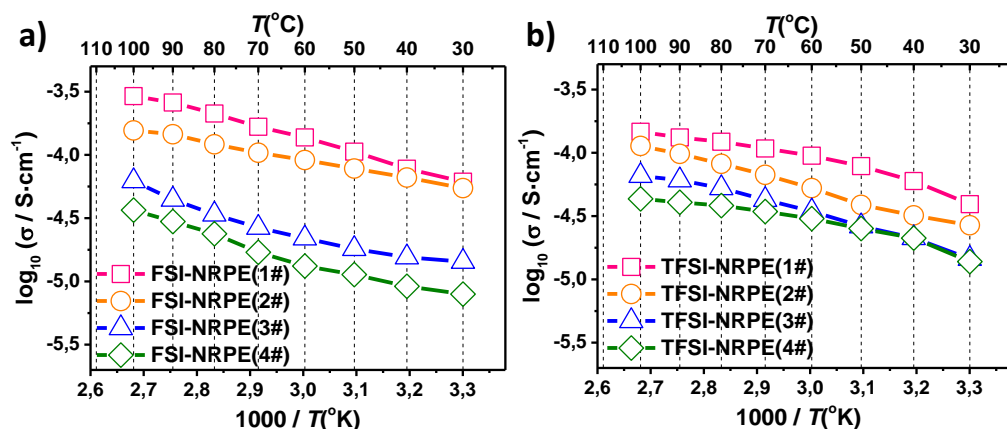
## 7.7. Electrochemical characterization

The study of properties such as ionic conductivity, Li-ion transference number, diffusion coefficient, electrochemical stability toward oxidation and compatibility with  $\text{Li}^{\circ}$  electrode is essential as these parameters will determine the suitability of the polymer electrolytes for their application in ASSLMs.

### 7.7.1. Ionic conductivity

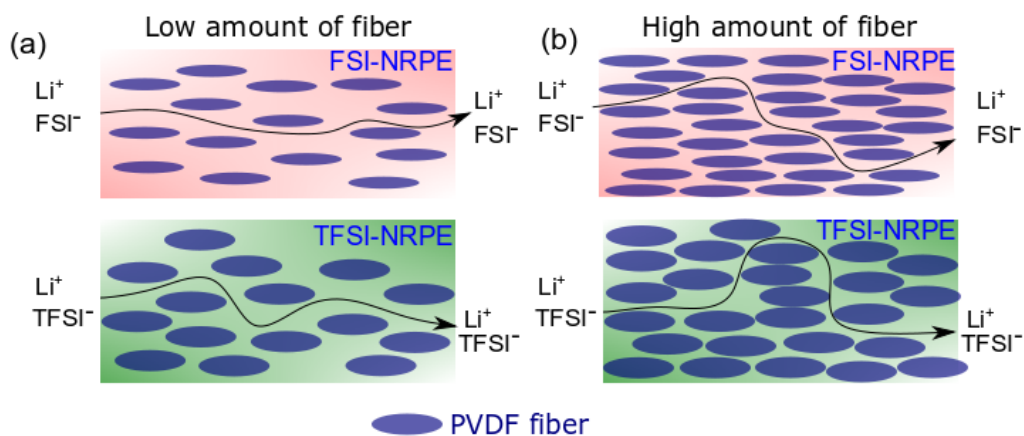
**Figure 7.8** shows the ionic conductivity for all the prepared **a)** FSI-NRPEs and **b)** TFSI-NRPEs materials. As it can be observed, both types of electrolytes follow the same tendency; higher ionic conductivities are achieved at lower amount of PVDF fibers. However, it is worth to mention that two differentiated regions are observed; low PVDF fiber amount (*ca.* 10 and 15 wt % PVDF) where the ionic conductivities are higher in the case of FSI-NRPEs than for TFSI-based ones, and high PVDF amount (*ca.* 20 and 25 wt % PVDF) where the opposite behavior is obtained.





**Figure 7.8.** Temperature dependence of ionic conductivity for all the prepared a) FSI-NRPEs and b) TFSI-NRPEs.

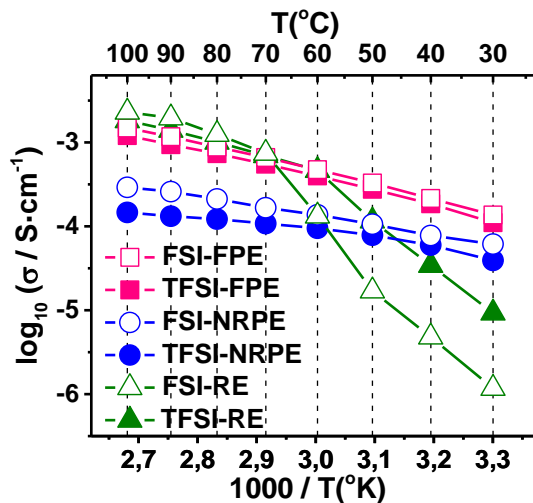
In the case of the samples with high electrolyte amount (*ca.* 10 and 15 wt % PVDF) the excess of electrolyte results in higher ionic conductivity values, being higher in the case of FSI-based electrolytes. These results are in accordance with the previous chapters where it has been explained that the smaller size of the FSI anion favors the ion mobility. This behavior could be explained by the higher swelling of PVDF nanofibers in TFSI-NRPEs, resulting in a higher degree of tortuosity for ion transport and, as a consequence, lower ionic conductivity values are obtained. This behavior is explained in **Figure 7.9a**.



**Figure 7.9.** Schematic illustration of the effect of tortuosity on the ion transport in FSI-NRPE and TFSI-NRPE.

However, when the amount of PVDF is increased the tortuosity is high for both types of electrolytes, **Figure 7.9b**, resulting in a big drop in the ionic conductivity, especially for LiFSI-NRPEs. In the case of TFSI-NRPEs, the fluorophilic nature of  $-\text{CF}_3$  group favors the interaction with the  $-\text{CF}_2$  groups from PVDF favoring the ionic transport and resulting in a relatively higher ionic conductivity (**Figure 7.5**).

For both types of NRPEs, 10 wt% PVDF fibers gave the highest ionic conductivity values for the measured temperature range. For this reason, these electrolytes were chosen as best candidates for further analysis. **Figure 7.10** shows the temperature dependence of ionic conductivities for both the FSI- and TFSI-based NRPEs, FPEs, as well as for PEO-based reference electrolytes (hereafter REs). All the Jeffamine-based PEs follow a continuous Vogel-Tamman-Fulcher behaviour, indicating a fully amorphous nature of the electrolytes; whereas the REs display a knee in ionic conductivity because of the melting transition of the crystallized PEO phase between 60 and 70 °C [15].



**Figure 7.10.** Temperature dependence of ionic conductivity for NRPEs, FPEs and reference PEO electrolytes.

At RT, NRPEs possess significantly higher ionic conductivities ( $\sim 10^{-4}$  S  $\text{cm}^{-1}$ ) than REs ( $\sim 10^{-5}$  –  $10^{-6}$  S  $\text{cm}^{-1}$ ) due to the high amorphicity of Jeffamine-based PEs. In comparison with the pristine FPEs, NRPEs show lower ionic conductivities and the difference between FSI and TFSI-based electrolytes is more pronounced. This

could be explained by the higher swelling of PVDF nanofibers in TFSI-NRPEs, resulting in a higher degree of tortuosity for ion transport, as schematically illustrated in **Figure 7.9a**.

### 7.7.2. Li-ion transference number

The contribution of Li-ion to the total ionic conductivity is quantified by the lithium-ion transference number ( $T_{Li^+}$ ) measurement via a combination of electrochemical impedance spectra (EIS) and polarization method described in **Chapter 2** section **2.4.5** [36]. **Table 7.4** summarizes the measured results of the parameters used to calculate the value of  $T_{Li^+}$  for the NRPEs at different temperatures. These results suggest an insignificant difference with the variation of temperature.

**Table 7.4.** The calculated values of Li-ion transference number ( $T_{Li^+}$ ) of various NRPEs at different temperatures.

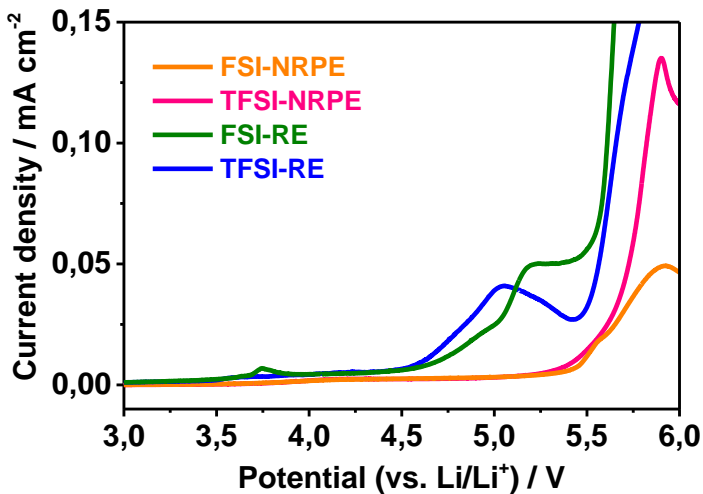
Electrolyte	$T/^\circ C$	$I_0/\mu A^{[a]}$	$I_s/\mu A^{[b]}$	$R_{b_0}^\circ/\Omega^{[c]}$	$R_{b_0}^s/\Omega^{[d]}$	$R_i^\circ/\Omega^{[e]}$	$R_i^s/\Omega^{[f]}$	$\Delta V/mV^{[g]}$	$T_{Li^+}$
<b>FSI-NRPE</b>									
	70	100	30	33	31	52	49	10	0.16
	60	62	20	41	40	107	108	10	0.13
	50	25	9	72	72	276	280	10	0.15
	40	3	5	113	112	591	587	10	0.12
	30	6	3	192	195	1332	1340	10	0.11
<b>TFSI-NRPE</b>									
	70	112	25	42	40	36	40	10	0.14
	60	64	17	60	60	80	84	10	0.15
	50	22	7	102	103	313	321	10	0.12
	40	11	4	157	157	666	675	10	0.12
	30	51	2	262	262	1494	1491	10	0.14

[a] Initial and [b] steady-state current obtained by dc polarization; [c] initial and [d] final resistances of the electrolytes measured by ac impedance method before and after polarization, respectively; [e] initial and [f] final resistances of interfacial layer between electrode/electrolyte measured by ac impedance method before polarization and after polarization, respectively; [g] the dc voltage subjected to the  $Li^\circ$  symmetrical cell.

In terms of salt type, the obtained results (*ca.* 0.15) suggest a negligible difference between the measured samples with the same EO/Li ratio for both LiTFSI and LiFSI, presenting typical  $T_{Li^+}$  values for salt-in-polymer systems.

### 7.7.3. Electrochemical stability toward oxidation

The anodic stability of the as-prepared NRPEs and PEO-based reference electrolytes was determined by linear sweep voltammetry (LSV). These LSV profiles show that the anodic stabilities of NRPEs are higher than those of the corresponding REs where oxidation currents at *ca.* 4 V vs. Li/Li<sup>+</sup> are observed due to the degradation of EO groups when the PEO is in renewed direct contact with the electrode [26]. This implies that the nanofibers reinforcement in NRPEs mitigates the electrochemical decomposition of EO units by minimizing the direct contact between the electrolyte and electrode.

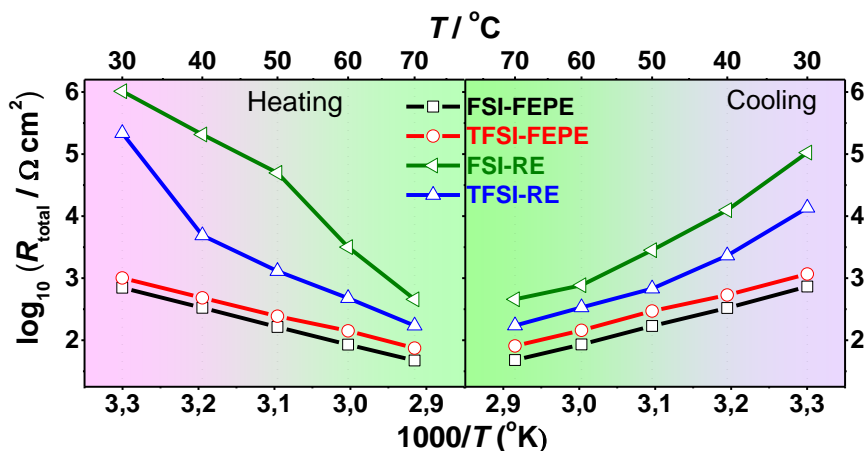


**Figure 7.11.** Linear sweep voltammetry profiles measured on stainless steel (SS) electrode at 70 °C.

### 7.7.4. Compatibility with Li<sup>o</sup> electrode

**Figure 7.12** shows the temperature dependence of the total resistance ( $R_{total}$ ) measured on Li<sup>o</sup> | Li<sup>o</sup> symmetric cells. Similar to the tendency observed in **Figure 7.10** for ionic conductivity,  $R_{total}$  for NRPEs changes gradually in the studied temperature range (30–70 °C) and a drastic decrease (or increase) in  $R_{total}$  is

observed for REs during the heating (or cooling) scan. This result suggests that solid electrolyte interphase (SEI) layer formed on  $\text{Li}^\circ$  electrode inherits the intrinsic properties of bulk electrolytes, and chemical decomposition of amorphous and conductive NRPE results in a less resistive SEI layer. See **Table A.7.1** for the comparison of interfacial resistance between NRPEs and REs. This behavior is similar to the one obtained for FPE itself in **Chapter 6**.

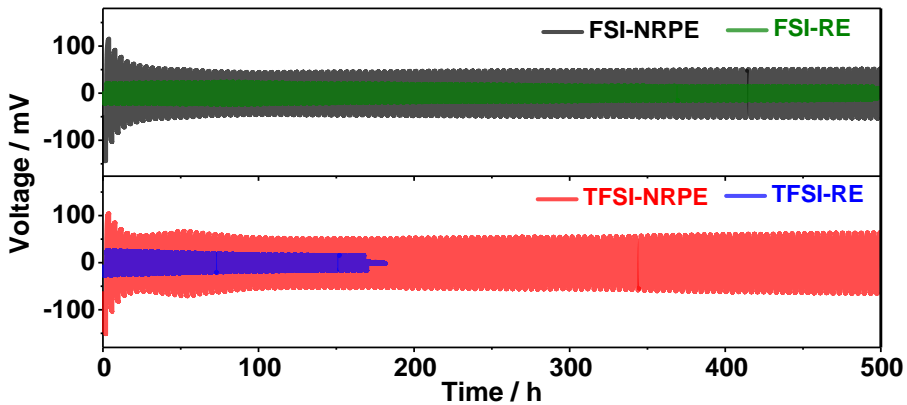


**Figure 7.12.** Total resistance ( $R_{\text{total}}$ ) of the  $\text{Li}^\circ$  symmetric cells using various electrolytes at heating and cooling scans.

Electrochemical impedance spectroscopy (EIS) plots of  $\text{Li}^\circ$  symmetric for NRPEs and PEO reference electrolytes at different temperatures are presented in **Figure A.7.2** and **Figure A.7.3** respectively. The simplified equivalent circuit used to fit collected EIS data is given in **Figure A.7.1** and the best fitted-results are summarized in **Table A.7.1**.

**Figure 7.13** further compares the voltage profiles for the  $\text{Li}^\circ$  plating/stripping test using  $\text{Li}^\circ$  symmetric cells at a current density of  $0.1 \text{ mA cm}^{-2}$  at  $70^\circ\text{C}$ . The TFSI-RE lasts only 160 h before the occurrence of internal short-circuit, whereas the rest of the electrolytes retain continuous cycling for more than 500 h without any internal short-circuit or impedance raise. This can be attributed to the good contact between the NRPEs and the electrode and the SEI-favourable  $\text{FSI}^-$  that can significantly improve the electrochemical stability of  $\text{Li}^\circ$  electrode with the electrolyte. Notice that the higher overpotential in NRPE-based cells than

that in the RE-based ones is probably associated with lower ionic conductivity of the former electrolyte at 70 °C.



**Figure 7.13.** Galvanostatic cycling of the  $\text{Li}^{\circ}$  symmetric cells at 70 °C with a current density of  $0.1 \text{ mA cm}^{-2}$  for NRPEs and REs.

Overall, these physicochemical and electrochemical characterizations clearly testify the suitability of NRPEs for  $\text{Li}^{\circ}$ -based rechargeable SSBs.

### 7.7.5. Cycling of $\text{Li}^{\circ}$ | $\text{LiFePO}_4$ cell performance

#### 7.7.5.1. Solvent-casting method in $\text{LiFePO}_4$ -based cathodes

The possibility of implementing the NRPEs in rechargeable ASSLMBs is further evaluated by the cycling performance of  $\text{Li}^{\circ}$  |  $\text{LiFePO}_4$  cells.

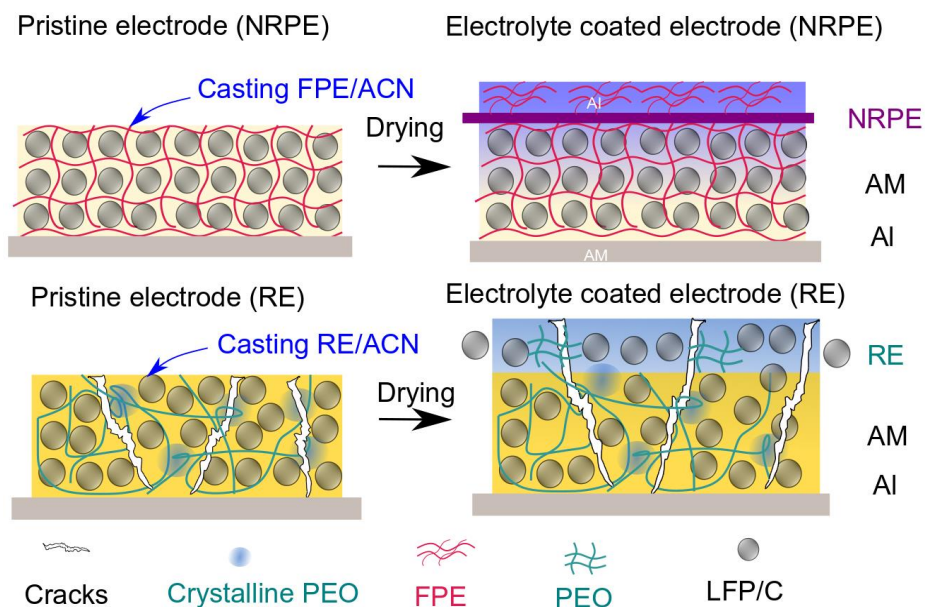
First,  $\text{LiFePO}_4$  based cathodes were prepared using 63 wt% LFP active material, 7 wt% C65 conductive carbon and 30 wt% SPE/LiX [(SPE = Jeffamine-based FPE, PEO) and (X = TFSI, FSI)] as polymer binder following the method reported in **Chapter 2** section **2.3.1**

However, the FPE presented really poor binding properties, resulting in a completely cracked electrode with delamination problems, as it can be observed in **Figure A.7.4**. Moreover, the sticky nature of the obtained NRPEs made the sample handling unmanageable. For this reason, so as to improve the wetting and contact

between PEs and porous LFP cathode, the electrolytes were in-situ casted on the top of the cathodes. In order to determine if this solvent casting method is suitable, PEO-based reference cathodes were obtained and compared with the Jeffamine-based ones using the same cathode composition.

Trying to improve the mechanical and binding properties of Jeffamine-based cathodes, 6 wt% Kynar® (1000 HD homopolymer) was added to the electrolyte slurry. The composition of the prepared cathodes was: 63 wt% LFP active material, 7 wt% C65 conductive carbon and 30 wt% SPE/LiX (X = TFSI, FSI) polymer binder, where 24 wt% is the corresponding polymer matrix and 6 wt% Kynar® (1000 HD homopolymer) using a mixture of ACN and 1-methyl-2-pyrrolidinone (NMP) (6 : 1 by volume) as solvent.

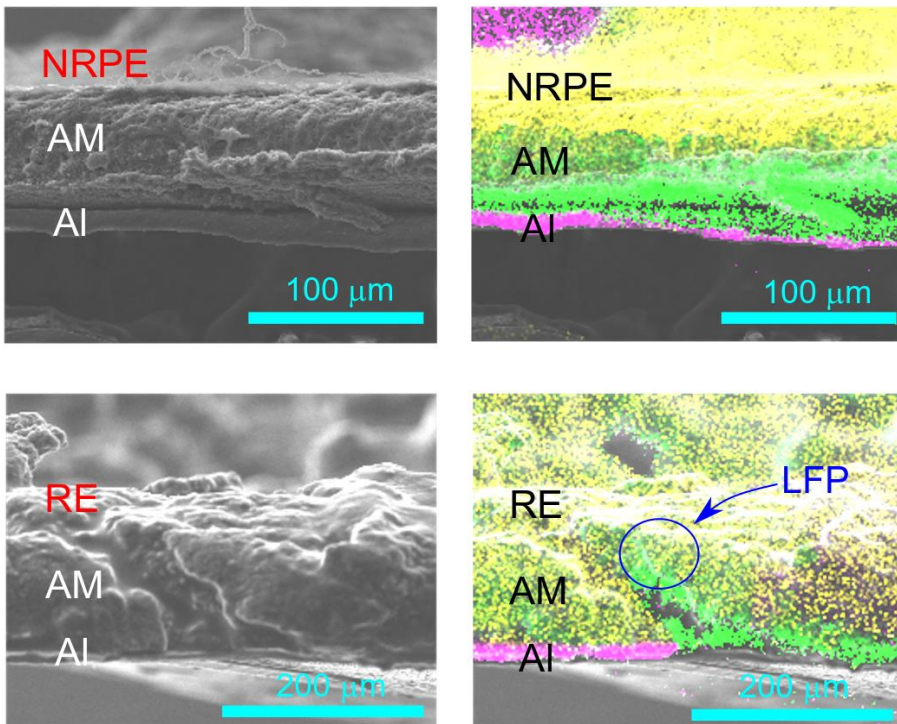
For sample preparation, the LFP based cathode was placed on the top of the stainless steel (SS) electrodes and the corresponding polymer electrolyte dissolved in acetonitrile (ACN) was cast on the top of it, using PVDF fibers as spacer in the case of NRPEs, as schematically illustrated in **Figure 7.14**. After solvent evaporation the samples were dried in a vacuum oven for 24 h at 50 °C.



**Figure 7.14.** Schematic illustration of the processing of the NRPE and RE-based cathodes.

In the case of NRPE, the PVDF nanofibers act as a protective layer, preventing the migration of active material (AM) into electrolyte solution, and thereby maintaining the integrity of the electrode. In sharp contrast, the direct casting of RE solution on the top of the cathode causes the dissolution of the binder and diffusion of electrode material particles into electrolyte phase and the breakdown of electrode. Such behaviour was ascertained by energy dispersive X-ray spectroscopy (EDX) mapping of the cross-sectional view of the as-prepared electrodes, as it is shown in **Figure 7.15**.

NRPE-based electrode shows three distinctive layers: 1) current collector as seen by the aluminium (Al) spectrum; 2) LFP cathode indicated by the iron (Fe); and 3) electrolyte bulk evidenced by fluorine (F) of the electrolyte salt. Yet, a blend between the Fe and F can be observed in RE-based electrode, which strongly suggests the breakdown of the cathode during the casting of the electrolyte.

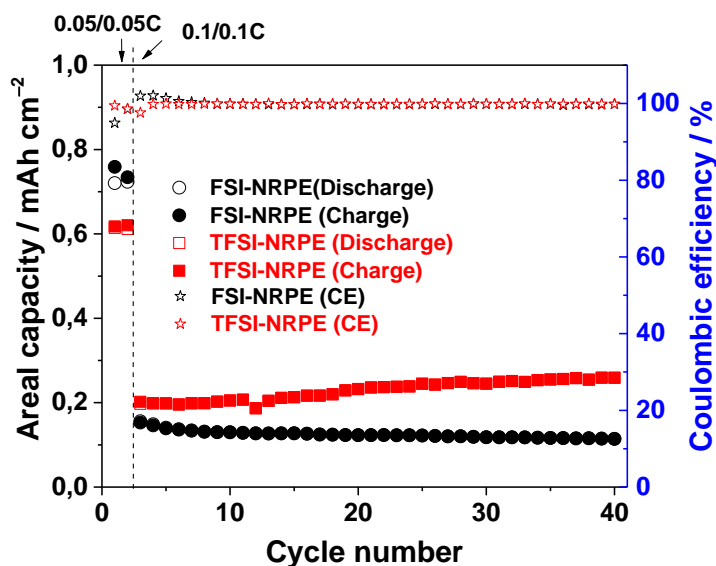


**Figure 7.15.** SEM and EDX images of the  $\text{LiFePO}_4$  cathodes (F in yellow, Fe in green and Al in pink).



### 7.7.5.2. Cycling of Li<sup>o</sup> | LiFePO<sub>4</sub> cell performance at RT

The feasibility of implementing NRPEs in rechargeable ASSLMBs is evaluated by the cycling performance of Li<sup>o</sup> | LiFePO<sub>4</sub> cells. **Figure 7.16** depicts the cell performance of FSI-NRPE and TFSI-NRPE under a constant charge/discharge rate of 0.1/0.1C at 30 °C. Both cells are cycled with excellent Coulombic efficiency (CE > 99%). The areal capacity of TFSI-NRPE-based cell is higher than that of the FSI-NRPE-based one. This difference can be attributed to the poor fluorophilicity of LiFSI which impedes the ion transport of LFP. Under a low C-rate of 0.05/0.05C, a high areal capacity of > 0.6 mAh cm<sup>-2</sup> is reached for both cells. This high cell capacity at RT outperforms most of the reported ones in literature, as it can be observed in **Table A.7.2**; e.g, 0.35 mAh cm<sup>-2</sup> for polycarbonate-based SPEs, 0.19 mAh cm<sup>-2</sup> for tetraglyme-added GPEs and 0.37 mAh cm<sup>-2</sup> for succinonitrile-containing PEs (**Table A.7.2** entries **3**, **5** and **11**, respectively).

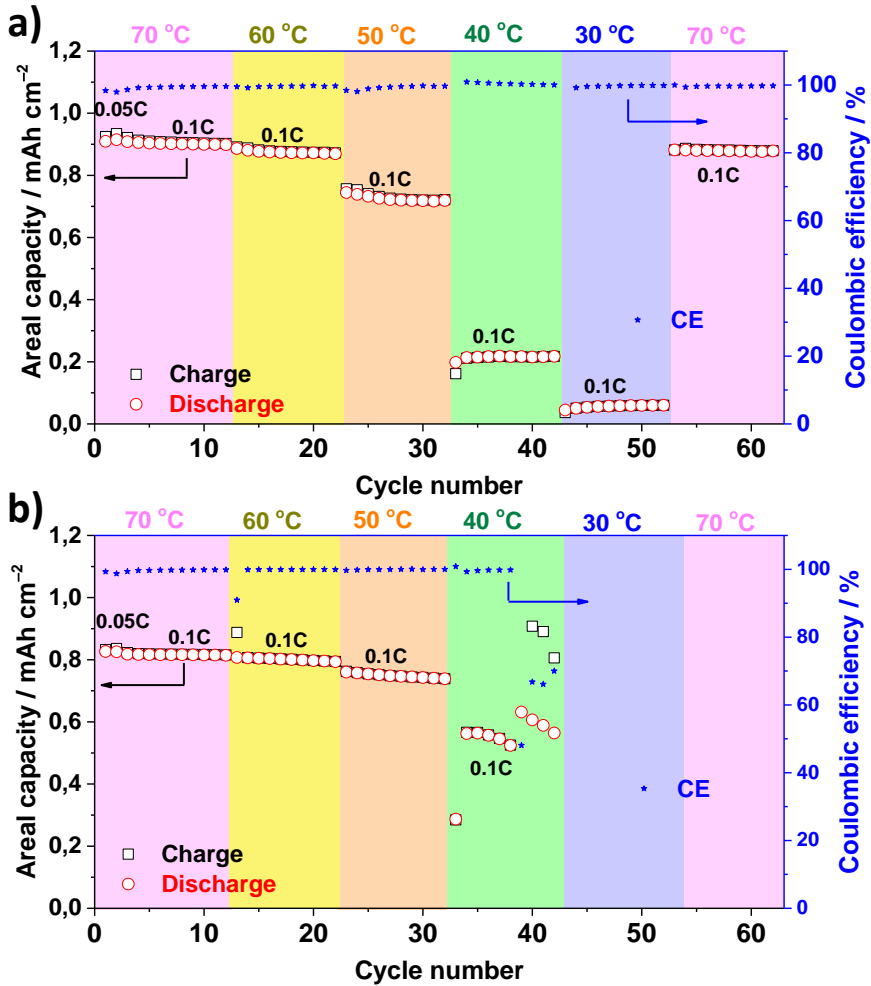


**Figure 7.16.** Areal charge/discharge capacities and Coulombic efficiency vs. cycle number for the cells using Li<sup>o</sup> | NRPEs | LFP cells at 30 °C.

### 7.7.5.3. Cycling of Li<sup>o</sup> | LiFePO<sub>4</sub> cell performance at different temperatures

**Figure 7.17** further shows the specific capacity and Coulombic efficiency vs. cycle number at various temperatures using **a)** FSI-NRPE and **b)** TFSI-NRPE. The

cell using TFSI-NRPE delivers a discharge capacity of  $0.8 \text{ mAh cm}^{-2}$  ( $159 \text{ mAh g}^{-1}$ ) at an elevated temperature of  $70^\circ\text{C}$ , and shows a slightly decreased capacity of  $0.75 \text{ mAh cm}^{-2}$  ( $145 \text{ mAh g}^{-1}$ ) after lowering the operational temperature down to  $50^\circ\text{C}$ . However, after prolonged cycling, the TFSI-NRPE-based cell encounters low CE due to formation of soft dendrites [26].



**Figure 7.17.** Areal charge/discharge capacities and Coulombic efficiency vs. cycle number for the cells using a)  $\text{Li}^+ | \text{FSI-NRPE} | \text{LFP}$  and b)  $\text{Li}^+ | \text{TFSI-NRPE} | \text{LFP}$  cells at variable temperature under a constant C-rate of 0.1/0.1C.

For the cell using FSI-NRPE (**Figure 7.17a**), an areal capacity of  $0.9 \text{ mAh cm}^{-2}$  ( $159 \text{ mAh g}^{-1}$ ) is obtained at  $70 \text{ }^\circ\text{C}$ , and decreasing to  $0.7 \text{ mAh cm}^{-2}$  ( $130 \text{ mAh g}^{-1}$ ) at  $50 \text{ }^\circ\text{C}$ . Further decrease of the temperature to  $40 \text{ }^\circ\text{C}$  results in a significant drop of capacity [*i.e.*,  $0.2 \text{ mAh cm}^{-2}$  ( $40 \text{ mAh g}^{-1}$ )], and it is tempting to associate this effect to a poorer miscibility between LiFSI + polyether and PVDF existing in both electrolyte and cathode below  $50 \text{ }^\circ\text{C}$ , resulting for the latter in reduced percolation. However, the capacity for LiFSI-NRPE reversibly regained a good Coulombic efficiency after several cycles when the temperature is returned to  $70 \text{ }^\circ\text{C}$ . This behaviour is attributable to the good SEI formation due to FSI<sup>-</sup> that keeps in the NRPE membranes. The decent cycling performance of NRPE-based cells affirms the technological feasibility of NRPE as safe and reliable electrolyte for accessing high-performance SSBs.

## 7.8. Conclusions

In this chapter the method for obtaining NRPEs by solvent casting method is described. These NRPEs present improved mechanical properties compared to the FPE itself, allowing the preparation of self-standing membranes. These electrolytes are completely amorphous with low  $T_g$  values, leading to a higher ionic conductivity than REs at RT ( $\sim 10^{-4} \text{ S cm}^{-1}$  vs.  $\sim 10^{-5} \text{ S cm}^{-1}$ ).

The addition of PVDF nanofibers into FPE does not affect the stability against Li<sup>o</sup> electrode ( $< 800 \text{ } \Omega \text{ cm}^2$  at  $30 \text{ }^\circ\text{C}$ ). As a result, the corresponding Li<sup>o</sup> | | LiFePO<sub>4</sub> cells show decent performances even at RT ( $\sim 0.7 \text{ mAh cm}^{-2}$  at  $30 \text{ }^\circ\text{C}$  and C/20). LiTFSI is more compatible with PVDF fibers giving higher areal capacity. However, TFSI ion does not protect the Li surface as effectively as FSI ion. Further optimization on the electrolyte formation such as the use of SEI-forming additives and novel salts could be beneficial for improving the energy density of NRPE-based SSBs. Therefore, NRPEs combining both rigid PVDF nanofibers and a high molecular weight but flowable polymer are believed to be one of the most appealing candidates for attaining high-performance SSBs in the near future.

**References**

- [1] W. Xu, J. Wang, F. Ding, X. Chen, E. Nasybulin, Y. Zhang, J.G. Zhang. Lithium metal anodes for rechargeable batteries. *Energ. Environ. Sci.* 2014; **7**(2), 513-537.
- [2] X.B. Cheng, R. Zhang, C.Z. Zhao, Q. Zhang. Toward safe lithium metal anode in rechargeable batteries: a review. *Chem. Rev.* 2017; **117**(15), 10403-10473.
- [3] C. Zhao, L. Liu, X. Qi, Y. Lu, F. Wu, J. Zhao, Y. Yu, Y.S. Hu, L. Chen. Solid-state sodium batteries. *Adv. Energy Mater.* 2018; **8**(17), 1703012.
- [4] Z. Gao, H. Sun, L. Fu, F. Ye, Y. Zhang, W. Luo, Y. Huang. Promises, challenges, and recent progress of inorganic solid-state electrolytes for all-solid-state lithium batteries. *Adv. Mater.* 2018; **30**(17), 1705702.
- [5] X. Judez, G.G. Eshetu, C. Li, L.M. Rodriguez-Martinez, H. Zhang, M. Armand. Opportunities for rechargeable solid-state batteries based on Li-intercalation cathodes. *Joule.* 2018; **2**(11), 2208-2224.
- [6] M. Keller, A. Varzi, S. Passerini. Hybrid electrolytes for lithium metal batteries. *J. Power Sources.* 2018; **392**, 206-225.
- [7] J.C. Bachman, S. Muy, A. Grimaud, H.H. Chang, N. Pour, S.F. Lux, O. Paschos, F. Maglia, S. Lupart, P. Lamp, L. Giordano, Y. Shao-Horn. Inorganic solid-state electrolytes for lithium batteries: mechanisms and properties governing ion conduction. *Chem. Rev.* 2016; **116**(1), 140-162.
- [8] Z. Zhang, Y. Shao, B. Lotsch, Y.S. Hu, H. Li, J. Janek, L.F. Nazar, C.W. Nan, J. Maier, M. Armand, L. Chen. New horizons for inorganic solid state ion conductors. *Energ. Environ. Sci.* 2018; **11**(8), 1945-1976.
- [9] H. Zhang, C. Li, M. Piszcz, E. Coya, T. Rojo, L.M. Rodriguez-Martinez, M. Armand, Z. Zhou. Single lithium-ion conducting solid polymer electrolytes: advances and perspectives. *Chem. Soc. Rev.* 2017; **46**(3), 797-815.
- [10] I. Aldalur, H. Zhang, M. Piszcz, U. Oteo, L.M. Rodriguez-Martinez, D. Shanmukaraj, T. Rojo, M. Armand. Jeffamine® based polymers as highly conductive polymer electrolytes and cathode binder materials for battery application. *J. Power Sources.* 2017; **347**, 37-46.
- [11] V. Di Noto, S. Lavina, G.A. Giffin, E. Negro, B. Scrosati. Polymer electrolytes: present, past and future. *Electrochim. Acta.* 2011; **57**, 4-13.

- [12] D.T. Hallinan, S.A. Mullin, G.M. Stone, N.P. Balsara. Lithium metal stability in batteries with block copolymer electrolytes. *J. Electrochem. Soc.* 2013; **160**(3), A464-A470.
- [13] X. Cheng, J. Pan, Y. Zhao, M. Liao, H. Peng. Gel polymer electrolytes for electrochemical energy storage. *Adv. Energy Mater.* 2018; **8**(7), 1702184.
- [14] M.B. Armand. Polymer Electrolytes. *Annu. Rev. Mater. Sci.* 1986; **16**(1), 245-261.
- [15] H. Zhang, C. Liu, L. Zheng, F. Xu, W. Feng, H. Li, X. Huang, M. Armand, J. Nie, Z. Zhou. Lithium bis(fluorosulfonyl)imide/poly(ethylene oxide) polymer electrolyte. *Electrochim. Acta.* 2014; **133**, 529-538.
- [16] M. Armand. The history of polymer electrolytes. *Solid State Ion.* 1994; **69**(3), 309-319.
- [17] S. Lascaud, M. Perrier, A. Vallee, S. Besner, J. Prud'homme, M. Armand. Phase diagrams and conductivity behavior of poly(ethylene oxide)-molten salt rubbery electrolytes. *Macromolecules.* 1994; **27**(25), 7469-7477.
- [18] B. Sun, J. Mindemark, K. Edström, D. Brandell. Realization of high performance polycarbonate-based Li polymer batteries. *Electrochem. Commun.* 2015; **52**, 71-74.
- [19] B. Sun, H.D. Asfaw, D. Rehnlund, J. Mindemark, L. Nyholm, K. Edström, D. Brandell. Toward solid-state 3D-microbatteries using functionalized polycarbonate-based polymer electrolytes. *ACS Appl. Mater. Interfaces.* 2018; **10**(3), 2407-2413.
- [20] C. Wang, H. Zhang, J. Li, J. Chai, S. Dong, G. Cui. The interfacial evolution between polycarbonate-based polymer electrolyte and Li-metal anode. *J. Power Sources.* 2018; **397**, 157-161.
- [21] G.B. Appetecchi, G.T. Kim, M. Montanino, M. Carewska, R. Marcilla, D. Mecerreyes, I. De Meatza. Ternary polymer electrolytes containing pyrrolidinium-based polymeric ionic liquids for lithium batteries. *J. Power Sources.* 2010; **195**(11), 3668-3675.
- [22] M. Li, L. Yang, S. Fang, S. Dong, S.I. Hirano, K. Tachibana. Polymer electrolytes containing guanidinium-based polymeric ionic liquids for rechargeable lithium batteries. *J. Power Sources.* 2011; **196**(20), 8662-8668.

[23] M. Li, L. Yang, S. Fang, S. Dong, S.I. Hirano, K. Tachibana. Polymerized ionic liquids with guanidinium cations as host for gel polymer electrolytes in lithium metal batteries. *Polym. Int.* 2012; **61**(2), 259-264.

[24] K. Yin, Z. Zhang, L. Yang, S.I. Hirano. An imidazolium-based polymerized ionic liquid via novel synthetic strategy as polymer electrolytes for lithium ion batteries. *J. Power Sources.* 2014; **258**, 150-154.

[25] K. Yin, Z. Zhang, X. Li, L. Yang, K. Tachibana, S.I. Hirano. Polymer electrolytes based on dicationic polymeric ionic liquids: application in lithium metal batteries. *J. Mater. Chem. A.* 2015; **3**(1), 170-178.

[26] I. Aldalur, M. Martinez-Ibañez, A. Krztoń-Maziopa, M. Piszcz, M. Armand, H. Zhang. Flowable polymer electrolytes for lithium metal batteries. *J. Power Sources.* 2019; **423**, 218-226.

[27] Y. Zhou, X. Wang, H. Zhu, M. Yoshizawa-Fujita, Y. Miyachi, M. Armand, M. Forsyth, G.W. Greene, J.M. Pringle, P.C. Howlett. Solid-state lithium conductors for lithium metal batteries based on electrospun nanofiber/plastic crystal composites. *ChemSusChem.* 2017; **10**(15), 3135-3145.

[28] X. Wang, H. Zhu, G.W. Greene, J. Li, N. Iranipour, C. Garnier, J. Fang, M. Armand, M. Forsyth, J.M. Pringle, P.C. Howlett. Enhancement of ion dynamics in organic ionic plastic crystal/PVDF composite electrolytes prepared by co-electrospinning. *J. Mater. Chem. A.* 2016; **4**(25), 9873-9880.

[29] Y. Zhou, X. Wang, H. Zhu, M. Armand, M. Forsyth, G.W. Greene, J.M. Pringle, P.C. Howlett. *N*-ethyl-*N*-methylpyrrolidinium bis(fluorosulfonyl)imide-electrospun polyvinylidene fluoride composite electrolytes: characterization and lithium cell studies. *Phys. Chem. Chem. Phys.* 2017; **19**(3), 2225-2234.

[30] J. Fang, X. Wang, T. Lin. Electrical power generator from randomly oriented electrospun poly(vinylidene fluoride) nanofibre membranes. *J. Mater. Chem.* 2011; **21**(30), 11088-11091.

[31] W.A. Yee, M. Kotaki, Y. Liu, X. Lu. Morphology, polymorphism behavior and molecular orientation of electrospun poly(vinylidene fluoride) fibers. *Polymer.* 2007; **48**(2), 512-521.

[32] P. Zhang, X. Zhao, X. Zhang, Y. Lai, X. Wang, J. Li, G. Wei, Z. Su. Electrospun doping of carbon nanotubes and platinum nanoparticles into the  $\beta$ -Phase

polyvinylidene difluoride nanofibrous membrane for biosensor and catalysis applications. *ACS Appl. Mater. Interfaces*. 2014; **6**(10), 7563-7571.

**[33]** K.M. Abraham, Z. Jiang, B. Carroll. Highly conductive PEO-like polymer electrolytes. *Chem. Mater*. 1997; **9**(9), 1978-1988.

**[34]** I. Aldalur, M. Martinez-Ibañez, M. Piszcz, L.M. Rodriguez-Martinez, H. Zhang, M. Armand. Lowering the operational temperature of all-solid-state lithium polymer cell with highly conductive and interfacially robust solid polymer electrolytes. *J. Power Sources*. 2018; **383**, 144-149.

**[35]** S.W. Choi, S.M. Jo, W.S. Lee, Y.R. Kim. An electrospun poly(vinylidene fluoride) nanofibrous membrane and its battery applications. *Adv. Mater*. 2003; **15**(23), 2027-2032.

**[36]** J. Evans, C.A. Vincent, P.G. Bruce. Electrochemical measurement of transference numbers in polymer electrolytes. *Polymer*. 1987; **28**(13), 2324-2328.





## Chapter 8

---

# Conclusions





## 8. Conclusions

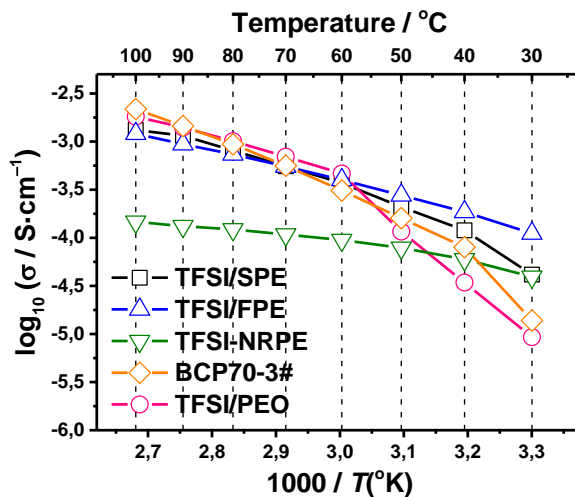
The main objective of this thesis work was the design and synthesis of novel polymer matrices that combine good mechanical properties and high ionic conductivity in order to decrease the operational temperature of all-solid-state lithium metal batteries (ASSLMBs). In order to overcome this challenge, this PhD work was focused on the synthesis of comb-like polymer electrolytes in which grafted units present extremely high chain flexibility.

In the first stage of this thesis, new type of comb-like polymer matrices based on imide ring and highly flexible Jeffamine<sup>®</sup> side chains comprising ethylene oxide (EO) and propylene oxide (PO) units were synthesized. It has been proven that the ratio between EO and PO units was a determining factor in order to find a good compromise between low crystallinity values and high ionic conductivity. EO units provide high ionic conductivity and good solvation power; whereas PO prevents the crystallization of the polymer chains and the glass transition temperature ( $T_g$ ) is decreased. On the other hand, the influence of the molecular weight ( $M_w$ ) of the chains on the mechanical properties was analysed, showing higher degree of entanglement for higher values of  $M_w$ . The polymer matrix based on Jeffamine M-2070 was selected as representative compound for further investigation in next chapters of the thesis. This decision was motivated by the low fraction of crystallinity and high ionic conductivity presented by this material even at room temperature (RT).

The influence of different sulfonimide salts on the properties of the solid polymer electrolytes (SPEs) was analysed; lithium bis (trifluoromethanesulfonyl) imide (LiTFSI) and lithium bis(fluorosulfonyl)imide (LiFSI). These selected salts present different properties in terms of Li metal compatibility. All the prepared SPEs showed high ionic conductivity at the temperature ranging from 70 °C to RT region, due to the high amorphicity of the polymer matrix, and obtaining the highest ionic conductivities with a molar ratio of EO/Li = 20. At this salt concentration the SPEs presents completely amorphous nature and low  $T_g$  values. These SPEs were also used as polymer binders in lithium iron phosphate (LiFePO<sub>4</sub>, LFP) based cathodes. The Li<sup>°</sup> || LFP cell using LiTFSI/SPE and LiFSI/SPE at 70 °C exhibited good cycling stability and high Coulombic efficiency. When decreasing the temperature, the Li<sup>°</sup> || LFP cell using LiFSI/SPE delivered decent specific/areal

capacity with good Coulombic efficiency. This was ascribed to SEI-favourable FSI<sup>-</sup> that could significantly improve the electrochemical stability of Li<sup>o</sup> electrode with the electrolyte.

Despite the outstanding electrochemical performance exhibited by these SPEs, they did not present sufficient mechanical properties to obtain self-standing membranes. To enhance the stiffness of the SPEs while keeping the good contact between the electrolyte and the electrodes, further modifications were carried out. In this context, a new family of tailor-made block copolymers based on the above mentioned SPE and amine terminated polystyrene (PS) were synthesized. Glassy polymers with high values of  $T_g$ , such as PS, could play the role of scaffold for polymer matrix. These new polymer electrolytes (PEs) showed improved mechanical properties at a very small expense of the ionic conductivity. The incorporation of the PS block into the Jeffamine-based polymer improved the electrochemical stability of SPEs vs. Li<sup>o</sup> electrode. The Li<sup>o</sup> || LFP cell using BCP-based electrolytes presented acceptable cycling stability and high Coulombic efficiency. However, these cells showed slightly deteriorated cell performance compared to the Jeffamine-based homopolymers. This behaviour was ascribed to the poor binding properties of the BCP in the cathode material due to the phase separation between different blocks.

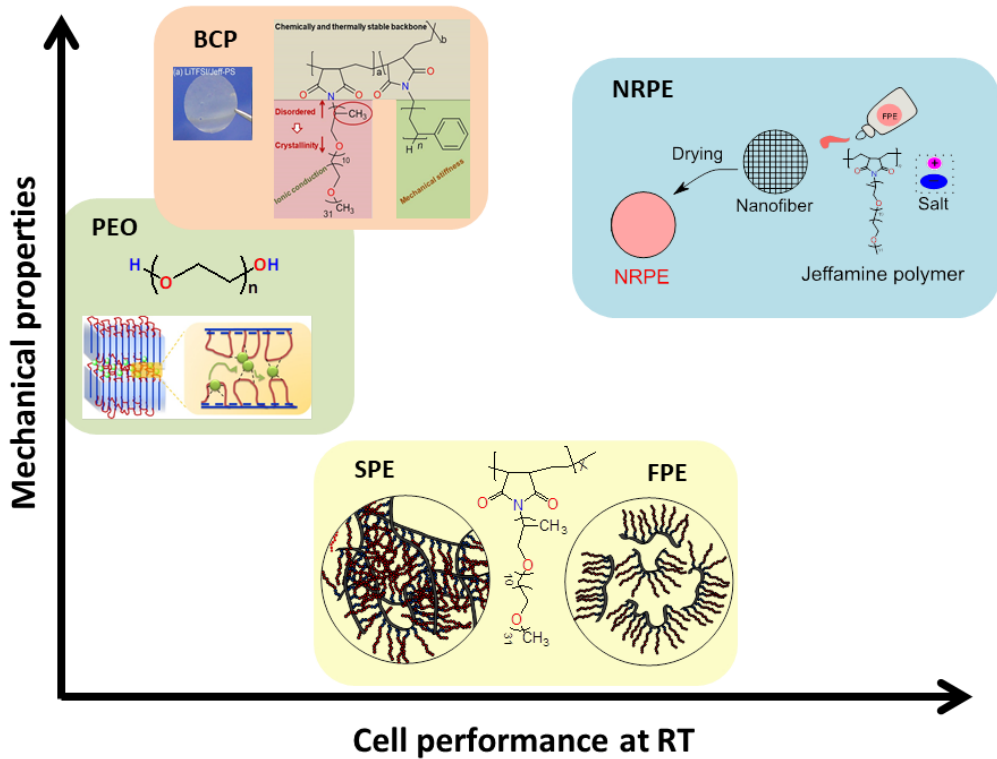


**Figure 8.1.** Temperature dependence of ionic conductivity for the TFSI- based electrolytes synthesized in this thesis work.

The BCP and PEO based electrolytes emphasize the major problem with Li metal cells. Apart from ionic conductivity the compatibility against electrode is a key factor for successful operation. As another alternative, physical modifications were carried out in the base SPE. The mechanical properties of the SPE were controlled by the modification of synthesis parameters, obtaining a flowable polymer electrolyte (FPE) as a result. The suppression of the entanglement on the Jeffamine-based polymers resulted in higher flexibility of the former matrix, thus giving lower  $T_g$  values and higher ionic conductivities. Moreover, the good adhesive properties presented by these novel materials endowed a better contact

between  $\text{Li}^\circ$  electrode and the electrolyte, thus retarding the dendrite formation. Due to the poor mechanical properties presented by these materials, in a first stage FPEs were used as a stable buffer layer between the  $\text{Li}^\circ$  electrode and poly(ethylene oxide) (PEO)-based membranes. As a consequence, the stability against  $\text{Li}^\circ$  electrode was significantly improved. Moreover the  $\text{Li}^\circ \parallel \text{LFP}$  cell using LiFSI/PEO membrane and LiFSI/FPE as buffer layer showed better cycling stability and high Coulombic efficiency even at different C-rates, compared to the reference LiFSI/PEO membranes at 70 °C. However, PEO did not allow the cycling of these cells at temperatures below the melting temperature (*ca.* 65 °C).

Due to the poor mechanical properties presented by the FPE, and the impossibility of decreasing the operational temperature of BCP and PEO-based cells, encourage to look for further modifications. In this regards, the FPE was blended with poly(vinylidene fluoride) (PVDF) fibers in order to provide robustness to the PE. These nanofiber reinforced polymer electrolytes (NRPEs) were self-standing and highly conductive at RT. Moreover, the stability against  $\text{Li}^\circ$  electrode was not affected by the incorporation of PVDF fibers, resulting in good cell performance of  $\text{Li}^\circ \parallel \text{LiFePO}_4$  cells even at RT.



**Figure 8.2.** Comparison of the mechanical properties and cell performance at RT for the electrolytes prepared in this thesis work.

In conclusion, the new polymer backbones presented in this PhD work represent reliable solutions for the scientific community for the development of all-solid-state lithium metal batteries in terms of safety, cost-effectiveness and environmentally friendly. Moreover, the extreme simplicity of the synthesis of all the polymers made in this study from commercial precursors suggests that they can be scaled up easily for commercial applications. Particularly, and taking into account all the conclusions arisen from this work, the synthesis of a block-copolymer based on PS and FPE could lead to a well-balanced ionic conductivity and mechanical properties, becoming a suitable candidate to meet the demand for this kind of batteries.

# Appendix

---







## Appendix:

A.1.	List of abbreviations and symbols .....	219
A.2.	SEM images of the cathodes .....	223
A.3.	Supplementary information Chapter 3 .....	224
A.4.	Supplementary information Chapter 4 .....	225
A.5.	Supplementary information Chapter 5 .....	228
A.6.	Supplementary information Chapter 6 .....	229
A.7.	Supplementary information Chapter 7 .....	235
	References .....	241
	List of contributions .....	243



**A.1. List of abbreviations and symbols**

ACN	Acetonitrile
$\Delta H_c$	Enthalpy of crystallization
$\Delta H_m$	Enthalpy of melting
Ar	Argon
$\Delta V$	DC voltage
ASSLMBs	All-solid-state lithium metal batteries
ATR-FTIR	Attenuated total reflectance Fourier-transform infrared spectroscopy
<i>B</i>	Pseudo-activation energy
BCP	Block copolymer
$\text{BF}_4^-$	Tetrafluoroborate
BSE	Back-scattered electron detector
C65	Conductive carbon
CDI	1,1-carbonyldiimidazole
$(\text{CD}_3)_2\text{SO}$	Deuterated dimethyl sulfoxide
CE	Coulombic efficiency
$\text{ClO}_4^-$	Perchlorate
$\text{CO}_2$	Carbon dioxide
CPE	Composite polymer electrolyte
<i>D</i>	Diffusion coefficient
DMA	Dynamic mechanical analysis
DMF	<i>N,N</i> -dimethylformamide
DMSO	Dimethyl sulfoxide
$\text{D}_2\text{O}$	Deuterium oxide
DSC	Differential scanning calorimeter
$E_a$	Activation energy
EDX	Energy dispersive X-ray spectroscopy
EES	Electrochemical energy storage
EIS	Electrochemical impedance spectroscopy
EO	Ethylene oxide
ETD	Secondary electron detector
$\text{Et}_3\text{N}$	Triethylamine

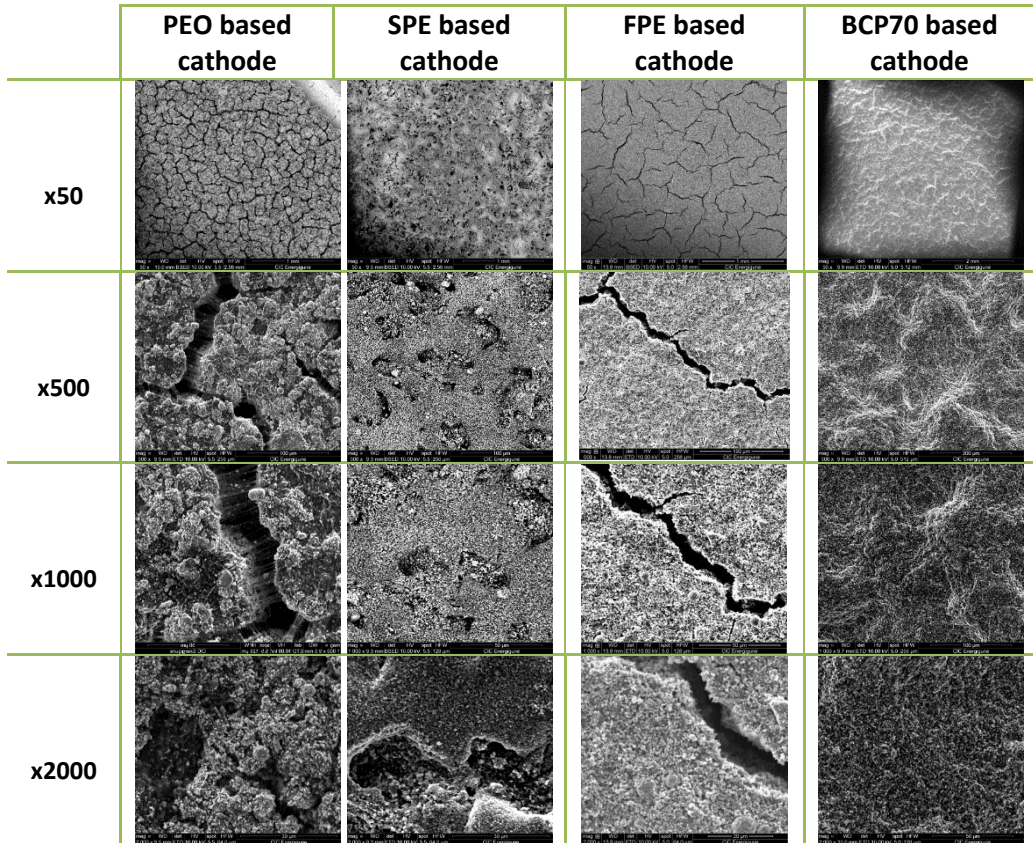
FP	Flowable polymer
FPE	Flowable polymer electrolyte
G'	Storage modulus
G''	Loss modulus
GPE	Gel polymer electrolytes
<sup>1</sup> H NMR	Hydrogen-1 nuclear magnetic resonance
HPE	Hybrid polymer electrolyte
<i>I</i> <sub>0</sub>	Initial current
IEA	International energy agency
<i>I</i> <sub>s</sub>	Steady-state current
ISE	Inorganic solid electrolytes
LCO	Lithium cobalt oxide
LFP	Lithium iron phosphate
Li	Lithium
LIB	Lithium-ion battery
LiFSI	Lithium bis(fluorosulfonyl)imide
LSV	Linear sweep voltammetry
LiTFSI	Lithium bis(trifluoromethanesulfonyl)imide
<i>M</i> <sub>w</sub>	Molecular weight
<i>η</i> <sup>*</sup>	Complex viscosity
N <sub>A</sub>	Nucleophilic addition
NMC	Manganese cobalt oxide
NMP	<i>N</i> -methyl-2-pyrrolidone
NMR	Nuclear magnetic resonance
NO <sub>x</sub>	Nitrogen oxide
NRPE	Nanofiber-reinforced polymer electrolyte
OCV	Open circuit voltage
PAN	Poly(acrylonitrile)
PC	Polycarbonate

PE	Polymer electrolyte
PEaMA	Poly(ethylene- <i>alt</i> -maleic)anhydride
PEC	Poly(ethylene carbonate)
PEG	Poly(ethylene glycol)
PEO	Poly(ethylene oxide)
PEO- <i>b</i> -PS	Poly(ethylene oxide)-block-polystyrene
PF <sub>6</sub> <sup>-</sup>	Hexafluorophosphate
PMMA	Poly(methyl methacrylate)
PO	Propylene oxide
PPO	Poly(propylene oxide)
PS	Polystyrene
PS-PEO	Poly(styrene- <i>b</i> -ethylene oxide)
P(TMC- <i>co</i> -CL)	Poly(trimethylene carbonate- <i>co</i> -caprolactone)
PVC	Poly(vinyl chloride)
PVDF	Poly(vinylidene fluoride)
PVDF-HFP	Poly(vinylidene fluoride- <i>co</i> -hexafluoropropylene)
$R_b^0$	Initial resistance of the bulk electrolytes
$R_b^s$	Final resistance of the bulk electrolytes
$R_i^0$	Initial resistance of the interfacial layers of the Li <sup>o</sup> electrode/electrolyte
$R_i^s$	Final resistance of the interfacial layers of the Li <sup>o</sup> electrode/electrolyte
RT	Room temperature
$R_{total}$	Total resistance
$\sigma$	Ionic conductivity
SE	Solid electrolyte
SEI	Solid electrolyte interphase
SEM	Scanning electron microscopy
SO <sub>x</sub>	Sulphur oxide
SP	Solid polymer
SPE	Solid polymer electrolyte
SS	Stainless steel
SSB	Solid state battery
STA	Simultaneous thermal analyser

$T_c$	Crystallization temperature
$T_d$	Decomposition temperature
TGA	Thermogravimetric analysis
TFT	$\alpha, \alpha', \alpha''$ -trifluorotoluene
THF	Tetrahydrofuran
$T_g$	Glass transition temperature
$T_{Li}^+$	Lithium transference number
$T_m$	Melting temperature
VTF	Vogel-Tamman-Fulcher
$\chi_c$	Crystallinity

## A.2. SEM images of the cathodes

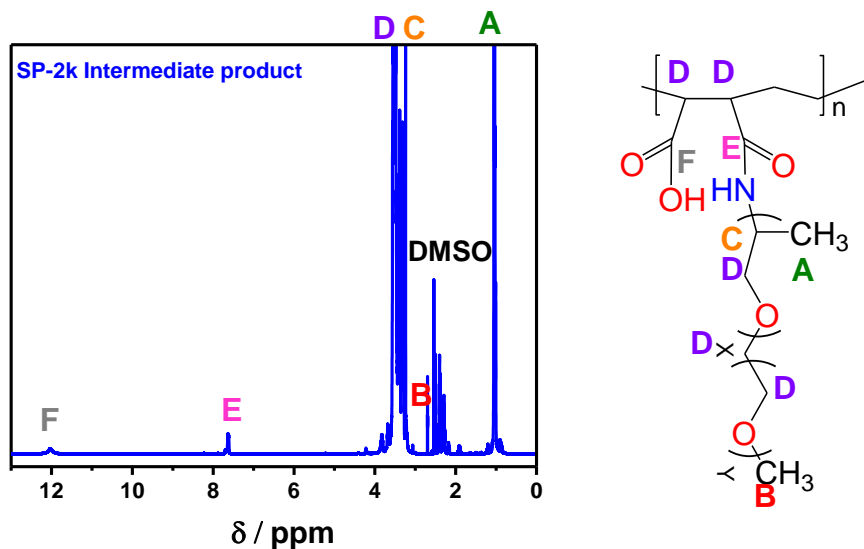
**Table A.2.1.** SEM images of the cathodes used during this thesis work using different magnifications.



### A.3. Supplementary information Chapter 3

#### A.3.1. Hydrogen-1 Nuclear magnetic resonance ( $^1\text{H}$ NMR)

The  $^1\text{H}$  NMR spectrum obtained for the intermediate product with the imide ring opened for SP-2k is depicted in **Figure A.3.1**. This technique was used to follow the imide ring closing reaction by changes in the signals related to  $-\text{NH}$  and  $-\text{OH}$  groups. The peaks at 1.2 and 3.6 ppm, named as **A** and **C** in the spectrum, correspond to the protons from  $-\text{CH}_3$  and  $-\text{CH}$  groups of the PO units in Jeffamine<sup>®</sup> side chains, respectively. The peak at 3.4 ppm, marked as **B**, corresponds to the terminal  $-\text{CH}_3$  of the EO units of the Jeffamine<sup>®</sup> side chains. Finally, the peak at 3.7 ppm, designated as **D**, corresponds to the protons from  $-\text{CH}/-\text{CH}_2$  group from the polymer backbone and  $-\text{CH}_2$  group from Jeffamine<sup>®</sup> side chains. The peaks, named as **E** and **F** in the spectrum, correspond to the  $-\text{NH}$  and  $-\text{OH}$  groups of the open ring.

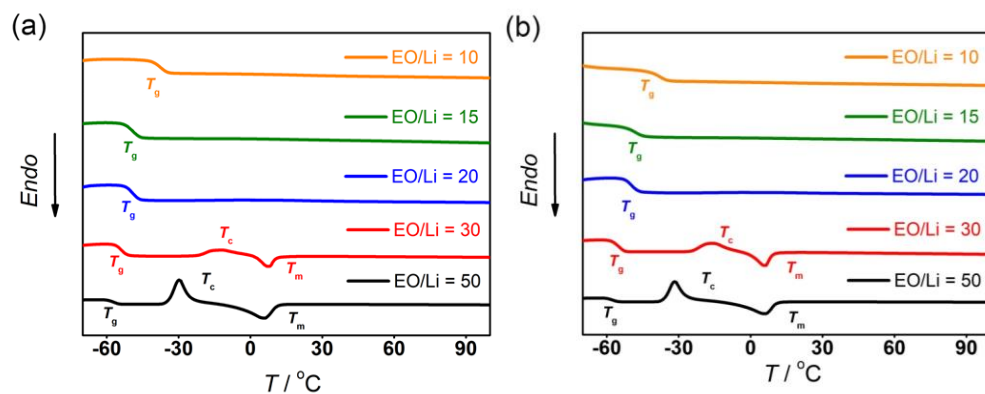


**Figure A.3.1.**  $^1\text{H}$  NMR spectrum for the intermediate product of SP-2k matrix.



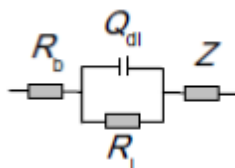
## A.4. Supplementary information Chapter 4

### A.4.1. Differential scanning calorimetry (DSC)



**Figure A.4.1.** DSC traces of the **a)** LiFSI/SPE and **b)** LiTFSI/SPE polymer electrolytes with different concentration of lithium salt at the second heating scan.

### A.4.2. Compatibility with Li<sup>o</sup> electrode



**Figure A.4.2.** The simplified equivalent circuit adopted to fit the collected electrochemical impedance spectra in **Figure 4.10**. In the circuit,  $R_b$ , bulk resistance of polymer electrolyte;  $R_i$ , Li/SPEs interface resistance;  $Q_{dl}$ , double layer capacity of Li/SPEs interface;  $Z$ , diffusive impedance [1].

**Table A.4.1.** The best-fitted results of the EIS spectra using the simplified equivalent circuit in A.4.2 for Li<sup>+</sup> symmetric cells with various electrolytes.

Samples	T <sup>[a]</sup> / °C	R <sub>b</sub> <sup>[b]</sup> / Ω cm <sup>2</sup>	R <sub>i</sub> <sup>[c]</sup> / Ω cm <sup>2</sup>	R <sub>total</sub> <sup>[d]</sup> / Ω cm <sup>2</sup>
<b>LiFSI/SPE (heating scan)</b>				
	25	490	1233	1723
	40	145	363	508
	50	80	189	269
	60	50	89	138
	70	33	41	74
<b>LiFSI/FPE (cooling scan)</b>				
	25	333	2818	3151
	40	126	570	696
	50	70	204	275
	60	45	85	131
	70	33	43	76
<b>LiFSI/PEO (heating scan)</b>				
	25	69631	620111	689741
	40	19133	120077	139211
	50	4098	29575	33673
	60	486	1690	2176
	70	68	250	319
<b>LiFSI/PEO (cooling scan)</b>				
	25	13306	58024	71330
	40	1614	6874	8488
	50	408	1531	1939
	60	104	430	535
	70	71	249	319
<b>LiTFSI/PEO (heating scan)</b>				
	25	31437	114749	146186
	40	680	2666	3347
	50	192	707	899
	60	62	271	333
	70	20	102	122
<b>LiTFSI/PEO (cooling scan)</b>				

---

25	1420	7857	9277
40	216	1377	1593
50	40	431	472
60	27	210	237
70	20	103	122

---

[a] Temperature at which the measurement was performed. [b] Bulk resistance. [c] Interfacial resistance. [d] Total resistance.

## A.5. Supplementary information Chapter 5

## A.5.1. Differential scanning calorimetry (DSC)

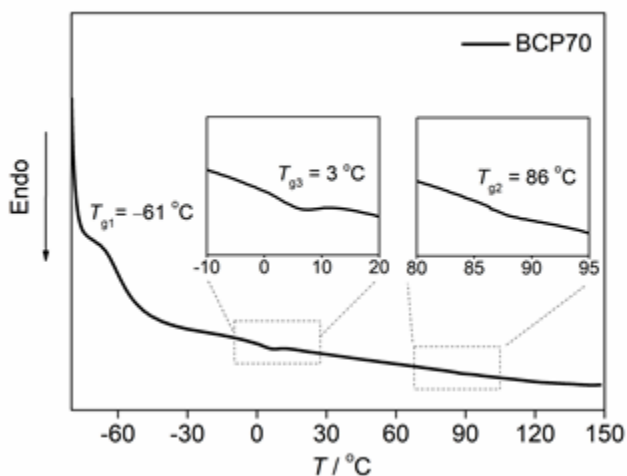


Figure A.5.1. DSC traces of BCP70 with the insets to make the glass transitions legible.

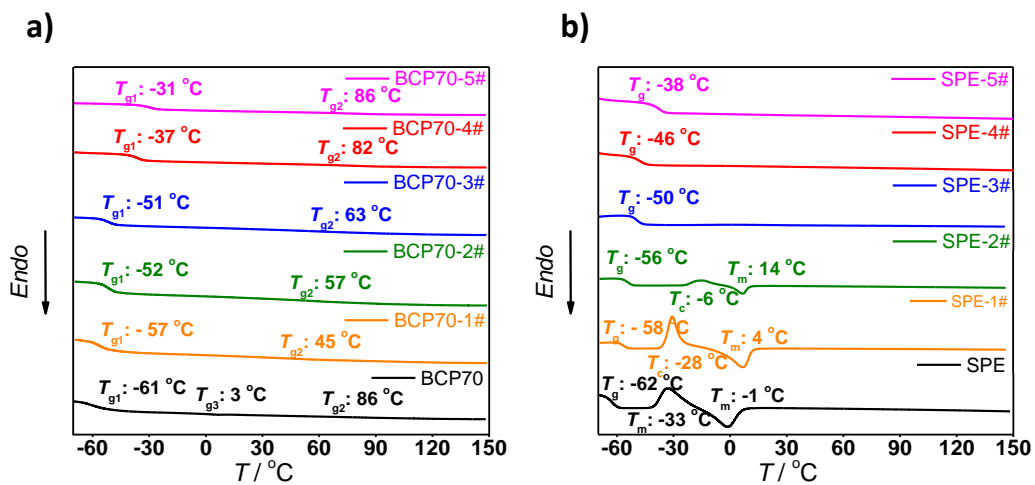


Figure A.5.2. DSC traces of a) BCP and b) SPE-based electrolytes.

## A.6. Supplementary information Chapter 6

### A.6.1. Attenuated total reflectance-Fourier-transform infrared spectroscopy (ATR-FTIR)

Characteristic signals assigned to TFSI<sup>-</sup> appear at  $\sim 1380\text{ cm}^{-1}$  (asymmetric ( $\nu_a$ ) stretching of SO<sub>2</sub>),  $\sim 1130\text{ cm}^{-1}$  (symmetric ( $\nu_s$ ) stretching of SO<sub>2</sub>),  $1060\text{ cm}^{-1}$  ( $\nu_a$  (SNS)),  $761\text{ cm}^{-1}$  ( $\nu_s$  (SNS)) [2]. Signals assigned to FSI<sup>-</sup> appear at  $\sim 1370\text{ cm}^{-1}$  ( $\nu_a$  (SO<sub>2</sub>)),  $1235\text{--}1150\text{ cm}^{-1}$  ( $\nu_s$ (SO<sub>2</sub>)),  $890\text{--}850\text{ cm}^{-1}$  ( $\nu_a$  (SNS)), and  $\sim 740\text{ cm}^{-1}$  ( $\nu_s$  (SNS) and  $\nu_s$  (SF)) [3].

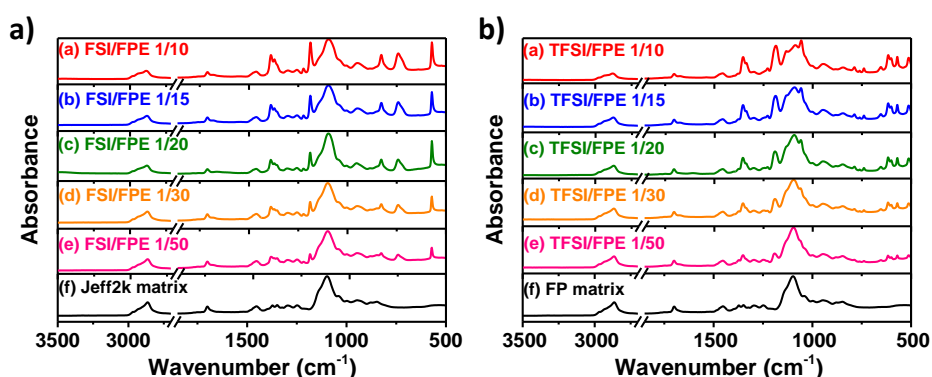


Figure A.6.1. ATR-FTIR spectra of the a) LiFSI/FPE and b) LiTFSI/FPE-based polymer electrolytes with all the studied lithium salt concentrations.

### A.6.2. Differential scanning calorimetry (DSC)

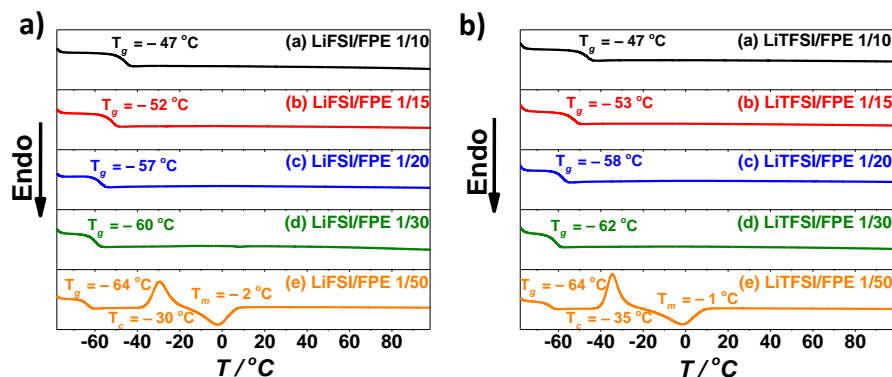


Figure A.6.2. DSC traces of the a) LiFSI/FPE and b) LiTFSI/FPE-based polymer electrolytes with different concentration of lithium salt at the second heating scan.

**Table A.6.1.** The characterization data for the phase behavior for the as-prepared electrolytes.

<b>Samples</b>	<b>EO/Li</b>	$T_g$ <sup>[a]</sup>	$T_c$ <sup>[b]</sup> ( $\Delta H_c$ ) <sup>[c]</sup>	$T_m$ <sup>[d]</sup> ( $\Delta H_m$ ) <sup>[e]</sup>
<b>LiFSI/SPE</b>				
	50	-58	-26 (21.9)	4 (22.4)
	30	-54	-13 (5.5)	7 (4.6)
	20	-49		
	15	-48		
	10	-37		
<b>LiTFSI/SPE</b>				
	50	-58	-28 (21.9)	4 (25.6)
	30	-56	-14 (3.3)	6 (3.8)
	20	-50		
	15	-46		
	10	-38		
<b>LiFSI/FPE</b>				
	50	-64	-30 (19.5)	-2 (20.5)
	30	-60		
	20	-57		
	15	-52		
	10	-47		
<b>LiTFSI/FPE</b>				
	50	-64	-35 (26.2)	-1 (27.3)
	30	-62		
	20	-58		
	15	-53		
	10	-47		
<b>LiFSI/PEO</b>	20	-47	3 (0.8)	63 (67)
<b>LiTFSI/PEO</b>	20	-45		65 (50)

[a] Glass transition temperature ( $^{\circ}\text{C}$ ); [b] Crystallization point ( $^{\circ}\text{C}$ ); [c] Enthalpy of crystallization ( $\text{J g}^{-1}$ ); [d] Melting point ( $^{\circ}\text{C}$ ); [e] Enthalpy of melting ( $\text{J g}^{-1}$ ).

## A.6.3. Ionic conductivity

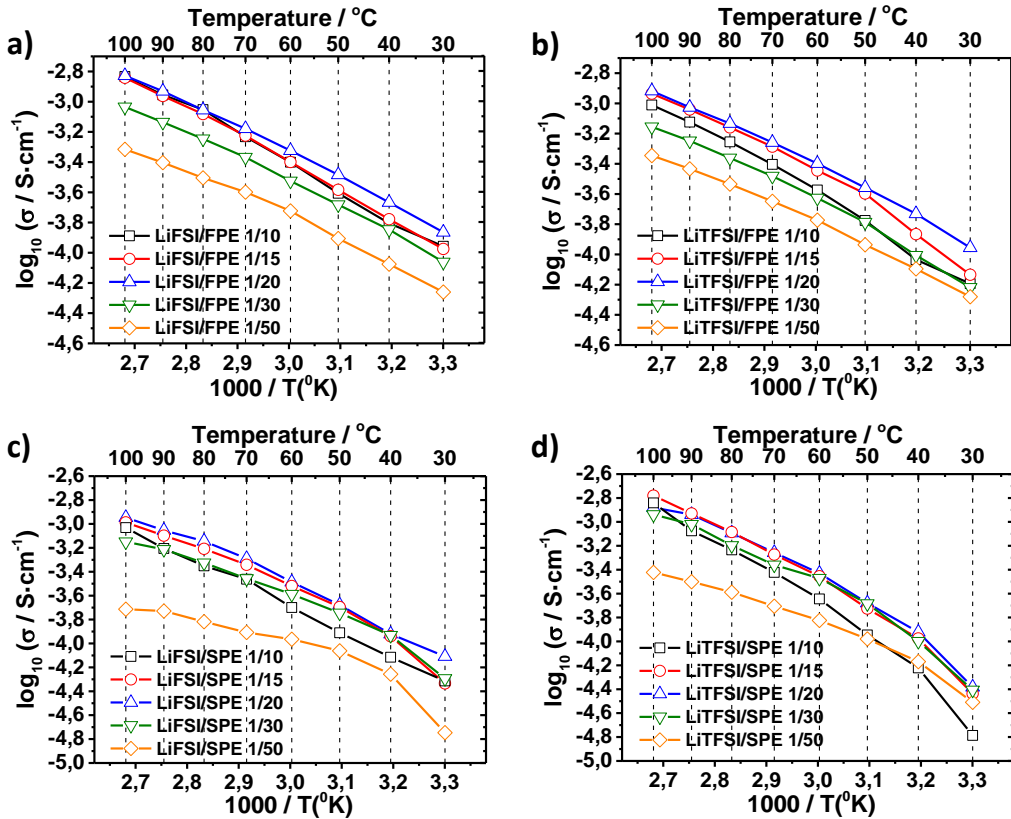


Figure A.6.3. Arrhenius plot of ionic conductivity for a) LiFSI/FPE, b) LiTFSI/FPE, c) LiFSI/SPE and d) LiTFSI/SPE with different salt concentration.

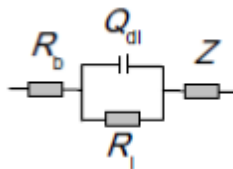
A.6.4. Compatibility with  $\text{Li}^0$  electrode

Figure A.6.4. The simplified equivalent circuit adopted to fit the collected electrochemical impedance spectra in Figure 6.14. In the circuit,  $R_b$ , bulk resistance of polymer electrolyte;  $R_i$ , Li/SPEs interface resistance;  $Q_{dl}$ , double layer capacity of Li/SPEs interface;  $Z$ , diffusive impedance [1].

**Table A.6.2.** The best-fitted results of the EIS spectra using the simplified equivalent circuit in A.6.4 for Li<sup>+</sup> symmetric cells with various electrolytes.

Samples	$T^{[a]} / ^\circ\text{C}$	$R_b^{[b]} / \Omega \text{ cm}^2$	$R_i^{[c]} / \Omega \text{ cm}^2$	$R_{\text{total}}^{[d]} / \Omega \text{ cm}^2$
<b>LiFSI/FPE (heating scan)</b>				
	25	273	568	841
	40	161	239	400
	50	80	74	154
	60	51	36	87
	70	36	8	43
<b>LiFSI/FPE (cooling scan)</b>				
	25	262	1198	1460
	40	132	431	563
	50	72	165	238
	60	47	78	126
	70	31	36	67
<b>LiTFSI/FPE (heating scan)</b>				
	25	234	843	1076
	40	92	237	330
	50	52	100	152
	60	31	43	74
	70	20	20	40
<b>LiTFSI/FPE (cooling scan)</b>				
	25	247	950	1198
	40	95	263	358
	50	48	99	147
	60	30	45	75
	70	19	21	41
<b>LiFSI/SPE (heating scan)</b>				
	25	490	1233	1723
	40	145	363	508
	50	80	189	269
	60	50	89	138
	70	33	41	74
<b>LiFSI/SPE (cooling scan)</b>				
	25	333	2818	3151
	40	126	570	696



	50	70	204	275
	60	45	85	131
	70	33	43	76
<b>LiTFSI/SPE (heating scan)</b>				
	25	750	7119	7870
	40	213	1213	1427
	50	128	568	695
	60	80	287	367
	70	54	182	236
<b>LiTFSI/SPE (cooling scan)</b>				
	25	491	9216	9706
	40	194	2142	2336
	50	119	935	1054
	60	76	364	439
	70	55	184	238
<b>LiFSI/PEO (heating scan)</b>				
	25	69631	620111	689741
	40	19133	120077	139211
	50	4098	29575	33673
	60	486	1690	2176
	70	68	250	319
<b>LiFSI/PEO (cooling scan)</b>				
	25	13306	58024	71330
	40	1614	6874	8488
	50	408	1531	1939
	60	104	430	535
	70	71	249	319
<b>LiTFSI/PEO (heating scan)</b>				
	25	31437	114749	146186
	40	680	2666	3347
	50	192	707	899
	60	62	271	333
	70	20	102	122
<b>LiTFSI/PEO (cooling scan)</b>				
	25	1420	7857	9277

Appendix

---

---

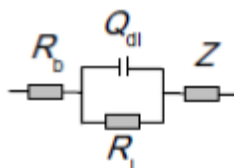
40	216	1377	1593
50	40	431	472
60	27	210	237
70	20	103	122

---

[a] Measured temperature. [b] Bulk resistance. [c] Interfacial resistance. [d] Total resistance.

## A.7. Supplementary information Chapter 7

### A.7.1. Compatibility with Li<sup>o</sup> electrode



**Figure A.7.1.** The simplified equivalent circuit adopted to fit the collected electrochemical impedance spectra in **Figure 7.12**. In the circuit,  $R_b$ , bulk resistance of polymer electrolyte;  $R_i$ , Li/SPEs interface resistance;  $Q_{dl}$ , double layer capacity of Li/SPEs interface;  $Z$ , diffusive impedance [1].

**Table A.7.1.** The best-fitted results of the EIS spectra using the simplified equivalent circuit in **A.7.1** for Li<sup>o</sup> symmetric cells with various electrolytes.

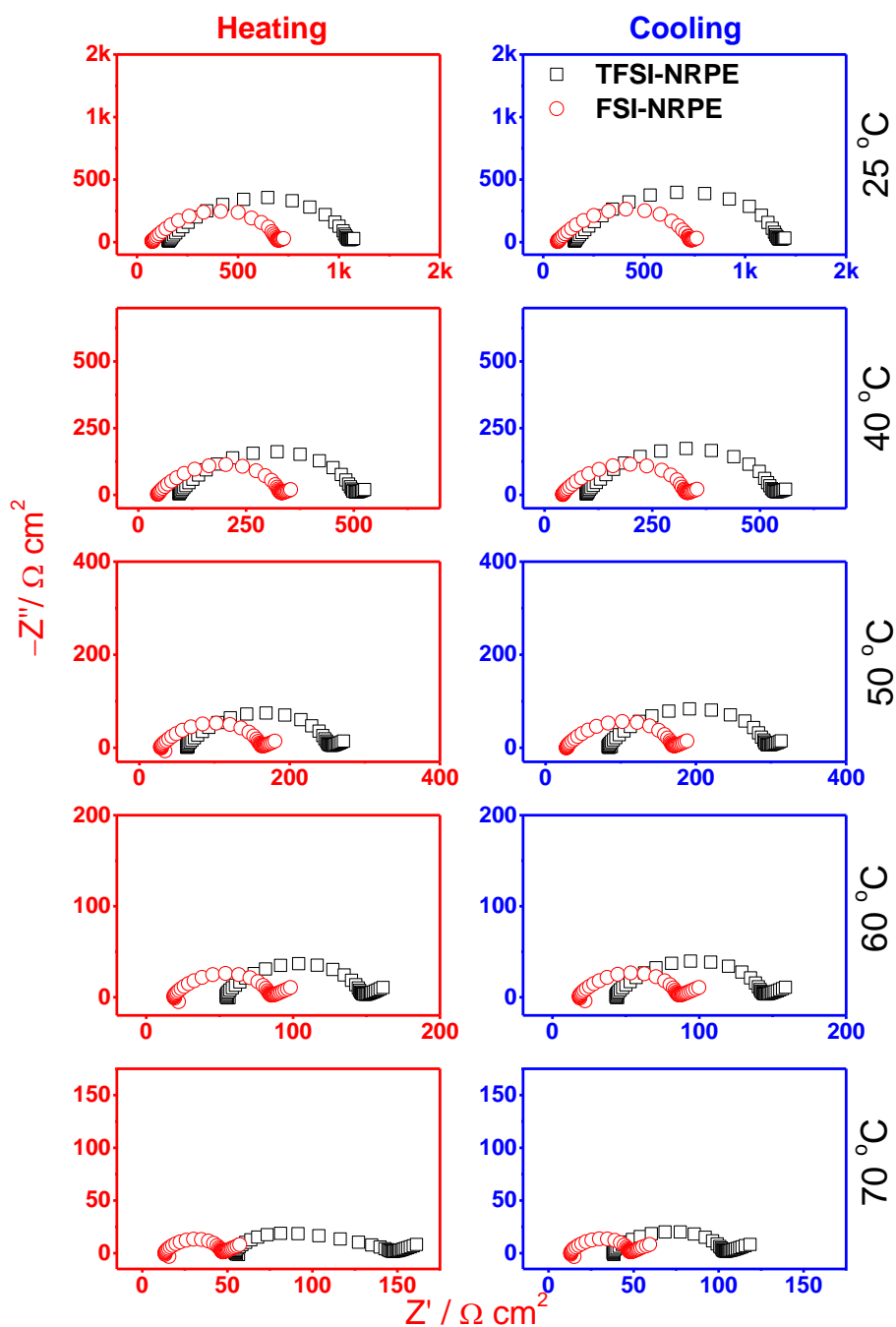
Samples	$T^{[a]}$ / °C	$R_b^{[b]}$ / $\Omega \text{ cm}^2$	$R_i^{[c]}$ / $\Omega \text{ cm}^2$	$R_{\text{total}}^{[d]}$ / $\Omega \text{ cm}^2$
<b>FSI-NRPE (heating scan)</b>				
	25	75	626	701
	40	45	288	333
	50	28	135	163
	60	19	66	85
	70	13	34	47
<b>FSI-NRPE (cooling scan)</b>				
	25	72	661	734
	40	42	288	331
	50	27	142	170
	60	18	68	86
	70	13	35	48
<b>TFSI-NRPE (heating scan)</b>				
	25	156	895	1051
	40	94	408	502
	50	63	191	254
	60	54	93	148

---

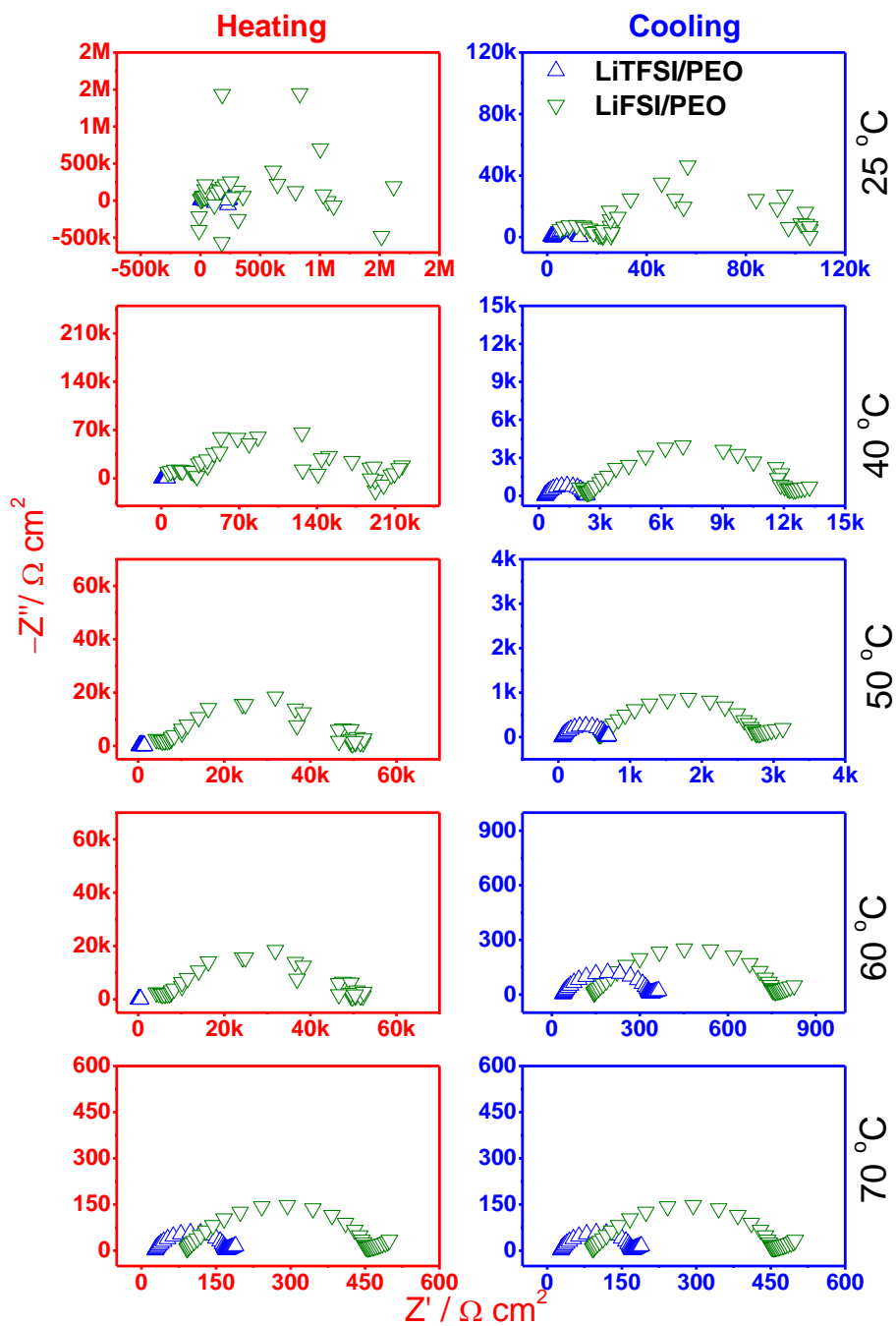
	70	30	48	78
<b>TFSI-NRPE (cooling scan)</b>				
	25	156	1012	1167
	40	97	438	536
	50	83	212	295
	60	43	101	145
	70	30	51	81
<b>FSI-RE (heating scan)</b>				
	25	69631	620111	689741
	40	19133	120077	139211
	50	4098	29575	33673
	60	486	1690	2176
	70	68	250	319
<b>FSI-RE (cooling scan)</b>				
	25	13306	58024	71330
	40	1614	6874	8488
	50	408	1531	1939
	60	104	430	535
	70	71	249	319
<b>TFSI-RE (heating scan)</b>				
	25	31437	114749	146186
	40	680	2666	3347
	50	192	707	899
	60	62	271	333
	70	20	102	122
<b>TFSI-RE (cooling scan)</b>				
	25	1420	7857	9277
	40	216	1377	1593
	50	40	431	472
	60	27	210	237
	70	20	103	122

---

[a] Measured temperature. [b] Bulk resistance. [c] Interfacial resistance. [d] Total resistance.

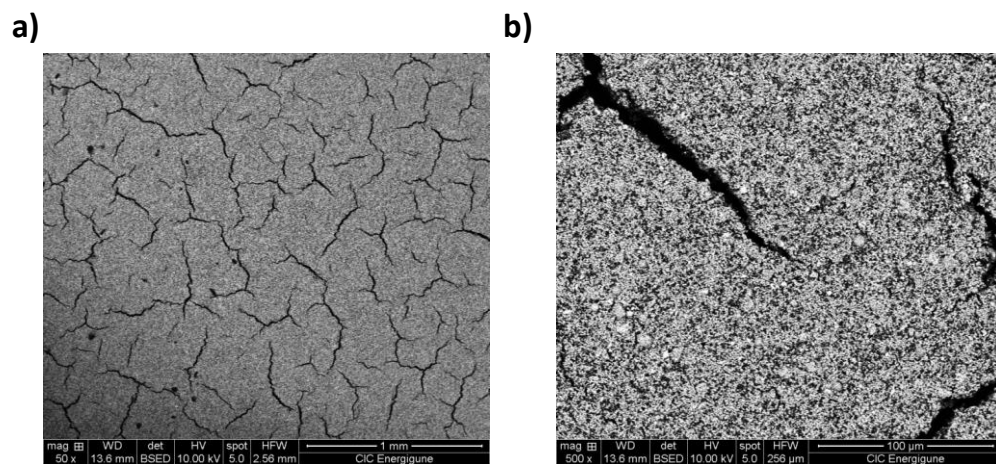


**Figure A.7.2.** Electrochemical impedance spectra of  $\text{Li}^+ || \text{Li}^+$  symmetric cell for NRPE with  $\text{EO/Li} = 20$  (X = TFSI, FSI).



**Figure A.7.3.** Electrochemical impedance spectra of  $\text{Li}^+ \parallel \text{Li}^+$  symmetric cell for PEO with EO/Li = 20 (X = TFSI, FSI).

### A.7.2. Solvent casting method in $\text{LiFePO}_4$ -based cathodes



**Figure A.7.4.** SEM images for FPE-based cathode with a magnification of **a)** x50 and **b)** x500.

### A.7.3. Cycling of Li<sup>o</sup> | LiFePO<sub>4</sub> cell performance at RT

**Table A.7.2.** State-of-art of the electrochemical performance of the Li-based cells solid and gel polymer electrolytes.

Entry	Electrolyte composition <sup>[a]</sup>	$T^{[b]}$ / °C	$\sigma^{[c]}$ / S cm <sup>-1</sup>	Areal capacity <sup>[d]</sup> / mAh cm <sup>-2</sup>	Cathode loading <sup>[e]</sup> / mg cm <sup>-2</sup>	Ref
1	PCL+TMC/LiTFSI	25	$4.1 \times 10^{-5}$	0.13	1.8–2.5	[4]
2	PPC+LAGP/LiFSI	RT	$10^{-4}$	0.35	2-3	[5]
3	PEC+PVDF-HFP/LiTFSI	30	$1.08 \times 10^{-4}$	0.35	2.5	[6]
4	Jeffamine/LiFSI	30	$10^{-4}$	0.1	6	[7]
5	POC+tetraglyme/LiTFSI	RT	$3.75 \times 10^{-5}$	0.19	1.2	[8]
6	BEMA+PEGMA/PY <sub>1.201</sub> TFSI	RT	$1 \times 10^{-3}$	0.25	3	[9]
7	PVDF-HFP/1g13LiTFSI- LiTFSI	25	$3.16 \times 10^{-4}$	0.29	2.0-2.5	[10]
8	PVDF- HFP+GBL/LiTFSI+S <sub>221</sub> TFSI	RT	$6.32 \times 10^{-4}$	0.33	2.0-2.5	[11]
9	PDADMATFSI/EMIM-TFSI	22	$3 \times 10^{-3}$	0.39	2.31	[12]
10	POSS-PEO+POSS-IL (EC/DMC)/LiTFSI EC/DMC	25	$4.8 \times 10^{-4}$	0.45	2.8	[13]
11	PP+PPC+SN/LiTFSI	25	$2.18 \times 10^{-4}$	0.37	2.65	[14]
<b>12</b>	<b>FSI-NRPE</b>	<b>30</b>	<b><math>6.4 \times 10^{-5}</math></b>	<b>0.25</b>	<b>6.0</b>	<b>This work</b>
<b>13</b>	<b>TFSI-NRPE</b>	<b>30</b>	<b><math>3.9 \times 10^{-5}</math></b>	<b>0.15</b>	<b>5.5</b>	<b>This work</b>

[a] Abbreviations are listed as follows: poly( $\epsilon$ -caprolactone) (PCL), trimethylene carbonate (TMC); lithium bis(trifluoromethanesulfonyl)imide (LiTFSI); poly(propylene carbonate) (PPC); Li<sub>1.5</sub>Al<sub>0.5</sub>Ge<sub>1.5</sub>(PO<sub>4</sub>)<sub>3</sub> (LAGP); Lithium bis(fluorosulfonyl)imide (LiFSI); poly(ethylene carbonate) (PEC); poly(vinylidene fluoride-co-hexafluoropropene) (PVDF-HFP); poly(oxo-carbonate) (POC); dimethacrylic oligomer bisphenol A ethoxylate dimethacrylate (BEMA); poly(ethylene glycol) methyl ether methacrylate (PEGMA); *N*-[2-(methacryloyloxy)ethyl]-*N*-methylpyrrolidinium bis(trifluoromethanesulfonyl)imide (PY<sub>1.201</sub>TFSI);  $\gamma$ -butyrolactone (GBL); 1,1,2,3,3-pentamethyl-2-propylguanidinium bis(trifluoromethanesulfonyl)imide (1g13TFSI); diethylmethylsulfonium bis(trifluoromethanesulfonyl)imide (S<sub>221</sub>TFSI); poly[diallyldimethylammonium bis(trifluoromethane)sulfonimide] (PDADMATFSI), 1-ethyl-3-methyl imidazolium bis(trifluoromethanesulfonyl)imide (EMIM-TFSI), pentaoxaheptadecan-1-ol silane (POSS), pentaoxaheptadecan-1-ol silane-co-poly ethylene oxide (POSS-PEO), ethylene carbonate/dimethyl carbonate (EC/DMC), polypropylene (PP), succinonitrile (SN). [b] Cycling temperature. [c] Ionic conductivity of the electrolytes. [d] Areal capacity of the cell. [e] Loading of active mass in the cathode. Color codes: Green (solid polymer electrolytes), blue (gel polymer electrolytes), red (polymers with properties between solid and gel) and yellow (present work).



## References

- [1] G.B. Appetecchi, S. Passerini. Poly(ethylene oxide)-LiN(SO<sub>2</sub>CF<sub>2</sub>CF<sub>3</sub>)<sub>2</sub> polymer electrolytes -II. Characterization of the interface with lithium. *J. Electrochem. Soc.* 2002; **149**(7), A891-A897.
- [2] J. Evans, C.A. Vincent, P.G. Bruce. Electrochemical measurement of transference numbers in polymer electrolytes. *Polymers.* 1987; **28**(13), 2324-2328.
- [3] I. Aldalur, H. Zhang, M. Piszcz, U. Oteo, L.M. Rodriguez-Martinez, D. Shanmukaraj, T. Rojo, M. Armand. Jeffamine<sup>®</sup> based polymers as highly conductive polymer electrolytes and cathode binder materials for battery application. *J. Power Sources.* 2017; **347**, 37-46.
- [4] J. Mindemark, B. Sun, E. Toermae, D. Brandell. High-performance solid polymer electrolytes for lithium batteries operational at ambient temperature. *J. Power Sources.* 2015; **298**, 166-170.
- [5] Y. Li, F. Ding, Z. Xu, L. Sang, L. Ren, W. Ni, X. Liu. Ambient temperature solid-state Li-battery based on high-salt-concentrated solid polymeric electrolyte. *J. Power Sources.* 2018; **397**, 95-101.
- [6] Y. Zhao, Y. Bai, Y. Bai, M. An, G. Chen, W. Li, C. Li, Y. Zhou. A rational design of solid polymer electrolyte with high salt concentration for lithium battery. *J. Power Sources.* 2018; **407**, 23-30.
- [7] I. Aldalur, M. Martinez-Ibañez, M. Piszcz, L.M. Rodriguez-Martinez, H. Zhang, M. Armand. Lowering the operational temperature of all-solid-state lithium polymer cell with highly conductive and interfacially robust solid polymer electrolytes. *J. Power Sources.* 2018; **383**, 144-149.
- [8] F. Ouhib, L. Meabe, A. Mahmoud, N. Eshraghi, B. Grignard, J.-M. Thomassin, A. Aqil, F. Boschini, C. Jérôme, D. Mecerreyes, C. Detrembleur. CO<sub>2</sub>-sourced polycarbonates as solid electrolytes for room temperature operating lithium batteries. *J. Mater. Chem. A.* 2019; **7**(16), 9844-9853.
- [9] C. Gerbaldi, J.R. Nair, S. Ferrari, A. Chiappone, G. Meligrana, S. Zanarini, P. Mustarelli, N. Penazzi, R. Bongiovanni. New electrolyte membranes for Li-based cells: Methacrylic polymers encompassing pyrrolidinium-based ionic liquid by single step photo-polymerization. *J. Membr. Sci.* 2012; **423-424**, 459-467.

**[10]** M. Li, L. Yang, S. Fang, S. Dong, Y. Jin, S.-i. Hirano, K. Tachibana. Li/LiFePO<sub>4</sub> batteries with gel polymer electrolytes incorporating a guanidinium-based ionic liquid cycled at room temperature and 50 °C. *J. Power Sources*. 2011; **196**(15), 6502-6506.

**[11]** M. Li, B. Yang, Z. Zhang, L. Wang, Y. Zhang. Polymer gel electrolytes containing sulfur-based ionic liquids in lithium battery applications at room temperature. *J. Appl. Electrochem*. 2013; **43**(5), 515-521.

**[12]** M. Safa, A. Chamaani, N. Chawla, B. El-Zahab. Polymeric ionic liquid gel electrolyte for room temperature lithium battery applications. *Electrochim. Acta*. 2016; **213**, 587-593.

**[13]** G. Yang, C. Chanthad, H. Oh, I.A. Ayhan, Q. Wang. Organic-inorganic hybrid electrolytes from ionic liquid-functionalized octasilsesquioxane for lithium metal batteries. *J. Mater. Chem. A*. 2017; **5**(34), 18012-18019.

**[14]** H. Yue, J. Li, Q. Wang, C. Li, J. Zhang, Q. Li, X. Li, H. Zhang, S. Yang. Sandwich-like poly(propylene carbonate)-based electrolyte for ambient-temperature solid-state lithium ion batteries. *ACS Sustain. Chem. Eng*. 2018; **6**(1), 268-274.

## LIST OF CONTRIBUTIONS

### Publications

- [1] I. Aldalur, M. Armand, H. Zhang. Jeffamine-based polymers for rechargeable batteries. (Submitted)
- [2] I. Aldalur, X. Wang, N. Goujon, M. Echeverría, M. Martínez-Ibañez, M. Piszcz, P. C. Howlett, M. Forsyth, M. Armand, H. Zhang. Nanofiber-reinforced polymer electrolytes toward room temperature solid-state lithium batteries. (Submitted)
- [3] H. Zhang, U. Oteo, H. Zhu, X. Judez, M. Martinez-Ibañez, I. Aldalur, E. Sanchez-Diez, C. Li, J. Carrasco, M. Forsyth, M. Armand. Enhanced lithium-ion conductivity of polymer electrolytes by selective introduction of hydrogen into the anion. *Angewandte Chemie*. 2019; **131**(23), 7911-7916.
- [4] I. Aldalur, M. Martinez-Ibañez, A. Krztoń-Maziopa, M. Piszcz, M. Armand, H. Zhang. Flowable polymer electrolytes for lithium metal batteries. *Journal of Power Sources*. 2019; **423**, 218-226.
- [5] U. Oteo, M. Martinez-Ibañez, I. Aldalur, E. Sanchez-Diez, J. Carrasco, M. Armand, H. Zhang. Improvement of the cationic transport in polymer electrolytes with (difluoromethanesulfonyl) (trifluoromethanesulfonyl)imide salts. *ChemElectroChem*. 2019; **6**(4), 1019-1022.
- [6] I. Aldalur, M. Martinez-Ibañez, M. Piszcz, H. Zhang, M. Armand. Self-standing highly conductive solid electrolytes based on block copolymers for rechargeable all-solid-state lithium-metal batteries. *Batteries & Supercaps*. 2018; **1**(4), 149-159.
- [7] X. Judez, M. Piszcz, E. Coya, C. Li, I. Aldalur, U. Oteo, Y. Zhang, W. Zhang, L.M. Rodriguez-Martinez, H. Zhang, M. Armand. Stable cycling of lithium metal electrode in nanocomposite solid polymer electrolytes with lithium bis(fluorosulfonyl)imide. *Solid State Ionics*. 2018; **318**, 95-101.
- [8] I. Aldalur, M. Martinez-Ibañez, M. Piszcz, L.M. Rodriguez-Martinez, H. Zhang, M. Armand. Lowering the operational temperature of all-solid-state lithium polymer cell

with highly conductive and interfacially robust solid polymer electrolytes. *Journal of Power Sources*. 2018; **383**, 144-149.

[9] I. Aldalur, H. Zhang, M. Piszcz, U. Oteo, L.M. Rodriguez-Martinez, D. Shanmukaraj, T. Rojo, M. Armand. Jeffamine® based polymers as highly conductive polymer electrolytes and cathode binder materials for battery application. *Journal of Power Sources*. 2017; **347**, 37-46.

## Works submitted to national or international conferences

[1] I. Aldalur, M. Martínez-Ibáñez, E. Sánchez-Díez, U. Oteo, M. Piszcz, H. Zhang, M. Armand. Highly conductive solid polymer electrolytes for all-solid-state lithium metal batteries. E-MRS Spring Meeting 2019, May 26-31, 2019 Nice (France).

[2] M. Martínez-Ibáñez, I. Aldalur, E. Sánchez-Díez, U. Oteo, M. Piszcz, H. Zhang, M. Armand. New polymer electrolytes for safe all-solid-state lithium metal batteries. 235<sup>th</sup> ECS Meeting, May 26-30, 2019 Dallas (United States).

[3] M. Martínez-Ibáñez, I. Aldalur, E. Sánchez-Díez, M. Piszcz, H. Zhang, L. M. Rodríguez-Martínez, M. Armand. Beyond PEO: new solid polymer electrolytes for decreasing the operational temperature of all-solid-state lithium metal batteries. 10<sup>th</sup> ECNP International conference of nanostructured polymers and nanocomposites, October 3-5, 2018 Donostia-San Sebastián (Spain).

[4] I. Aldalur, M. Martínez-Ibáñez, E. Sánchez-Díez, M. Piszcz, H. Zhang, M. Armand. Highly conductive solid polymer electrolytes for all-solid-state lithium metal batteries. E-MRS Fall Meeting 2018, September 16-20, 2018 Warsaw (Poland).

[5] M. Martínez-Ibáñez, I. Aldalur, E. Sánchez-Díez, M. Piszcz, H. Zhang, L. M. Rodríguez-Martínez, M. Armand. Solid polymer electrolytes for lithium batteries: enhancing the li-ion conductivity at ambient temperature. 69<sup>th</sup> annual meeting of the international society in electrochemistry, September 2-7, 2018 Bologna (Italy).

[6] M. Armand, M. Martínez-Ibáñez, I. Aldalur, E. Sánchez-Díez, I. Gracia, H. Zhang. Going further with polymer electrolytes. ISPE-XVI 16<sup>th</sup> International symposium on polymer electrolytes, June 24-29, 2018 Yokohama (Japan).

[7] H. Zhang, X. Judez, G. Eshetu, C. Li, I. Gracia, I. Aldalur, M. Martínez-Ibáñez, E. Sánchez-Díez, U. Oteo, O. Bondarchuk, L. M. Rodríguez-Martínez, M. Armand. Solid polymer electrolytes for safe and high energy density lithium-sulfur batteries. ISPE-XVI 16<sup>th</sup> International symposium on polymer electrolytes, June 24-29, 2018 Yokohama (Japan).

[8] X. Judez, H. Zhang, G. Eshetu, I. Aldalur, M. Martínez-Ibáñez, L. Otaegui, J. Zagorski, A. Llordés, M. Armand, C. Li, L. M. Rodríguez-Martínez. Towards

competitive lithium sulfur batteries. IDTechEX Show, April 11-13, 2018 Berlin (Germany).

**[9]** X. Judez, H. Zhang, C. Li, I. Aldalur, M. Piszcz, L. Otaegui, Evaluation of polymer-rich composite electrolytes for all-solid-state Li-S batteries. 3<sup>rd</sup> edition Power our future, July 3-5, 2017 Vitoria-Gasteiz (Spain).

**[10]** I. Aldalur, H. Zhang, M. Martínez-Ibáñez, M. Piszcz, L. M. Rodríguez-Martínez, T. Rojo, M. Armand. Highly conductive new polymer materials for battery application at ambient temperature. 3<sup>rd</sup> edition Power our future, July 3-5, 2017 Vitoria-Gasteiz (Spain).

**[11]** X. Judez, M. Piszcz, E. Coya, C. Li, I. Aldalur, U. Oteo, Y. Zhang, W. Zhang, L. M. Rodríguez-Martínez, M. Armand, H. Zhang. Stable cycling of lithium metal electrode in nanocomposite solid polymer electrolytes with lithium bis(fluorosulfonyl)imide. SSI-21, 21<sup>st</sup> International conference on solid state ionics, June 18-23, 2017 Padova (Italy).

**[12]** I. Aldalur, M. Piszcz, H. Zhang, L. M. Rodríguez-Martínez, T. Rojo, M. Armand. Jeffamine<sup>®</sup>-based polymer electrolytes for battery application. E-MRS Spring Meeting 2017, May 22-26, 2017 Strasbourg (France).

**[13]** X. Judez, H. Zhang, I. Aldalur, M. Piszcz, C. Li, L. Otaegui, J. Zagorski, L. Buannic, A. Llordés, T. Rojo, J. Kilner, M. Armand, L. M. Rodríguez-Martínez. Evaluation of solid electrolytes for all-solid-state Li-S batteries. LiS-M3 Lithium sulfur: mechanism, modelling & materials, April 26-27, 2017 London (United Kingdom).

**[14]** I. Aldalur, H. Zhang, M. Piszcz, L. M. Rodríguez-Martínez, T. Rojo, M. Armand. Jeffamine<sup>®</sup>-based polymer electrolytes. E ISPE-XV 15<sup>th</sup> International symposium on polymer electrolytes, August 15-19, 2016 Uppsala (Sweden).

## Internationally recognized awards

### **[1] Best Graduate Student Oral Presentation Award.**

Awarding entity: European Materials Research Society

Conference: E-MRS Spring Meeting 2019

### **[2] Graduate Student Award.**

Awarding entity: European Materials Research Society

Conference: E-MRS Fall Meeting 2018







